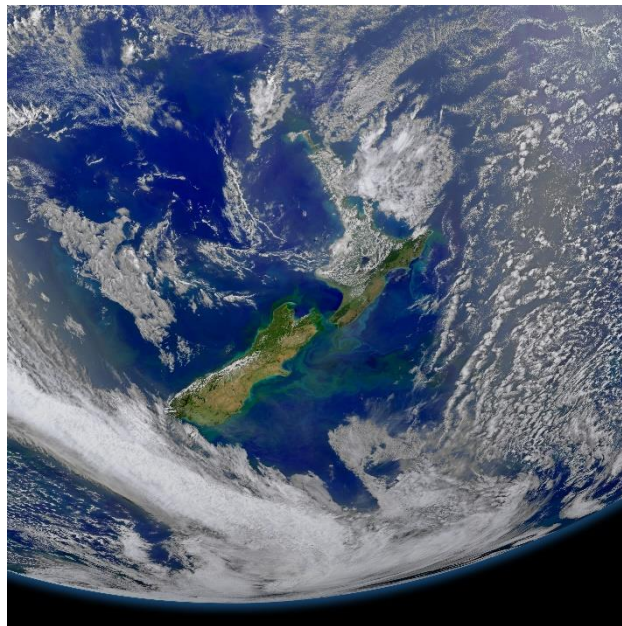


Monitoring ocean health: 2023 update on satellite indicators for surface temperature, productivity and suspended solids

Prepared for Ministry for the Environment

August 2023



Prepared by:
Matt Pinkerton
Mark Gall
Francois Thorat
Philip Sutton
Simon Wood

For any information regarding this report please contact:

Matt Pinkerton
Principal Scientist
+64 4 386 0369
m.pinkerton@niwa.co.nz

National Institute of Water & Atmospheric Research Ltd
Private Bag 14901, Kilbirnie, Wellington 6241

Phone +64 4 386 0300

NIWA CLIENT REPORT No: 2023217WN_rev1
Report date: August 2023
NIWA Project: MFE22302

Revision	Description	Date
Version 0.1	Draft report	28 June 2023
Version 1.0	Final version sent to client	09 August 2023
Version 1.1	Rev 1 version sent to client	28 August 2023

Quality Assurance Statement		
	Reviewed by:	David Bowden
	Formatting checked by:	Jess Moffat
	Approved for release by:	Mike Williams

VIIRS Image of New Zealand, 9 January 2015

© All rights reserved. This publication may not be reproduced or copied in any form without the permission of the copyright owner(s). Such permission is only to be given in accordance with the terms of the client's contract with NIWA. This copyright extends to all forms of copying and any storage of material in any kind of information retrieval system.

Whilst NIWA has used all reasonable endeavours to ensure that the information contained in this document is accurate, NIWA does not give any express or implied warranty as to the completeness of the information contained herein, or that it will be suitable for any purpose(s) other than those specifically contemplated during the Project or agreed by NIWA and the Client.

Contents

- Executive summary 8**
 - Ocean scale summary 8
 - Coastal scale summary 8
 - Recommendations 9

- 1 Introduction 11**
 - 1.1 Sea surface temperature 12
 - 1.2 Phytoplankton biomass and its primary productivity 13
 - 1.3 Total suspended solids 13
 - 1.4 Marine heatwaves 14

- 2 Methods 15**
 - 2.1 Satellite data sources 15
 - 2.2 Anomalies 20
 - 2.3 Descriptive regions 21
 - 2.4 Trend analysis 23
 - 2.5 Correlation analysis 24
 - 2.6 Marine heatwaves 25
 - 2.7 Trophic classes 25

- 3 Results 26**
 - 3.1 Ocean scale analyses 26
 - 3.2 Coastal scale analyses 43
 - Northland 65
 - Hauraki Gulf/Manukau/Kaipara 66
 - Bay of Plenty/East Cape/Hawke Bay 67
 - Wairarapa/South Taranaki Bight/Cook Straight/Marlborough 68
 - Canterbury/West Coast 70
 - Southland/Stewart Island 70
 - 3.3 Marine heatwaves 72

- 4 Discussion and conclusions 76**
 - 4.1 Satellite product limitations and uncertainties 76
 - 4.2 Ocean scale synopsis 80

4.3	Coastal scale synopsis.....	81
5	Recommendations.....	83
6	Acknowledgements	85
7	Glossary of abbreviations and terms	86
8	References.....	87
Appendix A	Descriptive sub-regions	97
Appendix B	Ocean SST and chl-a annual means	98
Appendix C	Ocean SST and chl-a annual anomalies.....	111
Appendix D	Ocean SST and chl-a time-series.....	124
Appendix E	Coastal SST, chl-a and TSS time-series	127
Appendix F	Oceanic MHW	130
Appendix G	Coastal MHW	133

Tables

Table 2-1:	Summary of satellite products.	16
Table 2-2:	Trend “likelihood” categories determined from posterior probability distributions of slope direction.	24
Table 2-3:	Trophic classes.	26
Table 3-1:	Ocean scale region trends in sea surface temperature over 40 years compared to global trends (1981-2023).	32
Table 3-2:	Ocean scale region trends in sea surface temperature over 20-years compared to global trends (2002-2023).	32
Table 3-3:	Ocean scale region trends in chlorophyll a from three different data sources (1997-2023).	38
Table 3-4:	Coastal scale region trends in sea surface temperature over 40 years (1981-2023) based on OISSTv2.1.	47
Table 3-5:	Coastal scale regional trends in sea surface temperature over 20-years (2002-2023) based on OISSTv2.1.	48
Table 3-6:	Coastal scale regional trends in sea surface temperature over 20-years (2002-2023) based on SCENZ SST v3.0.	48
Table 3-7:	Coastal scale regional trends in chlorophyll a from three data sources	55
Table 3-8:	Trend analysis for coastal region TSS.	61
Table 3-9:	Ocean scale regional linear trends for the marine heatwave cumulative intensity.	74
Table 3-10:	Coastal scale regional linear trends for the cumulative intensity.	76

Table A-1:	Co-ordinates defining descriptive regions.	97
Table F-1:	Trend analysis for four marine heatwave (MHW) metrics for the NZ EEZ.	130
Table G-1:	Trend analysis for four marine heatwave (MHW) metrics for the NZ coastal regions.	133

Figures

Figure 1-1:	Observation platform context to time and space scales of variability in physical and biological processes in the ocean.	12
Figure 2-1:	Ocean scale descriptive regions for which summary data were extracted.	22
Figure 2-2:	Coastal scale descriptive regions.	23
Figure 3-1:	Number of observations (N. Obs) used in the ocean scale analysis:	27
Figure 3-2:	Ocean scale long-term averages in environmental indicators	29
Figure 3-3:	Ocean scale spatial trends in sea surface temperature (SST: 1981-2023):	31
Figure 3-4:	Ocean scale time-series of sea surface temperature anomalies:	33
Figure 3-5:	Seasonal trends in SST (1981-2023).	34
Figure 3-6:	Trends in SST anomalies by month for EEZ and 4 descriptive regions.	35
Figure 3-7:	Ocean scale spatial trends in chlorophyll a (1997-2023):	37
Figure 3-8:	Time-series of chl-a anomalies:	39
Figure 3-9:	Ocean scale seasonal trends in chlorophyll a (chl-a, 1997-2023).	40
Figure 3-10:	Trends in chl-a by month for EEZ and 4 descriptive regions.	41
Figure 3-11:	Ocean scale spatial correlation between sea surface temperature and chlorophyll a (1997–2023).	42
Figure 3-12:	Coastal scale spatial coverage of observations (2002-2023)	44
Figure 3-13:	Coastal scale long-term averages in environmental indicators (2002-2023):	45
Figure 3-14:	Coastal scale spatial trends in sea surface temperature (2002-2022):	47
Figure 3-15:	Coastal scale regional sea surface temperature trend boxplot statistics.	49
Figure 3-16:	Coastal scale regional time-series of sea surface temperature (SST) anomalies.	49
Figure 3-17:	Coastal scale seasonal spatial trends in sea surface temperature (2002-2023).	50
Figure 3-18:	Coastal scale month trends in sea surface temperature anomalies.	51
Figure 3-19:	Coastal scale spatial trends in chlorophyll a (2002-2023).	53
Figure 3-20:	Coastal scale regional chlorophyll a trend boxplot statistics.	54
Figure 3-21:	Coastal scale regional time-series of trends in chlorophyll a (chl-a) anomalies.	56
Figure 3-22:	Coastal scale seasonal spatial trends in chlorophyll a (2002-2023).	57
Figure 3-23:	Coastal scale regional month timeseries trends in chlorophyll a (chl-a).	58
Figure 3-24:	Coastal: Spatial trends in TSS (2002-2023).	60
Figure 3-25:	TSS trends in coastal regions.	60
Figure 3-26:	Time-series of TSS anomalies for coastal bio-regions.	62
Figure 3-27:	Coastal: Seasonal spatial trends in TSS (2002-2023).	63
Figure 3-28:	Trends in TSS anomalies by month for coastal bio-regions.	64
Figure 3-29:	Northland: spatial trends in monthly anomalies of TSS (Total suspended solids) from MODIS-Aqua, 2002-2022.	66

Figure 3-30:	Hauraki Gulf/Manukau/Kaipara: spatial trends in monthly anomalies of TSS (Total suspended solids) from MODIS-Aqua, 2002-2022.	67
Figure 3-31:	Bay of Plenty/East Cape/Hawke Bay: spatial trends in monthly anomalies of TSS (Total suspended solids) from MODIS-Aqua, 2002-2022.	68
Figure 3-32:	Wairarapa/South Taranaki Bight/Cook Strait/Marlborough: spatial trends 2002-2022.	69
Figure 3-33:	Canterbury/West Coast: spatial trends in monthly anomalies of TSS (Total suspended solids) from MODIS-Aqua, 2002-2022.	70
Figure 3-34:	Southland/Stewart Island: spatial trends in monthly anomalies of TSS (Total suspended solids) from MODIS-Aqua, 2002-2022.	71
Figure 3-35:	Coastal: Kendall correlation coefficient between monthly anomalies (2002–2023).	72
Figure 3-36:	Ocean scale timeseries in marine heatwave metrics.	73
Figure 3-37:	Ocean scale regional timeseries in marine heatwave cumulative intensity (in °C days).	74
Figure 3-38:	Coastal scale regional timeseries in marine heatwave cumulative intensity (in °C days).	75
Figure B-1:	Oceanic: Mean annual chl-a and SST.	98
Figure C-1:	Oceanic: Annual mean chl-a and sea-surface temperature (SST) annual anomalies by year.	111
Figure D-1:	Oceanic: Monthly mean SST for descriptive New Zealand regions.	124
Figure D-2:	Oceanic: Monthly mean chl-a for descriptive New Zealand regions.	125
Figure E-1:	Coastal sea-surface temperature (SST) means by month for coastal bio-regions.	127
Figure E-2:	Coastal chl-a anomalies by month for coastal bio-regions.	128
Figure E-3:	Coastal TSS means by month for coastal bio-regions.	129
Figure F-1:	Trends in MHW metrics for the NZ oceanic region “Chatham Rise” between January 1982 and December 2022 (blue line).	131
Figure F-2:	Trends in MHW metrics for the NZ oceanic region “Tasman Sea” between January 1982 and December 2022 (blue line).	131
Figure F-3:	Trends in MHW metrics for the NZ oceanic region “Subtropical Water” between January 1982 and December 2022 (blue line).	132
Figure F-4:	Trends in MHW metrics for the NZ oceanic region “Subantarctic Water” between January 1982 and December 2022 (blue line).	132
Figure G-1:	Trends in MHW metrics for the NZ coastal region “North Eastern” between January 1982 and December 2022 (blue line).	134
Figure G-2:	Trends in MHW metrics for the NZ coastal region “Western North Island” between January 1982 and December 2022 (blue line).	134
Figure G-3:	Trends in MHW metrics for the NZ coastal region “Eastern North Island” between January 1982 and December 2022 (blue line).	135
Figure G-4:	Trends in MHW metrics for the NZ coastal region “North Cook Strait” between January 1982 and December 2022 (blue line).	135
Figure G-5:	Trends in MHW metrics for the NZ coastal region “South Cook Strait” between January 1982 and December 2022 (blue line).	136
Figure G-6:	Trends in MHW metrics for the NZ coastal region “West Coast South Island” between January 1982 and December 2022 (blue line).	136

Figure G-7:	Trends in MHW metrics for the NZ coastal region “East Coast South Island” between January 1982 and December 2022 (blue line).	137
Figure G-8:	Trends in MHW metrics for the NZ coastal region “Southland” between January 1982 and December 2022 (blue line).	137
Figure G-9:	Trends in MHW metrics for the NZ coastal region “Fiordland” between January 1982 and December 2022 (blue line).	138

Executive summary

Satellite observations were used to update and extend key indicators related to changes in sea surface conditions on both open-ocean (9 km) and coastal (0.5 km) scales in Aotearoa New Zealand. The study focused on three key properties: (1) sea-surface temperature (SST); (2) chlorophyll-a (chl-a) as an indicator of phytoplankton biomass and primary productivity; and (3) total suspended solids (TSS) as an indicator of coastal river plumes and bottom-sediment resuspension. The first two properties have previously been included in national-scale environmental reporting (2016, 2019), while the inclusion of TSS provides new insights into coastal regions. This report also includes an analysis of marine heatwave¹ metrics (MHWs). By leveraging multiple satellite products, this study enhances the robustness and temporal coverage of indicators, thereby significantly strengthening the reliability and accuracy of the analysis. These improvements provide a solid foundation for assessing changes around New Zealand and guides recommendations for future research and reporting.

Ocean scale summary

The oceans around New Zealand are warming (especially in winter) and the rate of warming has accelerated since the last report in 2019. Between 1981 and 2023, the area-weighted mean rate of surface warming in the New Zealand Exclusive Economic Zone (EEZ) was found to be +0.20°C per decade, exceeding the previous rate of +0.15°C per decade observed from 1981 to 2018 (Pinkerton et al., 2019). The EEZ has warmed 32% faster than the global average warming rate over the last 40 years and 2.4 times faster than the global average over the last 20 years (though we note there are areas of the global ocean warming faster and slower than the New Zealand region). Over the last 20 years, the fastest warming area around New Zealand was the Chatham region (more than 3 times higher than the mean global rate of warming over the same period) and the greatest acceleration in warming occurred in the Subantarctic region (3-fold increase from the 40-y to the 20-y analysis). Over the last 40 years there has been an increasing occurrence and intensity of marine heatwaves (MHW) around New Zealand, especially in the Tasman Sea region, with significant acceleration since 2010. These MHW events have become more frequent and longer-lasting.

We used changes in surface phytoplankton abundance (chl-a²) to indicate changes in ocean primary productivity. Increasing trends in chl-a were found in the Subtropical Front including a moderate increasing trend over the Chatham Rise (+2.2% of the median per decade), and a greater relative change in Subantarctic water to the south (+6.7% per decade). Conversely, a declining trend (-2.2% per decade) was identified in Subtropical waters located northeast of New Zealand. These findings generally align with previous analyses and our understanding of factors influencing primary productivity in the waters surrounding New Zealand. However, an unexpected decline in primary productivity in Subantarctic water was observed since 2020, where ongoing warming typically promotes increases in phytoplankton abundance. It is possible that some sort of threshold has been crossed in this region which calls for further investigation as it may have broader implications for the ecological dynamics of the Subantarctic at the global scale.

Coastal scale summary

Nearly all coastal waters surrounding New Zealand have experienced “virtually certain” surface warming over the last 40 y, and the warming over this period was faster than the global mean

¹ A marine heatwave is a period of more than 5 days when the water temperature is much higher than normal.

² The concentration of chlorophyll-a, the ubiquitous green pigment in algae, is commonly used as a metric of phytoplankton biomass.

warming rate by between 25% (eastern Te Ika-a-Māui North Island region) and 87% (East Coast Te Waipounamu South Island). In all but one region (eastern North Island), coastal warming was substantially higher over the last 20 y than over the last 40 y (increases of 50–146%) indicating widespread acceleration of coastal warming round New Zealand. The acceleration of coastal warming was particularly high around South Island, where 20-y warming rates in all regions were more than three times the global warming rate over the same period, and nearly 3.7 times as high as the global average in the Southern South Island region. Warming occurred year-round in most coastal regions, though generally greater warming occurred in summer/autumn than in winter/spring. Coastal MHW's have substantially increased in all coastal regions over the last 40 years and particularly since 2010. Coastal scale MHW events have generally become more frequent and longer-lasting.

Increases in chl-a were observed around the coasts of mid-lower North Island and all South Island, particularly during winter. In contrast, coastal regions along the west coast of Te Tai Tokerau Northland and northeast New Zealand shelf including the Hauraki Gulf, Te Tara-O-Te-Ika-A-Māui Coromandel, and Te Moana a Toi Bay of Plenty displayed decreasing trends in chl-a (productivity). Lower-than-normal chl-a was observed along the west coast of South Island during the MHW of December 2017 to March 2018 and December 2022 to January 2023.

Our analysis of total suspended solids (TSS) trends revealed complex patterns of increasing and decreasing trends at both broad (continental shelf) and small (local) scales. There were predominantly increasing TSS trends at the broad-scale, although with generally low confidence. On a smaller scale, both positive and negative TSS small-scale trend features were observed that could be indicative of localised changes associated with specific rivers, estuaries and harbours, and our report identifies areas where changes in TSS were likely to be influenced by variations in materials originating from river systems as opposed to climate drivers. These identified "hotspots" of TSS change provide valuable focal points to help prioritise future investigations.

Recommendations

The following recommendations aim to guide future studies, policy-making processes, and management approaches toward achieving improved understanding and stewardship of New Zealand's ocean and coastal systems:

1. **Link satellite-observations to marine biological resource and hazards:** Satellite data and analyses provide a basis to assess the links between changes to ocean and coastal environments and biological resources (such as fisheries, kai moana and Taonga species, and protected species such as seabirds, marine mammals, and reptiles). Linking biological response to environmental variability and change will take long-term commitment to new multi-trophic level monitoring and research. These programs should encompass both open ocean and coastal waters.
2. **Commit to improving and validating the quality of satellite products in the New Zealand region (coasts and oceans):** Satellite observations offer long-term, large-area, low-cost resource but new, targeted, local bio-optical research is needed to improve robustness of the data. Specifically, local validation and local tuning of the global data to the New Zealand region will provide more useful and reliable satellite observations in the future. In parallel, users require better information on data quality to ensure that new applications use satellite information appropriately, with due consideration of its weaknesses as well as its strengths.

3. **Foster collaboration and data sharing:** New Zealand could make more and better use of satellite capability if there was enhanced collaboration and data-sharing among coastal ecologists, satellite data scientists, management agencies and Māori principles of kaitiakitanga. More effective collaboration would improve the accuracy, resolution, accessibility and of satellite products and lead to new applications for coastal management. Ongoing developments and enhancements to the NIWA SCENZ portal³ streamline sharing of satellite products for New Zealand and enable timely analysis, empowering comprehensive exploration of patterns and monitoring of changes.
4. **Develop operational (near real-time) updating of satellite-based indicators:** Given the increasing pace of change in the ocean and coastal domains, more frequent updates of these satellite-based indicators would be useful. We recommend standardising the processing methodology and moving towards a more-frequent (and ideally semi-automated) update process. Exploring how to define baselines across multiple satellite and *in situ* time-series around New Zealand would be useful.
5. **Prioritise research efforts on coastal sediment:** Based on the identified coastal “hotspot” areas for TSS change, we recommend new field-based and integrative (i.e., *in situ* sampling, modelling, remote sensing, social and policy) research to understand the factors responsible for the observed changes in TSS over time. Knowledge of the interactions between land catchments, climate-related weather patterns, river/estuarine/continental shelf processes and human activities will improve the quality of satellite observations of TSS and advance their use to improve management of the effects of sediment on coastal ecosystems.
6. **Incorporate climate-aware responses into ocean and coastal resource management:** The information provided here could be used to adapt marine management strategies for the effects of climate variability/change including warming, MHW and changes to primary productivity and TSS. The information in the present report should be included alongside shifts in cloud cover, rainfall patterns, wave/current dynamics, sea-level rise when considering how to manage resources. For example some practical examples could include: changes to primary production in major fishing areas or juvenile fish locations may indicate potential trophic effects on stock productivity; trends in coastal primary productivity are relevant to aquaculture industry; marine reserves should be designed taking into account patterns of climate-driven oceanographic change; and patterns of change in TSS includes the effects of climate at the catchment scale.
7. **Expand work on MHW:** Investigate correlations between MHW metrics and primary production, chl-a, TSS; investigate trends in MHW metrics using a moving baseline; investigate seasonal drivers of MHWs around New Zealand; investigate trends in subsurface and bottom (seafloor) MHWs around New Zealand using models and in-situ time series (Argo floats, buoys); support a seasonal MHW forecast as recommended by Stevens et al. (2022); support long term biological monitoring across all coastal bioregions to better understand ecological impacts of MHWs.

³ <https://hub.arcgis.com/documents/NIWA::niwa-scenz-ocean-colour-application-1/explore>

1 Introduction

This report updates and enhances the indicators used by Te Papa Atawhai (Ministry for the Environment, MfE) and Tatauranga Aotearoa (Statistics NZ), for evaluating and communicating progress in sustainable environmental management within Aotearoa New Zealand consistent with the Environmental Reporting Act 2015. The goal is to provide an up-to-date assessment of the current state of New Zealand's marine environment. This report offers valuable insights into the status and trends of significant environmental indicators, equipping decision-makers, and stakeholders with essential knowledge for informed environmental management and conservation initiatives. Specifically, objectives focus on national indicators for oceanic and coastal sea surface temperature and primary productivity, building upon previous analyses (Pinkerton, 2015, 2016; Pinkerton et al., 2019). Additionally, this report introduces a new indicator for total suspended solids in coastal waters, and a new focused analysis on marine heatwave (MHW) metrics.

The physical conditions in New Zealand's coastal and oceanic waters exhibit substantial variation in response to local climate and weather, spanning a wide range of spatial and temporal scales. The marine realm is characterized by its remarkable diversity, heterogeneity, and dynamic nature, undergoing constant change. This profound variability means that *in situ* monitoring, using sensors installed at particular locations, or water samples followed by laboratory analysis, is fundamentally limited and cannot provide insights into change in the marine environment at the national scale and across appropriate time and space scales (Figure 1-1). Remotely-sensed observations which use sensors on Earth-orbiting satellites serve as a valuable solution to address this gap by providing frequent, long-term, wide-area, and spatially-resolved observations (Hooker et al., 1992; Murphy et al., 2001). Satellite observation is also cost-effective compared to *in situ* sampling, as a significant number of satellite products are freely accessible, courtesy of research funding especially in USA and Europe.

However, it is essential to recognize the limitations of satellite products in terms of coverage, resolution, accuracy, and consistency, which should be considered when using them as indicators. In this report, we present satellite products for sea surface temperature (SST), primary production (chlorophyll-a), and total suspended solids concentrations (TSS). Our analysis not only examines trends and patterns but also delves into the limitations and uncertainties associated with these measurements, providing valuable insights.

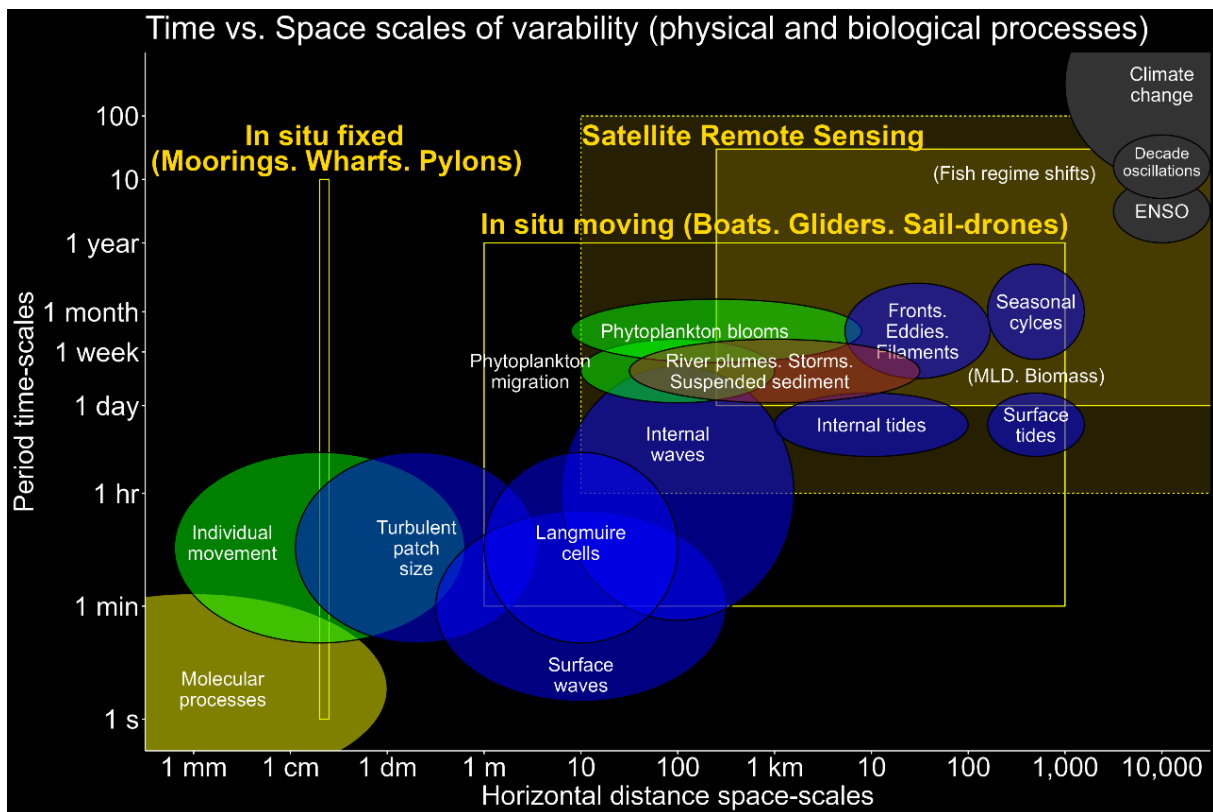


Figure 1-1: Observation platform context to time and space scales of variability in physical and biological processes in the ocean. Physical processes are in blue and biological processes are in green. River plumes, storms and suspended sediment resuspension events are highlighted as dark brown. Each observation platform (yellow) provides different scale insights. Satellite remote sensing is ideally suited to climate scale changes and provides broad and long-term coverage. Adapted from Dickey et al. (2006).

1.1 Sea surface temperature

Sea surface temperature (SST, °C) refers to the temperature of the uppermost layers of the ocean, typically within a metre from the surface. It exhibits spatial variations, generally showing warmer temperatures in the northern regions and cooler temperatures in the southern parts of New Zealand. Additionally, SST experiences seasonal fluctuations, with warmer temperatures prevailing during the summer months and cooler temperatures in winter. The complex dynamics influencing SST involve multiple factors, including radiative solar heating (absorption of incoming solar radiation by the upper ocean), evaporation from the ocean surface, sensible (conductive) heat exchange between the air and the sea, and the mixing of deeper water with surface waters through convective energy transfer. These interactions collectively shape the dynamic nature of SST in the marine environment.

SST is usually a useful indicator of the state of the well-mixed upper ocean layer (called the “mixed layer”), which typically varies between about 10 m and 300 m in depth (but can be outside this range). This upper ocean mixed layer is important because most oceanic primary production takes place within it and also because it is the part of the ocean in contact with the atmosphere and so affects exchange of gases between the atmosphere and ocean. SST is also affected by factors such as: (1) upwelling, where winds can bring colder (often nutrient-rich) water up from depth leading to phytoplankton blooms; (2) inflow of river water (which tends to be cooler than the sea in winter and warmer than the sea in summer); and (3) ocean and coastal currents.

The temperature of the ocean plays a crucial role in the emission of near infra-red radiation (NIR). By using sensors on Earth-orbiting satellites, it becomes possible to measure the NIR emitted by the ocean and consequently estimate the temperature of its surface waters. These satellite-based sensors have been employed since 1981, offering a valuable time series spanning over 40 years, enabling the assessment of sea surface temperature (SST) on a global scale. This extensive dataset provides a valuable resource for studying long-term temperature trends and variations in the world's oceans.

1.2 Phytoplankton biomass and its primary productivity

Phytoplankton are microscopic algae which are kept in suspension in the upper parts of the ocean by the movement of the water. Phytoplankton grow by the process of photosynthesis, whereby energy from the sun is captured by coloured compounds (pigments) in the algal cells and used to create organic matter. This process is called “primary productivity” because it is the primary process by which organic matter is produced from inorganic building blocks. Phytoplankton are consumed by microscopic animals (zooplankton) or die to form organic detritus. The grazers of phytoplankton and consumers of breakdown products are themselves consumed by larger animals in the marine food-web. Through these processes, primary productivity by phytoplankton in the upper layers of the ocean ultimately supports virtually⁴ all marine organisms including fish, mammals, seabirds and benthic biota like corals and sponges. Phytoplankton also play an important feedback role in the regulation of global climate, by forming organic matter that can be sequestered (stored long-term) in seabed sediments, and by releasing chemicals that can help clouds to form (Charlson et al., 1987).

Phytoplankton, similar to plants, imparts a green colour to the upper layers of the ocean, while pure seawater appears blue. Multiband, radiometric sensors on Earth-orbiting satellites can detect this change in water colour, enabling the estimation of phytoplankton biomass in near-surface waters using processing methods known as “algorithms”. The concentration of the main photosynthetic pigment, chlorophyll-a (chl-a), widely present in phytoplankton, serves as a reliable proxy for phytoplankton biomass (Gordon et al., 1988; Hooker et al., 1992; O'Reilly et al., 1998). These capabilities facilitate the study and assessment of phytoplankton dynamics and their ecological significance in the marine environment.

On a larger scale encompassing multiple years and large spatial extents, higher phytoplankton biomass serves as a reasonable indicator of increased primary productivity, although the relationship between the two is quantitatively more intricate (Friedland et al., 2012). In line with previous studies on indicators for the MfE, this report adopts chlorophyll-a (chl-a) as a proxy for primary productivity. This approach aligns with international research, where monitoring changes in the magnitude and patterns of chl-a has proven valuable in understanding shifts in fisheries, marine biogeochemistry, and climate-related alterations in ocean productivity (Murphy et al., 2001; Aiken et al., 2004; IOCCG, 2008).

1.3 Total suspended solids

The mass concentration of Total Suspended Solids (TSS) in the water column can arise from a mixture of particles derived from both organic and inorganic sources. In open-ocean areas, the predominant contribution to TSS is organic in nature, while in coastal regions with higher turbidity, the TSS is primarily composed of inorganic particles.

⁴ Some animals around deep-sea thermal vents obtain their energy from chemosynthetic processes rather than from phytoplankton.

On rocky coasts, studies of ecological problems caused by sedimentation⁵ from rivers and shoreline erosion inputs are widespread, have a long history, and are increasing globally acknowledged (Airoldi, 2003). Sedimentation can also adversely affect soft sediment ecosystems. After some early studies (McKnight 1969; Peterson 1985) there has been considerable recent research in New Zealand (and overseas) showing the potential for substantial impacts associated with smothering by terrestrial sediment deposits (e.g., Miller et al., 2002; Ellis et al., 2004; Lohrer et al., 2004). Many of the key papers were used to develop ANZECC⁶ guidelines for estuary sedimentation (Townsend & Lohrer, 2015) and recommendations for DOC research priorities for sediments in the CMA (part of Green et al., 2021).

The presence of suspended sediment in the water column has significant implications for filter-feeding organisms and can lead to reduced water clarity through increased light attenuation. Fine particulate material settling on the seabed can be resuspended by the combined forces of waves and currents, creating a dynamic interchange between suspended sediment and sedimentation processes. While sediment impacts have traditionally been assessed based on mass concentration alone (e.g., Hughes et al., 2015), it is important to recognise that water clarity can vary non-linearly with mass concentration. Water column light attenuation and visual clarity are influenced by factors such as the particle size distribution and their scattering properties (Stramski et al., 2004), potentially making water clarity aspects a more ecologically meaningful measure for primary producers and visually sighted organisms than the mass concentration of suspended matter (Smith & Davies-Colley, 2002; Davies-Colley et al., 2014; Hughes et al., 2015). Fine suspended sediment plays a crucial role in visual clarity and light penetration, while coarse sediment has a diminished impact, but, if present, can dominate mass concentration. Furthermore, fine suspended sediment serves as a more conservative tracer for pollutants compared to coarse sediments (Davies-Colley et al., 2014).

Satellite sensors that measure optical backscatter provide valuable insights for observing and analysing fine-suspended sediments in dynamic marine coastal environments (Pinkerton et al., 2019). By indirectly assessing the presence, distribution, and dynamics of suspended sediments, these sensors contribute to the assessment of spatial patterns and long-term climate-scale changes in river inputs, coastal erosion, and bottom resuspension across coastal bioregions. This information is crucial in monitoring the state of the marine environment and for informed decision-making and the implementation of sustainable practices in coastal management.

1.4 Marine heatwaves

Marine heatwaves (MHWs) are prolonged events of abnormally warm water that have significant impacts on marine ecosystems and the services they provide (Hobday et al., 2016, 2018; Smale et al., 2019; Smith et al., 2021). Globally, MHWs are increasing in duration, frequency, and intensity (Smale et al., 2019; Frolicher et al., 2018; Oliver et al., 2018, 2019) and several recent marine heatwave events have occurred in New Zealand. This global trend in MHW is expected to accelerate under future climate change, potentially pushing many marine organisms and ecosystems to their limits of resilience (Frolicher et al., 2018). The study of MHWs has seen a significant increase globally, driven by the severity of their impacts and the development of metrics and computer codes to characterize MHWs, using long-term satellite-based sea surface temperature data that is freely available (Banzon et al., 2016) and we apply these global methods to New Zealand in this report.

⁵ "Sedimentation" in this report means the deposition of sediment onto the seabed

⁶ Australian and New Zealand Environment and Conservation Council

2 Methods

2.1 Satellite data sources

2.1.1 Overview

In our analysis, we predominantly used satellite products that align with previous environmental reporting in New Zealand (Pinkerton et al., 2019). However, we have also incorporated new satellite products into the analysis to explore the variability between different approaches (see Table 2-1). This comprehensive approach allows us to gain a deeper understanding of the factors influencing variability and enhance the accuracy of our findings:

Ocean and coastal SST: The Optimum Interpolation Sea Surface Temperature (OISST) product (Reynolds et al., 2002) version 2 was used in Pinkerton et al. (2019) and this was updated to version 2.1 (Huang et al., 2021) for the present report. The time series was also extended to April 2023.

Ocean chl-a: In previous work in New Zealand, we developed methods to link observations from two ocean colour satellite sensors (SeaWiFS and MODIS-Aqua) into a consistent and lengthened time-series by adjusting both sets of measurements using a comparison between the times when both sensors were in operation (their overlap period). For consistency, we extend this time-series to April 2023, and also include new coastal products developed overseas by the Copernicus project (see below).

Coastal chl-a: Remote sensing of chl-a in optically-complex, coastal waters remains a scientifically-challenging area. For consistency, we repeat and extend the analysis from Pinkerton et al. (2019), using a coastal product generated in New Zealand from locally-received downlink data, but the methodology has been advanced as described in Gall et al. (2022). In this new analysis, we also include new coastal chl-a products developed overseas by the Copernicus project (see below).

Coastal TSS: Methods for the remote estimation of TSS concentrations in coastal waters are developing rapidly. For consistency, we repeat and extend the TSS analysis in the New Zealand coastal zone carried out for Te Papa Atawhai, the Department of Conservation (DOC) - Pinkerton et al., 2022) which used the SCENZ TSS v3.0 product. This product is based on observations by the MODIS-Aqua sensor, primarily received by the New Zealand satellite receiver in Lauder, and processed at NIWA at spatial 500 m spatial resolution. For comparison, in the present analysis we also include new coastal TSS products developed overseas by the Copernicus project (see below).

Copernicus: An approach for multi-sensor blending of ocean colour satellite observations has been developed and implemented overseas by various projects including GlobColour/Copernicus⁷ (Garnesson et al., 2019). A list of data products is available from Copernicus (2022)⁸. The overseas method uses multiple sensors (SeaWiFS, MERIS, MODIS-Aqua, VIIRS and OCLI) and provide a time-series of data slightly longer and likely more robust than we could achieve from just two sensors. In addition, a “gap-filled” product is available for some products (including chl-a) which aims to reduce the effect of cloud cover and sensor/algorithm failure on long-term observations (Volpe et al., 2018). In this study we compared the non-gap filled (“CHLM”) and gap-filled (“CHLGF”) Copernicus chl-a products because we are interested in the effects of this method on the time-series and trend analysis in the New Zealand ocean region.

⁷ marine.copernicus.eu

⁸ <https://catalogue.marine.copernicus.eu/documents/PUM/CMEMS-OC-PUM.pdf>

Validation: No new validation of satellite products using *in situ* measurements has been carried out in this study as this is beyond the scope of the project.

Table 2-1: Summary of satellite products. "Primary" dataset indicates the dataset most consistent with previous work for MfE. "Secondary" and "tertiary" datasets are used to extend the time series and/or provide comparison to different processing methods. Below the data source we give the spatial resolution and period covered (month-year).

Indicator	Primary dataset	Secondary dataset	Tertiary dataset
Ocean SST	OISST v2.1 1/4° -> 9km Sep 1981 – Apr 2023	None	None
Coastal SST	OISST v2.1 1/4° -> 500 m Sep 1981 – Apr 2023	MODISA sst 500 m Jul 2002 - Jun 2022	None
Ocean MHW	OISST v2.1 1/4° Sep 1981 – Apr 2023	None	None
Coastal MHW	OISST v2.1 1/4° Jan 1982 – Dec 2022	None	None
Ocean chl-a	MODISA+SW(NIWA) 9 km Sep 1997 - Apr 2023	CMEMS MO-CHL ¹ 4 km -> 9km Jul 1997 – Apr 2023	CMEMS gapfree ² 4 km -> 9 km Jul 1997 – Apr 2023
Coastal chl-a	SCENZ v4.0 CHL 500m Jul 2002 - Jun 2022	CMEMS CHLM ¹ 4 km -> 500m Jul 1997 – Apr 2023	CMEMS CHLGF ² 4 km -> 500 m Jul 1997 – Apr 2023
Coastal TSS	SCENZ v4.0 TSS 500m Jul 2002 - Jun 2022	CMEMS L3 SPM ³ 4 km -> 500 m Jul 1997 – Apr 2023	

Notes

- 1 Copernicus: cmems_obs-oc_glo_bgc-plankton_my_l3-multi-4km_P1M/CHL
- 2 Copernicus: cmems_obs-oc_glo_bgc-plankton_my_l4-gapfree-multi-4km_P1D/CHL
- 3 Copernicus: cmems_obs-oc_glo_bgc-transp_my_l4-multi-4km_P1M/SPM

2.1.2 Ocean scale sea surface temperature

The longest-running measurements of NIR for estimating SST are from the Advanced Very High Resolution Radiometer (AVHRR) series of satellite sensors operated by NOAA (National Oceanic and Atmospheric Administration of the USA). Through a series of overlapping and intercalibrated sensors, the AVHRR project has produced data since 1978 and continuous data since 1981. We used the AVHRR processed product called "OISSTv2.1" which is a 1/4° latitude/longitude daily SST estimate derived by Optimum Interpolation Sea Surface Temperature, version 2.1 (Reynolds et al., 2002; Huang et al., 2021). One-quarter of a degree spatial resolution is equivalent to about 28 km (longitude) and 15–25 km (latitude, 25° to 57°S) in the New Zealand region. The OISST data is processed to remove observation gaps caused by clouds, so this is a gap-free product (Huang et al., 2021). Data were interpolated by bilinear interpolation to the 9 km latitude-longitude to enable

intercomparison of trends in ocean chl-a. This dataset represents the longest satellite SST data available worldwide, and has been widely used internationally, so we do not include secondary or tertiary comparisons. The OISSTv2.1 dataset was also used for the ocean MHW analysis.

2.1.3 Coastal scale sea surface temperature

Two data sources were used for coastal SST: (1) the innermost pixels of the ocean scale OISSTv2.1 product; and (2) high-resolution (1 km) SST time-series obtained from MODIS-Aqua. Although the $\frac{1}{4}^\circ$ resolution OISSTv2.1 data are appropriate for oceanic analysis, the spatial resolution is relatively coarse for coastal investigations so comparison with higher resolution data is necessary. Higher-resolution SST datasets are available but are of much shorter duration and so of less value for investigating multi-decadal trends. We obtained MODIS-Aqua measurements using the SeaDAS v7.2 default 'sst' product (<https://seadas.gsfc.nasa.gov/>) which is derived from measurements of long-wave (11-12 μm) thermal radiation (NASA, 2018a) and started in 2002. SST products at 1 km were subsampled to 500 m on the New Zealand Transverse Mercator projection (NZTM) to match the other coastal products using bilinear interpolation. In order to confirm that the OISSTv2.1 data were appropriate for investigating longer-term trends in SST in coastal waters, Pinkerton et al. (2019) compared the coarse-scale OISSTv2 data with the fine-scale MODIS-Aqua SST data in the territorial waters. This work found that in the New Zealand coastal zone, the OISSTv2 data were highly correlated with the MODIS-Aqua 1 km measurements between 2002 and 2018 (SST: $R^2=0.972$, $N=256\ 687$; SST anomaly: $R^2=0.793$, $N=3\ 686$) with the conclusion that OISSTv2 data were suitable to track long term change in Aotearoa New Zealand territorial waters, and this analysis is not repeated here as the changes from OISSTv2 and OISSTv2.1 are relatively small.

2.1.4 Ocean scale chlorophyll a

Primary data used for ocean chl-a was the merged SeaWiFS and MODIS-Aqua dataset as used in previous study for MfE (e.g., Pinkerton et al., 2019). This merged dataset provides information from September 1997 (the advent of SeaWiFS) to April 2023 (MODIS-Aqua is still operational as of June 2023). Satellite products are periodically reanalysed to take into account improvements in processing methods. We used the most current SeaWiFS version R2018.0 and the most current MODIS-Aqua data version R2018.0 both as used in Pinkerton et al. (2019). Merging of the SeaWiFS and MODIS-Aqua time-series was carried out based on an approximately overlap period of 8 years (2002-2010), with most reliable overlap period of 2003 to 2007. We used the same process of blending chl-a measurements as previously (Pinkerton, 2016; Pinkerton, 2018; Pinkerton et al., 2019). Over all months and all years, MODIS-Aqua tended to give slightly higher chl-a values than SeaWiFS but the differences were very small (median difference in chl-a of $-0.0023\ \text{mg}\ \text{m}^{-3}$). We found that differences tended not to vary with chl-a concentration and there was no indication of a long-term (interannual) variation in the differences between SeaWiFS and MODIS-Aqua measurements (Pinkerton, 2016; Pinkerton, 2018).

We also used two new Copernicus (CMEMS⁹) chl-a products for comparison (Table 2-1): (1) the "cmems_obs-oc_glo_bgc-plankton_my_l3-multi-4km_P1M/CHL" product (here termed "CHLM") is a monthly, 4 km-resolution chl-a product that uses a blend of coastal (semi-analytical) and ocean (empirical) processing; and (2) the "cmems_obs-oc_glo_bgc-plankton_my_l4-gapfree-multi-4km_P1D/CHL" (called "CHLGF") is daily chl-a product based on the same processing as CHLM but gaps (due to clouds or algorithm fail) are filled using an Empirical Orthogonal Functions (EOF)

⁹ Copernicus Marine Environment Monitoring Service

techniques to characterise spatial and temporal patterns producing a gap-free product (Volpe et al., 2018). The CHLGF daily data were combined into monthly products.

2.1.5 Coastal scale chlorophyll a

The primary data source of coastal chl-a data for this study was from the NIWA-SCENZ¹⁰ CHL v4.0 product which is based on MODIS-Aqua observations at 500 m resolution over the period July 2002 – June 2022. NIWA-SCENZ (Seas, Coasts and Estuaries, New Zealand) is an online data repository, GIS-access and imaging portal, and time-series analysis tools (Gall et al., 2022). The method used previously (Pinkerton et al., 2019) was extended in two ways: (1) by developing methods to extrapolate satellite measurements from offshore into the area within ~2 km to the coast (an important area that is particularly important but difficult to observe); and (2) by improving the merging semi-analytic and empirical methods in coastal and ocean regions respectively to ensure consistency between coastal and ocean products in the continental shelf transition zone.

Data ingestion, calibration and mapping: Level 1A (top of atmosphere, uncalibrated) MODIS-Aqua data were acquired either by file transfer from NASA (data between 2002–2007) as full spatial-resolution 5-minute granules, or as direct broadcast data by the NIWA X-band receiver (after 2007). All direct broadcast data were calibrated and processed using NASA Collection 6 calibration files using NASA’s SeaDAS v7.2 (<https://seadas.gsfc.nasa.gov/>). Data were rejected for land, cloud cover, solar glint, white-cap reflection, atmospheric correction failure or in-water algorithm failure. Satellite products based on visible-band measurements were calculated at a spatial resolution of 500 x 500 m using paired bands (after Franz et al. 2006) and derived variables were projected to a New Zealand Transverse Mercator grid (NZTM2000; LINZ, 2017).

Atmospheric correction: The normal atmospheric correction process for ocean colour data (“dark pixel method”) does not apply to turbid waters but alternatives have been developed (Ruddick et al., 2000; Lavender et al., 2005; Wang & Shi, 2007). Pinkerton et al. (2019) investigated two atmospheric correction methods appropriate for turbid coastal New Zealand waters: (1) the NIR-short-wave infrared radiation (SWIR) switching algorithm (Wang & Shi, 2007); and (2) the MUMM model with the default MUMM alpha for MODIS of 1.945 (Ruddick et al., 2000). In a comparison in European coastal waters, it was found that the NIR-SWIR and MUMM methods performed similarly, but that “the MUMM algorithm gives a better quality product” (Ody et al., 2016) so the MUMM product was used in Pinkerton et al. (2019) and here.

In-water algorithms: Simple empirical methods (e.g., O’Reilly et al. 1998) can robustly estimate chl-a in ocean waters but typically perform poorly coastally (IOCGG 2000; Pinkerton et al. 2006). Two main types of semi-analytical in-water algorithms were tested in Pinkerton et al. (2019): (1) the Quasi-Analytical Algorithm (QAA) algorithm (Lee et al. 2002; Lee et al. 2009); and (2) the Garver-Siegel-Maritorena (GSM) algorithm (Garver & Siegel 1997; updated processing¹¹). Following Pinkerton et al. (2019) and Gall et al. (2022) we used the QAA approach here. Phytoplankton absorption was converted to an estimate of chl-a using the chl-specific absorption coefficient, $a_{ph}^*(488)$. The value of $a_{ph}^*(488)$ can vary seasonally and spatially, related to different phytoplankton species (varying cell physiology and pigments), different phytoplankton cell sizes, and the light environment (phytoplankton in more turbid waters may increase light harvesting pigments) (Kirk, 2011). Here, we used an average of values found for oceanic phytoplankton (Bricaud et al. 1995; Bissett et al. 1997),

¹⁰ <https://gis.niwa.co.nz/portal/apps/experiencebuilder/template/?id=9794f29cd417493894df99d422c30ec2>

¹¹ www.icess.ucsb.edu/OCisD/

and measurements in the lower reaches of New Zealand rivers and estuaries (Pinkerton, 2017; Pinkerton et al., 2019; Gall et al., 2022). The latter measurements were made as part of the National River Water Quality Network (NRWQN) project (Gall et al., 2022). MODIS data were interpolated to 500 m using paired bands where necessary (Franz et al. 2006).

Coastal extrapolation: Ocean colour satellite products are often missing for the 1-2 km closest to shore which is a problem for those particularly interested in this zone, including recreational users and coastal managers. The causes of this missing information include atmospheric correction issues due to near infra-red radiance from the land, shallow water (leading to algorithm fail), and pixel geolocation errors (where a coastal pixel is mis-located further offshore by up to ~1 km). In a development since Pinkerton et al., (2019), a method to extrapolate valid coastal data into the nearshore zone has been developed at NIWA and applied to the data used in the analysis presented here. First pixels erroneously located over the land are removed. Next, the data are “despeckled”, that is, individual pixels very different from those surrounding them are removed. Two methods are then used to estimate missing values within 5 km of the coast: (1) iterative nearest-neighbour smoothing with a 2.5 km smoothing window applied 3 times; (2) LOESS-extrapolation (LOcally WEighted Scatter-plot Smoother; Cleveland & Devlin, 1988) where the fitted variation in the property with distance offshore in 10 km-wide transects is used to estimate missing values. The smoothed and interpolated estimates were blended using weights based on their similarity to each other and to the surrounding data. The parameters used in this in-shore extrapolation scheme were optimised to maximise the proportion of missing data filled-in and the plausibility of the values. The method works well when spatial patterns and processes further offshore are representative of the very nearshore zone (<2 km from the coast), but it cannot provide information on small-scale processes that have no offshore expression. Given that coastal features are of the order of >10 km (Pinkerton et al., 2022), this limitation is not critical, but does highlight the need for using satellite products with a higher spatial resolution in the future to observe these very nearshore environments.

Onshore-offshore blending: It is important that there is not a discontinuity between the coastal chl-a data (processed using a semi-analytical method because of optical complexity) and ocean chl-a (processed using an empirical algorithm). Extending Pinkerton et al. (2019), two levels of blending were used to ensure that the ocean and coastal datasets were consistent across the inshore-offshore transition zone over the New Zealand continental shelf. First, in each daily image, we blended the QAA-chl-a and the MODIS-default chl-a product (NASA, 2018b) using a logistic-scaling of $b_{bp}(555)$ (Pinkerton et al., 2022; Gall et al., 2022). This is implemented in SCENZ data version v3.0 as currently active in NIWA-SCENZ. However, we found that this blending still led to issues in the transition zone where high backscatter offshore was caused by phytoplankton blooms, for example in areas off Horomaka Banks Peninsula in the western part of the Chatham Rise high productivity region. A second blending at the monthly level was hence developed and implemented for this work, leading to CHL product v4.0. The SCENZ product ADET v3.0 (Gall et al., 2022) was used in the blending as an index of “coastal influence”. ADET measures the amount of light absorption in the blue part of the spectrum (wavelength 443 nm) by detrital material, and can be a useful indicator of freshwater input into the coastal zone. Monthly climatological data on $\log(\text{ADET})$ in overlapping coastal sectors of width 21 km and extending between the coast and 50 km offshore were extracted around the New Zealand North and South Islands, and Stewart Island. The sectors overlapped by 14 km in the direction parallel to the coastline. The change in $\log(\text{ADET})$ with distance offshore from pure coastal (less than 3 km from the coast) to pure oceanic (more than 30 km from the coast) in each sector was used as a proxy for the degree of coastal influence on bio-optical properties. Although terrestrially-sourced suspended sediment in the upper water column can extend further than 30 km offshore,

coastal influence here is considered to be relatively short-lived and relatively uncommon at the national scale. The average estimate of “coastal influence” for each location was then used to weight estimates of coastal and ocean chl-a to produce the SCENZ CHL v4.0 product.

2.1.6 Coastal scale total suspended solids

The primary source of information on coastal TSS was the SCENZ v3.0 TSS product (Pinkerton et al., 2022; Gall et al., 2022). TSS was estimated from the total particulate backscatter product (BBP) which estimates the optical backscattering from all particulate material present in the near-surface water column. Technically, BBP is defined as the particulate backscatter coefficient at 555 nm (m^{-1}). In the SCENZ methodology, BBP v3.0 was estimated using the quasi-analytic algorithm (QAA v5; Lee et al. 2002; Lee et al. 2009) and converted to an estimate of gravimetric total suspended solids using an average mass-specific backscatter factor for the New Zealand coastal zone as described in detail by Pinkerton et al. (2022) and Gall et al. (2022). Suspended particulate material includes phytoplankton, particulate detritus and inorganic sediment and these different components have different optical characteristics and different mass concentrations, so that the conversion from BBP to a gravimetric quantity (TSS) is approximate.

In addition, the new Copernicus (CMEMS) SPM (suspended particulate matter) product was used for comparison (Table 2-1): “cmems_obs-oc_glo_bgc-transp_my_l4-multi-4km_P1M/SPM” (hereafter called SPMM). This is a monthly, 4 km-resolution gravimetric ($g\ m^{-3}$) product that uses coastal (semi-analytical) processing with a “global average” conversion of backscatter to gravimetric particulate matter concentration (Garnesson et al., 2019).

2.2 Anomalies

2.2.1 Annual anomalies

Annual anomalies were calculated as the mean value for a given year minus the long-term mean of a whole-number of years (Equation 1). For example, the 2000 chl-a anomaly is the mean value of chl-a for 2000 at a given pixel minus the long-term mean chl-a value for the same pixel. The mean is calculated on whole years to avoid bias due to different number of values in different seasons. In Equation 1, δ_Y is the annual anomaly for year Y, N_y is the total number of years of data, N_m is the total number of months of data per year, and $C_{y,m}$ is the chl-a or SST value for year y and month m.

$$\delta_Y = \frac{1}{N_m} \sum_m C_{Y,m} - \frac{1}{N_y N_m} \sum_y \sum_m C_{y,m} \quad \text{[Equation 1]}$$

2.2.2 Monthly anomalies (deseasonalisation)

Monthly anomalies were calculated as the average value for each month minus the long-term monthly mean (Equation 2). Here, $\delta_{y,m}$ is the anomaly for year y, month m; N_y is the total number of years of data, and $S_{y,m}$ is the satellite measure for year y and month m. For example, the monthly anomaly for January 2000 was calculated as the mean of January 2000 minus the long-term mean of all Januaries. Note that this implies a reference period against which anomalies are judged as the whole time series.

$$\delta_{y,m} = S_{y,m} - \frac{1}{N_y} \sum_y S_{y,m} \quad \text{[Equation 2]}$$

2.2.3 Reference period

The reference period for analysis is the time period over which the “climatological” monthly averages are calculated. The choice of appropriate reference periods for time-series analysis is important because it affects the anomalies from which trends are calculated but the choice is somewhat subjective, especially when there are multiple products spanning different time periods. In this work, we used a primary ocean reference period matching the SeaWiFS-MODIS time-series (i.e., the complete years 1998-2022). This reference period was also used for the OISSTv2.1 data. For the coastal chl-a and TSS data, we used a reference period matching the period of operation of the MODIS-Aqua sensor (i.e., complete years 2003-2022). The MHW analysis requires a different reference period, and the 30 y period 1983-2012 was chosen (see Section 2.6). Further research (beyond the present study) to consider defining appropriate reference periods for New Zealand indicator work would be useful.

2.3 Descriptive regions

2.3.1 Ocean scale

Monthly anomalies of chl-a and SST were extracted for the EEZ and four descriptive oceanic regions (Figure 2-1; Appendix A) which have not changed from previous environmental reporting (e.g., Pinkerton et al., 2019). These regions were chosen to include particularly productive regions and be characteristic of water masses (following Murphy et al., 2001), while noting that they do not cover (and do not need to cover) all locations in the EEZ. The four regions are: the Chatham Rise (Subtropical Front east of New Zealand); the Tasman Sea (including the Subtropical Front west of New Zealand); Subtropical Water (STW); and Subantarctic Water (SAW). All oceanic descriptive regions, including the EEZ region, exclude chl-a data in New Zealand territorial waters (within 12 nautical miles of the coast).

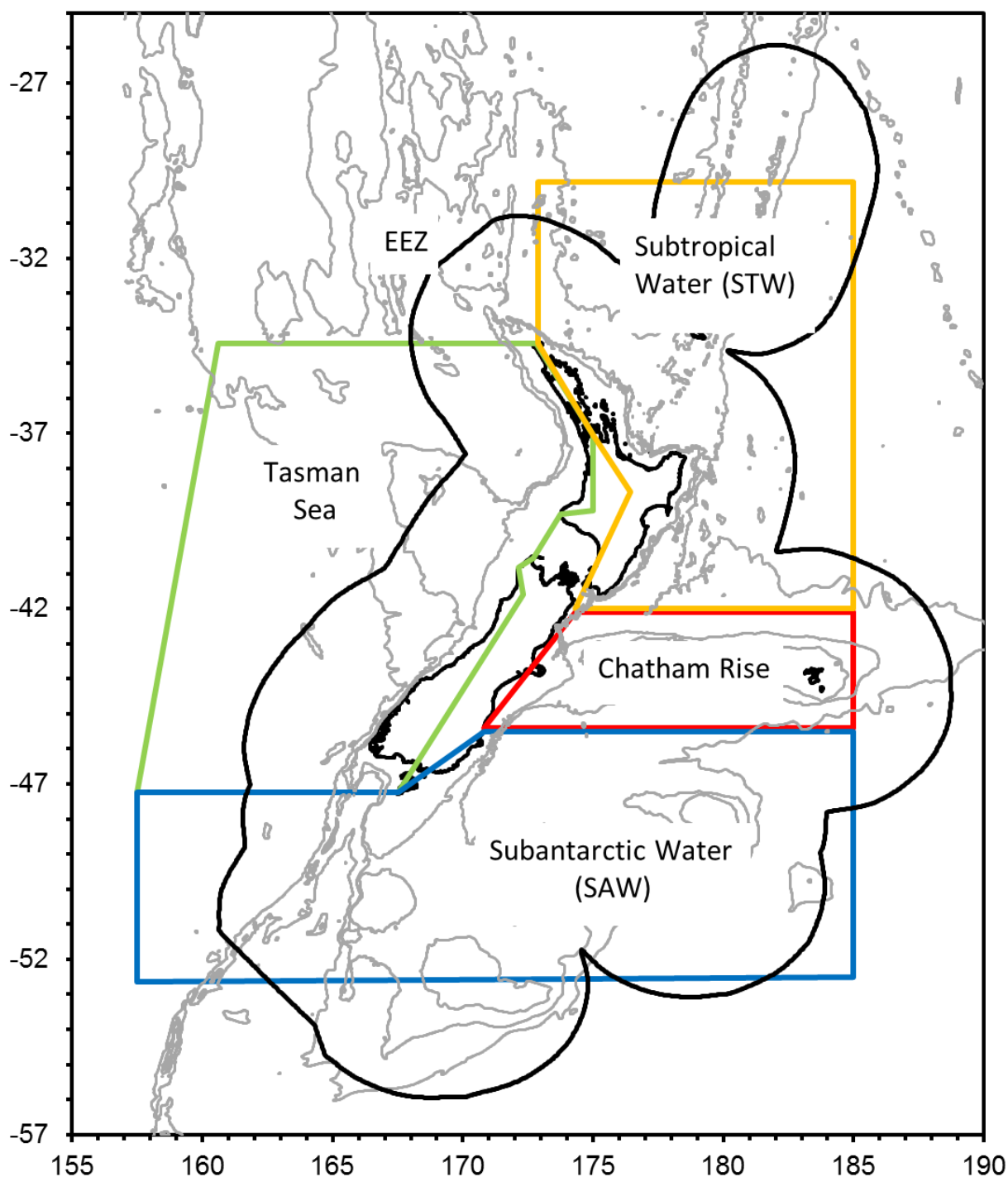


Figure 2-1: Ocean scale descriptive regions for which summary data were extracted. Depth contours are shown in grey at 500 m, 1000 m and 3000 m depths. Measurements in territorial waters (less than 12 nautical miles from the coast) were excluded from coastal analysis.

2.3.2 Coastal scale

Information on trends in chl-a and SST in coastal regions were summarised based on the New Zealand coastal bioregion analysis (Department of Conservation and Ministry of Fisheries, 2011) and extended to the territorial limit of 12 nautical miles offshore (Figure 2-2). This selection of coastal regions was considered more biologically-meaningful than dividing by Regional Council boundaries as was carried out in previously (Pinkerton et al., 2019) because Regional Council boundaries do not

necessarily align with oceanographic or biogeochemical differences round the coast. Only the 9 coastal regions around North and South Island were considered, not including Three Kings Islands, Chatham Islands, Snares Islands, because these are of comparable sizes and lie completely within the SCENZ domain.



Figure 2-2: Coastal scale descriptive regions. Summary analyses were only carried out for the 9 coastal regions around North and South Island, not including Three Kings Islands, Chatham Islands, Snares Islands. Boundaries are based on New Zealand coastal regions analysis (Department of Conservation and Ministry of Fisheries, 2011) and extend out to 12 nautical miles from the coast.

2.4 Trend analysis

Satellite data were deasonalised using monthly anomalies (Section 2.2.2) to remove the effect of seasonal cycles on the estimates of long-term change (trends). We compared an alternative method of deasonalising the data using a spline smooth by month, and the results were almost identical (data not shown). Temporal trends for each pixel were then determined by applying the Sen slope (Sen, 1968) method to these monthly anomalies. Statistical significance was assessed using Mann-Kendall Z statistic and p-values (Mann, 1945; Kendall, 1975). The null hypothesis in the Mann-Kendall test assumes that the data are independent and randomly ordered (Mann, 1945; Kendall, 1975). The existence of positive autocorrelation in the data increases the probability of detecting trends when none actually exists, and vice versa (Hamed & Rao, 1997). A number of correction methods for autocorrelation in the Mann-Kendall test exist and we used the method of Yue & Wang (2004). This correction method reduces the effective number of degrees of freedom if positive autocorrelation occurs and hence tends to reduce the risk of type 1 errors (false positives) but increases the risk of type 2 error (false negatives). The Sen slope and Mann-Kendall test are preferred over linear regression analysis because the method is non-parametric (distribution free) and does not require an

assumption that the data are normally distributed. In particular, the insensitivity of the Sen slope to outliers means that it is generally the preferred non-parametric method for estimating a linear trend (Hipel & McLeod, 1994).

We followed the trend direction assessment procedures and guidelines of McBride (McBride, 2005, 2019; McBride et al., 2014) to summarise trends into eight trend “likelihood” categories representing the confidence that the assessment of the slope is in the correct direction (i.e., positive or negative) rather than the confidence that the slope is different from zero (Table 2-2). Given that time-series of satellite observations are relatively short (at most ~40 years) and variability in such natural systems high, this is a more useful way of assessing the significance of a trend than whether the Mann-Kendall p-value is less than 0.05. In fact, Makowski et al. (2019) showed that Mann-Kendall p-values statistics in most cases have a direct correspondence with these likelihood categories proposed by McBride et al. (2014).

For chl-a and TSS, trends are given as an absolute magnitude and also expressed as a percentage of median values per decade to standardise change across measures of interest (Larned et al., 2016); both these metrics are informative. This normalisation to the median is not calculated for SST because the offset of the temperature scale used (° Celsius) is arbitrary and instead trend slopes for SST are only presented as an absolute magnitude of change per decade.

As outlined in McBride (2019), for freshwater quality assessment, the ecological or management significance of a trend (i.e., whether the trend is large enough relative to variability to be considered “important”) requires expert knowledge of the system. As there is a lack of accepted levels of importance thresholds for New Zealand waters (Dudley et al., 2017), we do not attempt to assess the ecological or management importance of trends.

Table 2-2: Trend “likelihood” categories determined from posterior probability distributions of slope direction. Mann-Kendall p-value statistics are also given which have, in this case, a direct correspondence with “frequentist” p-values (Makowski et al. 2019).

Mann-Kendal <i>p</i> -value	Probability of non-zero slope	McBride likelihood
0 – 0.01	0.995 – 1	Virtually certain
0.01 – 0.05	0.975 – 0.995	Very likely
0.05 – 0.10	0.950 – 0.975	Likely
0.1 – 0.33	0.835 – 0.950	Possible
0.33 – 0.66	0.665 – 0.835	About as likely as not
0.66 – 0.90	0.550 – 0.665	Unlikely
0.90 – 0.99	0.525 – 0.550	Very unlikely
0.99 – 1	0.5 – 0.525	Exceptionally unlikely

2.5 Correlation analysis

Correlation analysis can be used to understand the underlying drivers of oceanographic changes (Feng & Zhu, 2012; Kumar et al., 2016). For the ocean domain, the linear Pearson correlation coefficient between monthly anomalies in chl-a and SST were determined for each pixel separately, using the full overlap period. This correlation analysis investigates to what extent changes in chl-a

may be related to changes in ocean surface temperature. For the coastal region, correlations were carried out on a pixel-by-pixel basis between chl-a and SST, and between chl-a and TSS.

It is possible to carry out other correlate analyses, for example between MHW and chl-a anomalies, or between climate indices (such as ENSO) and SST, chl-a or TSS anomalies, but these are beyond the scope of the present study.

2.6 Marine heatwaves

A marine heatwave (MHW) is defined to occur when seawater temperature exceeds a seasonally-varying threshold (usually the 90th percentile temperature) for at least 5 consecutive days (Hobday et al., 2016). In this study, MHW metrics were calculated from the Daily Optimum Interpolation SST data (OISST, v2.1, Huang et al., 2021) between 1st January 1982 to 31st December 2022, with a fixed 30-year climatology (1 January 1983 to 31 December 2012; Hobday et al., 2016). Our analysis used the ‘heatwaveR’ R package version 0.4.6 (Schlegel & Smit, 2018). Five key MHW metrics were generated at each pixel (Thoral et al., 2022; Montie et al., 2023): (1) the number of MHW events, (2) the number of MHW days (time from start to end MHW dates, in days), (3) the mean and (4) max intensity (anomalies in relation to the climatological mean, in °C), and (5) the cumulative intensity (integrated intensity over events, in °C days). The spatially-resolved metrics were then combined per descriptive regions (EEZ, oceanic and coastal). In addition, a trend analysis (Mann-Kendall and Theil-Sen slope) was performed to determine significant changes in MHW metrics. As there was evidence of autocorrelation in some metrics time series, a modified Mann-Kendall (variance correction approach) was performed to account for autocorrelation using the ‘modifiedmk’ R package version 1.6 (Patakamuri et al., 2020). The Theil-Sen slope estimator was calculated on MHW metrics time series to determine the intensity and direction of change. Decadal trends were estimated by multiplying the Sen’s slope (yearly) by 10. For sake of clarity in the main report, we decided to focus and describe trends in the cumulative intensity metric as this measure contains information of both MHW duration and intensity (Schlegel et al., 2017). Other metrics can help capture the spatial and temporal variability of MHWs (Thoral et al., 2022), and other four metrics are given in Appendix F and Appendix G.

2.7 Trophic classes

“Trophic classes” are useful to broadly rate the biological productivity of a water body and are generally based on chl-a. For New Zealand lakes, regional councils historically have used a seven-class trophic level index (TLI) initially proposed by Burns et al. (2000), which has evolved into the trophic state (ecosystem health) system in the National Policy Statement for freshwater management (Freshwater NPS; MfE 2018). A 4-attribute state eutrophication system was used in the New Zealand Estuary Trophic Index (ETI - Robertson et al. 2016) and adapted by Plew et al. (2020) for four salinity estuary types. In this report, we suggest extending the euhaline type estuaries (>30 ppt salinity) chl-a ranges from Plew et al. (2020) to include oligotrophic, microtrophic and ultra-microtrophic classes for chl-a < 1 mg m⁻³, as guided by Morel et al. (1996) as these can be associated with oceanic waters surrounding New Zealand (Table 2-3). Nixon (1995) provided useful guidance on coastal marine eutrophication primary productivity ranges for oligotrophic (< 100 gC m⁻² day⁻¹), mesotrophic (100-300 gC m⁻² day⁻¹), eutrophic (301-500 gC m⁻² day⁻¹) and hypertrophic (>500 gC m⁻² day⁻¹) systems that can be broadly associated with the proposed trophic classes. Another useful guide is given in a worldwide compilation of 131 estuarine-coastal ecosystems (Cloern et al., 2014).

Table 2-3: Trophic classes. Proposed chlorophyll *a* concentration (chl-*a*, mg m⁻³) ranges for descriptive trophic classes used in New Zealand estuaries and oceans. Note: Microtrophic and Ultra-Microtrophic are not commonly present in the coasts and oceans around New Zealand.

Trophic class	Level	Lakes		Estuaries and ocean	
		Min (mg m ⁻³)	Max (mg m ⁻³)	Min (mg m ⁻³)	Max (mg m ⁻³)
Ultra-Micro	1	0.13	0.33	0.01	0.05
Microtrophic	2	0.33	0.82	0.05	0.10
Oligotrophic	3	0.82	2	0.1	1
Mesotrophic	4	2	5	1	3
Eutrophic	5	5	12	3	8
Supertrophic	6	12	31	8	12
Hypertrophic	7	31	~100	12	~50

Freshwater and Estuarine NPS states: A (Minimal); B (Moderate); C (High); D (Very High).

3 Results

3.1 Ocean scale analyses

3.1.1 Data coverage

The spatial distribution of data for the analyses (Figure 3-1 a and b) shows the greater number of observations of SST compared to chl-*a* for the New Zealand region: 500 points compared to a maximum of 310 points respectively (note the scale difference). The figure also shows the effect of systematically excluding data where the sun angle was low for ocean colour (chl-*a*) data, seen in the reduction in the number of observations available for analysis in the SeaWiFS-MODIS timeseries at greater latitudes (yellow to blue). The CMEMS products use a less strict requirement for sun-angle and more satellite sensors, has much better coverage south of the Chatham Rise in winter (Figure 3-1 c). The CMEMS gap-free product (Figure 3-1 d) has slightly better coverage than the CMEMS standard chl-*a* product, and although the gain appears small and confined to the extreme south of the EEZ on month averages, its calculation from gap-free daily maps is expected to provide more accurate statistics and analytical products (Sathyendranath, 2019; Liu, 2022).

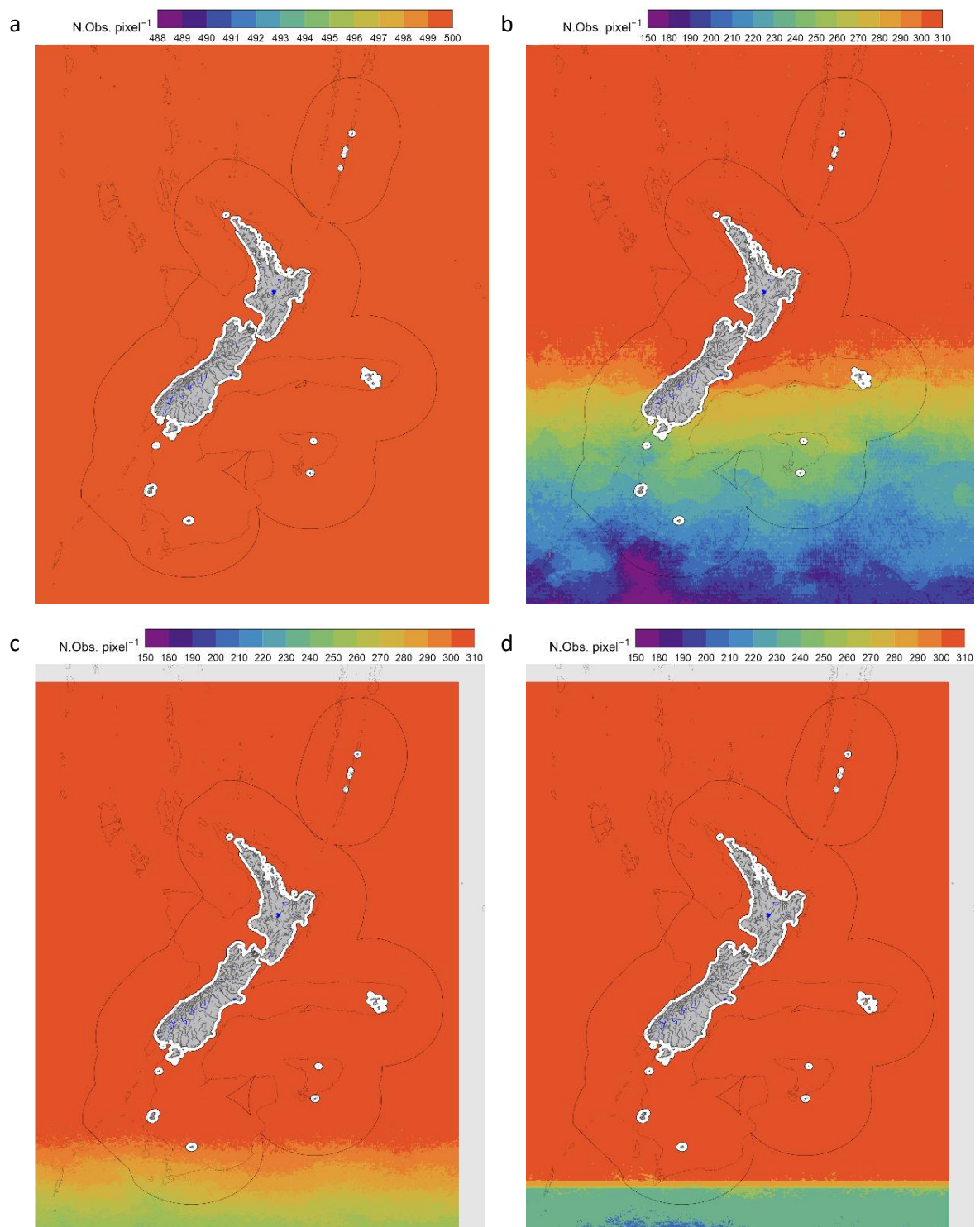


Figure 3-1: Number of observations (N. Obs) used in the ocean scale analysis: a: SST (1981–2023) from OISST v2.1; b: Chl-a (1997–2023) from primary dataset (MODISA+SW-NIWA; see Table 2-1); c: CHLM (1997–2023) from the secondary dataset (CMEMS MO-CHL); and d: CHLGF (1997–2023) from the tertiary dataset (CMEMS gap-free). The boundary of the New Zealand EEZ is also shown as are the 200 and 500 m depth contours. Note the different scale for SST in (a).

3.1.2 Mean spatial patterns

The long-term average, or spatial climatology, in SST (1981–2023) and chl-a (1997–2023) for the New Zealand oceanic region provides a useful overview of sea surface conditions and surface water masses, across fronts and continental shelves (Figure 3-2). Annual average SST varies with latitude principally, from about 25°C in northern Subtropical Water to ~7°C in southern Subantarctic Water (Figure 3-2 a). Variation in water temperature around the coast is also primarily related to latitude modified by water currents, with colder water masses to the south (Subantarctic) and warmer water masses to the north (Subtropical). The Southland Current pushes cold water eastwards round the bottom of South Island and then northwards past Ōtepoti Dunedin before being entrained eastwards by Chatham Rise. The East Auckland Current moves warm water down the upper east coast of North Island and brings warmer water to the Bay of Plenty.

In terms of the proposed ocean trophic classes (Table 2-3), most of the New Zealand ocean domain is oligotrophic (chl-a between 0.1 and 1 mg m⁻³), with microtrophic conditions (chl-a 0.05 - 0.1 mg m⁻³) in the extreme subtropical part of the EEZ (Figure 3-2 b-d). New Zealand Subtropical and Subantarctic waters are generally classified as oligotrophic with low chl-a concentrations. Higher oceanic chl-a is associated with the Subtropical front, which extends across the New Zealand domain at about 45°S, especially over Chatham Rise, and is typically classified as mesotrophic. Only around the coast are mesotrophic conditions (chl-a 1-3 mg m⁻³) present on an annual average scale.

Patterns in mean chl-a are very similar between the SeaWiFS-MODIS product (Figure 3-2 b) and the two CMEMS products (Figure 3-2 c-d). The difference in chl-a between the two CMEMS products is very small but there is an offset in chl-a of about 0.05 mg m⁻³ to the SeaWiFS-MODIS product, the latter being consistently higher (see Appendix D).

The mean annual SST and chl-a values for each year based on the merged SeaWiFS-MODIS product (Appendix B), and their anomalies (Appendix C), provide information on interannual variability. The annual plots display relatively low year-to-year variability in SST (about ±1°C between years) compared to year-to-year variability in chl-a of about ±25% between years.

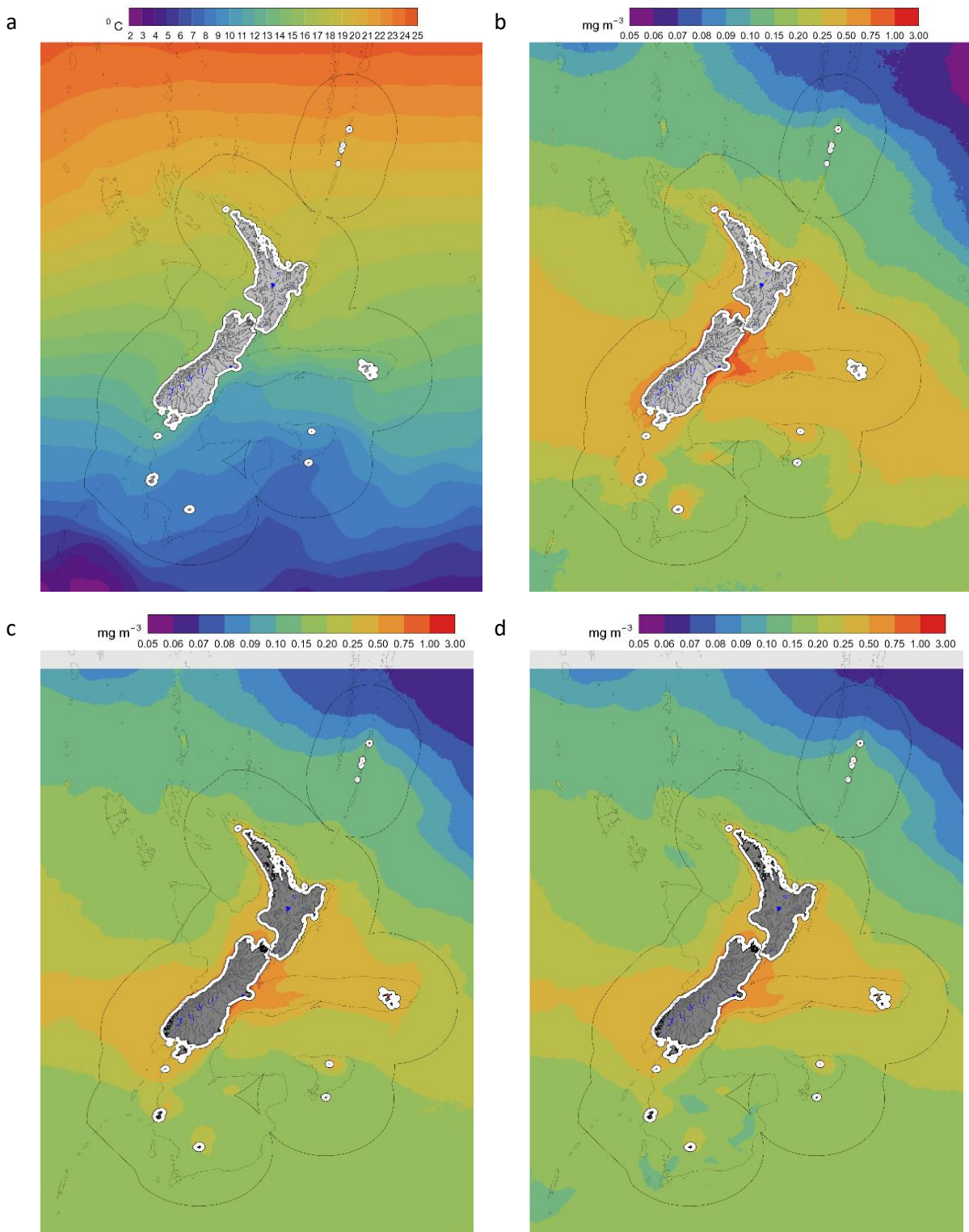


Figure 3-2: Ocean scale long-term averages in environmental indicators a: Sea-surface temperature (1981–2023) from OISST v2.1; b: Chl-a (1997–2023) from primary dataset (MODISA+SW-NIWA; see Table 2-1); c: CHLM (1997–2023) from the secondary dataset (CMEMS MO-CHL); and d: CHLGF (1997–2023) from the tertiary dataset (CMEMS gapfree). The boundary of the New Zealand EEZ is also shown as are the 200 and 500 m depth contours. Territorial waters (to 12 nautical miles offshore) are excluded from analysis.

3.1.3 Trends in sea surface temperature

Most of the oceans around New Zealand have warmed significantly between 1981 and 2023, as illustrated in their long-term positive trends (Figure 3-3 a), with “Virtually certain” trend likelihoods (Figure 3-3 b). Warming rates were highest in the Subtropical region and the Tasman Sea and lowest in Subantarctic Water. For the EEZ as a whole, the 40-y area-weighted mean rate of surface warming was 0.20°C per decade between 1981 and 2023 (Table 3-1), up from 0.15°C per decade between 1981 and 2018 (Pinkerton et al., 2019). Trends in SST in all descriptive regions were all positive, “virtually certain” and except for Subantarctic, were higher than the global average warming rate (Table 3-1). The 40-y global mean warming rate was 0.15°C per decade, with a global 25th–75th range of 0.09–0.23 °C per decade. In comparison, the EEZ 40-y warming rate was 32% higher than the mean global average warming rate, equivalent to the 65th percentile of global warming trend rates. The fastest warming New Zealand region was the Subtropical region (55% higher than the global average) followed by the Tasman region (53% higher than the global average). The 40-y warming rate of the Subantarctic region was 6% lower than the global average.

Warming is accelerating: the warming rates in the EEZ and all oceanic regions increased in the 20-y analysis (between 2002 and 2023) compared to the 40-y analysis (Table 3-2). The 20-y warming rate for the EEZ was nearly twice the 40-y warming rate. In the New Zealand Subantarctic region, the rate of increase of SST over the last 20 years is more than 3 times the rate over the last 40 years. The New Zealand 20-y warming rates are also accelerating faster than the global average. The 20-y warming rate in the Chatham region was found to be more than 3 times higher than the mean global rate of warming over the same period (Table 3-2).

The regional time-series plots (Figure 3-4) show that surface ocean warming in the New Zealand region has exhibited a non-linear pattern over the past four decades. Rather than a consistent upward trend, the data reveals the influence of multi-year climate variability, including phenomena like ENSO, overlaying the overall warming trend. For comparison, we show the mean global SST anomalies (Figure 3-4 a – red line), noting that the world’s oceans are highly heterogenous and include areas with very different trajectories of SST over time. In contrast to the relatively linear warming of global mean SST, the New Zealand EEZ has had periods of cooling (1985-1993; 2002-2010; 2018-2020) and rapid warming (1993-2002; 2010-2018; 2021-present). The smaller-scale climate variability that are apparent at the EEZ are “averaged out” when looking at the global scale. At the EEZ scale, the most recent rate of warming (since 2021) seems to be unprecedented in the satellite record (Figure 3-4 a). Similar patterns are evident in the regional time series where the underlying rate of warming seems to have increased in all regions from about 2009, and the warming since 2020 has been particularly rapid (Figure 3-4 b-e).

Spatial patterns in the seasonal (3-month average) warming rate of the surface ocean around New Zealand was highest in winter (especially to the north and east of the EEZ) and in autumn (especially in the Tasman Sea), and lowest in the summer (Figure 3-5). SST trends within each month were further used to examine seasonal changes in SST (Figure 3-6). At the EEZ scale, warming rates were highest between March and August (mid-autumn and late-winter), and the seasonal differences were quite modest (Figure 3-6 a). In the oceanic regions (Figure 3-6 b-e), a fairly consistent picture emerges with highest surface warming rates occurring mainly in autumn/winter: Chatham (April-August); Tasman (February-May); Subtropical (February-August); and Subantarctic (April-July).

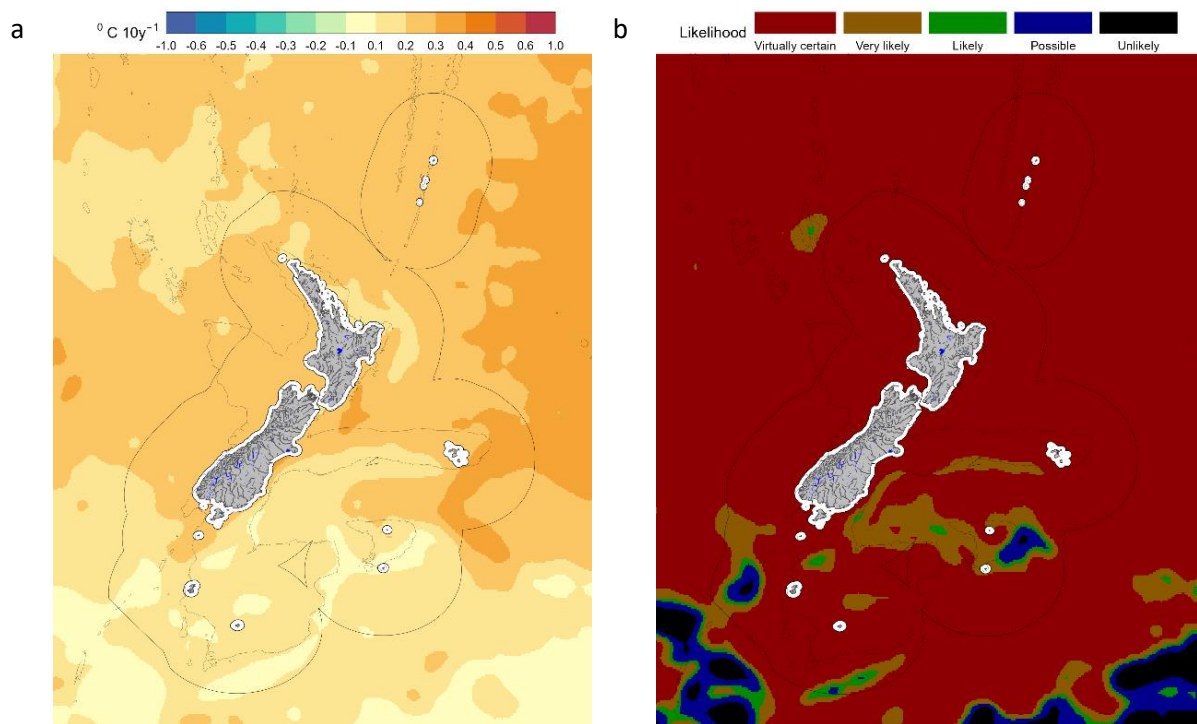


Figure 3-3: Ocean scale spatial trends in sea surface temperature (SST: 1981-2023): a: Sen-slope trends °C per decade based on OISSTv2.1 dataset, and **b:** Likelihood of non-zero trend based on Mann-Kendall analysis corrected for auto-correlation. Territorial waters (to 12 nautical miles offshore) are excluded from analysis.

Table 3-1: Ocean scale region trends in sea surface temperature over 40 years compared to global trends (1981-2023). The Mann Kendall test (using the Z statistic) was applied to SST monthly anomalies in the EEZ and descriptive regions based on the OISSTv2.1 product. Note: The “Sen slope/median” (typically calculated for other products) is not calculated for SST because the scale offset is non-zero. Mann-Kendall significance is shown: *** p<0.001; ** p<0.01; and * p<0.05.

Region	Mann-Kendall Z	Mann-Kendall p	Sen slope (°C decade ⁻¹)	Median (°C)	Mann-Kendall sig	McBride likelihood	Slope(40y) / global(40y)
EEZ	5.42	6.1E-08	0.20	14.0	***	Virtually certain	1.32
Chatham	4.78	1.8E-06	0.23	12.7	***	Virtually certain	1.46
Tasman	4.62	3.9E-06	0.24	15.5	***	Virtually certain	1.53
Subtropical	5.18	2.2E-07	0.24	18.1	***	Virtually certain	1.55
Subantarctic	3.21	1.3E-03	0.14	9.2	**	Virtually certain	0.94
Global	5.54	3.0E-08	0.15	18.2	***	Virtually certain	1

Table 3-2: Ocean scale region trends in sea surface temperature over 20-years compared to global trends (2002-2023). The Mann Kendall test (using the Z statistic) was applied to monthly anomalies in the EEZ and descriptive regions based on the OISSTv2.1 product. See also caption Table 3-1

Region	Mann-Kendall Z	Mann-Kendall p	Sen slope (°C decade ⁻¹)	Mann-Kendall sig	McBride likelihood	Slope(20y)/ global(20y)	Slope(20y)/ slope(40y)
EEZ	4.07	4.7E-05	0.41	***	Virtually certain	2.44	1.99
Chatham	3.94	8.2E-05	0.51	***	Virtually certain	3.04	2.25
Tasman	3.32	8.9E-04	0.44	***	Virtually certain	2.67	1.88
Subtropical	2.61	9.1E-03	0.29	**	Virtually certain	1.75	1.21
Subantarctic	4.26	2.1E-05	0.45	***	Virtually certain	2.72	3.14
Global	2.66	7.9E-03	0.17	**	Virtually certain	1	1.08

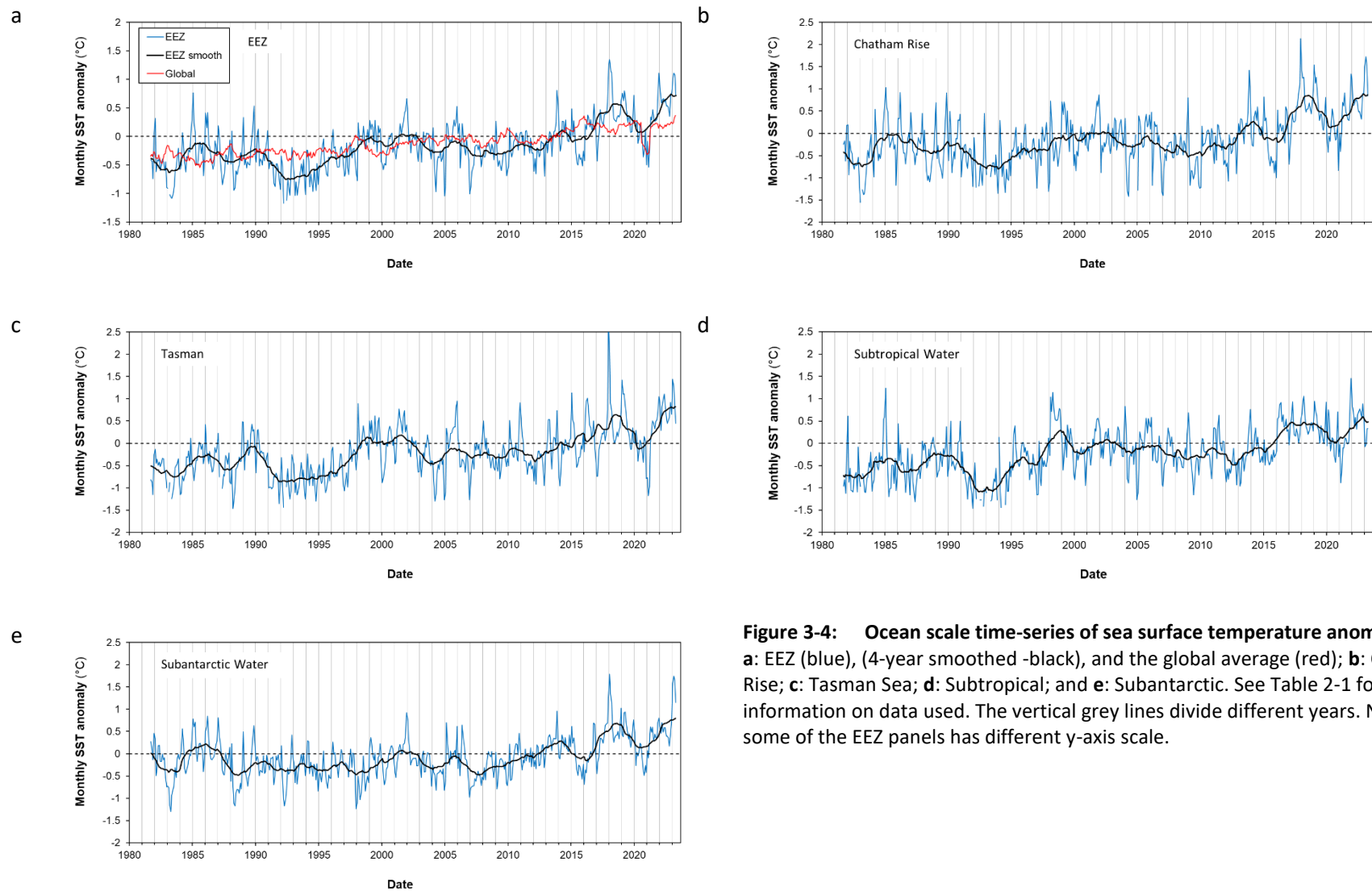


Figure 3-4: Ocean scale time-series of sea surface temperature anomalies: a: EEZ (blue), (4-year smoothed -black), and the global average (red); b: Chatham Rise; c: Tasman Sea; d: Subtropical; and e: Subantarctic. See Table 2-1 for more information on data used. The vertical grey lines divide different years. Note some of the EEZ panels has different y-axis scale.

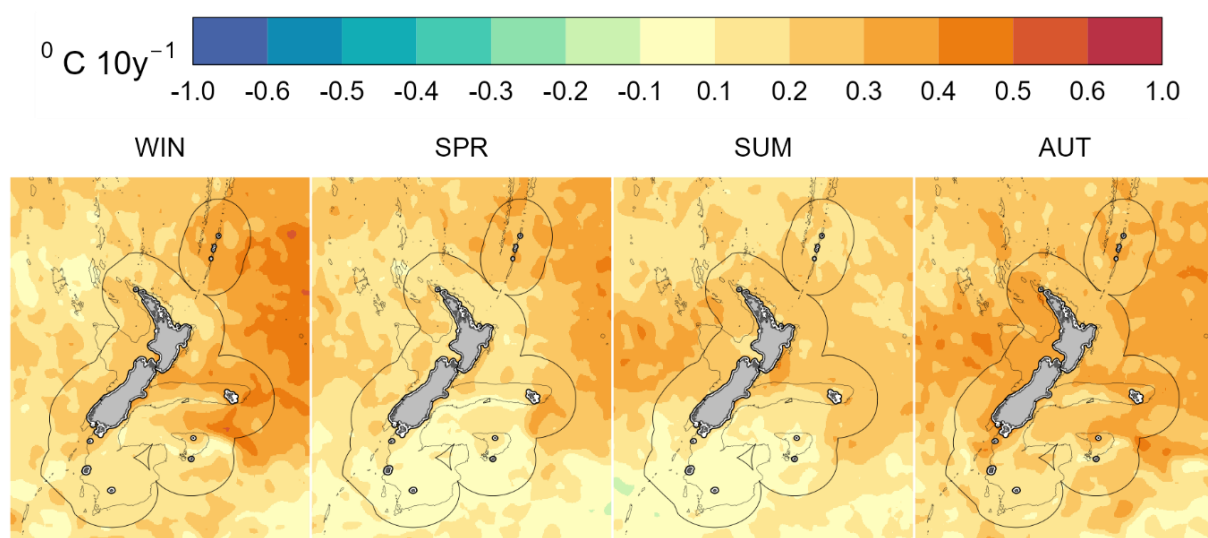


Figure 3-5: Seasonal trends in SST (1981-2023). Trends in SST (shown as $^{\circ}\text{C}$ per decade based on OISSTv2.1) are shown for each season separately (WIN=winter; SPR=spring; SUM=summer; AUT=autumn).

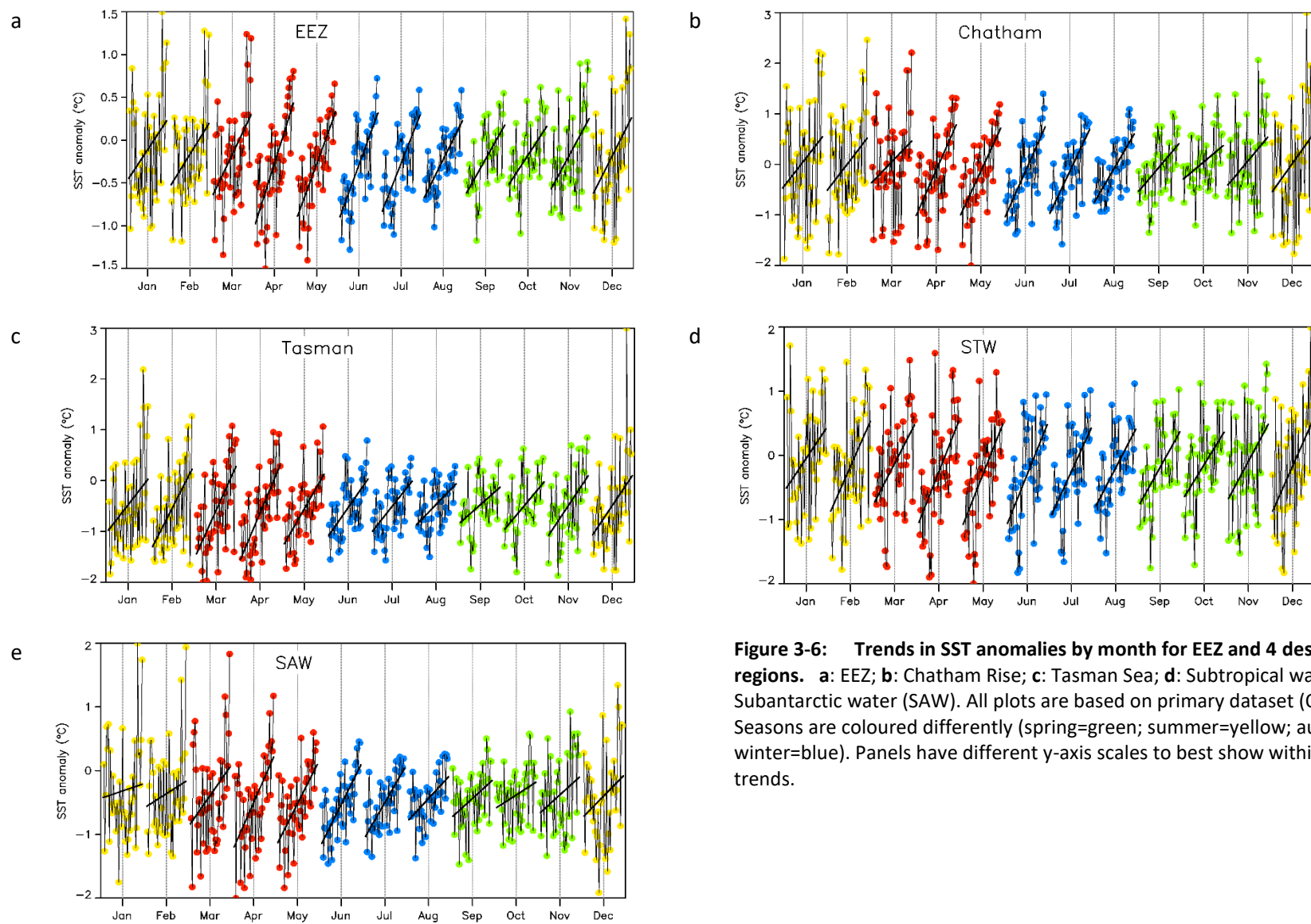


Figure 3-6: Trends in SST anomalies by month for EEZ and 4 descriptive regions. a: EEZ; b: Chatham Rise; c: Tasman Sea; d: Subtropical water (STW); e: Subantarctic water (SAW). All plots are based on primary dataset (OISST v2.1). Seasons are coloured differently (spring=green; summer=yellow; autumn=red; winter=blue). Panels have different y-axis scales to best show within-month trends.

3.1.4 Trends in chlorophyll a

Trends from the two CMEMS chl-a products were consistent with the NIWA blended chl-a product with similar results for trends within oceanic regions (Table 3-3), lending confidence to our interpretations based on the NIWA blended product alone. Significant positive trends in chl-a concentrations were observed in certain oceanic regions, notably in the Subtropical Front regions to the east (over the Chatham Rise) and west of New Zealand (Figure 3-7a). Additionally, notable positive trends were identified in Subantarctic waters located to the south. Conversely, substantial negative trends in chl-a concentrations are evident in the Subtropical Water located east of New Zealand, specifically northeast of Rēkohu/Wharekauri the Chatham Islands and in the regions encompassing Te Tai Tokerau Northland across the eastern coastline over the continental shelf and to the west. These negative trends extend to include the continental slope offshore of the Hauraki Gulf, eastern Te Tara-O-Te-Ika-A-Māui Coromandel and Te Moana a Toi Bay of Plenty, as well as progressing down the western coast of the North Island, reaching the northern parts of the South Island, and continuing halfway down the western coast of the South Island. Trends in chl-a over much of these areas was assessed as “virtually certain” (Figure 3-7 b, red).

At the scale of the EEZ a positive trend in chl-a was “about as likely as not” between 1997 and 2023 at +1.1% of the median per decade (Table 3-3). The CMEMS products gave consistent but slightly lower trends for the EEZ (0.6 – 1.2 % per decade) and similarly low confidence (“about as likely as not” and “unlikely”). Decreasing trends in chl-a were “possible” in Subtropical Waters (-2.2% per decade), and positive trends were “virtually certain” in Subantarctic waters (+6.7% per decade). A positive trend was “possible” in the Chatham Rise region and +2.2% per decade, while “very unlikely” in the Tasman region (-0.2% per decade).

Despite the offset in the absolute estimates of chl-a between the SeaWiFS-MODIS product (Figure 3-2 b) and the two CMEMS products (Figure 3-2 c-d), the anomalies are very consistent (Figure 3-8) – the thin black line (SeaWiFS-MODIS) is virtually indistinguishable from the blue and red lines (CMEMS). Regional chl-a time-series display non-linear patterns and long-term (multi-year to decade) climate variability (Figure 3-8). In the Chatham Rise, Tasman Sea and Subtropical regions (Figure 3-8 b-d), chl-a appears to have had four phases: (1) increases from 1997 to a peak in 2010; (2) decreases from 2010 to a low in 2016; (3) another increase to a peak in 2020; and (4) a general decrease over the past few years to 2023. The changes in chl-a in the Subantarctic region (Figure 3-8 e) were generally lower than other regions, except for a rapid rise from 2018 to a peak in 2020, followed by a decline to 2023. There has been a notably decline in chl-a levels across all four oceanic regions during the period of 2020-2023. The rate of reduction in chl-a during this recent period appears exceptionally rapid and if it continues, would surpasses previous records captured by satellite observations.

There was spatial variation in chl-a trends within and between seasons (3-month, Figure 3-9) compared to overall (Figure 3-7). Largest decreases in chl-a generally occurred in spring and summer in southern Subtropical waters, while largest positive trends in chl-a are seen in Subantarctic waters in summer, with the southland current boundary in particular showing prominence (Figure 3-9). Trends in chl-a were generally smallest during winter.

At the finer monthly scale, timeseries at the EEZ scale (Figure 3-10 a), indicated positive trends in chl-a from March-August (early-autumn to late-winter) and generally no trends in most other months, except for a large positive trend during November. The seasonal pattern of chl-a in the Chatham rise region (Figure 3-10 b) was characterised by peaks in chl-a in late-spring (November) and late-summer

(February), and low chl-a during mid-winter (July). Increasing trends in chl-a occurred in all months from late-autumn (April) to late-spring (November), with no change or decreasing trends in the summer (Figure 3-10 b). In the Tasman Sea region (Figure 3-10 c), chl-a peaked in late-spring (November) and was lowest in late-summer (February) to early autumn (March). There were small increasing trends in chl-a in winter months, while there was either no change or small decreasing trends in all other months. In the Subtropical region (Figure 3-10 d), the seasonal pattern was similar in shape to the Tasman region, with a prominent early-mid spring bloom (September-October) and lower chl-a in late-summer (February). Decreasing trends in chl-a were found during spring and summer, progressing to no change in autumn, and small increases during some winter months. In the Subantarctic waters region (Figure 3-10 e), chl-a seasonal patterns were similar to those in the Chatham Rise region (Figure 3-10 b), with peaks in late spring (November) and early autumn (March). Note that there was no data for early winter (June) in the NIWA dataset for this region because of low sun angle. Chl-a trends were positive in this region in all months, with the greatest rates of change in late autumn (May) and late spring (November).

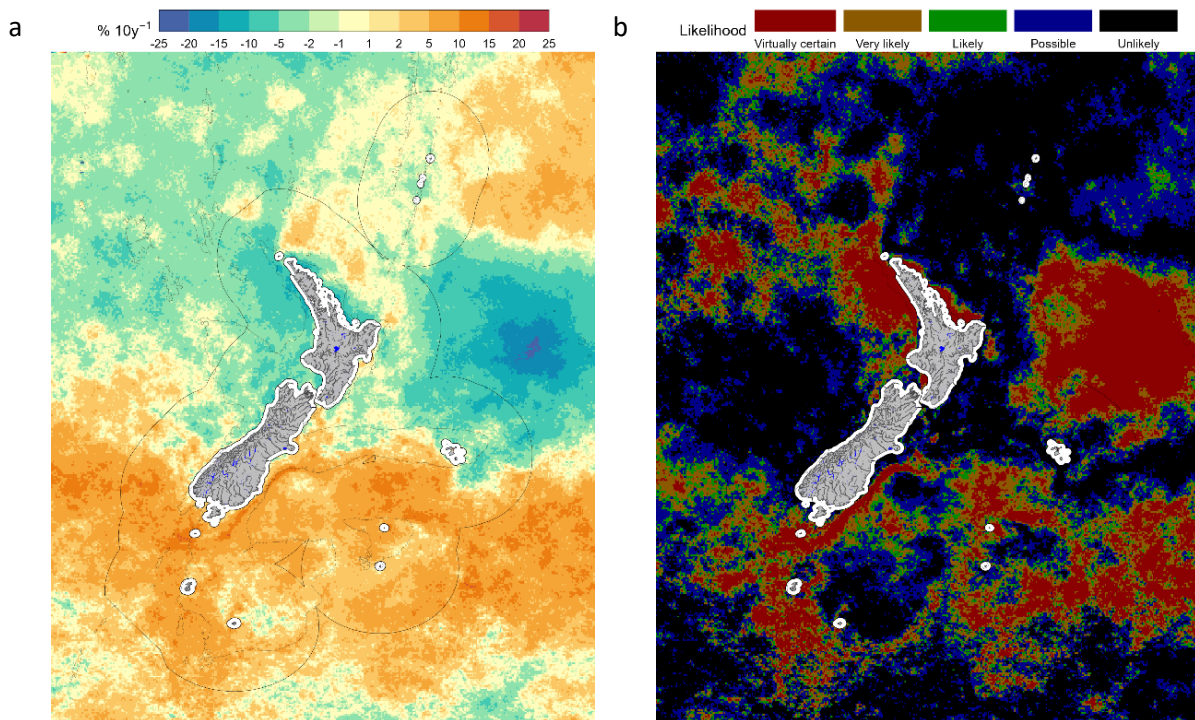


Figure 3-7: Ocean scale spatial trends in chlorophyll a (1997-2023): a: Sen-slope trends as a proportion of the median value (% per decade); and b: Likelihood of non-zero trend based on Mann-Kendall analysis corrected for auto-correlation. Data are from the merged SeaWiFS-MODIS-Aqua dataset.

Table 3-3: Ocean scale region trends in chlorophyll a from three different data sources (1997-2023). The Mann Kendall test (using the Z statistic) was applied to monthly anomalies in the EEZ and descriptive regions. See text for more details. Mann-Kendall significance (sig) is shown: *** $p < 0.001$; ** $p < 0.01$; * $p < 0.05$

Region	Mann-Kendall Z	Mann-Kendall p	Sen slope ($\text{mg m}^{-3} 10\text{y}^{-1}$)	Median chl-a (mg m^{-3})	Trend/median ($\% 10\text{y}^{-1}$)	Mann-Kendall sig	McBride likelihood
SeaWiFS-MODIS-Aqua (NIWA)							
EEZ	0.85	0.39	0.0024	0.21	1.1		About as likely as not
Chatham	1.12	0.26	0.0086	0.39	2.2		Possible
Tasman	-0.08	0.94	-0.0005	0.22	-0.2		Very unlikely
Subtropical	-1.23	0.22	-0.0034	0.16	-2.2		Possible
Subantarctic	3.59	0.00	0.0136	0.20	6.7	***	Virtually certain
CHLM (CMEMS)							
EEZ	0.41	0.68	0.0011	0.18	0.6		Unlikely
Chatham	0.76	0.45	0.0048	0.31	1.6		About as likely as not
Tasman	-0.01	0.99	-0.0001	0.18	0.0		Exceptionally unlikely
Subtropical	-0.75	0.45	-0.0019	0.14	-1.4		About as likely as not
Subantarctic	1.83	0.07	0.0048	0.17	2.9		Likely
CHLGF (CMEMS)							
EEZ	0.82	0.41	0.0020	0.17	1.2		About as likely as not
Chatham	1.08	0.28	0.0062	0.30	2.1		Possible
Tasman	0.16	0.87	0.0008	0.18	0.5		Unlikely
Subtropical	-0.57	0.57	-0.0013	0.14	-1.0		About as likely as not
Subantarctic	2.29	0.022	0.0057	0.16	3.5	*	Very likely

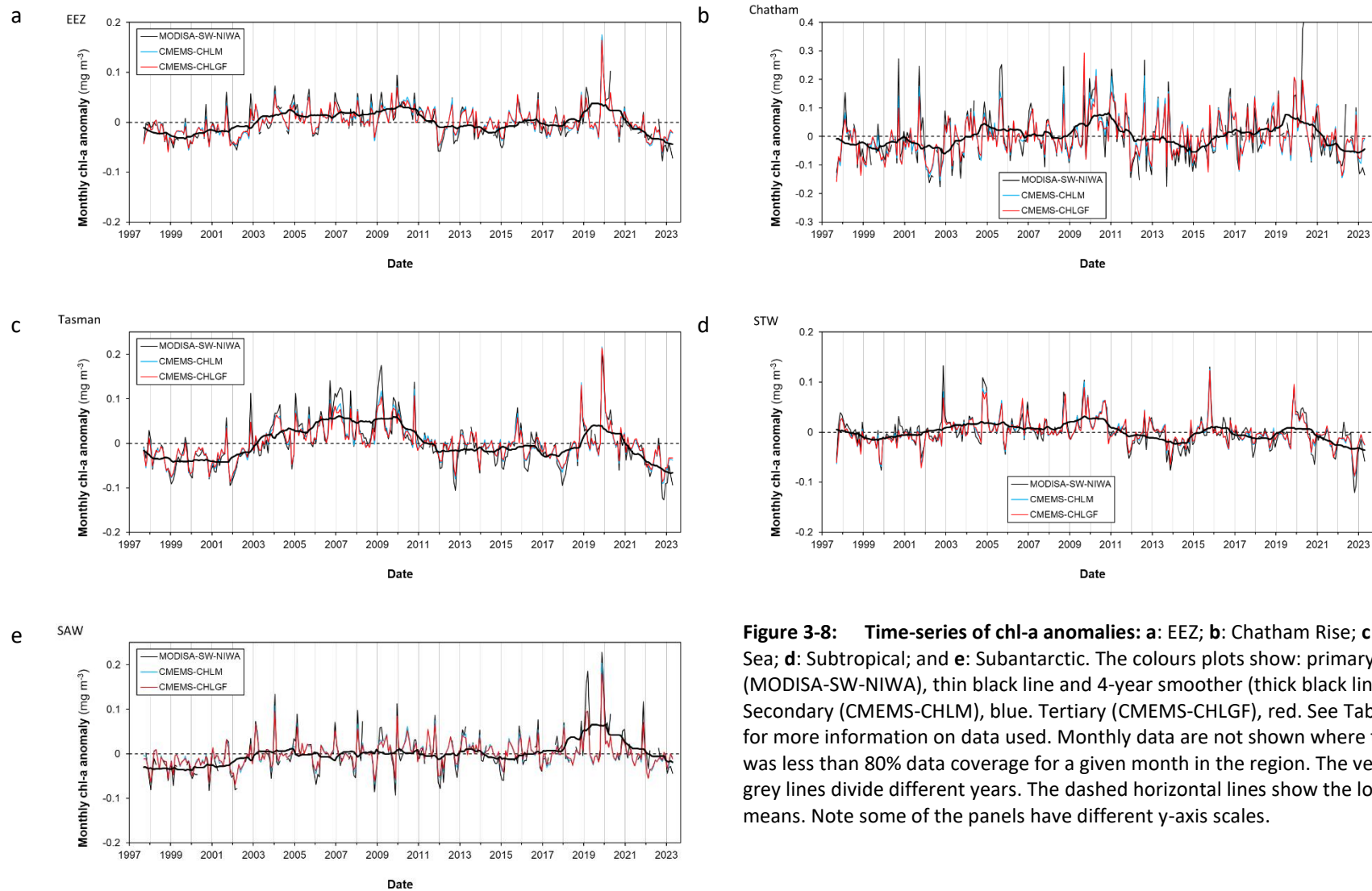


Figure 3-8: Time-series of chl-a anomalies: a: EEZ; b: Chatham Rise; c: Tasman Sea; d: Subtropical; and e: Subantarctic. The colours plots show: primary (MODISA-SW-NIWA), thin black line and 4-year smoother (thick black line). Secondary (CMEMS-CHLM), blue. Tertiary (CMEMS-CHLGF), red. See Table 2-1 for more information on data used. Monthly data are not shown where there was less than 80% data coverage for a given month in the region. The vertical grey lines divide different years. The dashed horizontal lines show the long-term means. Note some of the panels have different y-axis scales.

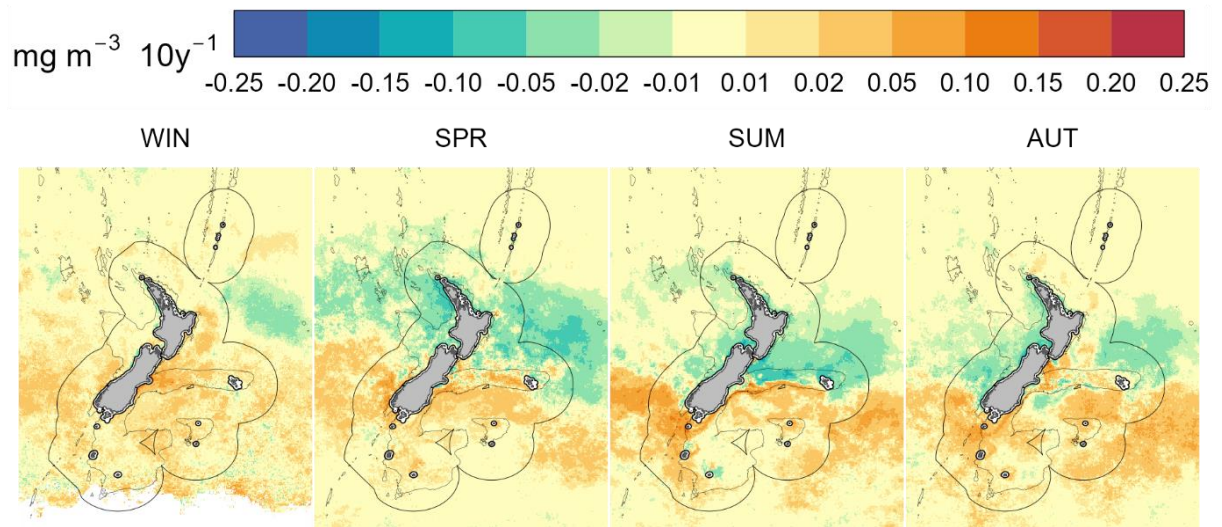


Figure 3-9: Ocean scale seasonal trends in chlorophyll a (chl-a, 1997-2023). Trends in chlorophyll-a concentration (chl-a, shown as mgChl-a m^{-3} per decade based on MODISA-SW NIWA dataset) are shown for each season separately (WIN=winter; SPR=spring; SUM=summer; AUT=autumn).

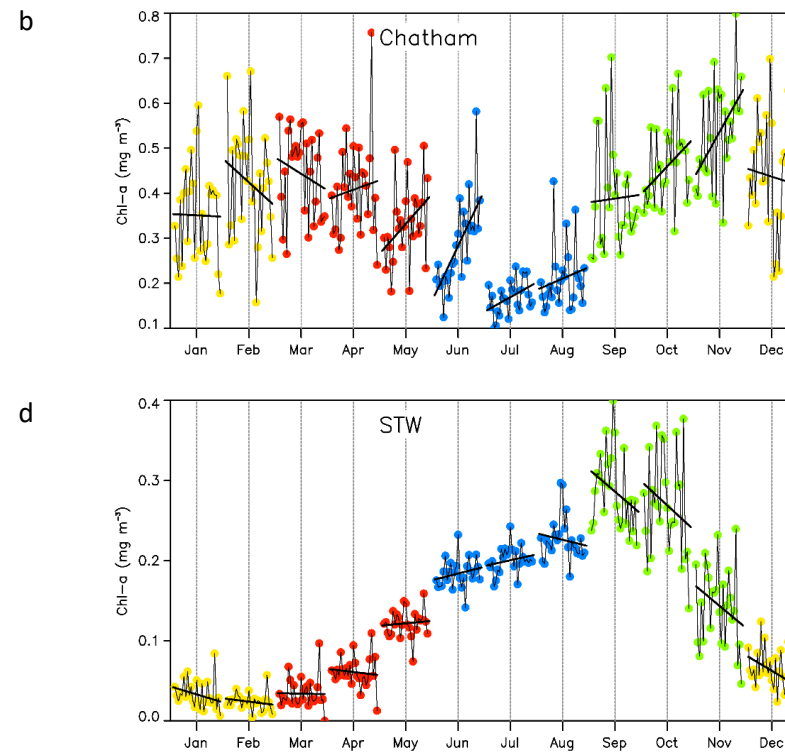
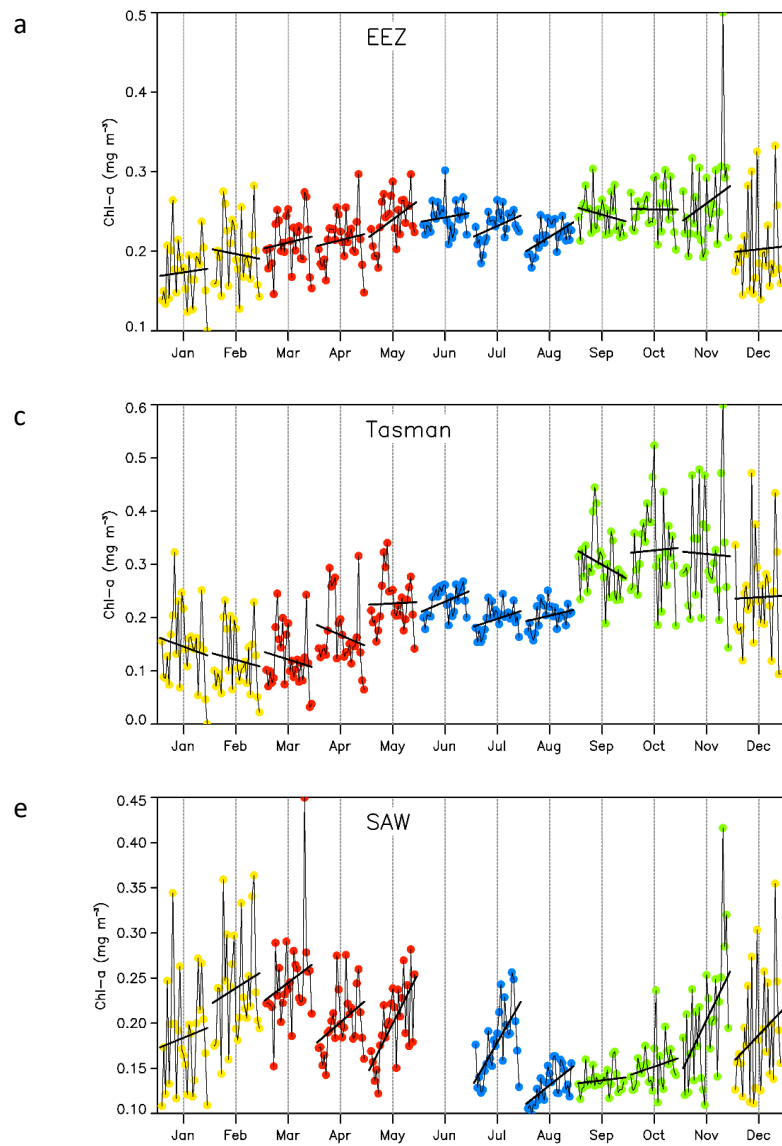


Figure 3-10: Trends in chl-a by month for EEZ and 4 descriptive regions. a: EEZ; b: Chatham Rise; [panels below] c: Tasman Sea; d: Subtropical Water (STW); e: Subantarctic Water (SAW). All plots are based on primary dataset (MODISA-SW-NIWA) chl-a only. Seasons are coloured differently (spring=green; summer=yellow; autumn=red; winter=blue). Note all panels have different y-axis scales to show within month trends.

3.1.5 Spatial correlations

Correlations between monthly anomalies of chl-a and SST for each pixel between 1997 and 2023 (Figure 3-11) were found to be generally negative in Subtropical Water and the Tasman Sea, and positive in Subantarctic Water, consistent with previous analyses between 1997 and 2018 (Pinkerton et al., 2019). In Subtropical Water and the Tasman Sea, when the surface water is warmer than normal, surface chl-a tends to be lower than normal (negative correlation). In northern portions of Subantarctic Water, the reverse is true, when the surface water is warmer than normal, chl-a tends to increase (positive correlation), particularly so around the Southland Current and southern extent of the subtropical convergence zone.

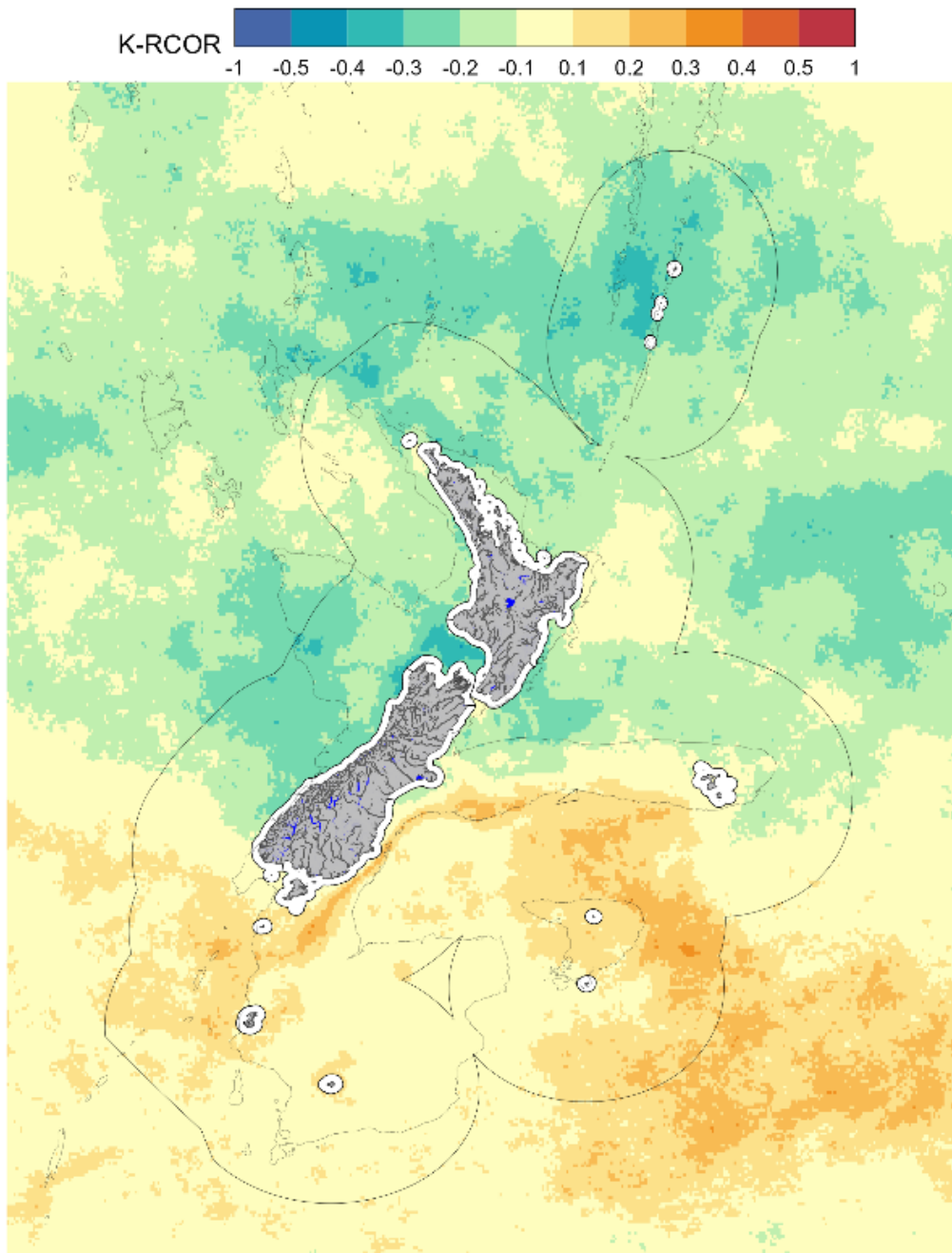


Figure 3-11: Ocean scale spatial correlation between sea surface temperature and chlorophyll a (1997–2023). The linear Kendall regression correlation coefficient (K-RCOR) was computed between anomalies.

3.2 Coastal scale analyses

3.2.1 Data coverage

The spatial distribution of satellite observations for the coastal analyses (Figure 3-12) is influenced by a range of factors:

1. Reduced data coverage close to the coast (within ~4 km) was due to a combination of processing failures in SeaDAS software from a combination of atmospheric correction failure in highly turbid waters, land adjacency effects (bright land pixels), in-water algorithm failure due to factors including, bottom reflection in clear, shallow waters. Data were extrapolated and smoothed to fill in data gaps (see Section 2.1.5) in this nearshore zone and the increase in data coverage obtained using this method is not shown in Figure 3-12. Instead, the coverage shown in Figure 3-12 is indicative of the number of actual observations before the filling-in process;
2. The decrease in data coverage to the south of Stewart Island was due to low solar elevations in winter which leads to failure of NASA's quality-control routines in SeaDAS;
3. Decreases in the quantity of data quantity at the extreme edges of the coastal domain was due to failure of the in-water algorithm in clear oceanic environments; and
4. Residual broad-scale patterns in data availability (e.g., greater number of available ocean colour observations in areas like Bay of Plenty, Hawke Bay, Cook Strait) was primarily influenced by the distribution of cloud cover (i.e., these areas tend to be sunnier than normal).

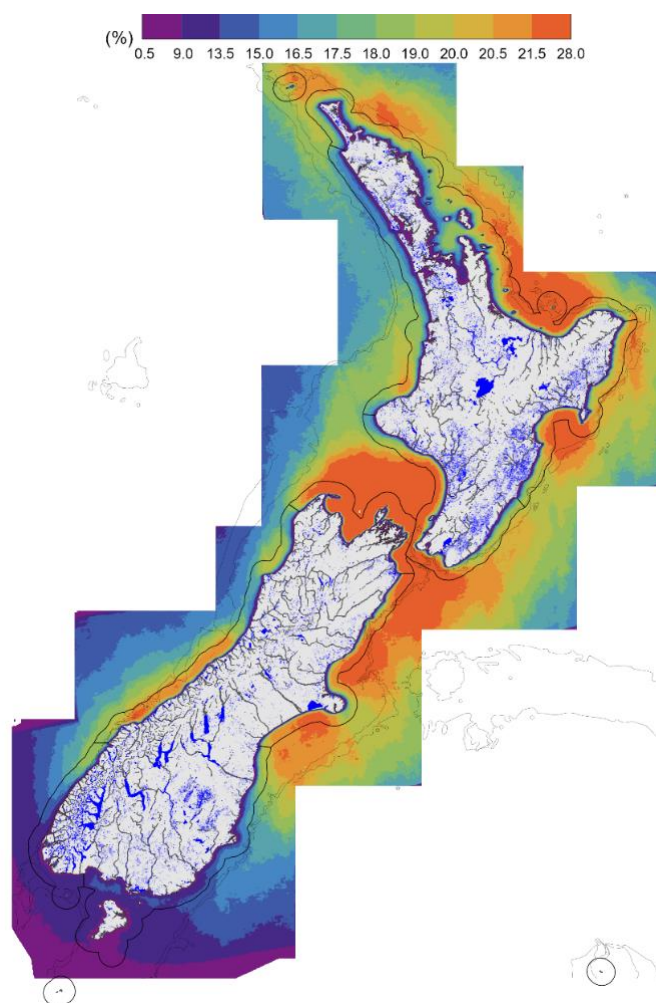


Figure 3-12: Coastal scale spatial coverage of observations (2002-2023) The colour shows the % of potential satellite observations that provided valid ocean colour products. The boundary of the New Zealand territorial sea and coastal regions are also shown, along with the 200 and 500 m depth contours.

3.2.2 Mean spatial patterns

Sea surface temperature around the coast was primarily related to latitude, with colder Subantarctic water to the south and warmer Subtropical water to the north (Figure 3-13 a). The influence of alongshore coastal currents was important, for example the Southland Current along the south-eastern coast of the South Island which transports colder water further north around Banks Peninsula, and the East Auckland Current off the north-eastern coast of the North Island which transports warmer water south towards the Bay of Plenty.

Coastal chl-a concentrations (Figure 3-13 b) were highest closer to land, typically classifying as mesotrophic ($1-3 \text{ mg m}^{-3}$), reducing offshore to oligotrophic ($0.1-1 \text{ mg m}^{-3}$). The general spatial pattern and offshore gradient typically followed the underlying bathymetry but elevated coastal phytoplankton abundances blended into offshore elevations in the area to the east of Banks Peninsula at the extreme west of the Chatham Rise.

Total suspended solids (TSS) concentration spatial patterns (Figure 3-13 c) were similar to chl-a (Figure 3-13 c) with an offshore-to-inshore gradient, with lower concentrations offshore and higher relative concentrations inshore. TSS was particularly elevated in areas associated with shallower shelf regions and larger river inflows.

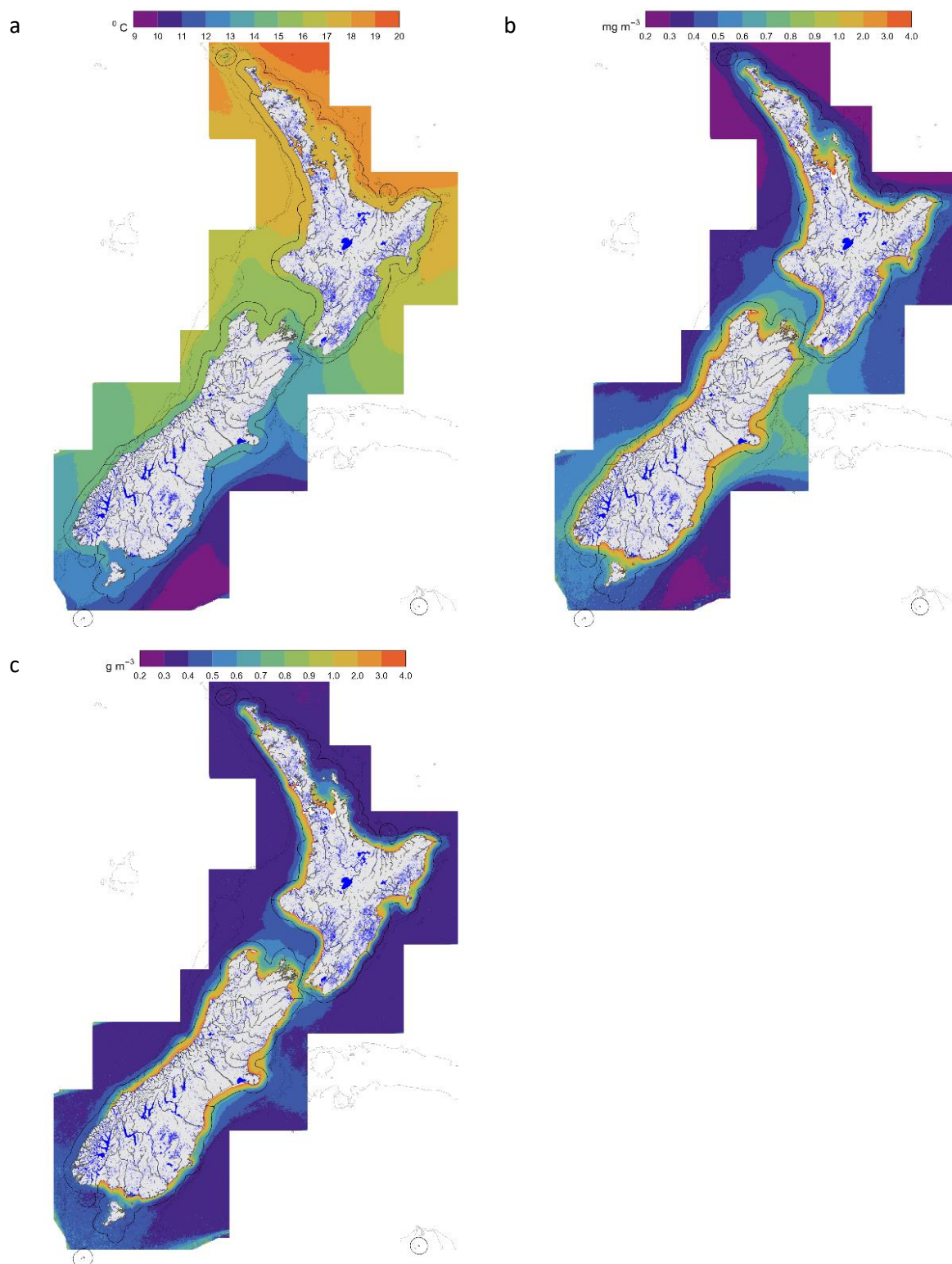


Figure 3-13: Coastal scale long-term averages in environmental indicators (2002-2023): a: SST (°C); b: Chl-a (mg m⁻³); and c: TSS (g m⁻³). Refer to Figure 3-12 for further details.

3.2.3 Trends in sea surface temperature

Surface water over most of the New Zealand coastal region warmed during the last 20 years (2002-2023 period) with the exception of waters to the east of central New Zealand, where there was either no change or a small negative (cooling) trend off the Wairarapa coast (Figure 3-14 a). Most of the warming trend is “virtually certain” and the cooling in the Eastern North Island region “possible” (Figure 3-14 b). Coastal areas round the South Island seem generally warmed at a faster rate over the last 20 years than coastal waters around North Island.

SST trends in the nine coastal regions were analysed over two periods, ~20 years (2002-2023) and ~40 years (1981-2023). The 40-y analysis was carried out only on the OISSTv2.1 product (Table 3-4) and the 20-y analysis on both OISSTv2.1 (Table 3-5) and the SCENZ SST v3.0 product (Table 3-6). Over the last 40 years, we found “virtually certain” warming in all coastal regions at rates between 0.23 – 0.29 °C per decade (Table 3-4). New Zealand 40-y coastal warming rates in all coastal regions were greater than the global mean warming rate over the same period, by between 25% (North Eastern region) and 87% (East Coast South Island). We note that there is a wide range of SST warming rates worldwide.

Over the last 20 years, trends in SST were very consistent between the OISSTv2.1 and SCENZ SST v3.0 products (Table 3-5, Table 3-6). Based on both SST products, except for Eastern North Island, there was “virtually certain” or “very likely” 20-y surface ocean warming in the New Zealand coastal regions at rates of between 0.36 – 0.61 °C per decade (Table 3-5, Table 3-6, Figure 3-15). Based on OISSTv2.1, warming rates over the past 20 years were 50–146% higher than equivalent warming rates over the last 40 years in all regions except Eastern North Island where the 20-y warming rate was a quarter of the 40-y rate (Table 3-5). The acceleration of the coastal warming was particularly high around South Island, where 20-y warming rates in all coastal region were more than three times the global warming rate over the same period, and nearly 3.7 times the global average in the Southern South Island region (Table 3-5).

SST time-series for the coastal regions (Figure 3-16) showed evidence for multi-year climate variability on which was superimposed an overall warming trend. The warming trend since 2002 seems to have dominated multi-year climate variability in most coastal regions. The occurrence of marine heatwaves (MHW) in some coastal regions is apparent in these timeseries; note the high SST anomalies in coastal regions such as in January 2018 in the South Cook Strait region (Figure 3-16 e) and December 2021 in the Western North Island region (Figure 3-16 e).

Seasonally coastal warming was greatest in summer and autumn, except off the Wairarapa coast (East Coast South Island region, Figure 3-17). Month trends within regions reinforces this pattern (Figure 3-18), with particularly strong warming trends in all regions between late spring (November) and late autumn (May). SST anomalies in the anomalous Eastern North Island region were flat during winter months (June-August).

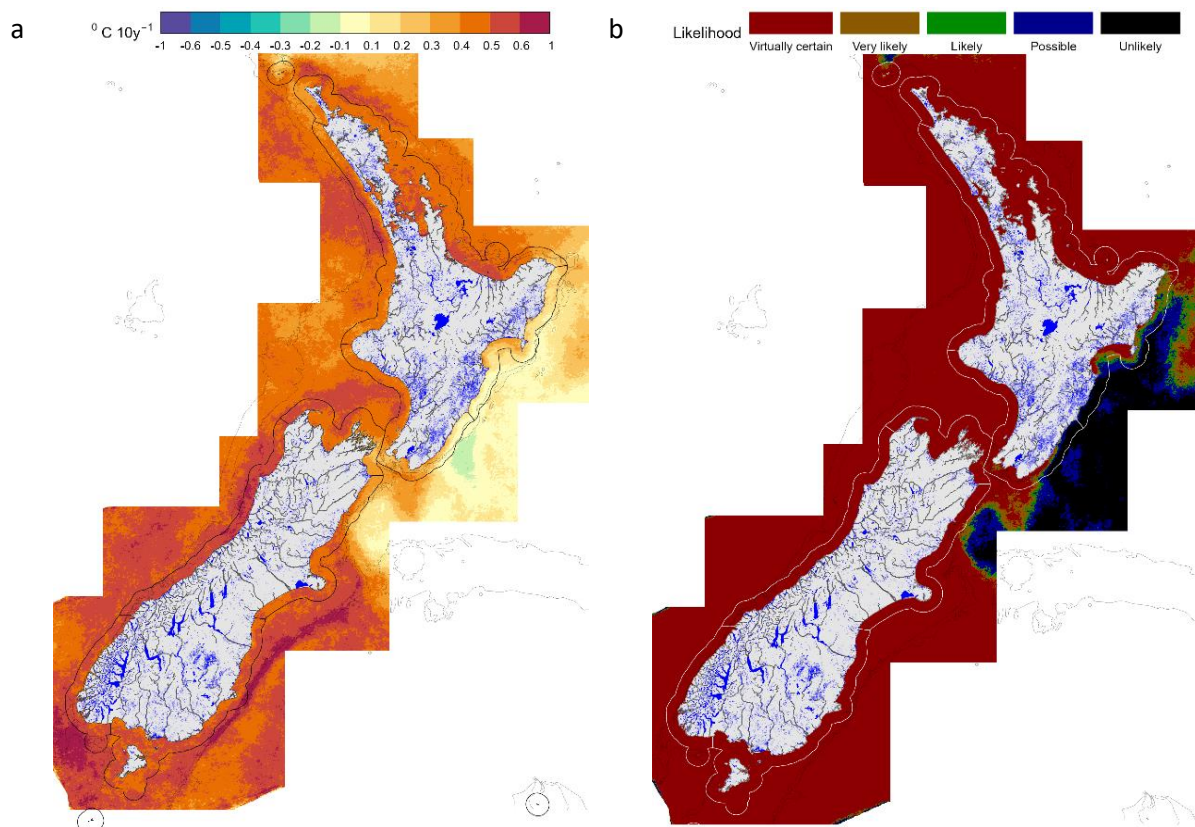


Figure 3-14: Coastal scale spatial trends in sea surface temperature (2002-2022): a: Sen-slope trends in sea surface temperature (SST) shown as °C per decade based on MODIS-Aqua dataset (SCENZ SST v3.0); and b: Likelihood of non-zero trend in SST based on Mann-Kendall analysis corrected for auto-correlation.

Table 3-4: Coastal scale region trends in sea surface temperature over 40 years (1981-2023) based on OISSTv2.1. The Mann Kendall (M-K) test (using the Z statistic) was applied to monthly anomalies in the coastal descriptive regions based on the OISSTv2.1 product. NI=North Island; SI=South Island. Note: The “Sen slope/median” (typically calculated for other products) is not calculated for SST because the scale offset is non-zero. Mann-Kendall significance (sig) is shown: *** p<0.001; ** p<0.01; and * p<0.05.

Region	M-K Z	M-K p	Sen slope °C/10y	Median °C	M-K sig	McBride likelihood	Slope(40y) / global(40y)
North Eastern	3.61	3.1E-04	0.19	17.5	***	Virtually certain	1.25
Western NI	4.78	1.8E-06	0.26	16.9	***	Virtually certain	1.70
Eastern NI	4.30	1.7E-05	0.25	16.0	***	Virtually certain	1.60
North Cook Strait	4.39	1.1E-05	0.25	14.8	***	Virtually certain	1.61
South Cook Strait	4.10	4.2E-05	0.23	14.9	***	Virtually certain	1.51
West Coast SI	3.65	2.7E-04	0.23	14.5	***	Virtually certain	1.50
East Coast SI	6.13	8.6E-10	0.29	12.8	***	Virtually certain	1.87
Fiordland	3.77	1.6E-04	0.24	13.3	***	Virtually certain	1.57
Southern SI	4.24	2.3E-05	0.26	12.1	***	Virtually certain	1.67

Table 3-5: Coastal scale regional trends in sea surface temperature over 20-years (2002-2023) based on OISSTv2.1. The Mann Kendall (M-K) test was applied to monthly anomalies in the coastal descriptive regions based on the OISSTv2.1 product. See also caption Table 3-4.

Region	M-K Z	M-K p	Slope °C/10y	M-K sig	McBride likelihood	Slope(20y)/global(20y)	Slope(20y)/slope(40y)
North Eastern	3.29	1.0E-03	0.40	**	Virtually certain	2.40	2.07
Western NI	3.59	3.3E-04	0.45	***	Virtually certain	2.69	1.71
Eastern NI	0.54	5.9E-01	0.06		About as likely as not	0.38	0.25
North Cook Strait	2.57	1.0E-02	0.37	*	Very likely	2.25	1.50
South Cook Strait	3.02	2.5E-03	0.46	**	Virtually certain	2.79	1.99
West Coast SI	3.56	3.7E-04	0.52	***	Virtually certain	3.14	2.27
East Coast SI	4.41	1.0E-05	0.54	***	Virtually certain	3.23	1.86
Fiordland	3.93	8.6E-05	0.60	***	Virtually certain	3.58	2.46
Southern SI	3.96	7.4E-05	0.61	***	Virtually certain	3.68	2.37

Table 3-6: Coastal scale regional trends in sea surface temperature over 20-years (2002-2023) based on SCENZ SST v3.0. The Mann Kendall (M-K) test was applied to monthly anomalies in the coastal descriptive regions based on the SCENZ SST v3.0 product. See also caption Table 3-4.

Region	M-K Z	M-K p	Slope °C/10y	M-K sig	McBride likelihood	Slope(20y)/global(20y)	Slope(20y)/Slope(40y)
North Eastern	4.82	1.4E-06	0.45	***	Virtually certain	2.71	2.34
Western NI	4.75	2.0E-06	0.44	***	Virtually certain	2.67	1.70
Eastern NI	1.55	0.12	0.16		Possible	0.96	0.65
North Cook Strait	3.46	5.5E-04	0.36	***	Virtually certain	2.17	1.45
South Cook Strait	4.04	5.2E-05	0.45	***	Virtually certain	2.70	1.93
West Coast SI	4.15	3.3E-05	0.54	***	Virtually certain	3.22	2.32
East Coast SI	5.00	5.8E-07	0.44	***	Virtually certain	2.66	1.54
Fiordland	4.45	8.7E-06	0.52	***	Virtually certain	3.10	2.14
Southern SI	4.61	4.0E-06	0.51	***	Virtually certain	3.07	1.98

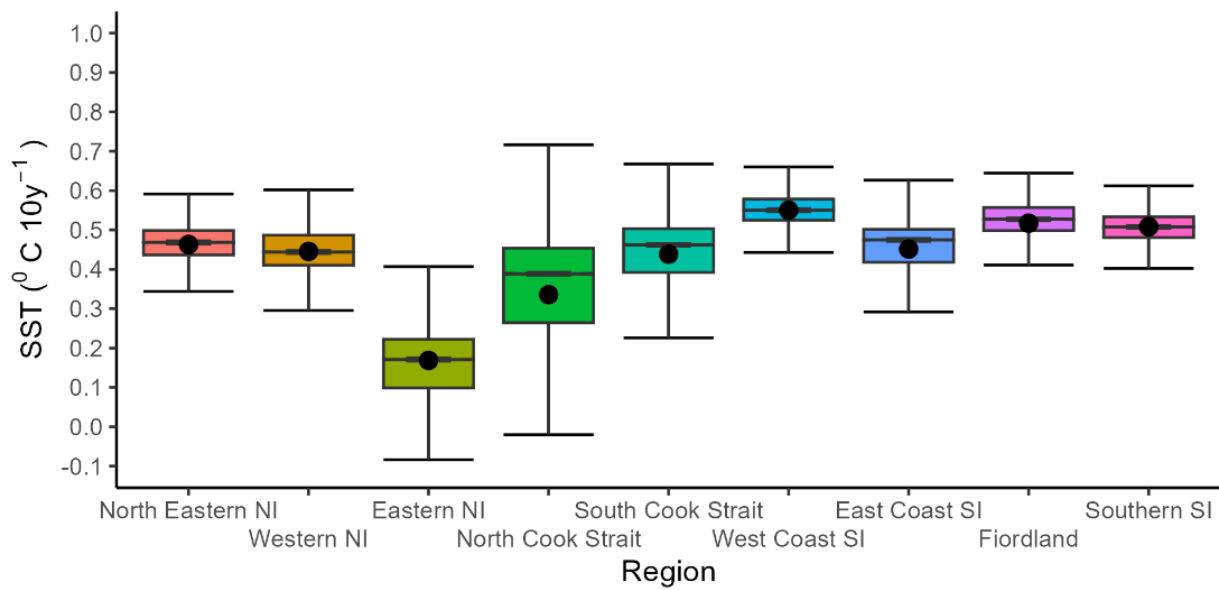


Figure 3-15: Coastal scale regional sea surface temperature trend boxplot statistics. The distribution of 20-year trends (2002-2023) in each of the coastal regions was based on NIWA SCENZ SST 3.0 ($^{\circ}\text{C}$ per decade). Boxes show the 25th – 75th percentiles, dots the mean, horizontal line the median and the bars the full range.

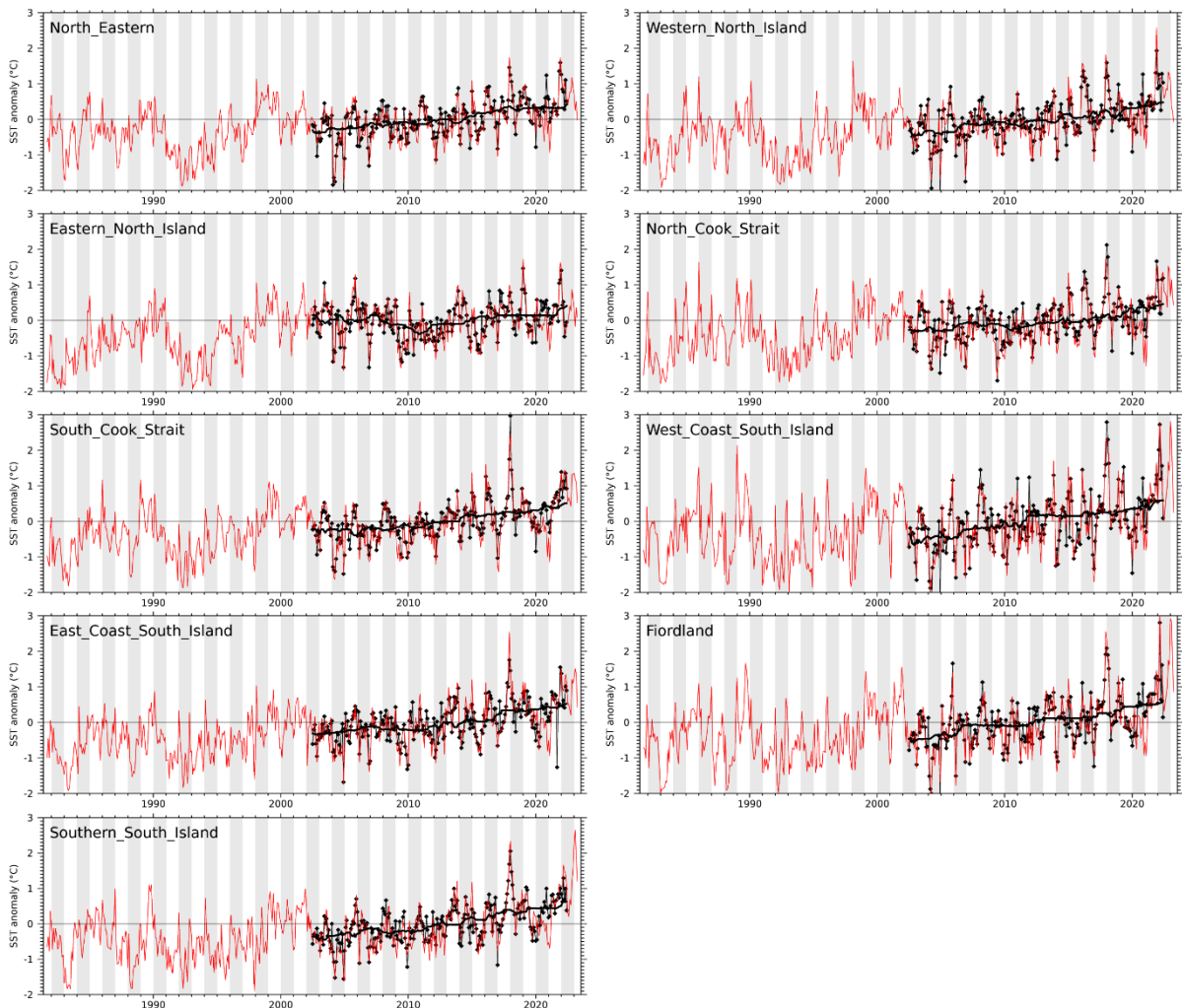


Figure 3-16: Coastal scale regional time-series of sea surface temperature (SST) anomalies. MODIS-Aqua (SCENZ SST v3.0) from 2002 are shown black with a 4-year smoothed trend (thick black line). OISSTv2.1 data from 1981 are shown red for comparison.

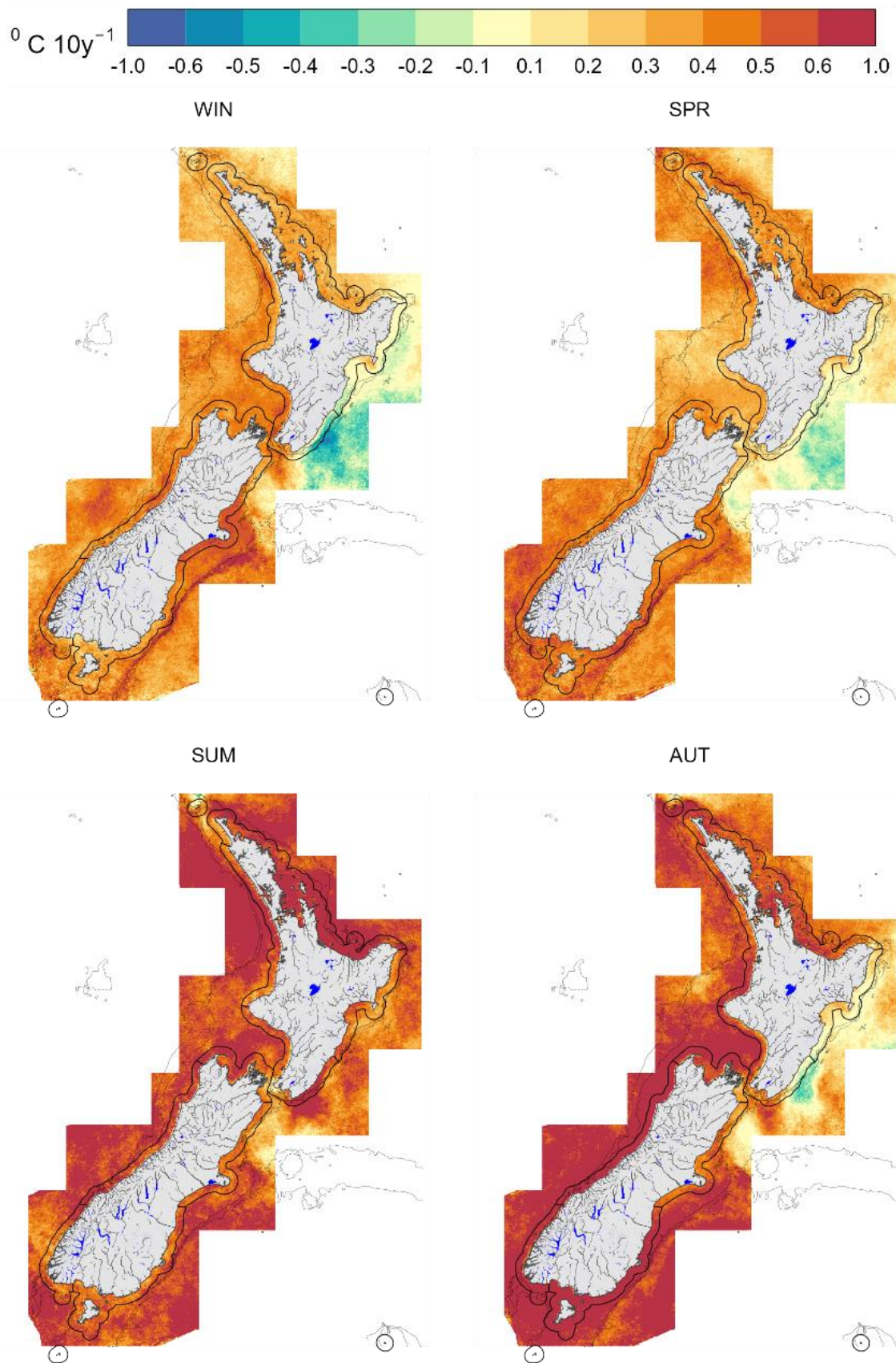


Figure 3-17: Coastal scale seasonal spatial trends in sea surface temperature (2002-2023). Trends in SST (shown as $^{\circ}\text{C}$ per decade based on SCENZ SST v3.0) are shown for each season separately (WIN=winter; SPR=spring; SUM=summer; AUT=autumn).

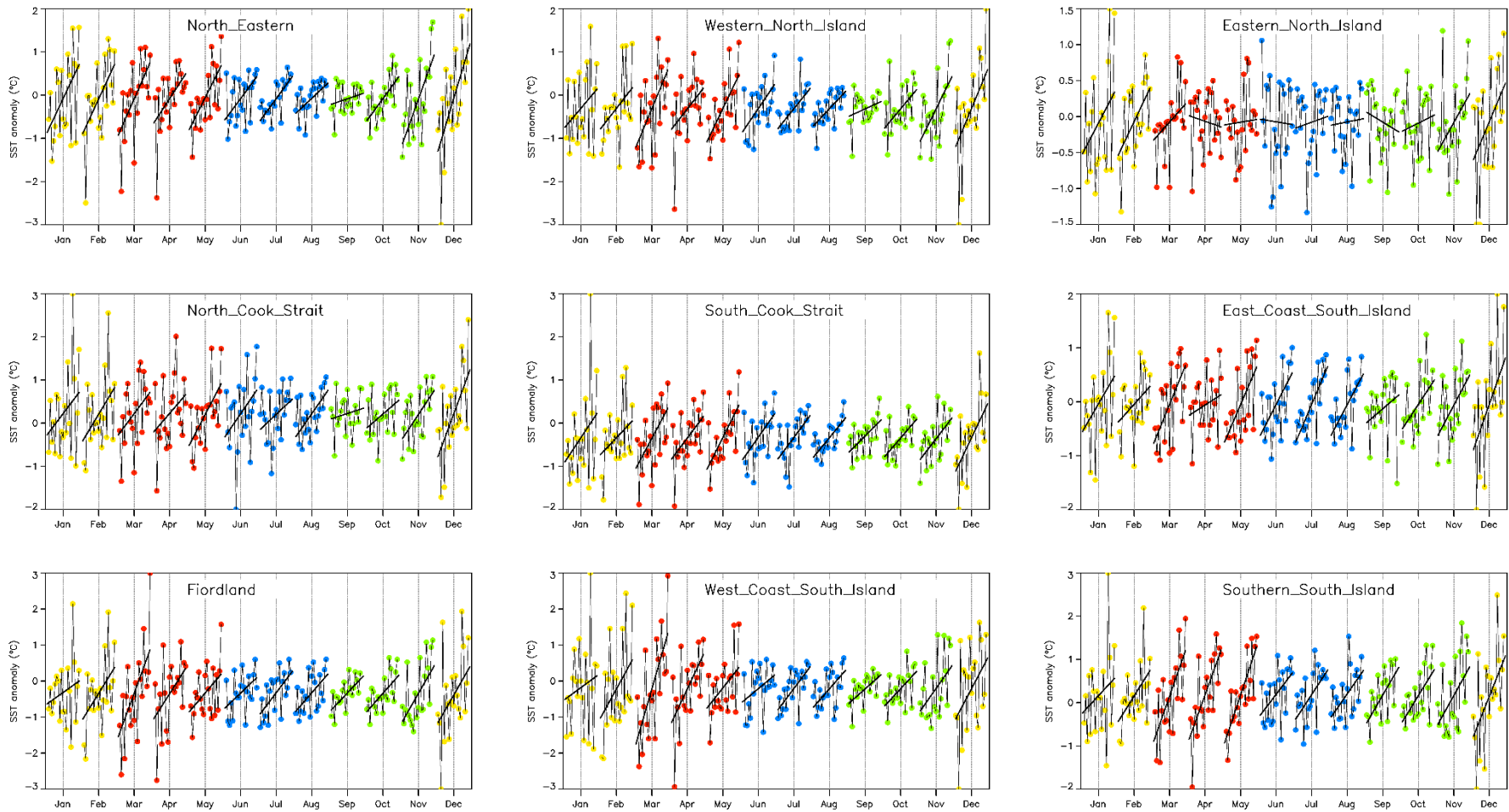


Figure 3-18: Coastal scale month trends in sea surface temperature anomalies. All analyses based on MODIS-Aqua (SCENZ SST v3.0) from 2002.

3.2.4 Trends in chlorophyll a

Chl-a increased (positive trends) in many coastal regions around the South Island (Figure 3-19 a), yet only parts of these display “virtually certain” trends (Figure 3-19 b). Of note are “virtually certain” increases: around Pelorus and Queen Charlotte Sounds and down the upper western coast of the South Island to north of Kaikoura and offshore to STC waters; around Southland and Stewart Island; offshore from the boundary of the southland current into Subantarctic waters to the west of the South Island; and an area of Subtropical waters east of the Kaipara coast.

Areas where chl-a decreased (negative trends) included: along the north-east New Zealand shelf, Hauraki Gulf into the outer Firth of Thames, Coromandel and into the Bay of Plenty; west of Northland down to Kaipara and Manukau Harbours; around Mahia Peninsula; and offshore from Golden and Tasman Bays (Figure 3-19 a). However, confidence in these trends were generally low, with only small areas within these regions having “virtually certain” decreasing trends in chl-a (Figure 3-19 b), e.g., around Kaipara and Manukau Harbours and the outer Firth of Thames. A more detailed area-specific analysis is required to identify “local” (i.e., small spatial scale) chl-a trends that may be associated with particular rivers, estuaries or harbours and is not included here.

Considering the coastal regions and based on all three coastal chl-a datasets, regional trends in chl-a were predominantly positive (Table 3-7, Figure 3-20), with negative trends found only in the North Eastern North Island (“about as likely as not”). Using the SCENZ CHL v4.0 product, above “likely” positive trends in chl-a were evident in only the three southern-most regions (East Coast South Island, Fiordland, Southern South Island). The relative magnitudes of the trends in chl-a in regions were relatively large, varying from +7.5% of the median per decade in Fiordland, to -2.0% per decade in the North Eastern North Island.

Analyses of trends in coastal chl-a based on the two CMEMS products were consistent with each other and generally larger and more significant than for those based on the shorter SCENZ CHL v4.0 analysis (Table 3-7). Differences in the positive CMEMS trends arose because of low chl-a anomalies in most regions during the period 1997-2002, which is included in the CMEMS analysis but not in the SCENZ analysis.

The three data sources (SCENZ CHL v4.0 products and the two CMEMS products) showed good agreement (Figure 3-21) which provides confidence in the use of these data sources in the present and future analysis. There was little evidence in these time-series of strong multi-year climate variability as with SST (Figure 3-16). Instead, trends and multi-year variations in chl-a were relatively small compared to month-to-month variability. For example high anomalies in February 2023 in the Eastern North Island (Figure 3-21 c), in November 2005 and July 2010 in the East Coast South Island (Figure 3-21 g), and particularly low chl-a anomalies from December 2017 to January 2018 and December 2022 to January 2023 in the West Coast South Island (Figure 3-21 f). We note that these low chl-a anomalies on the West Coast South Island correspond to the occurrence of marine heatwaves in this region (see below).

Seasonally, winter trends in chl-a were positive almost everywhere except the west coast of Northland, whereas summer trends tended to be negative in most regions except offshore from the southland current and around the top eastern portion of the South Island (Figure 3-22). Within-month trends in North Eastern (Figure 3-23 a) and Eastern (Figure 3-23 b) North Island regions were generally negative during spring and early autumn (March), and positive/neutral in other months. In the Western North Island (Figure 3-23 b), negative trends in chl-a occurred in winter as well as spring

and summer. In the more southerly regions (Figure 3-23 d-i), positive chl-a trends between early autumn (May) and late winter (August) was the clearest consistent pattern across these regions.

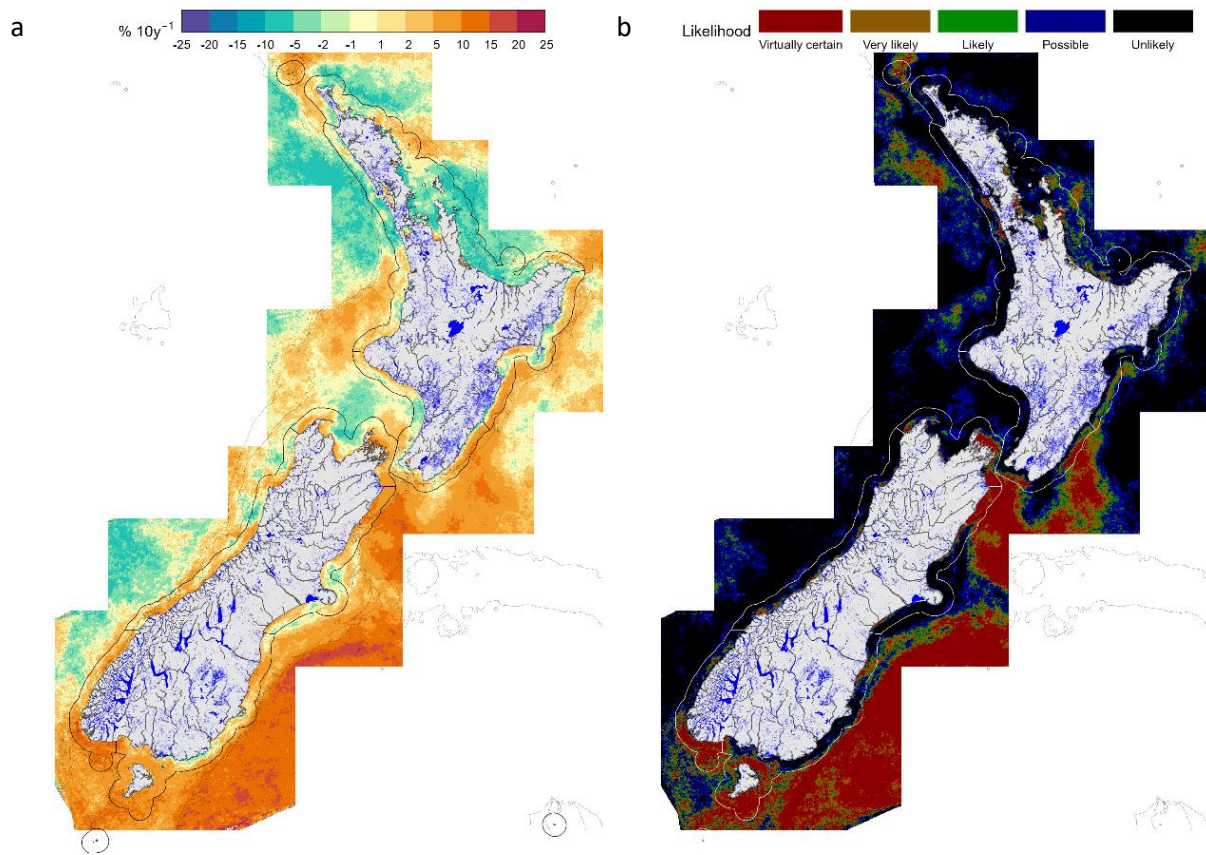


Figure 3-19: Coastal scale spatial trends in chlorophyll a (2002-2023). a: Sen-slope trends in chl-a as a proportion of the median chl-a value (% per decade); and b: Likelihood of non-zero trend in chl-a based on Mann-Kendall analysis corrected for auto-correlation. Data are from the NIWA SCENZ v4.0 coastal chl-a dataset.

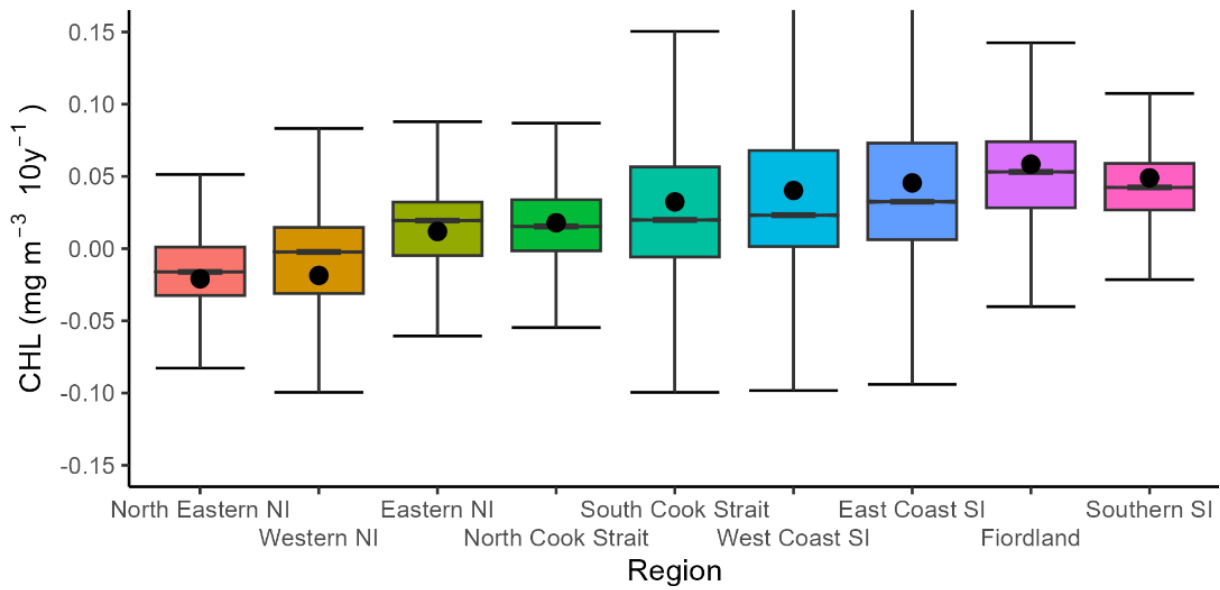


Figure 3-20: Coastal scale regional chlorophyll a trend boxplot statistics. The distribution of trends (2002-2023) in each of the coastal regions based on NIWA Chl-a (mg m^{-3}). Boxes show the 25th – 75th percentiles, dots the mean, horizontal line the median and the bars the full range (truncated in some cases).

Table 3-7: Coastal scale regional trends in chlorophyll a from three data sources The Mann Kendall (M-K) test (using the Z statistic) is applied to monthly anomalies in the coastal regions, 2002–2023. Trends are shown per decade ($10y^{-1}$). Mann Kendall significance (sig) is shown: *** $p < 0.001$; ** $p < 0.01$; * $p < 0.05$.

Area	M-K Z	M-K p	Sen slope ($mg\ m^{-3}\ 10y^{-1}$)	Median ($mg\ m^{-3}$)	Slope/median ($\% 10y^{-1}$)	M-K Sig	McBride likelihood
SCENZ CHL v4.0 (2002-2022)							
North Eastern	-0.87	0.383	-0.012	0.59	-2.0		About as likely as not
Western North Island	0.01	0.991	0.000	0.95	0.0		Exceptionally unlikely
Eastern North Island	1.10	0.273	0.018	0.83	2.1		Possible
North Cook Strait	1.22	0.223	0.019	0.73	2.5		Possible
South Cook Strait	1.03	0.302	0.018	0.87	2.1		Possible
West Coast South Island	0.81	0.420	0.034	1.20	2.8		About as likely as not
East Coast South Island	1.79	0.073	0.044	1.22	3.6		Likely
Fiordland	2.32	0.020	0.052	0.70	7.5	*	Very likely
Southern South Island	2.77	0.006	0.042	0.76	5.6	**	Virtually certain
CHLM (CMEMS 1997-2023)							
North Eastern	-1.30	0.193	-0.014	0.42	-3.5		Possible
Western North Island	2.24	0.025	0.032	0.63	5.1	*	Very likely
Eastern North Island	3.95	0.000	0.044	0.54	8.3	***	Virtually certain
North Cook Strait	2.72	0.007	0.032	0.56	5.8	**	Virtually certain
South Cook Strait	2.68	0.007	0.050	0.67	7.4	**	Virtually certain
West Coast South Island	1.63	0.103	0.044	0.94	4.7		Possible
East Coast South Island	4.58	0.000	0.084	0.79	10.6	***	Virtually certain
Fiordland	1.85	0.064	0.028	0.53	5.4		Likely
Southern South Island	2.70	0.007	0.024	0.54	4.4	**	Virtually certain
CHLGF (CMEMS, 1997-2023)							
North Eastern	-0.87	0.385	-0.010	0.40	-2.4		About as likely as not
Western North Island	2.71	0.007	0.038	0.58	6.5	**	Virtually certain
Eastern North Island	4.46	0.000	0.048	0.51	9.5	***	Virtually certain
North Cook Strait	2.89	0.004	0.034	0.53	6.3	**	Virtually certain
South Cook Strait	2.96	0.003	0.051	0.65	7.8	**	Virtually certain
West Coast South Island	1.58	0.115	0.039	0.85	4.6		Possible
East Coast South Island	4.75	0.000	0.084	0.76	11.1	***	Virtually certain
Fiordland	2.08	0.038	0.027	0.48	5.6	*	Very likely
Southern South Island	3.35	0.001	0.028	0.51	5.5	***	Virtually certain

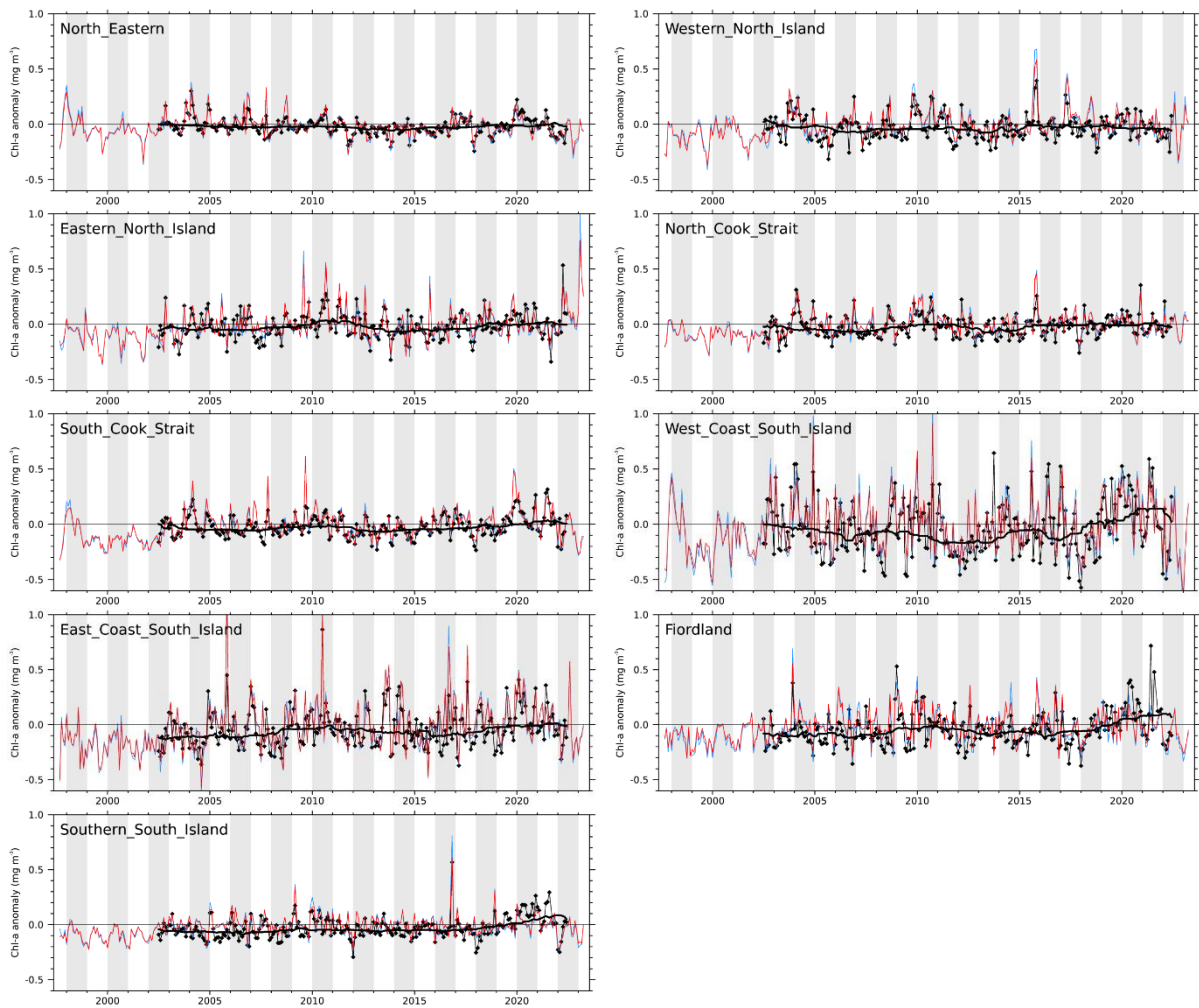


Figure 3-21: Coastal scale regional time-series of trends in chlorophyll a (chl-a) anomalies. MODIS-Aqua (SCENZ CHL v4.0) from 2002 are shown black with a 4-year smoothed trend (thick black line). CMEMS CHLM (blue) and CMEMS CHL-gap-free (red) are shown for comparison (but note that the lines so closely over-lie each other that often the underlying lines often cannot be easily seen).

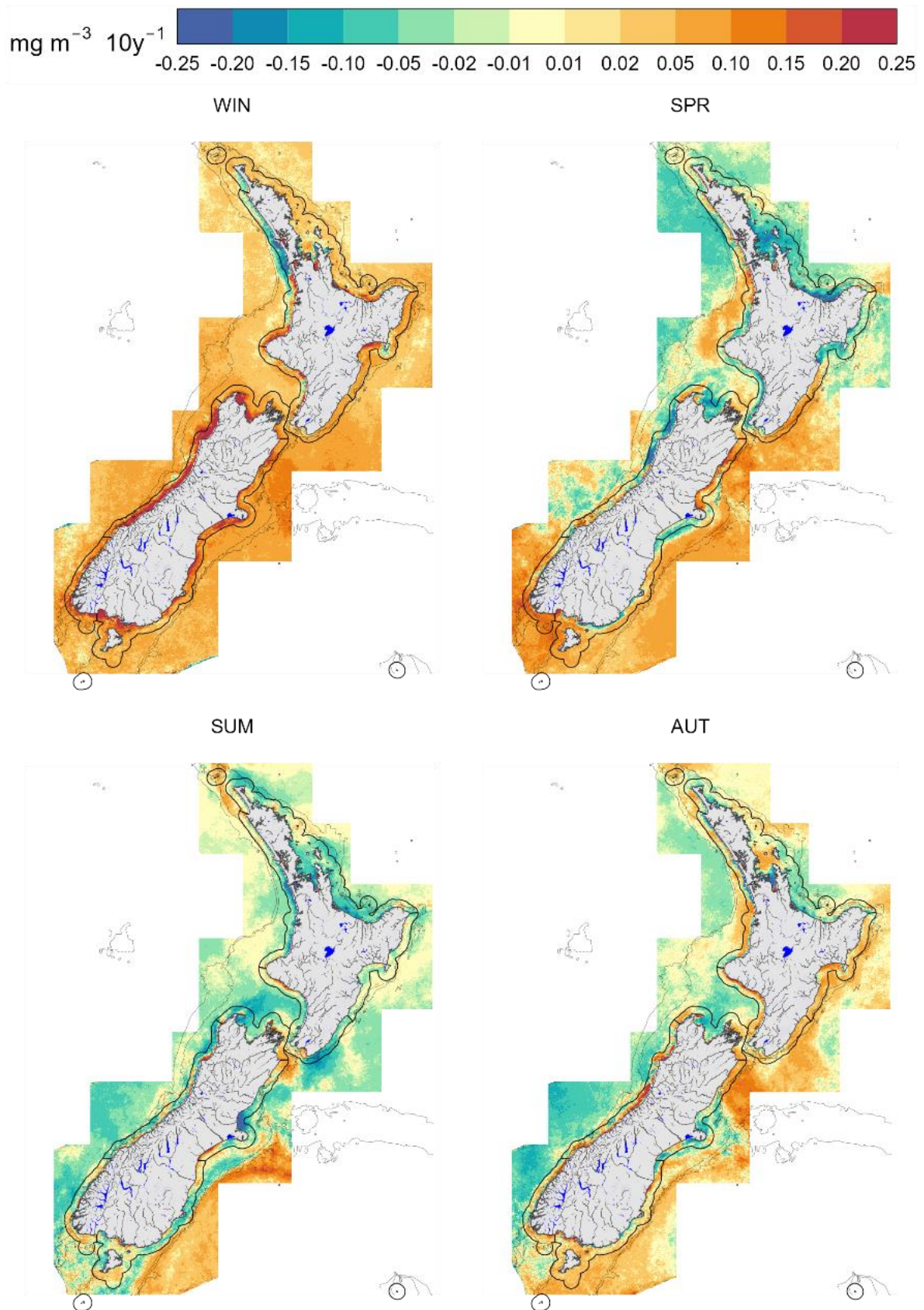


Figure 3-22: Coastal scale seasonal spatial trends in chlorophyll a (2002-2023). Trends in chl-a (shown as mg m^{-3} per decade based on SCENZ CHL v4.0) are shown for each season separately (WIN=winter; SPR=spring; SUM=summer; AUT=autumn).

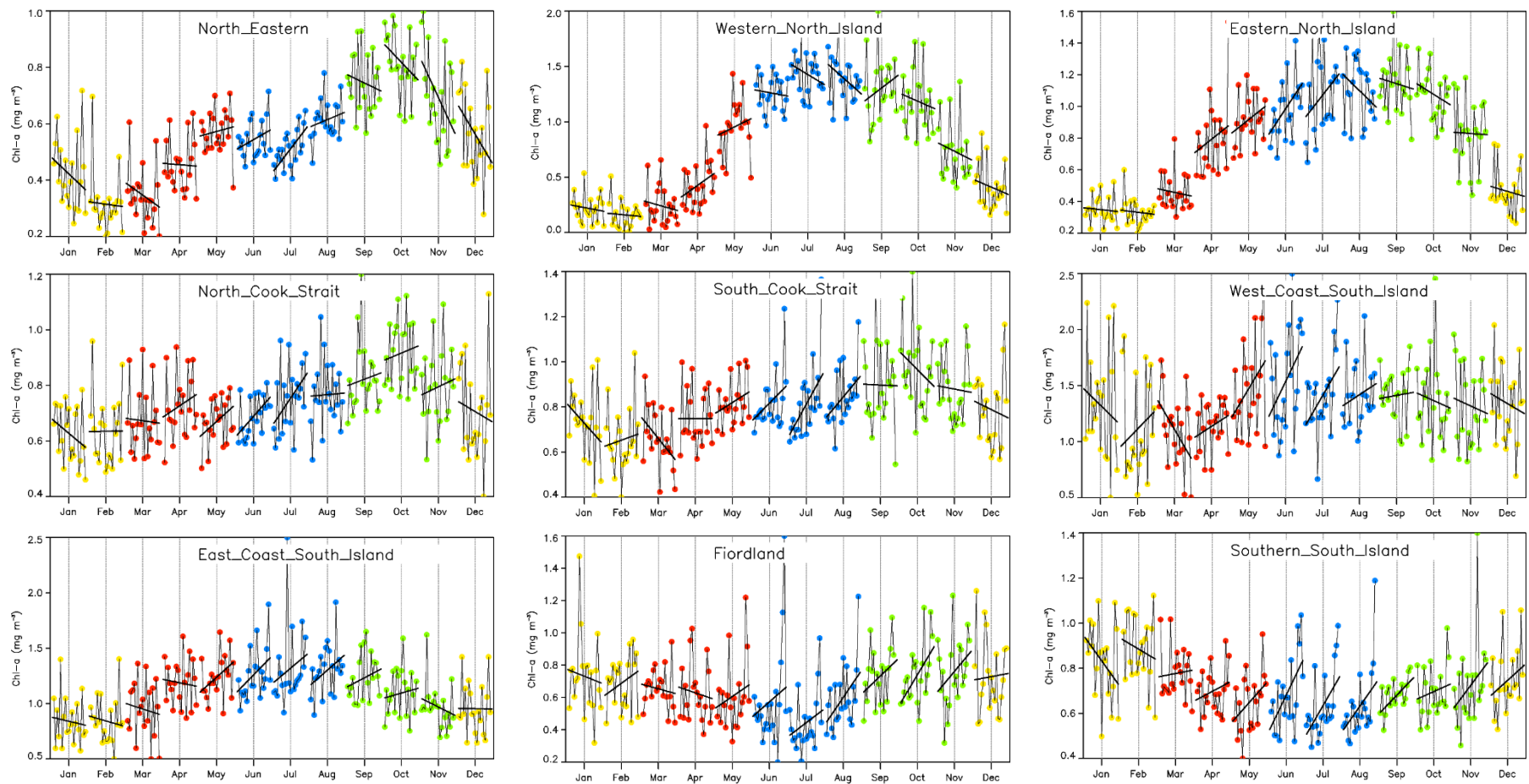


Figure 3-23: Coastal scale regional month timeseries trends in chlorophyll a (chl-a). All analyses based on MODIS-Aqua (SCENZ CHL v4.0).

3.2.5 Trends in total suspended solids

The spatial analysis presented in Figure 3-24 a, shows complex patterns of increasing and decreasing trends in TSS in the New Zealand coastal zone from 2002 to 2023. In contrast to SST and chl-a, which exhibited clear and discernible broad-scale patterns, changes in TSS did not display clear patterns across the coastal zone. Most of the observed TSS trends were deemed "unlikely", with a few noteworthy exceptions (Figure 3-24 b). Particularly, "virtually certain" increasing trends were found in the regions north of the Coromandel Peninsula, the east coast of the North Island, the offshore area of Tauihu-o-te-Waka Marlborough Sounds, Te Rua-o-Te-Moko Cloudy Bay and the eastern region of the upper South Island, and Te Rua-o-Te-Moko Fiordland. The only region demonstrating a "virtually certain" decreasing trend was around the Kaipara Harbour. Our analysis underscores the significant variability in TSS trends within coastal regions, as evidenced by the wide interquartile box widths in Figure 3-25

Trends in TSS in the coastal regions were predominantly positive (Table 3-8). Based on the SCENZ TSS v3.0 product, trends in only one region were negative (Western North Island, "about as likely as not"), and the positive trend in TSS in only one region (Fiordland) was considered "very likely". The magnitudes of the trends in TSS in the coastal regions based on the SCENZ TSS v3.0 product were reasonable in magnitude, varying from +5.8% of the median per decade for the Fiordland region, to -1.3% per decade for the Western North Island region.

Time-series of TSS anomalies based on CMEMS SPM were very consistent with those from SCENZ TSS (Figure 3-26; compare black and red lines). However, there were differences in TSS trends between the SCENZ TSS and CMEMS SPM analyses resulting from the difference in time periods (SCENZ TSS: 2002-2022; CMEMS SPM: 1997-2023). In particular, trends in TSS based on the CMEMS dataset in two northern regions (the Western and Eastern North Island regions) were assessed as "very likely" and negative/positive (respectively), compared to these being much less significant using SCENZ TSS data. The difference between these analyses arises because the CMEMS products include additional observations at the start (1997-2002) and end (2022-2023) of the SCENZ TSS product. TSS anomalies in these two regions (Western and Eastern North Island) in the early period (1997-2002) were neutral/negative (respectively), whereas the anomalies in the later period (2022-2023) were negative/positive (respectively). The addition of these data was enough to change the trend results, highlighting the importance of exercising caution when interpreting linear trends across different timespans.

As for chl-a, there was little evidence in these time-series of strong multi-year climate variability on TSS; both trends and multi-year variations in TSS were relatively small compared to month-to-month variability (Figure 3-26). The increasing trend in TSS in Fiordland seems to be associated with an increase in TSS from about 2019; before this, TSS anomalies in Fiordland show no evidence of change (Figure 3-26 h). The high positive TSS anomaly (+1.0 g m⁻³ based on the CMEMS TSS product, SPMM) in late summer (February) 2023, in the Eastern North Island region is likely associated with sediment brought into the coastal zone by Cyclone Gabrielle (Figure 3-26 c).

Trends in TSS were complex when analysed in seasonal (3-month) and monthly time frames (Figure 3-27 and Figure 3-28 respectively). Winter (June-August), which generally showed the strongest trends in TSS, and overall increases in TSS were observed across most regions, except for Western North Island, where a consistent seasonal decreasing trend was evident (Figure 3-28 b). In spring (September-November), there were few strong trends in coastal regions, except for an increase in TSS observed in Fiordland (Figure 3-28 h). During summer (December-February), there were few

noteworthy trends observed in any specific month or coastal region. In autumn, March trends were generally negative, while April shows neutral trends and in May, some regions exhibited positive trends (increases) in TSS, although not consistently across all regions.

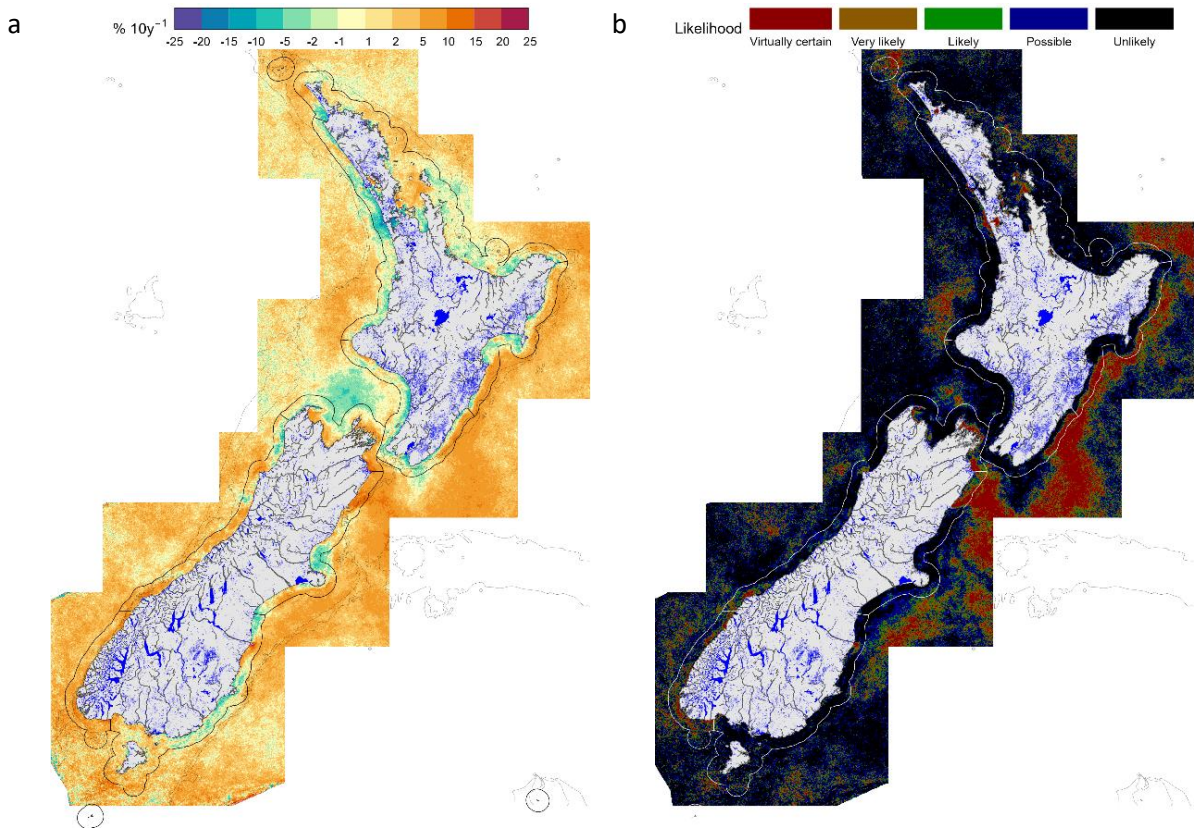


Figure 3-24: Coastal: Spatial trends in TSS (2002-2023). a: Sen-slope trends in TSS as a proportion of the median value (% per decade). b: McBride likelihood of non-zero trend in TSS based on Mann-Kendall analysis corrected for auto-correlation. Data are from the NIWA SCENZ TSS v3.0.

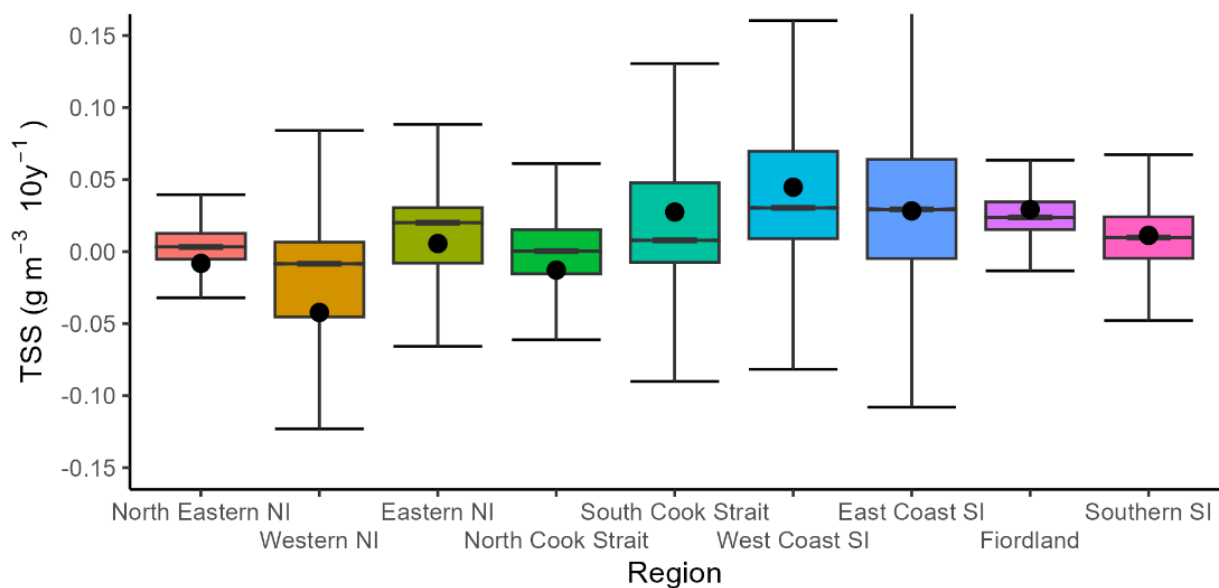


Figure 3-25: TSS trends in coastal regions. The distribution of trends (2002-2023) in each of the coastal regions based on NIWA SCENZ TSS (g m^{-3}). Boxes show the 25th – 75th percentiles, dots the mean, horizontal line the median and the bars the full range (truncated in some cases).

Table 3-8: Trend analysis for coastal region TSS. The Mann Kendall (M-K) test (using the Z statistic) was applied to monthly TSS anomalies in the coastal regions, 2002–2023. Trends are shown per decade ($10y^{-1}$). Mann Kendall significance (sig) is shown: *** $p < 0.001$; ** $p < 0.01$; * $p < 0.05$.

Area	M-K Z	M-K P	Sen slope ($g\ m^{-3}\ 10y^{-1}$)	Median ($g\ m^{-3}$)	Slope/median (% $10y^{-1}$)	M-K Sig	McBride likelihood
SCENZ TSS v3.0 (2002-2022)							
North Eastern	0.27	0.785	0.002	0.43	0.4		Unlikely
Western North Island	-0.60	0.547	-0.010	0.77	-1.3		About as likely as not
Eastern North Island	1.53	0.127	0.021	0.63	3.3		Possible
North Cook Strait	0.19	0.851	0.002	0.60	0.3		Unlikely
South Cook Strait	1.01	0.315	0.012	0.74	1.7		Possible
West Coast South Island	1.19	0.235	0.033	0.85	3.9		Possible
East Coast South Island	1.10	0.272	0.038	0.96	4.0		Possible
Fiordland	2.40	0.016	0.023	0.40	5.8	*	Very likely
Southern South Island	0.66	0.508	0.009	0.50	1.9		About as likely as not
SPMM (CMEMS, 1997-2023)							
North Eastern	-1.92	0.054	-0.010	0.58	-1.7		Likely
Western North Island	-2.09	0.036	-0.057	1.54	-3.7	*	Very likely
Eastern North Island	2.17	0.030	0.056	1.28	4.4	*	Very likely
North Cook Strait	0.34	0.736	0.008	1.11	0.7		Unlikely
South Cook Strait	1.25	0.213	0.022	1.33	1.7		Possible
West Coast South Island	1.00	0.316	0.045	1.71	2.6		Possible
East Coast South Island	1.52	0.129	0.077	2.21	3.5		Possible
Fiordland	2.54	0.011	0.019	0.52	3.7	*	Very likely
Southern South Island	-0.50	0.620	-0.007	0.74	-0.9		About as likely as not

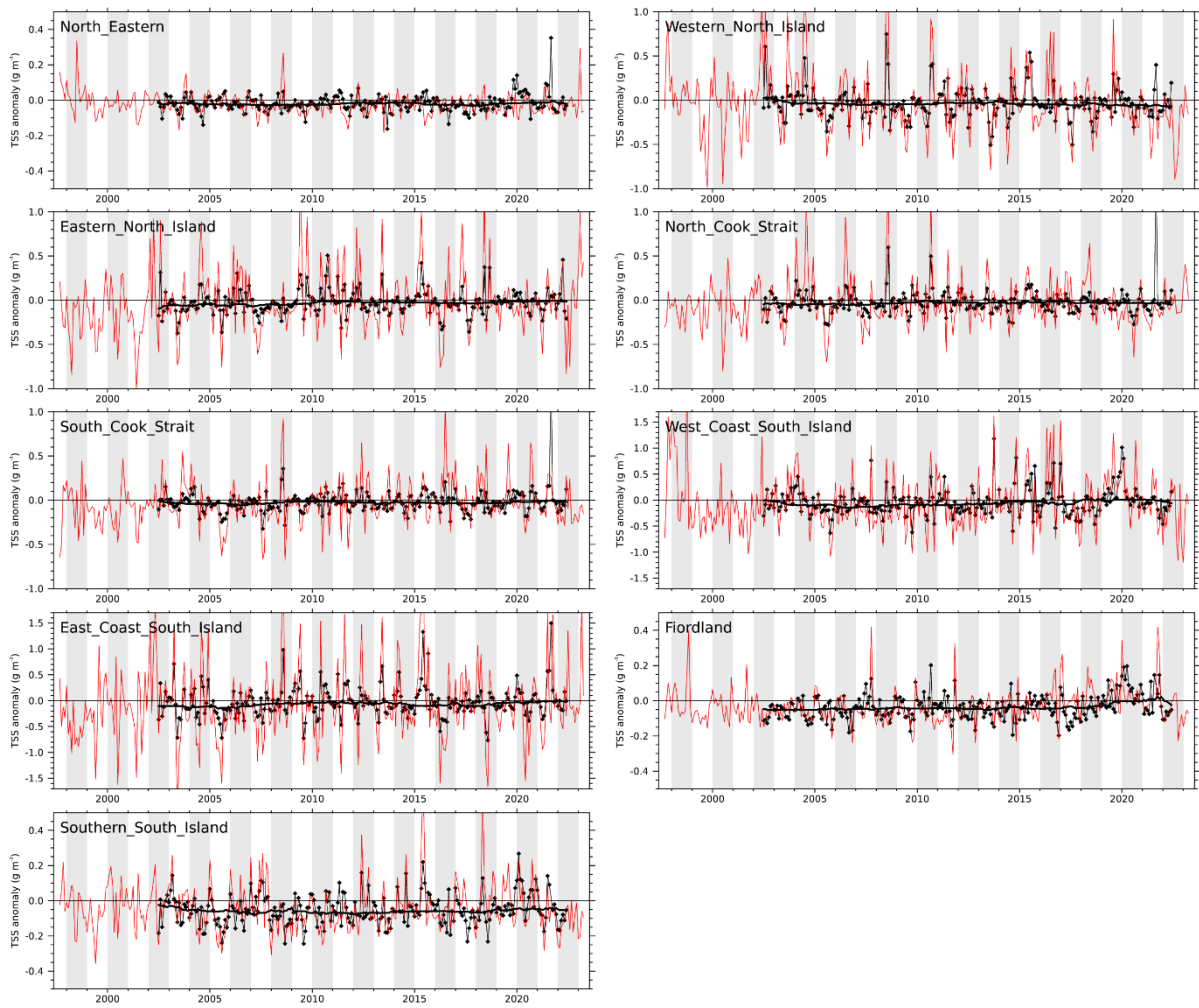


Figure 3-26: Time-series of TSS anomalies for coastal bio-regions. MODIS-Aqua (SCENZ TSS v3.0) from 2002 are shown black with a 4-year smoothed trend (thick black line). CMEMS SPM data are shown red for comparison.

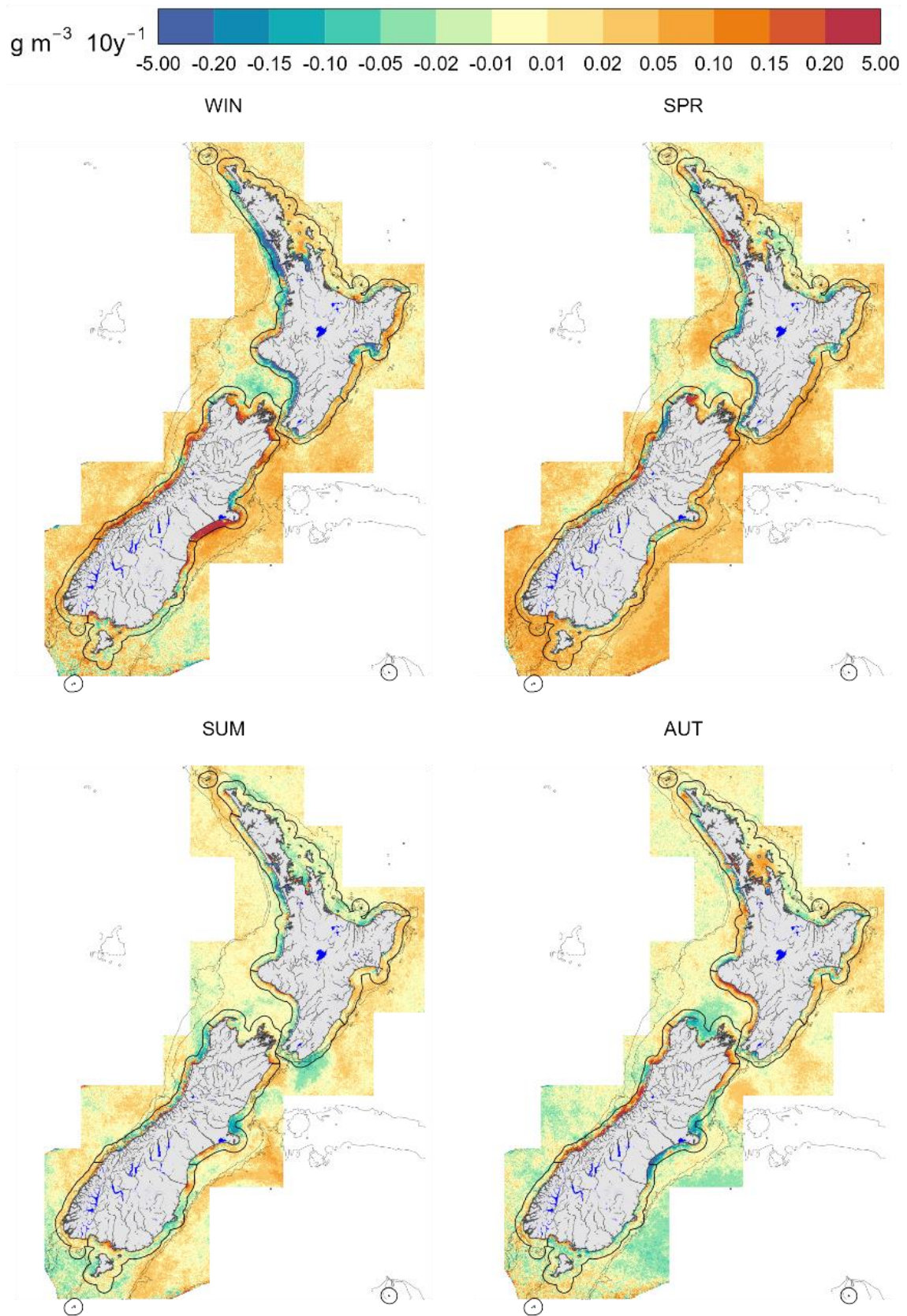


Figure 3-27: Coastal: Seasonal spatial trends in TSS (2002-2023). Trends in TSS (shown as g m^{-3} per decade based on SCENZ TSS v3.0) are shown for each season separately (WIN=winter; SPR=spring; SUM=summer; AUT=autumn).

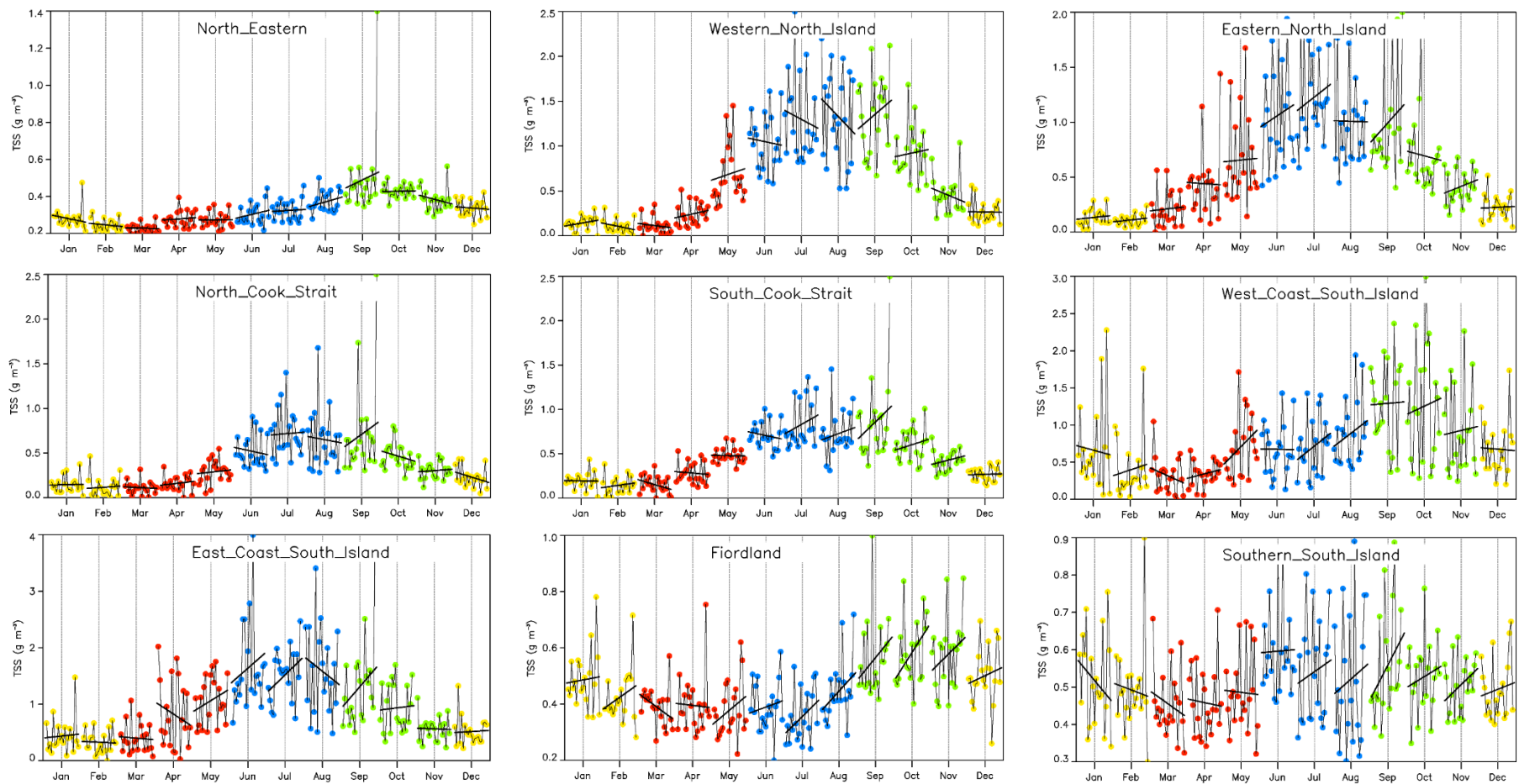


Figure 3-28: Trends in TSS anomalies by month for coastal bio-regions. MODIS-Aqua (SCENZ TSS v3.0) from 2002 are shown black with a 4-year smoothed trend (thick black line). CMEMS SPM data are shown red for comparison.

3.2.6 Regional scale focus on total suspended solids

Following Pinkerton et al. (2022), spatial maps of trends in TSS in six regions are shown as “zoomed-in” versions of the coastal TSS trend analysis (Figure 3-24) with features of interest (including estuaries and river mouths) also shown: Northland (Figure 3-29); Hauraki Gulf/Manukau/Kaipara (Figure 3-30); Bay of Plenty/East Cape/Hawke Bay (Figure 3-31); Wairarapa/South Taranaki Bight/Cook Strait/Marlborough (Figure 3-32); Canterbury/West Coast (Figure 3-33); and Southland/Stewart Island (Figure 3-34).

Trends in TSS that occur near estuaries and river mouths and which appear more likely to be related to land-use changes (i.e., changes in suspended sediment, river flow and/or changes in nutrients leading to trends in phytoplankton productivity) are highlighted below. Our initial interpretation of the spatial patterns in TSS trends is based on the following rationale:

- Changes to TSS that are consistent over moderate-large spatial scales (i.e., more than about 30 km alongshore or extending across the width of the continental shelf) are likely due to large-scale (climate) drivers, such as changes to phytoplankton primary production and/or changes to resuspension of sediment by currents and waves.
- Small-scale changes in TSS (of the order of less than 10s of km) are more likely due to local drivers. Where these small-scale changes are located near mouths of major rivers and estuaries, the TSS trends may be related to changes in land-use and weather patterns that affect material discharged by the rivers. Increases in sediment run-off and increases in nutrients (which fertilise phytoplankton production) will tend to lead to increases in TSS, and vice versa.

These should be considered as unconfirmed hypotheses. Definitive attribution of causes of changes will require additional data to be considered and/or new fieldwork or modelling to be carried out.

Northland

TSS across most of the coastline of Northland decreased between 2002-2022, likely driven by coastal warming leading to lower primary productivity (less phytoplankton-derived particulate material in the water column). However, at the northern tip of Northland (marked “A” in Figure 3-29) there is a large area of positive TSS trends for which the causes are not known. This area of increasing TSS does not appear to be associated with riverine input and is more likely of phytoplankton origin, i.e., increasing primary production perhaps because of increasing upwelling of nutrient-rich water along this coast.

There is a patchwork of decreasing trends in some harbours/regions down the east coast of Northland set against generally increasing TSS trends. Parengarenga Harbour System has decreasing trends in TSS, as does Rangaunu Harbour, and all the harbours and estuaries down the east coast of Northland to the Hauraki Gulf including Bay of Islands and Whangarei Harbour (though there are increasing trends at the mouth of the Waipu River). The reasons for these localised decreasing/increasing trends of TSS are not known but are consistent with changes to suspended sediment inflow in the rivers, reduced resuspension and/or reduced primary production associated with river influence. On the west coast of Northland, there is evidence of a general decrease in TSS including near the Hokianga Harbour System (in contrast with Pinkerton et al., 2022). Further south between Hokianga and Kaipara Harbours, there is predominant decreasing trends in TSS off the west

coast and it is not known if these are associated with the discharge of small rivers and streams, or are related to changes in the patterns of resuspension of benthic sediment or other causes.

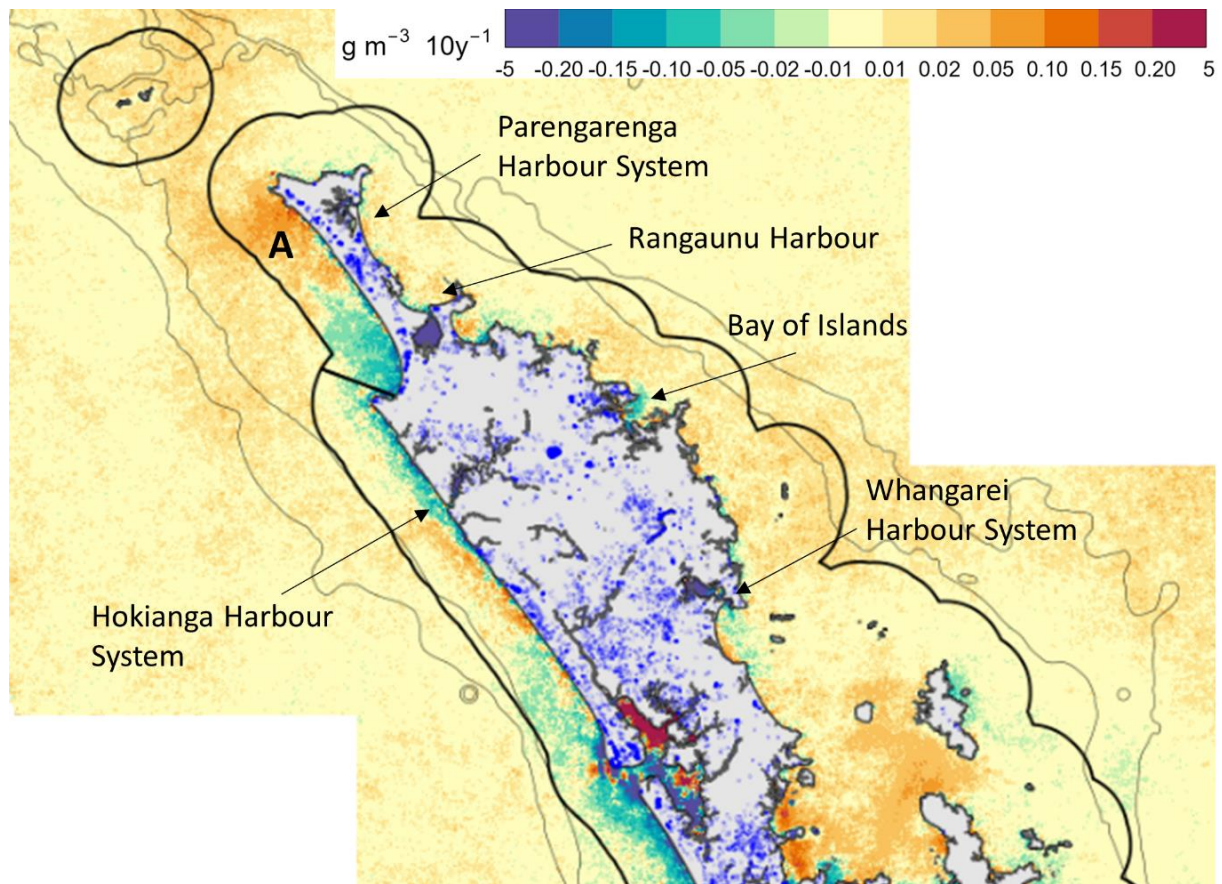


Figure 3-29: Northland: spatial trends in monthly anomalies of TSS (Total suspended solids) from MODIS-Aqua, 2002-2022. Sen-slope (linear) trends in TSS from deseasonalised monthly satellite estimates are shown as colours (red=increasing trends; green/purple=decreasing trends). All trends are shown, regardless of statistical significance. No data or no analysis (including land) is shown grey. Rivers/lakes/inland waters are shown bright blue and are not included in trend analysis. The contours show 250 m and 500 m depth. [Hauraki Gulf/Manukau/Kaipara](#)

There is evidence of areas of both increasing and decreasing TSS in the Kaipara Harbour, but TSS trends are predominantly (but not exclusively) decreasing at its mouth. Patterns of change in TSS in the satellite observations are consistent with increasing inflows of suspended sediment and/or nutrients into Kaipara Harbour and increasing deposition rates of sediment within the Harbour.

In the outer Hauraki Gulf, north of Waiheke Island (marked “A”, Figure 3-30), there are increasing trends in TSS, which are likely driven by increasing primary productivity. These extend into the coast on the west of the Hauraki Gulf either side of Whangaparaoa (perhaps associated with the Okura River and Puhoi Rivers).

South of Waiheke Island in most of the Firth of Thames, we see decreasing TSS, consistent with decreasing primary production (i.e., lower growth rates of phytoplankton) or decreasing suspended sediment. There are several small-scale areas of increasing TSS along parts of the south-western Tikapa Moana-O-Hauraki Firth of Thames which are suggestive of increasing input of suspended sediment from land run off. There are decreasing TSS trends in the south-eastern Firth of Thames likely associated with the Waihou/Piako Rivers. There is evidence of decreasing TSS in the Waitemata

Harbour System, in Manukau Harbour System and offshore to the west of Manukau. Further south, the satellite products suggest increasing sediment run off from the Waikato River, but no major increase in TSS outflow from the Whāingaroa Raglan, Aotea or Kawhia Harbour Systems.

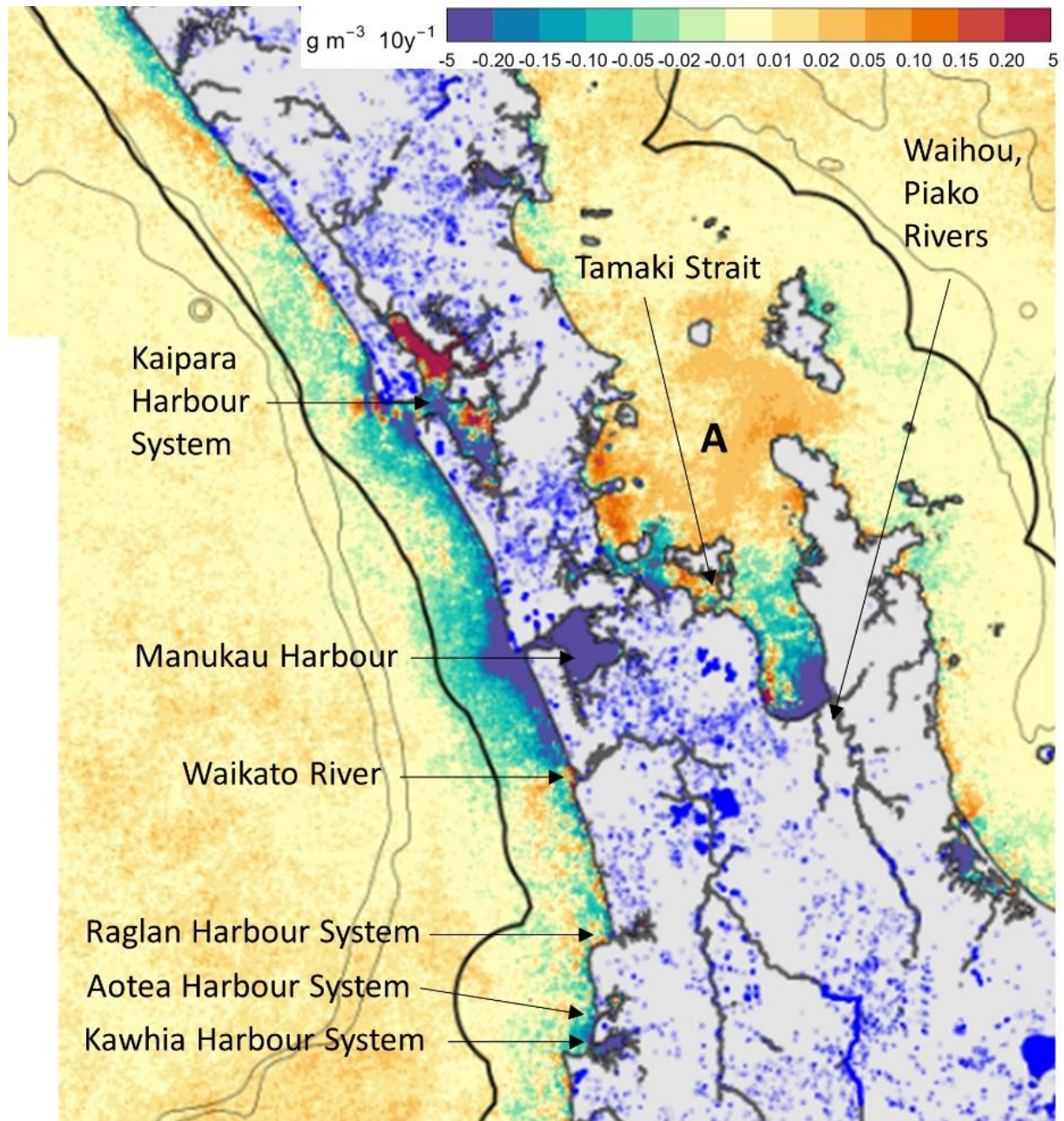


Figure 3-30: Hauraki Gulf/Manukau/Kaipara: spatial trends in monthly anomalies of TSS (Total suspended solids) from MODIS-Aqua, 2002-2022. See caption Figure 3-29 for more details.

Bay of Plenty/East Cape/Hawke Bay

The main situation through Bay of Plenty, around East Cape and through Te Matau-a-Māui Hawke Bay is decreasing trends in TSS between 2002-2022, consistent with lower primary productivity (less phytoplankton-derived particulate material in the water column) superimposed on which are smaller-scale (localised) increases in TSS consistent with increasing suspended sediment and/or increasing primary production. Areas of increasing TSS are seen close to the outflow of the Tauranga Harbour System (at least in some areas), associated with the Whakatane River (in Bay of Plenty), and

from the Waiapu River (eastern East Cape). No increase is seen near the and Uawa River. In Hawke Bay, there is generally decreasing broad-scale TSS, but evidence of increasing TSS (consistent with land-use drivers) from the Mohaka River. There are decreasing trends in TSS near the mouth of the Ahuriri Estuary and Ngaruroro River.

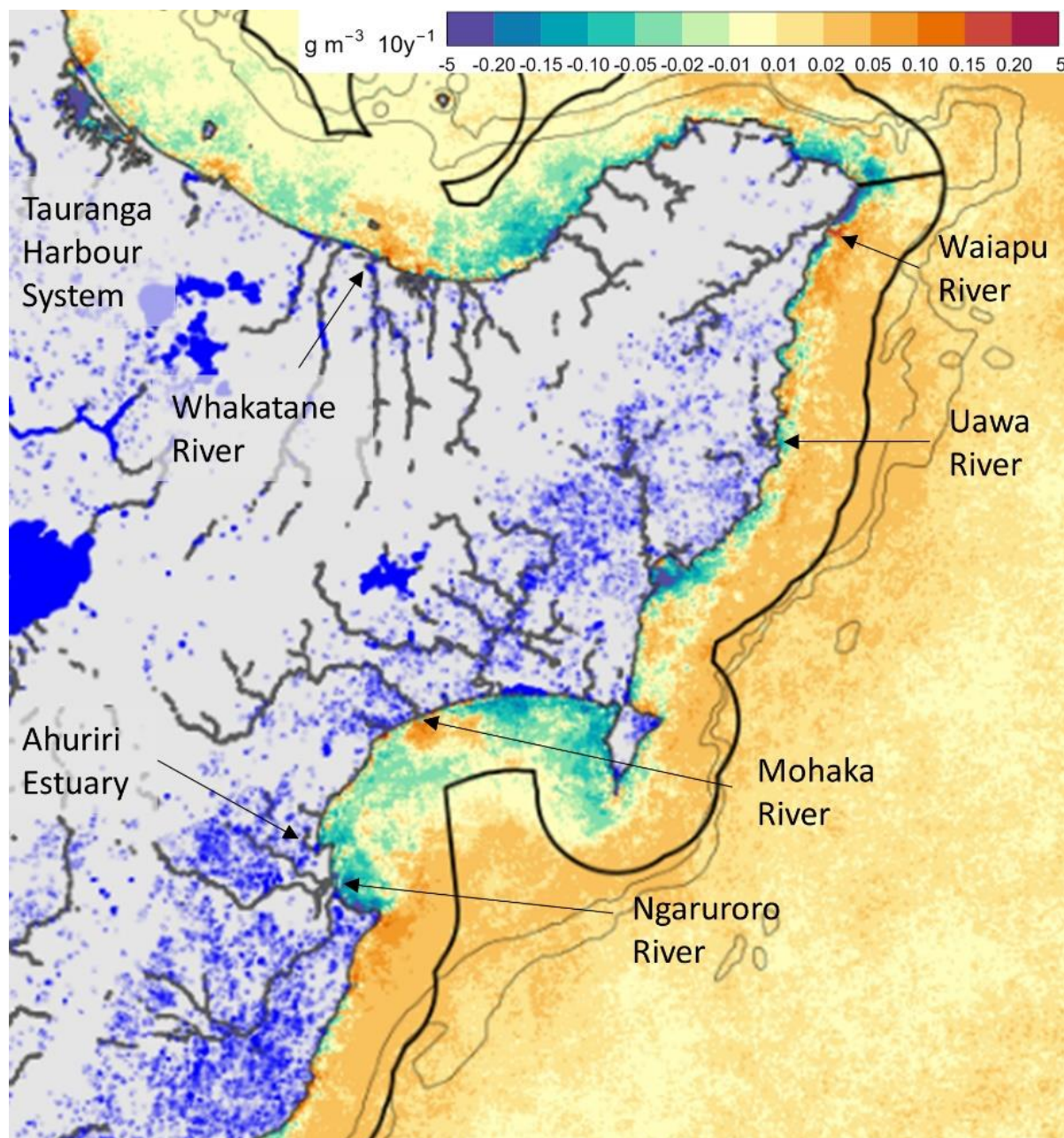


Figure 3-31: Bay of Plenty/East Cape/Hawke Bay: spatial trends in monthly anomalies of TSS (Total suspended solids) from MODIS-Aqua, 2002-2022. See caption Figure 3-29 for more details.

Wairarapa/South Taranaki Bight/Cook Strait/Marlborough

TSS decreased along most of the coastline of the lower North Island between 2002-2022, consistent with large-scale coastal warming leading to lower primary productivity (less phytoplankton-derived particulate material in the water column). There is evidence of decreasing TSS in Wellington Harbour. Increasing trends in TSS were observed close to the mouths of Kaipokonui Stream and Waingongoro River (both Taranaki region), and Patanui Stream (eastern Wairarapa).

Moving to South Island, there were increasing trends in TSS between 2002-2022 in Golden and Tasman Bays, which contrast with decreasing trends further offshore. The widespread nature of these increases in TSS suggest that increased phytoplankton production is likely the main driver, but there may be an increase in riverine input of particulate material and/or changes to mixing. Increased mixing (for example due to windier conditions) would lead to particulate material staying in suspension longer or benthic sediment being resuspended more often.

Increasing trends in TSS in Cloudy Bay and Clifford Bay were also observed and may be associated with the Wairau and Awatere Rivers. Trends in TSS in the Marlborough Sounds are unreliable because these areas are really too narrow to get reliable satellite estimates of TSS using base data of 500 m spatial resolution. Decreasing trends in TSS west of Farewell Spit are consistent with reduced phytoplankton production (which may be related to reduced upwelling or lower mixing). Small-scale increasing trends in TSS are observed at the outflow of the Little Wanganui River (but not Karamea River).

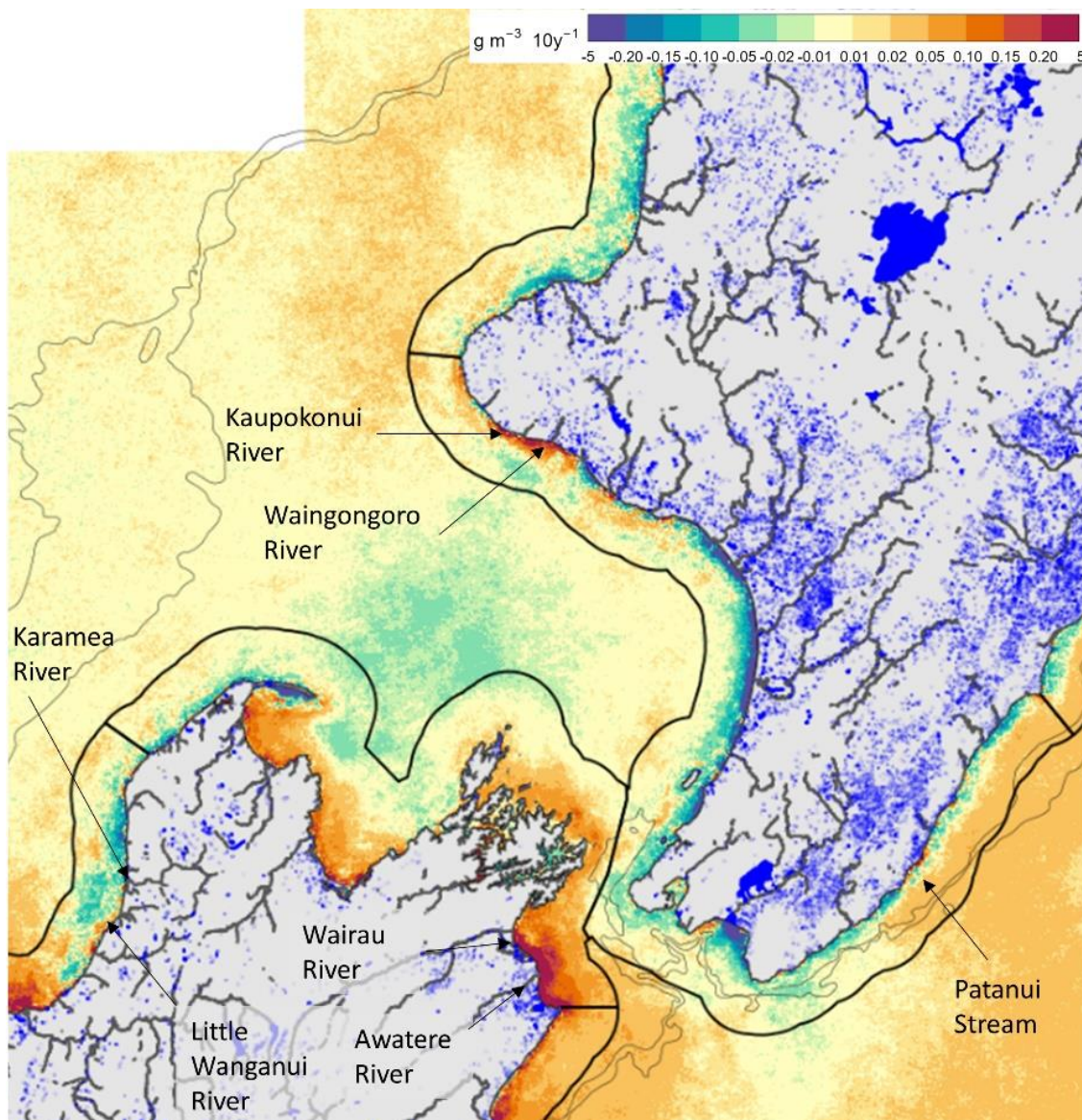


Figure 3-32: Wairarapa/South Taranaki Bight/Cook Strait/Marlborough: spatial trends in monthly anomalies of TSS (Total suspended solids) from MODIS-Aqua, 2002-2022. See caption Figure 3-29 for more details.

Canterbury/West Coast

On the west coast of South Island, the satellite products shows generally increasing trends in TSS, with some rather indistinct patches of decreasing trends. These patterns are consistent with large-scale coastal warming leading to increasing phytoplankton productivity and biomass, but also consistent with increasing suspended sediment run off from west coast rivers. For example, there is evidence of increasing trends in TSS close to the terminal reaches of rivers including the Mokihiui, Buller, Grey and Whataroa Rivers, but it's not always possible to resolve changes near to these rivers separately. On the east coast of South Island, there is a complex picture of increasing and decreasing trends in TSS in the satellite products but some trends at the river mouths are spatially distinct. For instance, there is evidence of increasing TSS offshore of rivers including the Waiiau Toa/Clarence, Hurunui, Rakaia, Rangitata and Waitaki Rivers.

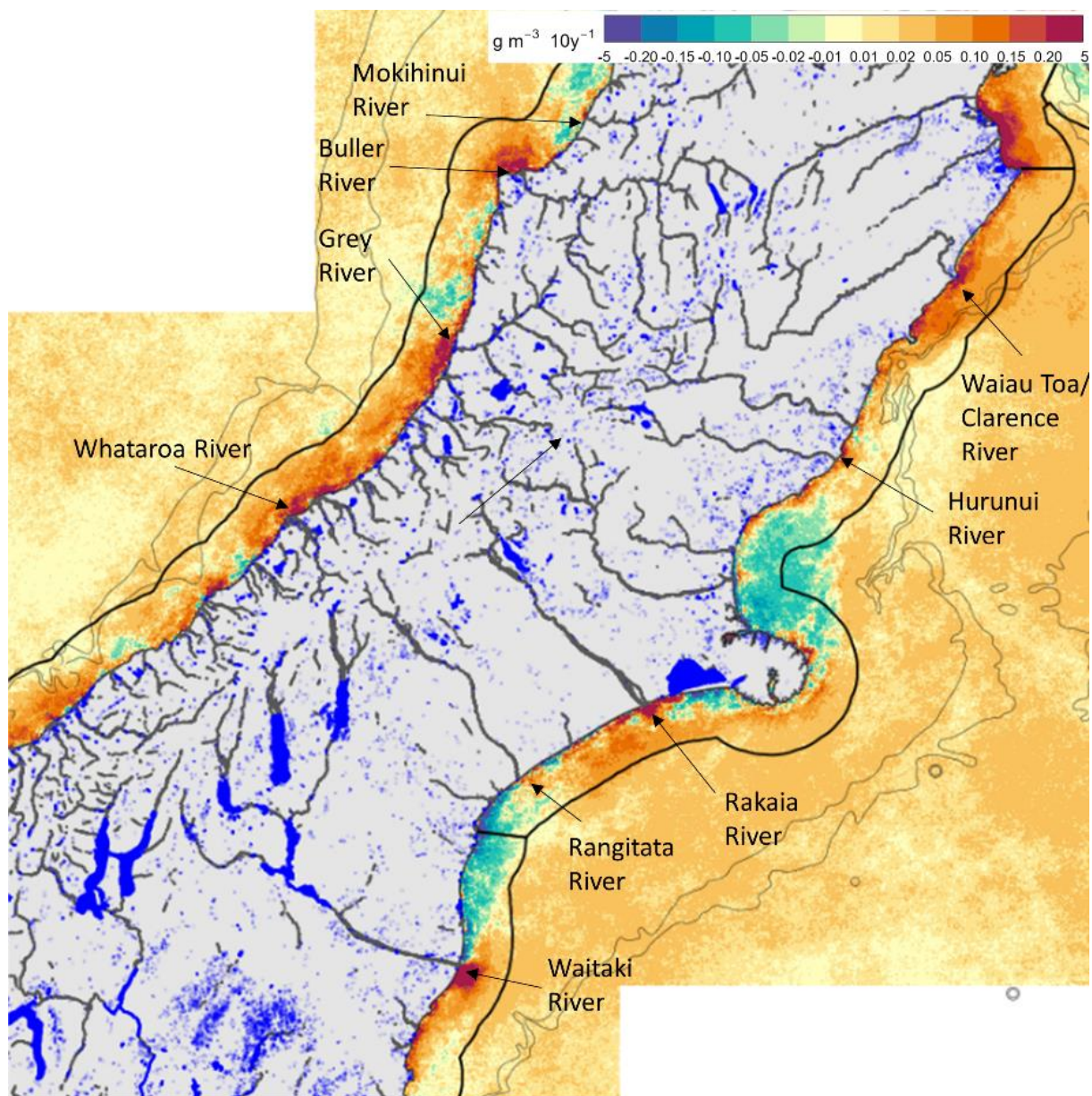


Figure 3-33: Canterbury/West Coast: spatial trends in monthly anomalies of TSS (Total suspended solids) from MODIS-Aqua, 2002-2022. See caption Figure 3-29 for more details. [Southland/Stewart Island](#)

Around the south of South Island between 2002-2022, the predominant pattern is increasing trends in TSS along the west and south coasts (including around Rakiura Stewart Island), and decreasing TSS trends on the east coast. TSS seems to have increased particularly near the mouth of Kakanui, Clutha and Waiau Rivers. The fiords are generally too narrow to get reliable TSS trends from satellite products.

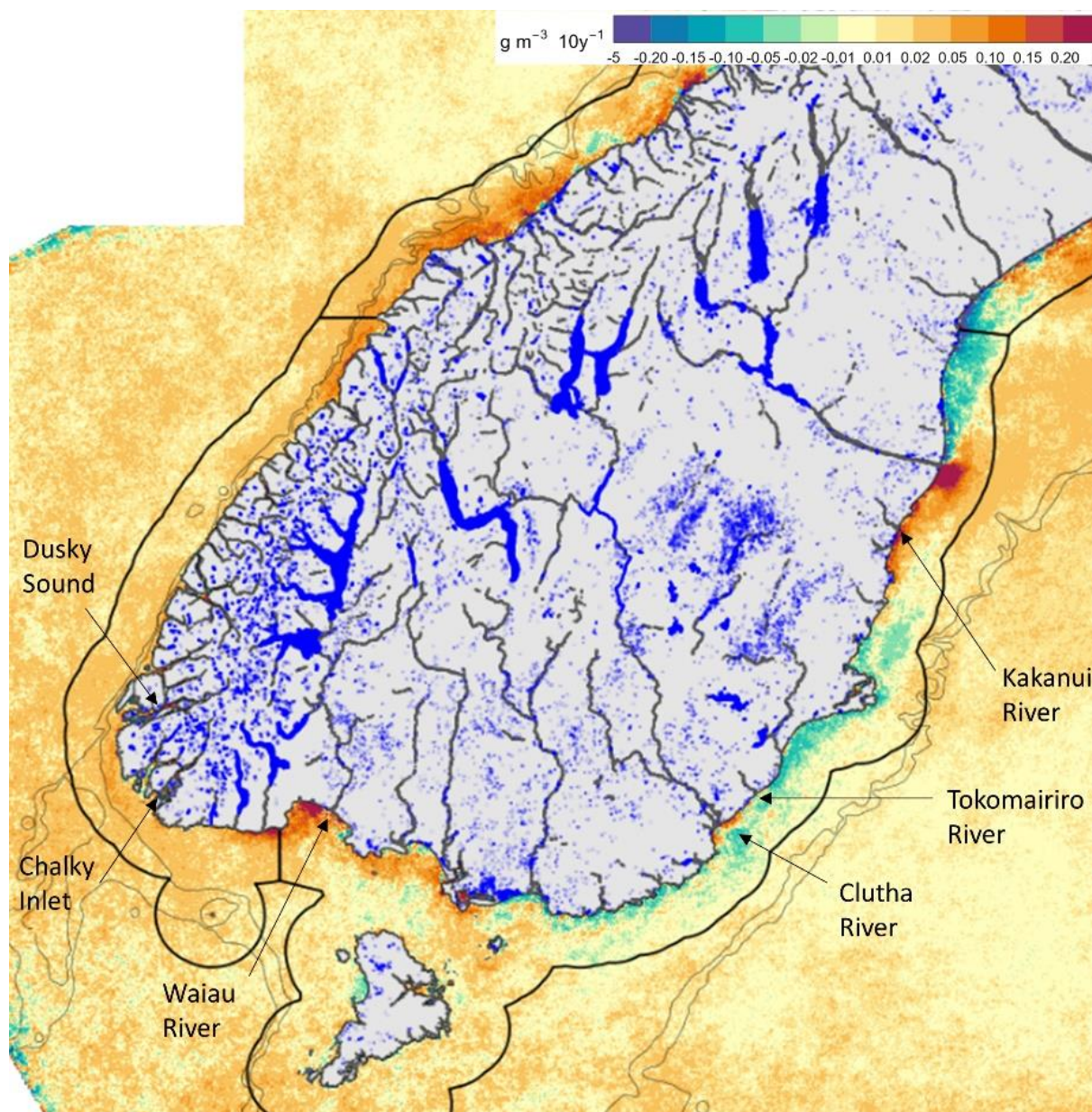


Figure 3-34: Southland/Stewart Island: spatial trends in monthly anomalies of TSS (Total suspended solids) from MODIS-Aqua, 2002-2022. See caption Figure 3-29 for more details. [Spatial correlations](#)

Correlations between monthly anomalies of SST and chl-a for each pixel in the coastal domain 2002-2023 (Figure 3-35a) were found to be predominantly negative and consistent with coastal warming leading to lower coastal chl-a (likely lower primary productivity). This relationship was much stronger around North Island than around South Island, and some coastal areas showed the opposite relationship (coastal warming correlated with increasing productivity): parts of Kaipara Harbour, Manukau Harbour, inner Hauraki Gulf (including Firth of Thames, Tamaki Strait), Tauranga Harbour, off Whāingaroa Raglan, Te Marlborough Sounds, inner Mohua Golden Bay and Te Tai-o-Aorere

Tasman Bays, and South Canterbury Bight. A positive relationship between SST and chl-a anomalies was also seen over a large offshore area south of Stewart Island and stretching west past Hautere Solander Island.

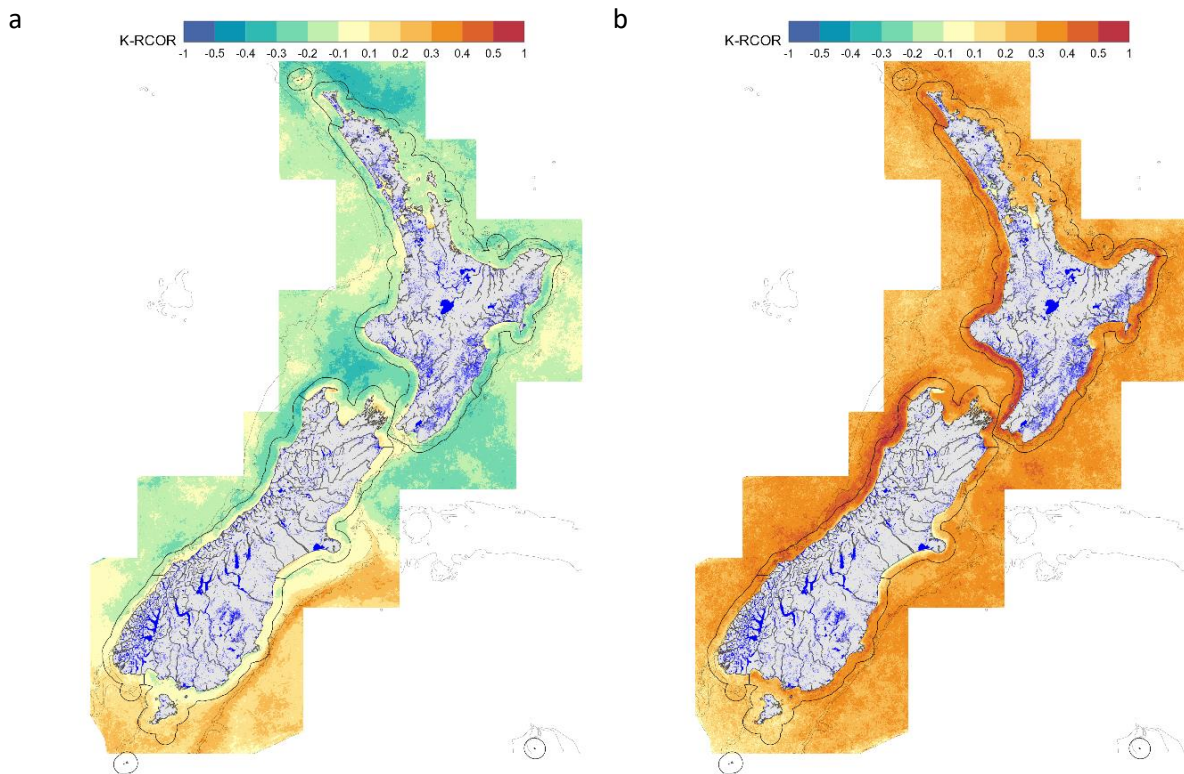


Figure 3-35: Coastal: Kendall correlation coefficient between monthly anomalies (2002–2023). a: Correlation between chl-a and SST; b: Correlation between chl-a and TSS. All data from NIWA SCENZ based on MODIS-Aqua. The 250 m and 500 m depth contours are also shown.

3.3 Marine heatwaves

3.3.1 Oceanic scale

Time-series for the New Zealand EEZ shows that the LOESS-fitted trends for all five MHW metrics (number of days, number of events, mean intensity, maximum intensity, and cumulative intensity) have been increasing since 2010 (Figure 3-36). Three MHW metrics (number of days, number of events, and cumulative intensity) have been generally increasing since 1981 but accelerating since about 2010. MHW cumulative intensity has also been increasing and accelerating in the four oceanic regions (Figure 3-37) with high confidence (“virtually certain” or “very likely”) positive linear trends (Table 3-9). The magnitudes of the trends are very high compared to the median values equating to relative increases of between +37.5 % median per decade in the Subantarctic Waters region and +107% per decade in the Tasman region. For the EEZ, the trend in the MHW cumulative metric is +55.1% of the median per decade. Most of the increase in the cumulative MHW intensity metric in the EEZ and in the four oceanic regions was associated with more MHW days and events rather than higher mean or maximum intensity (Appendix F).

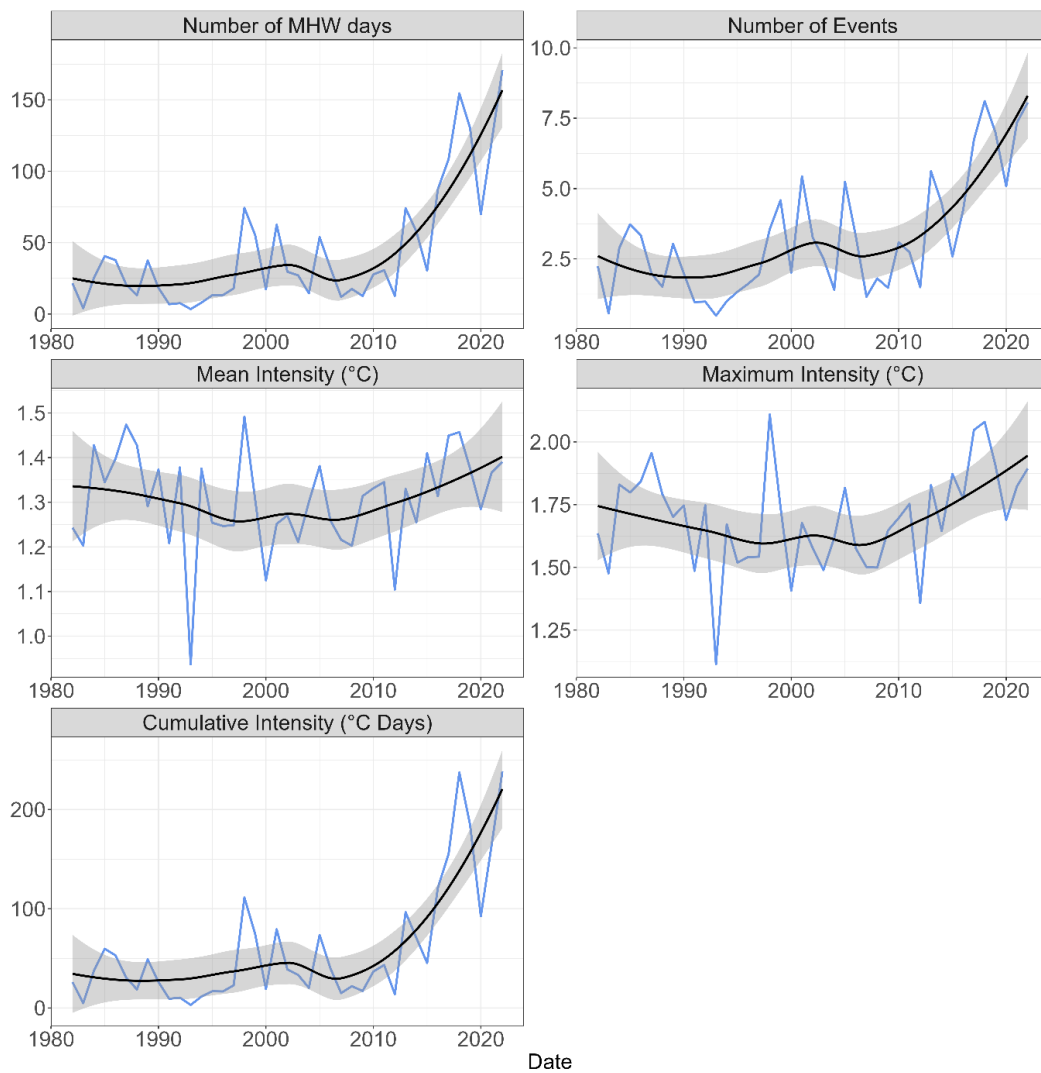


Figure 3-36: Ocean scale timeseries in marine heatwave metrics. Analysis was carried out between January 1982 and December 2022 (blue line) with the LOESS-fitted smooth (black) and confidence intervals (grey). The metrics are yearly, and grid-cell averaged.

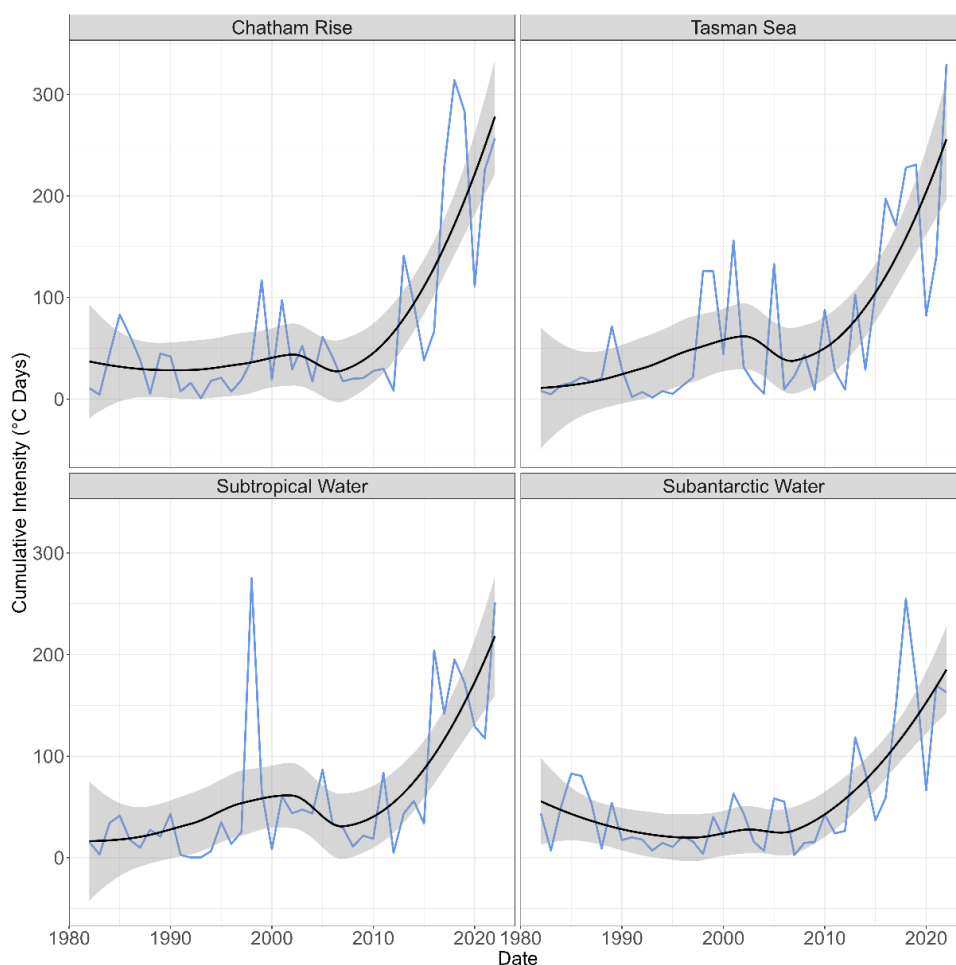


Figure 3-37: Ocean scale regional timeseries in marine heatwave cumulative intensity (in °C days). Analysis was carried out between January 1982 and December 2022 (blue line) with the LOESS-fitted smooth (black) and confidence intervals (grey). The metrics are yearly, and grid-cell averaged.

Table 3-9: Ocean scale regional linear trends for the marine heatwave cumulative intensity. The modified Mann Kendall (M-K) test is applied to the yearly-averaged metrics. Corrected Zc: Z statistic after variance correction. Mann Kendall significance is shown: *** p<0.001; ** p<0.01; * p<0.05.

Region	M-K Zc	M-K p	Sen slope (°C days decade ⁻¹)	Median (°C days)	Trend/median (% decade ⁻¹)	M-K significance	McBride likelihood
EEZ	3.32	9E-04	20.8	37.6	55.1	***	Virtually certain
Chatham	2.74	6E-03	20.1	38.2	52.7	**	Virtually certain
Tasman	4.83	1E-06	29.5	27.7	106.7	***	Virtually certain
Subtropical	4.82	1E-06	22.6	34.3	66.1	***	Virtually certain
Subantarctic	2.44	2E-02	15.0	40.1	37.5	*	Very likely

3.3.2 Coastal scale

Time-series of cumulative MHW intensity for all coastal regions have been increasing over the period of satellite observation (Figure 3-38) with “virtually certain” confidence in linear trend slopes (Table 3-10). As for the oceanic analysis, most of the increase in cumulative MHW intensity for the coastal regions is associated with more MHW days and events, though for many (but not all) of the coastal

regions there have been highly-significant increases in MHW mean intensity and MHW maximum intensity (Appendix G). The magnitudes of the trends in the cumulative MHW metric in the coastal regions are very high compared to the median values (Table 3-10), being between +50.0% of the median per decade in the North Cook Strait region and +89.5% per decade in the South Cook Strait region.

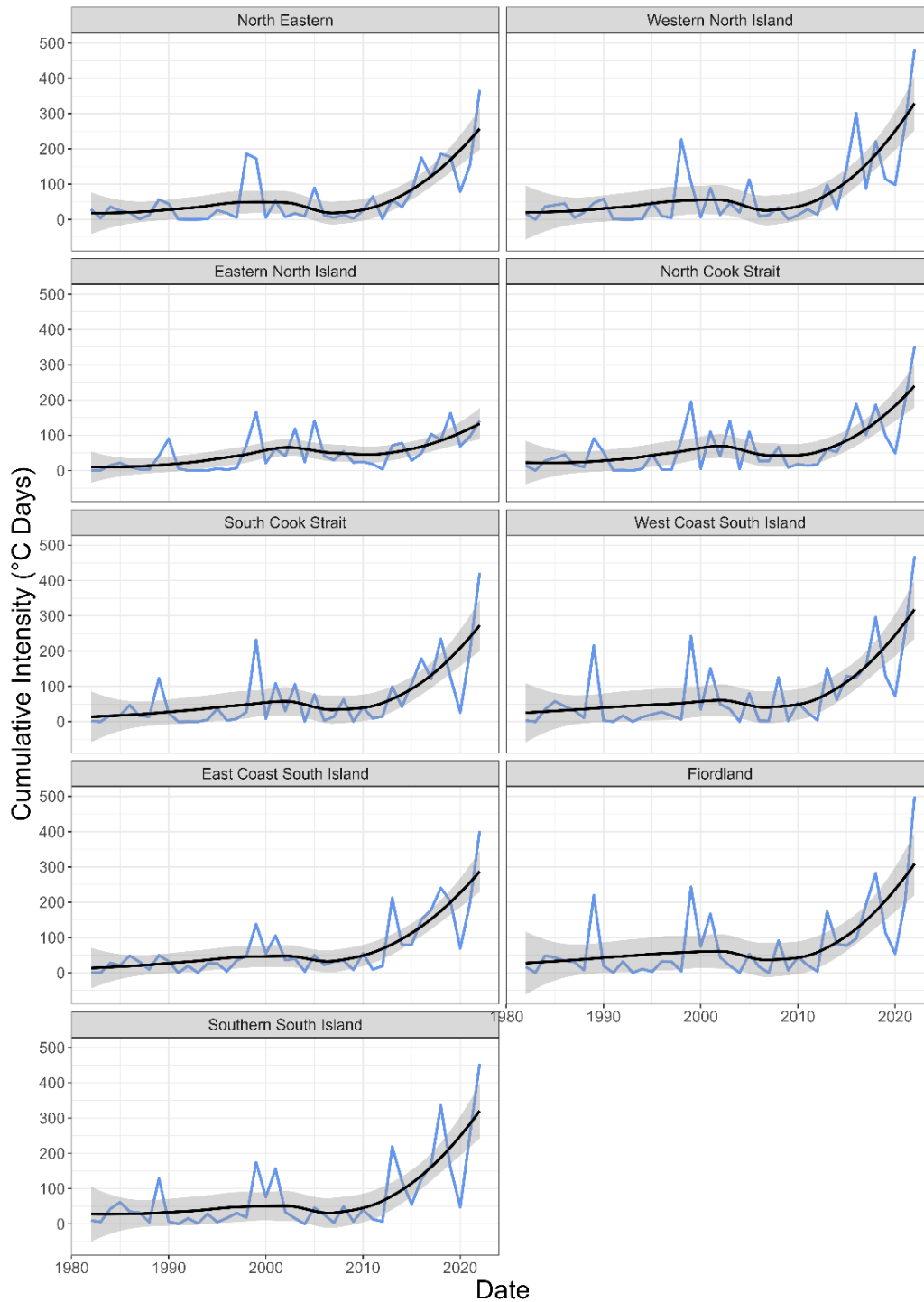


Figure 3-38: Coastal scale regional timeseries in marine heatwave cumulative intensity (in °C days). Analysis was carried out between January 1982 and December 2022 (blue line) with the LOESS-fitted smooth (black) and confidence intervals (grey). The metrics are yearly, and grid-cell averaged.

Table 3-10: Coastal scale regional linear trends for the cumulative intensity. The modified Mann Kendall (M-K) test was applied to the yearly-averaged metrics. Corrected Zc: Z statistic after variance correction. Mann Kendall Significance is shown: *** p<0.001; ** p<0.01; * p<0.05.

Descriptive region	M-K Zc	M-K p	Sen slope (°C days decade ⁻¹)	Median (°C days)	Trend/median (% decade ⁻¹)	M-K sig	McBride likelihood
North Eastern	3.03	2E-03	17.5	25.1	69.5	**	Virtually certain
Western North Island	3.96	1E-06	21.4	34.4	62.2	***	Virtually certain
Eastern North Island	9.41	5E-21	19.8	28.2	70.1	***	Virtually certain
North Cook Strait	4.33	2E-05	20.4	40.7	50.0	***	Virtually certain
South Cook Strait	4.27	2E-05	23.4	26.1	89.5	***	Virtually certain
West Coast South Island	3.96	7E-05	26.5	34.8	75.9	***	Virtually certain
East Coast South Island	3.76	2E-04	25.3	34.7	73.1	***	Virtually certain
Fiordland	3.69	2E-04	21.2	34.6	61.3	***	Virtually certain
Southern South Island	2.88	4E-03	20.8	33.5	62.1	**	Virtually certain

4 Discussion and conclusions

This report significantly enhances the suite of indicators used previously by the Ministry for the Environment and Statistics NZ to assess and communicate progress regarding ocean health and sustainable environmental management in New Zealand. By providing an up-to-date evaluation of the marine environment (from 2018), it offers valuable insights to inform decision-makers and stakeholders. Specifically, the report focuses on national indicators for sea surface temperature, primary productivity (via phytoplankton biomass – chlorophyll a), and introduces new indicators for total suspended solids and marine heatwave metrics.

4.1 Satellite product limitations and uncertainties

4.1.1 Spatial and temporal coverage

Satellite-based observation is a cost-effective solution to national-scale environmental monitoring but there are limitations and caveats to this approach, and this section summarises the effects of factors such as spatial resolution (ocean vs coastal scales), uncertainty, duration, and consistency associated with satellite measurements. Satellite remote sensing excels in capturing the variability of physical and biological processes across various scales in the surface ocean, outperforming other platforms (Figure 1-1, Dickey, 2006). For a comprehensive understanding of sampling coverage and observation representativeness in satellite remote sensing of coastal water quality in New Zealand, we refer to the results and detailed discussion provided in Pinkerton et al. (2022) and Gall et al. (2022) and summarised here.

The capability of Earth-orbiting satellites to observe the ocean directly is primarily limited by the day/night cycle and cloud cover, known to vary regionally, seasonally, in response to weather patterns, and transient and episodic events (Wilson & Jetz, 2016). Cloud cover can present a significant challenge in acquiring satellite data at less than about monthly time-scales. In New Zealand, the proportion of valid observations varies spatially and temporally, showing an inverse correlation with cloud cover (Figure 3-1, Figure 3-12). Despite this limitation, we anticipate that the majority of the ocean and coastal scale analysis will effectively capture long-term patterns and trends through monthly averaging. We have observed that the absence of observations for an entire month

due to cloud cover is uncommon, with such instances being rare and primarily limited to very low latitudes. However, there are systematic data gaps in chl-a in Subantarctic Water during winter due to low solar elevation, i.e., the sun is so low in the sky when the satellite is overhead that there is not enough light leaving the water to allow a reliable measurement of ocean colour. See Section 4.1.4 below for discussion of the effects of this.

As demonstrated in Aurin et al. (2013), the optimal scale (pixel size) for resolving spatial heterogeneity varies with distance from shore, about 0.5 km or smaller for inshore coastal areas containing river plumes, about 0.75 km over the continental shelf, and increasing to > 1.35 km for the open ocean. Given the diverse regions under study, it is necessary to conduct spatial scale analyses tailored to each area. In this regard, our ocean scale dataset (4 km) and coastal scale dataset (0.5 km) provide adequate coverage and resolution to meet these requirements.

4.1.2 Sea surface temperature

The primary sea surface temperature (SST) data used in this study is the OI-SST v2.1 dataset developed by Huang et al. (2021). This dataset combines observations from various platforms, including Advanced Very High-Resolution Radiometer (AVHRR) satellite data, ships, buoys, and Argo floats, on a regular global grid using optimal daily interpolation analysis. By interpolating and filling in spatial gaps, a comprehensive SST map is generated. The methodology includes bias adjustment of satellite and ship observations, referenced to buoys, to account for platform differences and sensor biases. OI-SST is a part of NOAA's Climate Data Records (CDRs), which are extensively vetted time series measurements meeting the standards set by the National Research Council (NRC)¹⁰. The use of OI-SST in previous New Zealand environmental reporting (Pinkerton et al., 2019) replaced the NIWA SST record, as it is a more reliable and widely used product for understanding global SST trends. However, it is noted that long-term, *in situ* measurement of SST is important in the nearshore environment and in estuaries as the occurrence of local scale MHWs can be decoupled from the surrounding shelf sea (Cook et al., 2022).

4.1.3 Net primary productivity

Phytoplankton, the photosynthetic organisms, and primary producers of aquatic ecosystems, play a crucial role in the carbon cycle by converting inorganic carbon into organic compounds using light energy. The concentration of chlorophyll-a (chl-a) is widely recognized as a proxy for phytoplankton biomass, as most phytoplankton contain this green pigment (e.g., Gordon et al., 1988). However, different phytoplankton species and physiological states can have varying chl-a contents, which can lead to differences between patterns of chl-a and measurements of phytoplankton biomass in terms of carbon concentration or numerical abundances. Nonetheless, satellite-observed chl-a remains the most used metric worldwide and in New Zealand for assessing trends in phytoplankton abundance (e.g., Dunstan et al., 2018 and Pinkerton et al., 2021).

The concentration of chl-a is (quantitatively) not the same as net primary productivity (NPP): the vertically-integrated rate of growth of phytoplankton after allowing for respiration (units of mg carbon m⁻² d⁻¹). Various methods exist for estimating NPP from satellite products (e.g., Platt & Sathyendranath, 1993; Antoine & Morel, 1996a,b; Behrenfeld & Falkowski, 1997; Behrenfeld et al., 2005; Westberry et al., 2008), and variations in chl-a typically account for the majority (~70%) of the variability in satellite-based NPP estimates. However, different NPP estimation methods can yield divergent results (Campbell et al., 2002), and the suitability of available satellite-based NPP estimates for the New Zealand region remains uncertain (Schwarz et al., 2008). When monitoring changes in marine productivity, the simpler and more comprehensible proxy of chl-a is often preferred over

satellite-based NPP estimates (Aiken et al., 2004; O'Reilly & Sherman, 2016), and we have followed this approach in the present report, as done previously (e.g., Pinkerton et al., 2019). It is reasonable to expect that, for the purpose of examining long-term trends and variability in ocean productivity around New Zealand, changes in satellite-observed chl-a are indicative of changes in NPP.

Typically, the majority of NPP in the ocean occurs through phytoplankton growth in the mixed-layer, although in some cases, phytoplankton may also thrive at the base of the mixed-layer, forming deep chlorophyll maxima (DCM - Campbell et al., 2002; Aiken et al., 2004). Both satellite estimates of chl-a and NPP do not provide information about the DCM. While prototype methods for detecting and estimating trends in DCM have been proposed (Pinkerton et al., 2021), these approaches have not yet been validated for the New Zealand region and are not utilized in the present report. It is anticipated that the contribution of the DCM to NPP will be relatively minor, about 15% (Campbell et al., 2002; Behrenfeld et al., 2005; Westberry et al., 2008).

4.1.4 Oceanic phytoplankton biomass (chlorophyll-a concentration)

Discrepancies in oceanic chl-a measurements obtained from different satellite sensors can be attributed to multiple factors including: variations in overpass times; sensor designs and performance (Brewin et al., 2014); spectral bands and processing algorithms for both in-water and atmospheric corrections (Pinkerton et al., 2005; Gordon, 1997); and sensor degradation rates over time (Barnes et al., 2001; Eplee et al., 2001). International research teams, exemplified by NASA, invest significant effort in mitigating these variations to establish consistent, long-term datasets for climate-related monitoring and research. Nonetheless, a persistent offset in chl-a measurements persists in the coastal ocean between the two CMEMS products and the SeaWiFS-MODIS-Aqua blended product (Figure D-1), likely due to algorithmic differences. While this discrepancy does not impact the conclusions of the present report, further investigation is warranted to understand this discrepancy.

The use of the SeaWiFS-MODIS-Aqua blended product for environmental reporting (Pinkerton et al., 2019), and in this report, has revealed the existence of systematic data gaps in chl-a primarily caused by low sun angles during the winter season in the Subantarctic region. These data gaps were accommodated as in previous work (e.g., Pinkerton et al., 2019) by excluding periods where less than 80% of data in a given region were available in a month. In the present report, we also compared trends from the SeaWiFS-MODIS product with two CMEMS products that have fewer systematic gaps. Differences between the SeaWiFS-MODIS trends and trends based on the two CMEMS products were small in all areas except the Subantarctic region. In this southern-most region, we found that the magnitude and confidence of trends in chl-a from SeaWiFS-MODIS were likely over-estimated because of the data gaps (Table 3-3). As suggested by Pinkerton et al. (2019), using optimal interpolation or other methods to fill in missing chl-a data in Subantarctic regions in winter months reduced biases in chl-a trend analysis and should be used in future work. In other ocean and coastal regions, the consistency of chl-a trends between SeaWiFS-MODIS and the two CMEMS products gave confidence in the present and previous analysis.

4.1.5 Coastal phytoplankton biomass (chlorophyll-a concentration)

The processing of ocean colour satellite data to estimate chl-a concentrations in the coastal zone, where suspended sediment and coloured dissolved organic matter (CDOM) can intermittently occur, presents ongoing scientific challenges, and remains an active area of research (Siegel et al., 2000; Babin et al., 2003b; Pinkerton et al., 2005, 2018). Uncertainties in satellite-derived chl-a estimates in the coastal zone can be significant and exhibit temporal and spatial variations. In the context of the New Zealand coastal zone, comparisons between *in situ* chl-a measurements (e.g., Dudley et al.,

2017; Dudley & Jones-Todd, 2018) have been conducted to assess data quality (Pinkerton et al., 2019). The study by Pinkerton et al. (2019) revealed that the SCENZ coastal chl-a product was less biased than open-ocean chl-a products due to its reduced sensitivity to sediment in the water. While further evaluation of coastal chl-a data quality and its impact on chl-a trends goes beyond the scope of the present report, it is noteworthy that the NIWA SCENZ CHL v4.0 anomaly product exhibits strong agreement with two new coastal chl-a data products from the European Copernicus project (Figure 3-21). This consistency provides robust support for the conclusions drawn in this report, as well as previous studies based on SCENZ chl-a data.

4.1.6 Total suspended solids

The estimation of gravimetric concentrations of TSS in the coastal zone using satellite data is rendered imprecise by changes to the type of particulate material in time and space, (Pinkerton et al., 2022). Optical backscatter, although suitable for remote estimation, exhibits a variable relationship with sediment concentration (g m^{-3}) across different regions and over time because it depends on the type and size of particles. For instance, a small concentration of fine particles like mud in suspension can generate higher backscatter values than a larger concentration of coarse sediment like sand. In this study, we have used a single relationship between TSS and backscatter across locations and time, so the trends and patterns in TSS strictly measure changes in optical backscatter rather than absolute gravimetric TSS. This approach is reasonable, as patterns in backscatter are highly likely to indicate changes in TSS *within a specific region*, which aligns with the primary objective of this report. Moreover, the agreement between TSS anomalies (SCENZ v3.0) and the CMEMS SPM product further reinforces the validity of our findings.

4.1.7 Marine heatwaves

Since the definition of MHWs by Hobday et al. (2016), the number of scientific studies reporting trends, drivers, and biological impacts of MHWs has rapidly increased (Smith et al., 2021; Sen Gupta et al., 2023). Globally, there is overwhelming evidence that MHWs are becoming longer, stronger, and more frequent (Holbrook et al., 2019; Thorat et al., 2022). Future projections also indicate that the increasing trend will continue to the point that many oceanic regions will reach a quasi-permanent MHW state by the end of the 21st century (Oliver et al., 2019; Behrens et al., 2022), given the use of a fixed baseline. There is currently a scientific debate whether using a shifting baseline would be more appropriate to characterise future MHWs (Sen Gupta, 2023; Amaya et al., 2023; Chiswell 2022). On one hand, a fixed baseline better reflects the escalating biological impacts from MHWs that are increasingly reported in the literature (Sen Gupta 2023; Smith et al., 2023). On the other hand, a shifting baseline can be useful to separate extreme heating events from the background warming of the ocean and the “new normal” (Amaya et al., 2023). In this report, we used the recommended fixed and 30-year-long baseline (1983-2012 period) as this is consistent with recent studies documenting trends in MHW metrics globally and around New Zealand (Marin et al., 2021; Thorat et al., 2022, Cook et al., 2022; Montie et al., 2023). This report built on the methods and results from global (Thorat et al., 2022) and New Zealand (Montie et al., 2023) coastal regions about trends in MHW metrics based on satellite products. More specifically, here we have extended the study of Montie et al. (2023) by a year (year 2022 included) as well as providing trends for four oceanic regions not covered by Montie et al. (2023). A synthesis of MHW results is given below in Sections 4.2 (ocean MHW) and 4.3 (coastal MHW).

4.2 Ocean scale synopsis

The ocean surface surrounding New Zealand has warmed over the last 40 years and this rate of warming has accelerated over the last 20 years. Between 1981 and 2023, the area-weighted mean rate of surface warming in the New Zealand Exclusive Economic Zone (EEZ) was +0.20°C per decade on average. This represents an increase from the previous rate of +0.15°C per decade observed between 1981 and 2018 (Pinkerton et al., 2019) and is 32% higher than the global average warming rate over the same period (though we note there are areas of the global ocean warming faster and slower than the New Zealand region). The 40-y ocean warming rates were found to be highest in the Subtropical and the Tasman regions (55% and 53% higher than the global average respectively), while the lowest 40-y warming rate was observed in the Subantarctic region (6% lower than the global average). Autumn and winter exhibited the strongest ocean warming patterns. The 20-y warming rate for the EEZ was nearly twice the 40-y warming rate, and 2.4 times as high as the global mean warming rate over the same period. The fastest warming area over the last 20 years was the Chatham region (more than 3 times higher than the mean global rate of warming over the same period) and the greatest acceleration in warming occurred in the Subantarctic region (3-fold increase from the 40-y to the 20-y analysis).

Multi-year climate variability, such as those associated with the El Niño-Southern Oscillation (ENSO), overlay the overall warming trend. Recent rapid warming has been attributed to the "triple dip" La Niña conditions persisting from 2020 to 2023. In the New Zealand region, La Niña events are typically linked to northeast wind anomalies, resulting in warmer air and surface ocean temperatures (Sutton & Roemmich, 2001). The recent La Niña conditions, coupled with blocking atmospheric high-pressure systems east of New Zealand, align with this pattern. Additionally, the reduced strength winds associated with La Niña have contributed to large-scale and persistent Marine Heatwaves (MHWs - Salinger et al., 2020; Salinger et al., 2023). These MHWs have played a role in the observed changes across the EEZ. Looking ahead, the strong warming trend since 2020 may alleviate to some extent with the establishment of El Niño conditions in the second half of 2023. El Niño conditions tend to associate with stronger and more frequent westerly winds in summer, and southerly winds in winter, and produce generally cooler sea temperature conditions around New Zealand.

Likely in response to warming and associated changes in nutrients and mean upper-ocean irradiance, positive trends in ocean primary productivity were found in specific regions around New Zealand and for the EEZ as a whole (+1.1% median chl-a per decade). Notably, the Subtropical Front, including the Chatham Rise, exhibited a significant increase in chl-a with a rate of +2.2% median chl-a per decade. Similarly, the Subantarctic water to the south of New Zealand showed a substantial positive trend in chl-a with a rate of +6.7% median chl-a per decade. In contrast, a decreasing trend in ocean productivity was indicated in the Subtropical Water to the northeast of New Zealand, with a rate of -2.2% median chl-a per decade.

The changes in oceanic primary productivity in response to warming were qualitatively consistent with alterations in the water column structure. Surface warming tends to result in a shallower mixed layer depth, leading to reduced surface nutrient availability. However, it also increases the mean mixed-layer irradiance, which influences primary production (Uddstrom & Oien, 1999; Murphy et al., 2001). These interactions between warming and the water column structure play a crucial role in shaping the productivity trends observed in different regions of the ocean around New Zealand.

In the New Zealand region, the correlation between chl-a and SST generally followed expected patterns, with negative correlations observed in Subtropical Water and the Tasman Sea, and positive

correlations in Subantarctic Water, consistent with previous analyses (Pinkerton et al., 2019). In Subtropical Water and the Tasman Sea, warmer surface water tended to result in lower chl-a levels and reduced primary productivity. Conversely, in Subantarctic Water, warmer surface water was associated with increased chl-a and likely increased primary productivity. However, the decreases in chl-a observed in the Subantarctic region since 2020, despite warming water there, suggest the possibility of a crossed threshold where further warming might further inhibit rather than enhance primary productivity. This anomalous change was seen in the SeaWiFS-MODIS product as well as the two CMEMS chl-a products that had fewer data gaps due to persistent clouds or low solar elevation. Further investigation is needed to understand the underlying mechanisms and potential inhibitory effects of continued warming on primary productivity in the Subantarctic region.

Small changes in mean environmental temperatures can have significant implications, leading to amplified occurrences of extreme climate events (van der Wiel & Bintanja, 2021). In the context of New Zealand's warming waters, there has been an observable increase in the frequency and intensity of MHWs (Thoral et al., 2022; Montie et al., 2023). Notably, MHW events are becoming more frequent, lasting for longer durations, and (to a lesser degree) exhibiting higher mean and maximum intensities. The rates of increase in some MHW metrics are substantial, with a trend of +55.1% of the median per decade observed in the cumulative MHW metric for the EEZ. The largest oceanic MHW trend, reaching +107% per decade, was recorded in the Tasman Sea region. The most intense year in terms of cumulative intensity was observed in 2022 in the Tasman Sea whereas cumulative intensity was maximum in 2018 for the Chatham Rise and the Subantarctic Waters, and in 1998 (although close to the 2022 level) for the Subtropical Waters. This suggests that the background warming of SST is not the sole driver of MHWs, and that the role of broader-scale oceanographic and meteorological events (like El-Nino) are to be included in future MHW forecast systems (Stevens et al., 2022). The impact of MHW on primary production generally aligned with the patterns described earlier: MHW events seem to have generally reduced primary productivity in northern waters while increasing productivity in Subantarctic waters (Montie et al., 2020). However, further comprehensive analysis specific to the New Zealand region is needed to fully understand these dynamics. The higher prevalence and intensity of MHW are highly likely to have increasingly profound effects on organisms and ecological communities in New Zealand's ocean, extending beyond phytoplankton.

4.3 Coastal scale synopsis

Nearly all coastal waters surrounding New Zealand have experienced “virtually certain” surface warming over the last 40 y, and the warming over this period was faster than the global mean warming rate by between 25% (North Eastern region) and 87% (East Coast South Island). In all but one region (Eastern North Island), coastal warming was substantially higher over the last 20 y than over the last 40 y, indicating widespread acceleration of warming. The acceleration of the coastal warming was particularly high around South Island, where 20-y warming rates in all coastal regions were more than three times the global warming rate over the same period, and nearly 3.7 times the global average in the Southern South Island region (Table 3-5).

MHWs in New Zealand's territorial waters have shown a substantial increase over the past four decades, particularly since 2010 consistent with the work of Montie et al. (2023). This upward trend is characterized by more frequent occurrences of events that last for extended durations. To a lesser degree, these MHW events have also exhibited slightly higher maximum and mean intensities, indicating that MHW are getting hotter. The cumulative MHW metric, which considers the combined effect of these factors, has significantly increased in coastal regions, with trends of +50.0% to +89.5% of the median per decade. Additionally, the year 2022 showed record values of cumulative intensity

in all coastal regions excluding the Eastern North Island. Particularly notable rates of increase in MHW have been observed in the southern Cook Strait and along the west coast of the South Island, suggesting that ecosystems in these areas are likely to face increasing impacts from MHW events. Compared to the global coastal zone, the New Zealand territorial seas are experiencing on average more MHW days (~150 vs ~75 days in 2021) and more MHW events (~7.5 vs 4 events), but do not see specifically higher mean intensity (~1.3 °C in 2021) or maximum intensity (~1.8 °C in 2021). As a result, the cumulative intensity of MHW around New Zealand was two times higher than for the global coastal zone on average (~200 vs ~100 °C days in 2021; Thorat et al., 2022).

Satellite remote sensing of water constituents such as phytoplankton and sediment in coastal areas is more complex compared to open ocean regions due to the proximity of land, which affects atmospheric correction, the diverse mixture of coloured materials present, such as phytoplankton, sediment, and colored dissolved organic matter (CDOM), and the greater temporal and spatial variability inherent to coastal systems. Consequently, uncertainties in coastal satellite products are higher, and accurately assessing this uncertainty remains a challenge. However, despite these difficulties, there is a notable level of consistency observed among coastal satellite products from different sources (SCENZ versus CMEMS), providing confidence in the robustness of the analyses and results and conclusions presented in this study.

Coastal primary productivity is influenced by a combination of oceanic conditions, such as cross-shelf intrusions, local coastal effects, including upwelling of deep nutrient-rich waters to the surface, and impacts of land runoff from river plume stormflows (Pinkerton et al., 2005, 2006). Nearshore areas generally exhibit higher chl-a concentrations, indicating greater phytoplankton abundance. As you move further offshore, chl-a tends to decrease. However, in the area to the east of Banks Peninsula at the extreme west of the Chatham Rise, chl-a is elevated. This is associated with the highly productive waters of the subtropical convergence zone.

Coastal warming along the lower North Island and South Island was generally associated with elevated chl-a, especially during winter, indicating increased phytoplankton biomass and primary productivity at the base of the food web. However, lower-than-normal productivity was noted along the west coast of the South Island during two MHW events: December 2017 to March 2018 and December 2022 to January 2023. Conversely, negative trends in chl-a (decreases in biomass and likely primary productivity) were observed along the west coast of Northland and the northeast shelf including the Hauraki Gulf, Coromandel, and the Bay of Plenty.

The same processes that transport nutrients from rivers to the coastal zone can also carry suspended sediment. In New Zealand's coastal zone, there is a growing recognition of the ecological importance of sediment (Lohrer et al., 2004; Townsend & Lohrer, 2015; Green et al., 2021), leading to the use of satellite remote sensing to investigate patterns and trends in TSS (e.g., Pinkerton et al., 2022). Expanding on this research, our study examined the complex mixture of increasing and decreasing trends in TSS between 2002 and 2023 within the New Zealand coastal zone. At the scale of territorial sea bio-regions, positive trends in TSS were prevalent, although often with low confidence, except for the Fiordland region exhibited a strong positive trend in TSS (+5.8% median TSS per decade). The observed TSS trends are likely influenced by a combination of factors, including modifications to sediment and nutrient input from rivers and estuaries, climate change effects (such as temperature, water-column structure, wave climate, and coastal currents), and other factors such as coastal development.

Changes to TSS arise from multiple causes. Alterations in climate-related weather patterns, such as shifts in cloud cover, affects rainfall patterns within land catchments resulting in changes in river plume stormflow events. Additionally, the projected erosion caused by rising sea levels acts in conjunction with shifts in waves and currents, affect the distribution and settling/resuspension of sediment in the coastal zone. The multiplicity of factors affecting TSS means that site-specific (local area) patterns and trends in TSS often deviate from the patterns observed at broader regional scales. While our study did not investigate the specific causes behind the changes in TSS observed in the satellite products, we conducted small-scale regional analyses to identify notable locations where TSS, and therefore water clarity, exhibited significant changes. These "hotspots" of TSS change can be used to prioritize focused *in situ* and modelling studies. By pinpointing rivers, estuaries, and harbours where evidence suggests a shift in TSS was plausibly due to altered material input from rivers, we provide valuable insights into the likely underlying processes driving these changes. The identification of these hotspots offers valuable guidance for future research to enhance our understanding of the dynamics and implications of TSS changes in the New Zealand coastal zone.

5 Recommendations

The following recommendations aim to guide future studies, policy-making processes, and management approaches toward achieving improved understanding and stewardship of New Zealand's ocean and coastal systems.

1. **Link satellite-observations to marine biological resource and hazards:** Satellite data and analyses provide a basis to assess the links between changes to ocean and coastal environments and biological resources (such as fisheries, kai moana and Taonga species, and protected species such as seabirds, marine mammals, and reptiles). Linking biological response to environmental variability and change will take long-term commitment to new multi-trophic level monitoring and research. These programs should encompass both open ocean and coastal waters.
2. **Commit to improving and validating the quality of satellite products in the New Zealand region (coasts and oceans):** Satellite observations offer long-term, large-area, low-cost resource but new, targeted, local bio-optical research is needed to improve robustness of the data. Specifically, local validation and local tuning of the global data to the New Zealand region will provide more useful and reliable satellite observations in the future. In parallel, users require better information on data quality to ensure that new applications use satellite information appropriately, with due consideration of its weaknesses as well as its strengths.
3. **Foster collaboration and data sharing:** New Zealand could make more and better use of satellite capability if there was enhanced collaboration and data-sharing among coastal ecologists, satellite data scientists, management agencies and Māori principles of kaitiakitanga. More effective collaboration would improve the accuracy, resolution, accessibility and of satellite products and lead to new applications for coastal management. Ongoing developments and enhancements to the NIWA SCENZ portal¹² streamline sharing of satellite products for New Zealand and enable timely analysis, empowering comprehensive exploration of patterns and monitoring of changes.

¹² <https://hub.arcgis.com/documents/NIWA::niwa-scen-z-ocean-colour-application-1/explore>

4. **Develop operational (near real-time) updating of satellite-based indicators:** Given the increasing pace of change in the ocean and coastal domains, more frequent updates of these satellite-based indicators would be useful. We recommend standardising the processing methodology and moving towards a more-frequent (and ideally semi-automated) update process. Exploring how to define baselines across multiple satellite and *in situ* time-series around New Zealand would be useful.
5. **Prioritise research efforts on coastal sediment:** Based on the identified coastal “hotspot” areas for TSS change, we recommend new field-based and integrative (i.e., *in situ* sampling, modelling, remote sensing, social and policy) research to understand the factors responsible for the observed changes in TSS over time. Knowledge of the interactions between land catchments, climate-related weather patterns, river/estuarine/continental shelf processes and human activities will improve the quality of satellite observations of TSS and advance their use to improve management of the effects of sediment on coastal ecosystems.
6. **Incorporate climate-aware responses into ocean and coastal resource management:** The information provided here could be used to adapt marine management strategies for the effects of climate variability/change including warming, MHW and changes to primary productivity and TSS. The information in the present report should be included alongside shifts in cloud cover, rainfall patterns, wave/current dynamics, sea-level rise when considering how to manage resources. For example some practical examples could include: changes to primary production in major fishing areas or juvenile fish locations may indicate potential trophic effects on stock productivity; trends in coastal primary productivity are relevant to aquaculture industry; marine reserves should be designed taking into account patterns of climate-driven oceanographic change; and patterns of change in TSS includes the effects of climate at the catchment scale.
7. **Expand work on MHW:** Investigate correlations between MHW metrics and primary production, chl-a, TSS; investigate trends in MHW metrics using a moving baseline; investigate seasonal drivers of MHWs around New Zealand; investigate trends in subsurface and bottom (seafloor) MHWs around New Zealand using models and in-situ time series (Argo floats, buoys); support a seasonal MHW forecast as recommended by Stevens et al. (2022); support long term biological monitoring across all coastal bioregions to better understand ecological impacts of MHWs.

6 Acknowledgements

This project received funding from the Ministry for the Environment (MfE) through NIWA project MFE22302. The research conducted aligns with the NIWA Oceans Programme "Structure and function of marine ecosystems," which is supported by the Ministry for Business, Innovation and Employment (MBIE). We extend our gratitude to Lance Morell from the Ministry for the Environment for his project leadership. We also thank David Bowden from NIWA for providing valuable comments on an earlier version of this work. We acknowledge the NASA Goddard Space Flight Center and OrbImage Inc. (USA) for providing access to SeaWiFS data, as well as the NASA MODIS project for their courtesy in sharing MODIS data. The European Space Agency (ESA) is acknowledged for granting access to MERIS data. All SeaWiFS, MODIS, and MERIS data were obtained through the NASA Ocean Biology Distributed Active Archive Center (OB.DAAC). We also acknowledge the National Oceanic and Atmospheric Administration (NOAA, USA) for providing access to AVHRR data. This study utilized data from the E.U. Copernicus Marine Service Information, specifically cmems obs-oc glo bgc-plankton my l3-multi-4km P1M/CHL, cmems obs-oc glo bgc-plankton my l4-gapfree-multi-4km P1D/CHL, and cmems obs-oc glo bgc-transp my l4-multi-4km P1M/SPM.

7 Glossary of abbreviations and terms

Algorithm	A mathematical recipe for combining data.
Annual anomaly	How different one year is from the average.
Atmospheric correction	The process of estimating ocean colour from the signal received by a radiometric sensor at the top of the atmosphere. This involves estimating and removing the signal which comes from the scattering of light in the atmosphere.
AVHRR	Advanced Very High-Resolution Radiometer (USA)
CDOM	Coloured dissolved organic matter
Chlorophyll-a / chl-a	The ubiquitous pigment in marine phytoplankton.
CMEMS	Copernicus Marine Environment Monitoring Service
Copernicus	The Copernicus Programme is the European Union's Earth Observation Programme ¹³
EEZ	Exclusive Economic Zone
GSM	Garver-Siegel-Maritorena
MERIS	Medium Resolution Imaging Spectro-radiometer (European Space Agency).
MLD	Mixed layer depth
MODIS	Moderate Resolution Imaging Spectro-radiometer (NASA). There are two MODIS sensors, Terra and Aqua.
Monthly anomaly	How different one month is from the average (e.g., the difference between January 2000 and an average January).
MUMM	Scientific Service Management Unit of the Mathematical Model of the North Sea
NASA	National Aeronautics and Space Administration of the USA
NOAA	National Oceanic and Atmospheric Administration of the USA
NPP	Net primary productivity (rates of growth of phytoplankton)
NZTM	New Zealand Transverse Mercator Eastings and Northings
PAR	Photosynthetically active radiation (light between 400 and 700 nm)
QAA	Quasi-Analytical Algorithm
Radiometric	Pertaining to the measurement of the intensity of light.
SeaWiFS	Sea-viewing Wide Field-of-view Sensor (OrbImage/NASA)
SSIF	Strategic Science Investment Fund
VIIRS	Visible Infrared Imaging Radiometer Suite (VIIRS) (USA)

¹³ <https://marine.copernicus.eu/>

8 References

- Aiken, J, Moore, G.F, Holligan, P.M. (2004) Remote sensing of oceanic biology in relation to global climate change. *Journal of Phycology*, 28(5): 579-590.
- Airoidi, L. (2003) The effects of sedimentation on rocky coast assemblages. *Oceanography and Marine Biology*, (Annual Review) 41: 161–236.
- Amaya, D, Jacox, M.G, Fewings, M.R, Saba, V.S, Stuecker, M.F, Rykaczewski, R.R., Ross, A.C., Stock, C.A., Capotondi, A., Petrik, C.M., Bograd, S.J., Alexander, M.A., Cheng, W., Hermann, A.J., Kearney, K.A., Powell, B.S. (2023) Marine heatwaves need clear definitions so coastal communities can adapt. *Nature*, 616(7955), 29-32.
- Antoine, D, Morel, A. (1996a) Oceanic primary production 1: Adaptation of a spectral light-photosynthesis model in view of application to satellite chlorophyll observations. *Global Biogeochemical Cycles*, 10: 43-55.
- Antoine, D, Morel, A. (1996b) Oceanic primary production 2: Estimation of global scale from satellite (Coastal Zone Color Scanner) chlorophyll. *Global Biogeochemical Cycles*, 10: 57-69.
- Aurin, D, Mannino, A, Franz, B. (2013) Spatially resolving ocean color and sediment dispersion in river plumes, coastal systems, and continental shelf waters. *Remote Sensing of Environment*, 137: 212–225.
- Babin, M, Stramski, D, Ferrari, G.M, Claustre, H, Bricaud, A, Obolensky, G, Hoepffner, N. (2003) Variations in the light absorption coefficients of phytoplankton, nonalgal particles, and dissolved organic matter in coastal waters around Europe. *Journal of Geophysical Research*, 108(C7): 1-20.
- Banzon, V, Smith, T.M, Chin, T.M, Liu, C, Hankins, W.A (2016) long-term record of blended satellite and in situ sea-surface temperature for climate monitoring, modeling and environmental studies. *Earth Syst. Sci. Data*, 8(1): 165–176 (2016).
- Barnes, R.A, Eplee, R.E, Schmidt, M, Patt, F.S, McClain, C.R. Calibration of SeaWiFS. (2001) 1: Direct techniques. *Applied Optics*, 40: 6682-6700.
- Behrenfeld, M.J, Boss, E, Siegel, D.A, Shea, D.M. (2005) Carbon-based ocean productivity and phytoplankton physiology from space. *Global Biogeochemical Cycles*, 19(1): GB1006.
- Behrenfeld, M.J, Falkowski, P.G. (1997) Photosynthetic rates derived from satellite-based chlorophyll concentration. *Limnology and Oceanography*, 42: 1-20.
- Behrens, E, Rickard, G, Rosier, S, Williams, J, Morgenstern, O, Stone, D. (2022) Projections of Future Marine Heatwaves for the Oceans Around New Zealand Using New Zealand's Earth System Model. *Frontiers in Climate*, 19.
- Bissett, W.P, Patch, J.S, Carder, K.L, Lee, Z.P. (1997) Pigment packaging and Chl a-specific absorption in high-light oceanic waters. *Limnology and Oceanography*, 42(5): 961–968.

- Brewin, R.J.W, Mélin, F, Sathyendranath, S, Steinmetz, F, Chuprin, A, Grant, M. (2014) On the temporal consistency of chlorophyll products derived from three ocean-colour sensors. *ISPRS Journal of Photogrammetry and Remote Sensing*, 97: 171–184.
- Bricaud, A, Babin, M, Morel, A, Claustre, H. (1995) Variability in the chlorophyll-specific absorption coefficients of natural phytoplankton: analysis and parametrisation. *Journal of Geophysical Research*, 100: 13321–13332.
- Burns, N, Bryers, G, Bowman, E. (2000) Protocol for monitoring trophic levels of New Zealand lakes and reservoirs., Lakes Consulting Client Report: 99/2 for MfE, March 2000. Available (July 2023): <https://environment.govt.nz/assets/Publications/Files/Protocol-for-monitoring-trophic-levels-of-New-Zealand-lakes-and-reservoirs.pdf>
- Campbell, J, with 22 co-authors (2002) Comparison of algorithms for estimating ocean primary production from surface chlorophyll, temperature, and irradiance. *Global Biogeochemical Cycles*, 16(3): 9.1-9.15.
- Charlson, R, Lovelock, J, Andreae, M. et al. (1987) Oceanic phytoplankton, atmospheric sulphur, cloud albedo and climate. *Nature*, 326, 655–661. <https://doi.org/10.1038/326655a0>
- Chiswell, S.M. (2022) Global Trends in Marine Heatwaves and Cold Spells: The Impacts of Fixed Versus Changing Baselines. *Journal of Geophysical Research: Oceans*, 127(10): e2022JC018757.
- Cleveland, W.S, Devlin, S.J. (1988) Locally Weighted Regression: An Approach to Regression Analysis by Local Fitting. *Journal of the American Statistical Association*, 83(403): 596-610.
- Cloern, J.E, Foster, S, Kleckner, A. (2014) Phytoplankton primary production in the world's estuarine-coastal ecosystems. *Biogeosciences*, 11(9): 2477-2501.
- Cook, F, Smith, R.O, Roughan, M, Cullen, N.J, Shears, N, Bowen, M. (2022) Marine heatwaves in shallow coastal ecosystems are coupled with the atmosphere: Insights from half a century of daily in situ temperature records. *Frontiers in Climate*, 4: 1012022.
- Copernicus (2022) Copernicus Marine Product User Manual for Ocean Colour Products. Eds: S. Colella; E. Böhm; C. Cesarini; P. Garnesson; J. Netting; B. Calton, November 2022. Pp 124. Available from: <https://catalogue.marine.copernicus.eu/documents/PUM/CMEMS-OC-PUM.pdf>
- Davies-Colley, R.J, Ballantine, D.J, Elliott, A.H, Swales, A, Hughes, A.O, Gall, M.P. (2014) Light attenuation – a more effective basis for the management of fine suspended sediment than mass concentration? *Water Science Technology*, 69: 1867–1874. doi:10.2166/wst.2014.096.
- Department of Conservation and Ministry of Fisheries (2011) Coastal marine habitats and marine protected areas in the New Zealand Territorial Sea: a broad scale gap analysis. Wellington, New Zealand. Available (June 2023): Coastal marine habitats and marine protected areas in the New Zealand Territorial Sea : a broad scale gap analysis (doc.govt.nz)

- Dickey, T, Lewis, M, Chang, G. (2006) Optical oceanography: Recent advances and future directions using global remote sensing and in situ observations. *Reviews of Geophysics*, 44(1), <https://doi.org/10.1029/2003RG000148>
- Dudley, B, Jones-Todd, C. (2018) New Zealand Coastal Water Quality Assessment Update. *NIWA Client Report 2018096CH* for Ministry for the Environment, May 2018. Pp 34.
- Dudley, B, Zeldis, J, Burge, O. (2017). New Zealand Coastal Water Quality Assessment. *NIWA Client Report 2016093CH* prepared for Ministry for the Environment. February 2017. Pp 84.
- Dunstan, P.K, Foster, S.D, King, E, Risbey, J, O’Kane, T.J, Monselesan, D, Hobday, A.J, Hartog, J.R, Thompson, P.A. (2018) Global patterns of change and variation in sea surface temperature and chlorophyll a. *Scientific Reports*, 8: 14624. doi.org/10.1038/s41598-018-33057-y
- Ellis, J, Nicholls, P., Craggs, R., Hofstra, D., Hewitt, J. (2004) Effect of terrigenous sedimentation on mangrove physiology and associated macrobenthic communities. *Marine Ecology Progress Series*, 270: 71-82.
- Eplee, R.E, Robinson, W.D, Bailey, S.W, Clark, D.K, Werdell, P.J, Wang, M, Barnes, R.A, McClain, C.R. Calibration of SeaWiFS (2001) 2: Vicarious techniques. *Applied Optics*, 40: 6701-6718.
- Feng, J.F, L. Zhu (2012) Changing trends and relationship between global ocean chlorophyll and sea surface temperature. *Procedia Environmental Sciences*, 13: 626-631.
- Franz, B.A, Werdell, P.J, Meister, G, Kwiatkowska, E.J, Bailey, S.W, Ahmad, Z, McClain, C.R. (2006) MODIS land bands for ocean remote sensing applications. Proc Ocean Optics XVIII, Montreal, Canada, 9-13 October 2006.
- Friedland, K.D, Stock, C, Drinkwater, K.F, Link, J.S, Leaf, R.T, Shank, B.V, Rose, J.M, Pilskalns, C.H, Fogarty, M.J. (2012) Pathways between primary production and fisheries yields of Large Marine Ecosystems. *PLoS One*, 7(1): e28945. [doi:10.1371/journal.pone.0028945](https://doi.org/10.1371/journal.pone.0028945)
- Frolicher, T.L., Fischer, E.M, Gruber, N. (2018) Marine heatwaves under global warming. *Nature*, 560: 360–364. doi.org/10.1038/s41586-018-0383-9.
- Gall, M.P, Pinkerton, M.H, Steinmetz, T, Wood, S. (2022) Satellite remote sensing of coastal water quality in New Zealand. *New Zealand Journal of Marine and Freshwater Research*, 56:3: 585-616, DOI: 10.1080/00288330.2022.2113410
- Garnesson, P, Mangin, A, Fanton d’Andon, O, Demaria, J, Bretagnon, M. (2019). The CMEMS GlobColour chlorophyll a product based on satellite observation: Multi-sensor merging and flagging strategies. *Ocean Science*, 15(3), 819-830.
- Garver, S.A, Siegel, D.A. (1997) Inherent optical property inversion of ocean color spectra and its biogeochemical interpretation: I. Time series from the Sargasso Sea. *Journal of Geophysical Research*, 102: 18,607-18,625.
- Gordon, H.R. (1997) Atmospheric correction of ocean colour imagery in the Earth Observing system era. *Journal of Geophysical Research*, 102, 17081-17106.

- Gordon, H.R, Brown, O.B, Evans, R.H, Brown, J.W, Smith, R.C, Baker, K.S, Clark, D.K. (1988) A semianalytic radiance model of ocean colour. *Journal of Geophysical Research*, 93(D9): 10909-10924.
- Green, M.O, Walker, J, Nicol, S. (2021) Steering our waka through turbid waters: research priorities over the next 5 years for sediments in the coastal marine area of Aotearoa New Zealand. Prepared for the Department of Conservation by RMA Science, Hamilton: 69.
- Hamed, K.H, Rao, A.R. (1997) A modified Mann-Kendall trend test for autocorrelated data. *Journal of Hydrology*, 204(1-4): 182–96. doi:10.1016/s0022-1694(97)00125-x.
- Hipel, K.W, McLeod, A.I. (1994) Time Series Modelling of Water Resources and Environmental Systems. Elsevier, Amsterdam.
- Hobday, A.J, Alexander, L.V, Perkins, S.E, Smale, D.A, Straub, S.C, Oliver, E.C., ... Wernberg, T. (2016). A hierarchical approach to defining marine heatwaves. *Progress in Oceanography*, 141: 227-238.
- Hobday, A.J, Oliver, E.C.J, Sen Gupta, A, Benthuyesen, J.A, Burrows, M.T, Donat, M.G, Holbrook, N.J, Moore, P.J, Thomsen, M.S, Wernberg, T, Smale, D.A. (2018) Categorizing and naming marine heatwaves. *Oceanography*, 31:162–173.
- Holbrook, N.J, Scannell, H.A, Sen Gupta, A, Benthuyesen, J.A, Feng, M, Oliver, E.C. et al. (2019). A global assessment of marine heatwaves and their drivers. *Nature communications*, 10(1): 2624.
- Hooker, S.B, Esaias, W.E, Feldman, G.C, Gregg, W.W, McClain, C.R. (1992) An overview of SeaWiFS and ocean colour. NASA Technical Memorandum 194566 (SeaWiFS Technical Report Series) Volume 1, NASA Goddard Space Flight Center, Maryland, USA. 24 p.
- Huang, B, Liu, C, Banzon, V, Freeman, E, Graham, G, Hankins, B, Smith, T, Zhang, H.M. (2021). Improvements of the daily optimum interpolation sea surface temperature (DOISST) version 2.1. *Journal of Climate*, 34: 2923–2939.
- IOCCG, (2008) Why Ocean Colour? The Societal Benefits of Ocean Colour Technology, eds Platt T, et al. Reports of the International Ocean-Colour Coordinating Group, No. 7 (IOCCG , Dartmouth, NS, Canada), 83–102.
- Kendall, M.G. (1975) Rank Correlation Methods. Griffin, London, UK.
- Kirk, J.T.O. (2011) Light and photosynthesis in aquatic ecosystems. Cambridge University Press, Cambridge: 649.
- Kumar, G.S, Prakash, S, Ravichandran, M, Narayana, A.C. (2016) Trends and relationship between chlorophyll-a and sea surface temperature in the central equatorial Indian Ocean. *Remote Sensing Letters*, 7: 1093-1101.
- Larned, S, Snelder, T, Unwin, M, McBride, G.B. (2016) Water quality state and trends in New Zealand rivers, 2004–2013. *New Zealand Journal of Marine and Freshwater Research*, 50: 389–417. doi:10.1080/00288330.2016.1150309

- Lavender, S.J, Pinkerton, M.H, Moore, G.F, Aiken, J, Blondeau-Patissier, D. (2005) Modification to the atmospheric correction of SeaWiFS ocean colour images over turbid waters. *Continental Shelf Research*, 25(4): 539-555.
- Lee, Z.P, Carder, K.L, Arnone, R.A. (2002) Deriving inherent optical properties from water color: A multi- band quasi-analytical algorithm for optically deep waters. *Applied Optics*, 41: 5755- 5772.
- Lee, Z.P, Lubac, B, Werdell, J, Arnone, R. (2009) An Update of the Quasi-Analytical Algorithm (QAA v5). Open file online at: [http://www.ioccg.org/groups/Software/OCA/QAA v5.pdf](http://www.ioccg.org/groups/Software/OCA/QAA_v5.pdf), 9 pp., 2009.
- LINZ (2017). New Zealand transverse mercator grid (NZTM2000). <https://www.linz.govt.nz/data/geodetic-system/datums-projections-and-heights/projections/new-zealand-transverse-mercator-2000> [Accessed 1/10/2020]
- Lohrer, A.M, Berkenbusch, K, Thrush, S.F, et al. (2004) Terrestrially derived sediment: how much is too much for marine microbenthic communities? *Marine Ecology Progress Series*, 273: 121–38.
- Makowski, D, Ben-Shachar, M.S, Chen, S.H.A, Lüdecke, D. (2019) Indices of Effect Existence and Significance in the Bayesian Framework. *Frontiers in Psychology*, 10:2767. doi: 10.3389/fpsyg.2019.02767.
- Mann, H.B. (1945) Nonparametric tests against trend. *Econometrica*, 13: 245-259.
- Marin, M, Feng, M, Phillips, H.E, Bindoff, N.L. (2021). A global, multiproduct analysis of coastal marine heatwaves: Distribution, characteristics, and long-term trends. *Journal of Geophysical Research: Oceans*, 126(2): e2020JC016708.
- McBride, G.B. (2005) Using statistical methods for water quality management: Issues, problems, and solutions. John Wiley & Sons, New York. doi:10.1002/0471733199.
- McBride, G.B. (2019) Has Water Quality Improved or Been Maintained? A Quantitative Assessment Procedure. *Journal of Environmental Quality*, 48: 412–420. doi:10.2134/jeq2018.03.0101.
- McBride, G.B, Cole, R, Westbrooke, I, Jowett, I.G. (2014) Assessing environmentally significant effects: A better strength-of-evidence than a single P value? *Environmental Monitoring and Assessment*, 186(5): 2729–2740. doi:10.1007/s10661-013-3574-8.
- McKnight, D.G. (1969) A recent, possible catastrophic burial in a marine molluscan community. *New Zealand Journal Marine and Freshwater Research*, 3: 177–79.
- MfE (2018) A Guide to attributes in Appendix 2 of the national policy statement for freshwater management (as amended 2017). Ministry for the Environment Wellington.
- Miller, D.C, Muir, C.L, Hauser, O.A. (2002) Detrimental effects of sedimentation on marine benthos: what can be learned from natural processes and rates? *Ecological Engineering*, 19: 211–232.

- Montie, S, Thomsen, M.S, Rack, W, Broady, P.A. (2020) Extreme summer marine heatwaves increase chlorophyll a in the Southern Ocean. *Antarctic Science*. doi:10.1017/S0954102020000401
- Montie, S, Thoral, F, Smith, R.O, Cook, F, Tait, L.W, Pinkerton, M.H, ... Thomsen, M.S. (2023) Seasonal trends in marine heatwaves highlight vulnerable coastal ecoregions and historic change points in New Zealand. *New Zealand Journal of Marine and Freshwater Research*, 1-26.
- Morel, A, Antoine, D, Babin, M, Dandonneau, Y. (1996) Measured and modeled primary production in the northeast Atlantic (EUMELI JGOFS program): the impact of natural variations in photosynthetic parameters on model predictive skill. *Deep Sea Research Part I: Oceanographic Research Papers*, 43(8): 1273-1304.
- Murphy, R.J, Pinkerton, M.H, Richardson, K.M, Bradford-Grieve, J, Boyd, P.W. (2001) Phytoplankton distributions around New Zealand derived from SeaWiFS remotely-sensed ocean colour data. *New Zealand Journal of Marine and Freshwater Research*, 35: 343-362, 2001.
- NASA Goddard Space Flight Center; Ocean Ecology Laboratory; Ocean Biology Processing Group (2018a) SeaWiFS Ocean Color Reprocessing 2018.0 <https://oceancolor.gsfc.nasa.gov/reprocessing/r2018/seawifs/> (Accessed May 2018).
- NASA Goddard Space Flight Center; Ocean Ecology Laboratory; Ocean Biology Processing Group (2018b) MODIS/Aqua Ocean Color Reprocessing 2018.0 <https://oceancolor.gsfc.nasa.gov/reprocessing/r2018/aqua/> (Accessed May 2018).
- Nixon, S.W. (1995) Coastal marine eutrophication: a definition, social causes, and future concerns. *Ophelia*, 41(1): 199-219.
- O'Reilly, J.E, Maritorena, S, Mitchell, G, Siegel, D.A, Carder, K.L, Garver, S.A, Kahru, M, McClain, C.R. (1998) Ocean colour algorithms for SeaWiFS. *Journal of Geophysical Research*, 103(C11): 24: 937-24,953.
- O'Reilly, J.E, Sherman, K. (2016) Chapter 5.1: Primary productivity and trends. In IOC-UNESCO and UNEP (2016). *Large Marine Ecosystems: Status and Trends*. United Nations Environment Programme, Nairobi, Pp 91-99.
- Ody, A, Doxaran, D, Vanhellefont, Q., et al. (2016) Potential of high spatial and temporal ocean color satellite data to study the dynamics of suspended particles in a micro-tidal river plume. *Remote Sensing*, 8: 245. doi:10.3390/rs8030245.
- Oliver, E.C, Burrows, M.T, Donat, M.G, Sen Gupta, A, Alexander, L.V, Perkins-Kirkpatrick, S. E, et al. (2019). Projected marine heatwaves in the 21st century and the potential for ecological impact. *Frontiers in Marine Science*, 6: 734.
- Oliver, E.C.J, Burrows, M.T, Donat, M.G, et al. (2018) Longer and more frequent marine heatwaves over the past century. *Nat. Commun.* <https://doi.org/10.1038/s41467-018-03732-9>.

- Oliver, E.C.J, Burrows, M.T, Donat, M.G, et al. (2019) Projected marine heatwaves in the 21st century and the potential for ecological impact. *Frontiers in Marine Science*, doi.org/10.3389/fmars.2019.00734.
- Patakamuri, S.K, O'Brien, N, Patakamuri, M.S.K. (2020) Package 'modifiedmk'. Cran. R-project.
- Peterson, C.H. (1985) Patterns of lagoonal bivalve mortality after heavy sedimentation and their paleoecological significance. *Paleobiology*, 11: 139–53.
- Pinkerton, M, Gall, M, O'Callaghan, J, Thorall, F, Swales, A. (2022) Monitoring coastal suspended sediment in Aotearoa New Zealand: utility of satellite remote sensing. *NIWA Client Report 2022106WN*. Prepared for Department of Conservation, May 2022, pp 113.
- Pinkerton, M.H. (2015) Ocean colour satellite observations of phytoplankton in the New Zealand EEZ, 1997–2014. *NIWA Client Report MfE15302-WLG2015-9*. Prepared for Ministry for the Environment, January 2015. Pp 59.
- Pinkerton, M.H. (2016) Ocean colour satellite observations of phytoplankton in the New Zealand EEZ, 1997–2016. *NIWA Client Report WLG2016-19*. Prepared for Ministry for the Environment, March 2016. Pp 43.
- Pinkerton, M.H. (2017) Satellite remote sensing of water quality and temperature in Manukau Harbour. *NIWA Client Report 2017092WN* produced for Watercare Services Ltd, Pp 76.
- Pinkerton, M.H, Gall, M, Wood, S, Zeldis, J. (2018) Measuring the effects of mariculture on water quality using satellite ocean colour remote sensing. *Aquaculture Environment Interactions*, 10:529-545.
- Pinkerton, M.H, Moore, G.F, Lavender, S.J, Gall, M.P, Oubelkheir, K, Richardson, K.M, Boyd, P.W, Aiken, J. (2006) A method for estimating inherent optical properties of New Zealand continental shelf waters from satellite ocean colour measurements. *New Zealand Journal of Marine and Freshwater Research*, 40(2): 227-247.
- Pinkerton, M.H, P. Boyd; S. Deppeler; A. Hayward; J. Hofer; S. Moreau (2021) Evidence for the impact of climate change on primary producers in the Southern Ocean. *Frontiers of Marine Science*, doi: 10.3389/fevo.2021.592027.
- Pinkerton, M.H, Richardson, K.M, Boyd, P.W, Gall, M.P, Zeldis, J, Oliver, M.D, Murphy, R.J. (2005) Intercomparison of ocean colour band-ratio algorithms for chlorophyll concentration in the Subtropical Front east of New Zealand. *Remote Sensing of Environment*, 97: 382-402.
- Pinkerton, M.H, Sutton, P.J.H, Wood, S. (2019) Satellite indicators of phytoplankton and ocean surface temperature for New Zealand. *NIWA Client Report 2018180WNrev1*. Prepared for the Ministry for the Environment. Wellington, New Zealand.
- Platt, T, Sathyendranath, S. (1993) Estimators of primary production for interpretation of remotely sensed data on ocean color. *Journal of Geophysical Research*, 98: 14561-14567.

- Plew, D.R, Zeldis, J.R, Dudley, B.D, Whitehead, A.L, Stevens, L.M, Robertson, B.M, Robertson, B.P. (2020) Assessing the eutrophic susceptibility of New Zealand estuaries. *Estuaries and Coasts*, 43(8): 2015-2033.
- Reynolds, R.W, Rayner, N.A, Smith, T.M, Stokes, D.C, Wang, W. (2002) An improved in situ and satellite SST analysis for climate. *Journal of Climate*, 15: 1609-1625.
- Robertson, B, Stevens, L, Robertson, B, Zeldis, J, Green, M, Madarasz-Smith, A, Plew, D, Storey, R, Hume, T, Oliver, M. (2016) NZ estuary trophic index screening tool 1. Determining eutrophication susceptibility using physical and nutrient load data. Prepared for Environlink tools project: Estuarine trophic index 47: 0-1.
- Ruddick, K.G, Ovidio, F, Rijkeboer, M. (2000) Atmospheric correction of SeaWiFS imagery for turbid coastal and inland waters. *Applied Optics*, 39:897-912.
- Salinger, M.J, Diamond, H.J, Bell, J, Behrens, et al. (2023) Coupled Ocean-Atmosphere Summer Heatwaves in the New Zealand Region: an update. *Weather and Climate*, 42 (1).
- Salinger, M.J, Renwick, J, Diamond, H.J, et al. (2020)\ Unparalleled coupled ocean-atmosphere summer heatwaves in the New Zealand region: drivers, mechanisms and impacts. *Climatic Change*. <https://doi.org/10.1007/s10584-020-02730-5>.
- Schlegel, R.W, Oliver, E.C, Wernberg, T, Smit, A.J. (2017) Nearshore and offshore co-occurrence of marine heatwaves and cold-spells. *Progress in Oceanography*, 151: 189-205.
- Schlegel, R.W, Smit, A.J. (2018) Heatwaver: A central algorithm for the detection of heatwaves and cold-spells. *Journal of Open Source Software*. 3(27): 821.
- Schwarz, J.N, Gall, M, Pinkerton, M.H, Kennan, S. (2008) Primary production in the subtropical convergence zone: Comparison of in-situ measurement methods and remote estimates. *Proceedings of Ocean Optics XIX*, Barga, Italy, 6-10 October 2008.
- Sen Gupta, A. (2023) Marine heatwaves: definition duel heats up. *Nature*, 617(7961), 465-465.
- Sen Gupta, A, Ryan, S, Hernaman, V. (2023) Advances in marine heatwave interactions. *Frontiers in Climate*, 5: 1177781.
- Sen, P.K. (1968) Estimates of the regression coefficient based on Kendall's tau. *Journal of the American Statistical Association*, 63: 1379-1389.
- Siegel, D.A, Wang, M, Maritorena, S, Robinson, W. (2000) Atmospheric correction of satellite ocean color imagery: the black pixel assumption. *Applied Optics*, 39: 3582-3591.
- Smale, D.A, Wernberg, T, Oliver, E.C.J, et al. (2019). Marine heatwaves threaten global biodiversity and the provision of ecosystem services. *Nature Climate Change*, 9: 306-312. doi.org/10.1038/s41558-019-0412-1.

- Smith, D.G, Davies-Colley, R.J. (2002) If visual water clarity is the issue, then why not measure it? Proceedings of NWQMC. Available (May 2022): <https://acwi.gov/monitoring/nwqmc.org/NWQMC-Proceedings/Papers-Alphabetical%20by%20First%20Name/David%20Smith2.pdf>.
- Smith, K.E, Burrows, M.T, Hobday, A.J, King, N.G, Moore, P.J, Sen Gupta, A. et al. (2023) Biological impacts of marine heatwaves. *Annual Review of Marine Science*, 15: 119-145.
- Smith, K.E, Burrows, M.T, Hobday, A.J, Sen Gupta, A, Moore, P.J, Thomsen, M. et al. (2021) Socioeconomic impacts of marine heatwaves: Global issues and opportunities. *Science*, 374(6566), eabj3593.
- Smith, K.E, Smith, K.E, Burrows, M.T, et al. (2021). Socioeconomic impacts of marine heatwaves: Global issues and opportunities. *Science*, 374. eabj3593 (2021).
- Stevens, C.L, Spillman, C.M, Behrens, E, Broekhuizen, N, Holland, P, Matthews, Y, et al. (2022) Horizon Scan on the benefits of ocean seasonal forecasting in a future of increasing marine heatwaves for Aotearoa New Zealand. *Frontiers in Climate*, 92.
- Stramski, D, Boss, E, Bogucki, D, Voss, K.J. (2004) The role of seawater constituents in light backscattering in the ocean. *Progress in Oceanography*, 61(1): 27-56.
- Sutton, P J, Bowen, M. (2019) Ocean temperature change around New Zealand over the last 36 years. *New Zealand Journal of Marine and Freshwater Research*, 53(3), 305-326.
- Sutton, P.J.H, Roemmich, D. (2001) Ocean temperature climate off north-east New Zealand. *N.Z. Journal of Marine and Freshwater Research*, 35: 553-565.
- Thoral, F, Montie, S, Thomsen, M.S, Tait, L.W, Pinkerton, M.H, Schiel, D.R. (2022). Unravelling seasonal trends in coastal marine heatwave metrics across global biogeographical realms. *Scientific Reports*, 12(1), 7740.
- Townsend, M, Lohrer, D. (2015) ANZECC Guidance for Estuary Sedimentation. *NIWA Client Report HAM2015-096*, September 2015.
- Uddstrom, M.J, Oien, N.A. (1999) On the use of high resolution satellite data to describe the spatial and temporal variability of sea surface temperatures in the New Zealand Region. *Journal of Geophysical Research (Oceans)*, 104(C9): 20729–20751.
- van der Wiel, K, Bintanja, R. (2021) Contribution of climatic changes in mean and variability to monthly temperature and precipitation extremes. *Nature Communications Earth and Environment*, <https://doi.org/10.1038/s43247-020-00077-4>.
- Volpe, G, Nardelli, B.B, Colella, S, Pisano, A, Santoleri, R. (2018) Operational Interpolated Ocean Colour Product in the Mediterranean Sea. *New Frontiers in Operational Oceanography*, 227-244.
- Wang, M, Shi, W. (2007) The NIR-SWIR combined atmospheric correction approach for MODIS ocean color data processing. *Optics Express*, 15(24): 15722-15733.

- Westberry, T, Behrenfeld, M.J, Siegel, D.A, Boss, E. (2008) Carbon-based primary productivity modeling with vertically resolved photo-acclimation. *Global Biogeochemical Cycles*, 22(2): GB2024.
- Wilson, A.M, Jetz, W. (2016) Remotely sensed high-resolution global cloud dynamics for predicting ecosystem and biodiversity distributions. *PLoS Biol*, 14(3): e1002415. doi:10.1371/journal.pbio.1002415.
- Yue, S, Wang, C.Y. (2004) The Mann–Kendall test modified by effective sample size to detect trend in serially correlated hydrological series. *Water Resources Management*, 18: 201–218.

Appendix A Descriptive sub-regions

Table A-1: Co-ordinates defining descriptive regions.

Region	Co-ordinates of boundary	
	Latitude	Longitude
Chatham Rise	-42	174.3
	-45.5	170.8
	-45.5	185
	-42	185
Tasman Sea	-34.43	160.6
	-47.25	157.5
	-47.25	167.5
	-41.6	172.3
	-40.82	172.14
	-40.55	172.7
	-39.3	173.75
	-39.2	175
	-37.05	175
-34.43	172.8	
Subtropical Water (STW)	-29.82	172.87
	-34.43	172.87
	-37.05	175
	-38.67	176.44
	-42	174.3
	-42	185
	-29.82	185
Subantarctic Water (SAW)	-45.5	170.8
	-47.25	167.5
	-47.25	157.5
	-52.64	157.5
	-52.52	185
	-45.5	185

Appendix B Ocean SST and chl-a annual means

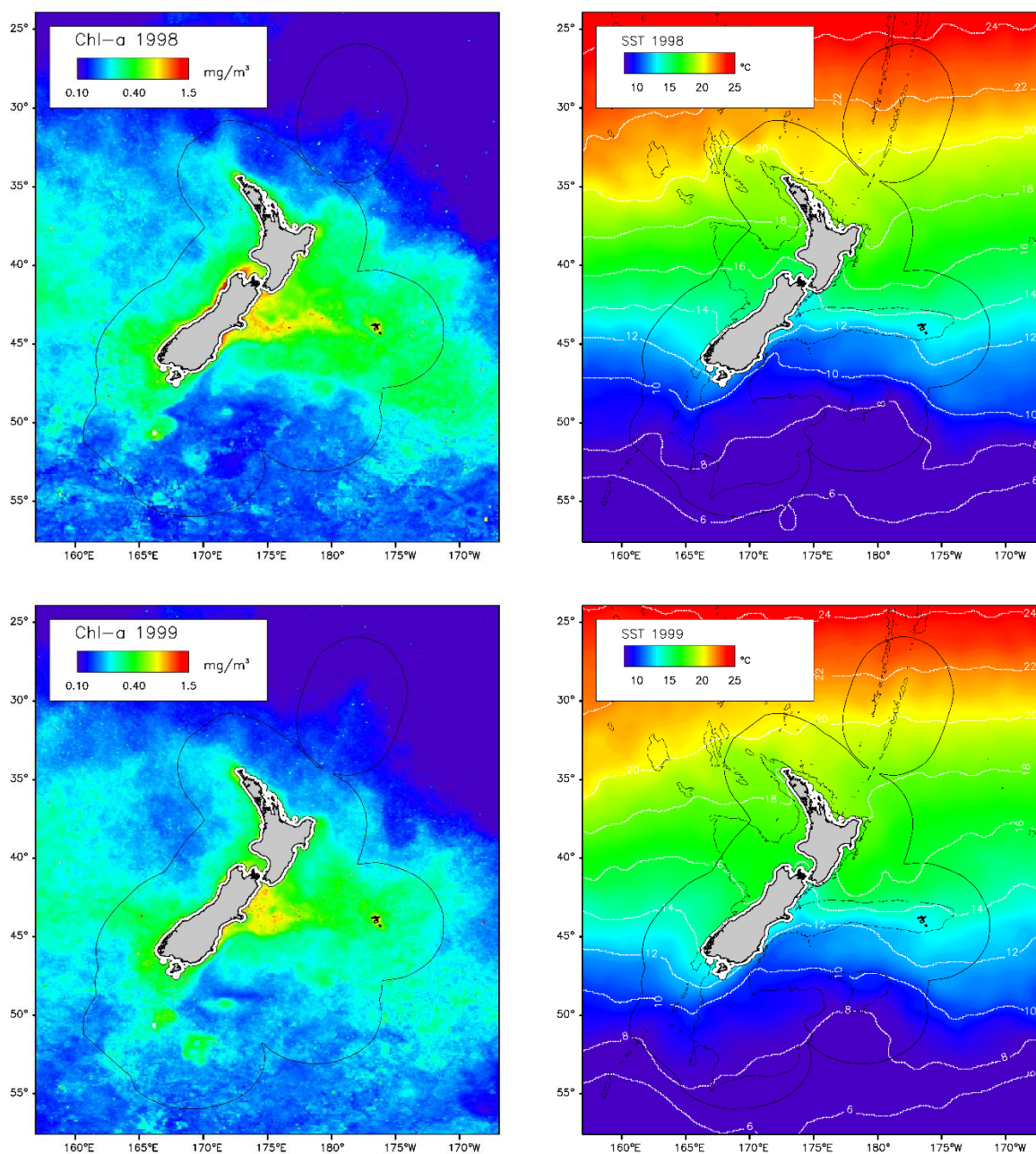


Figure B-1: Oceanic: Mean annual chl-a and SST. Left: Mean annual chl-a by year from the merged dataset of SeaWiFS and MODIS-Aqua. Right: Mean annual SST from OISST v2.1 remapped to 9 km resolution with white contours showing 2° isotherms. The boundary of the New Zealand EEZ is also shown. Territorial seas (to 12 nautical miles offshore) are excluded from analysis (shown white).

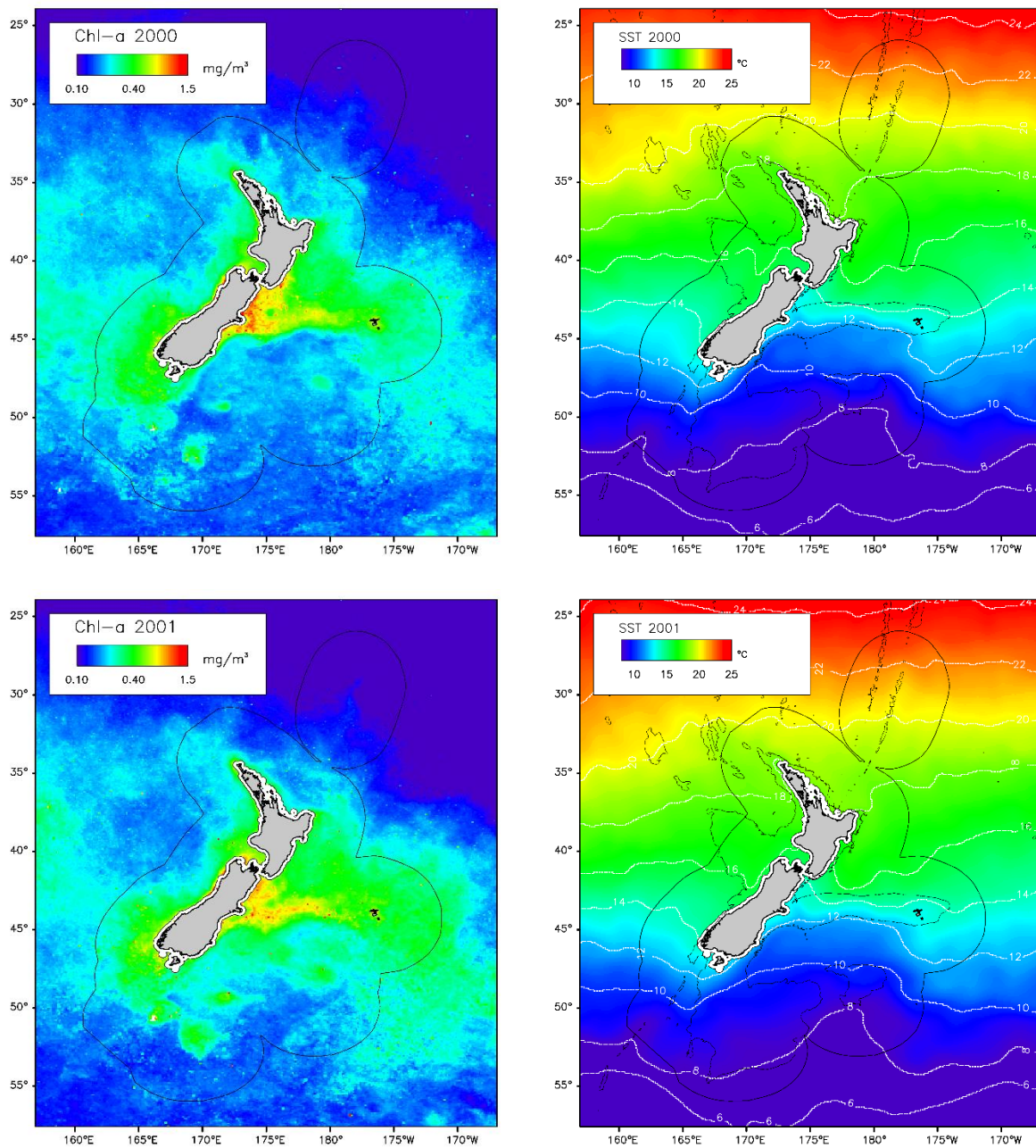


Figure B-1: Oceanic: Mean annual chl-a and SST. (Continued) Left: Mean annual chl-a by year from the merged dataset of SeaWiFS and MODIS-Aqua. Right: Mean annual SST from OISST v2.1 remapped to 9 km resolution with white contours showing 2° isotherms. The boundary of the New Zealand EEZ is also shown. Territorial seas (to 12 nautical miles offshore) are excluded from analysis (shown white).

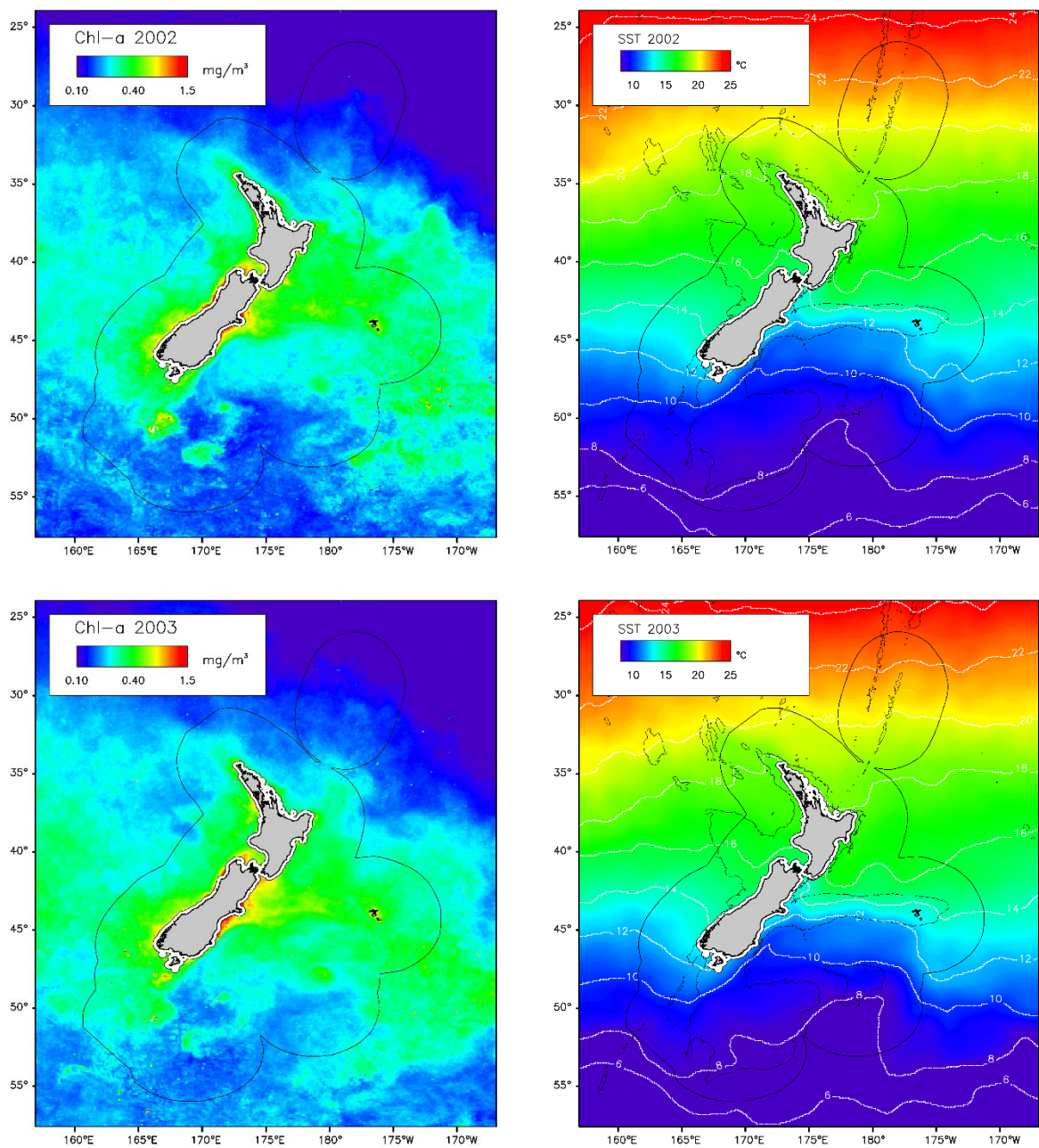


Figure B-1: Oceanic: Mean annual chl-a and SST. (Continued) Left: Mean annual chl-a by year from the merged dataset of SeaWiFS and MODIS-Aqua. Right: Mean annual SST from OISST v2.1 remapped to 9 km resolution with white contours showing 2° isotherms. The boundary of the New Zealand EEZ is also shown. Territorial seas (to 12 nautical miles offshore) are excluded from analysis (shown white).

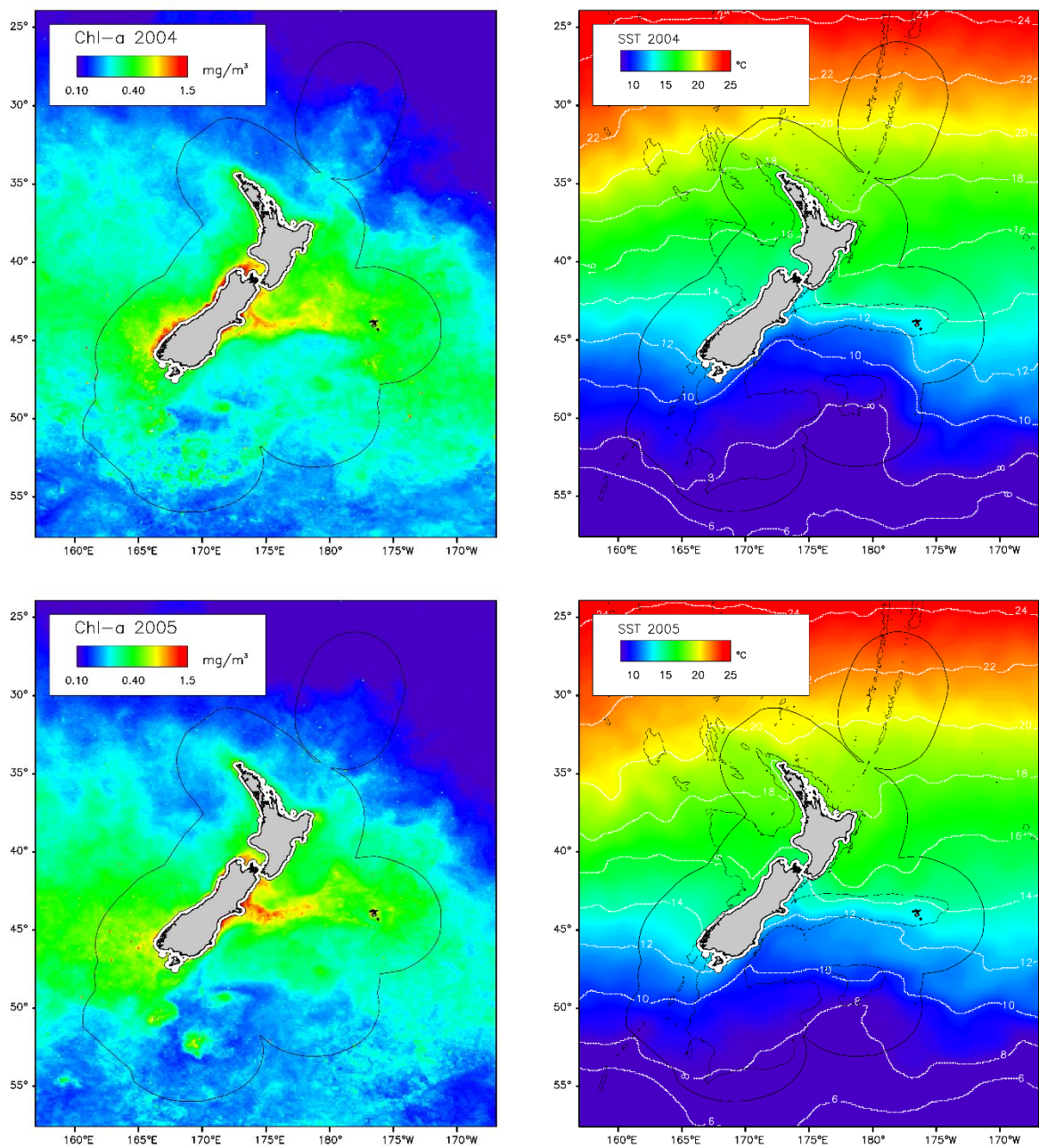


Figure B-1: Oceanic: Mean annual chl-a and SST. (Continued) Left: Mean annual chl-a by year from the merged dataset of SeaWiFS and MODIS-Aqua. Right: Mean annual SST from OISST v2.1 remapped to 9 km resolution with white contours showing 2° isotherms. The boundary of the New Zealand EEZ is also shown. Territorial seas (to 12 nautical miles offshore) are excluded from analysis (shown white).

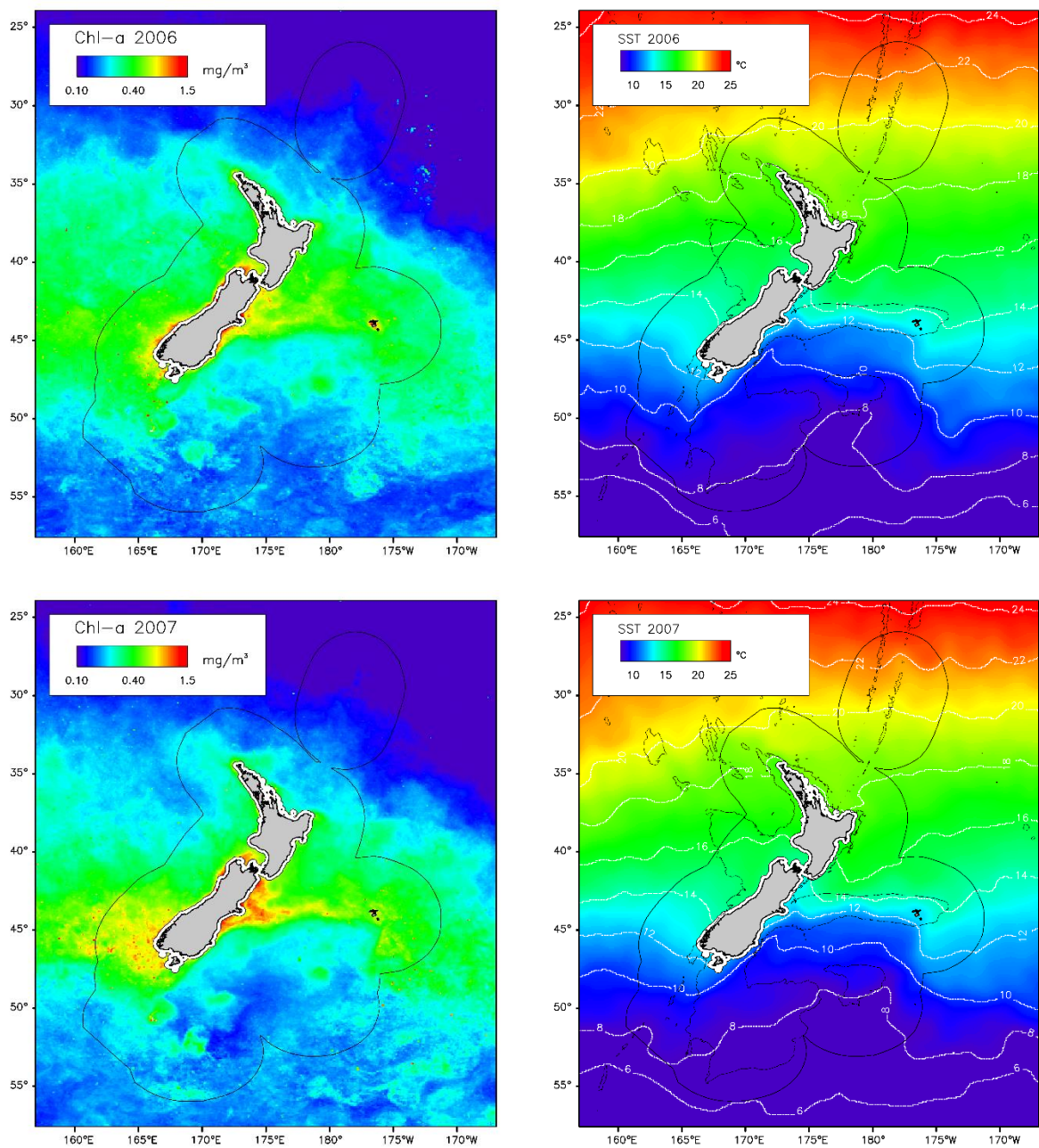


Figure B-1: Oceanic: Mean annual chl-a and SST. (Continued) Left: Mean annual chl-a by year from the merged dataset of SeaWiFS and MODIS-Aqua. Right: Mean annual SST from OISST v2.1 remapped to 9 km resolution with white contours showing 2° isotherms. The boundary of the New Zealand EEZ is also shown. Territorial seas (to 12 nautical miles offshore) are excluded from analysis (shown white).

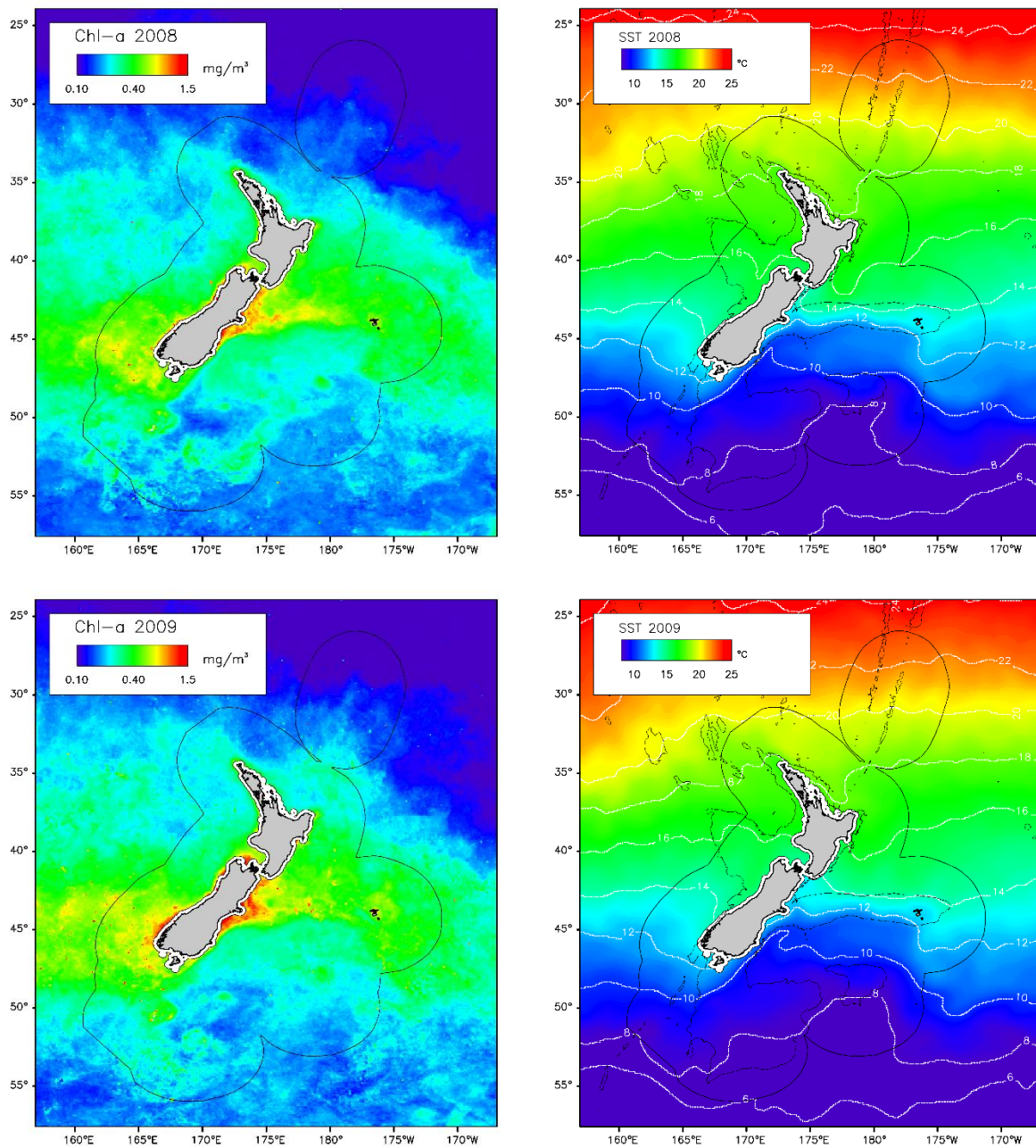


Figure B-1: Oceanic: Mean annual chl-a and SST. (Continued) Left: Mean annual chl-a by year from the merged dataset of SeaWiFS and MODIS-Aqua. Right: Mean annual SST from OISST v2.1 remapped to 9 km resolution with white contours showing 2° isotherms. The boundary of the New Zealand EEZ is also shown. Territorial seas (to 12 nautical miles offshore) are excluded from analysis (shown white).

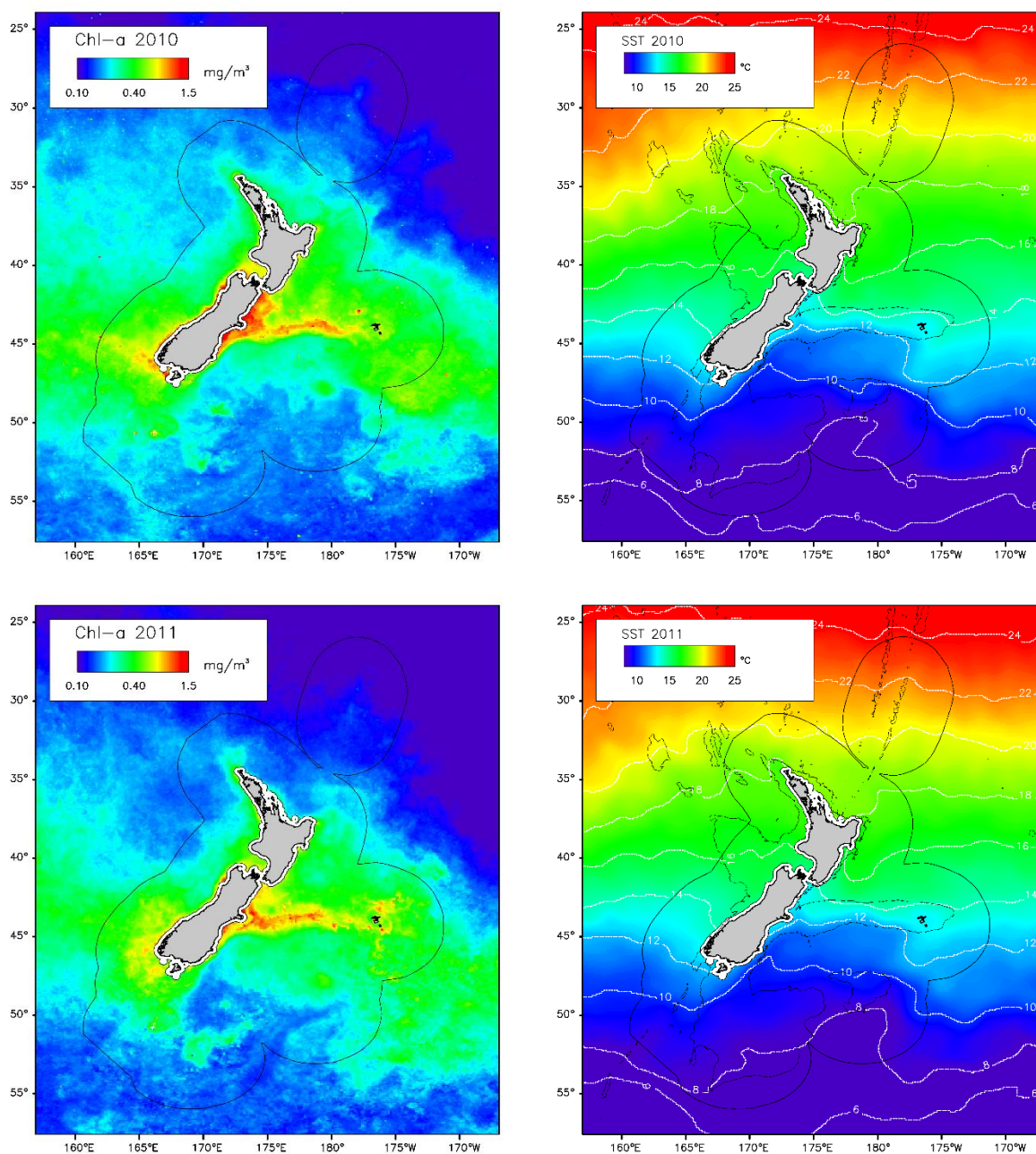


Figure B-1: Oceanic: Mean annual chl-a and SST. (Continued) Left: Mean annual chl-a by year from the merged dataset of SeaWiFS and MODIS-Aqua. Right: Mean annual SST from OISST v2.1 remapped to 9 km resolution with white contours showing 2° isotherms. The boundary of the New Zealand EEZ is also shown. Territorial seas (to 12 nautical miles offshore) are excluded from analysis (shown white).

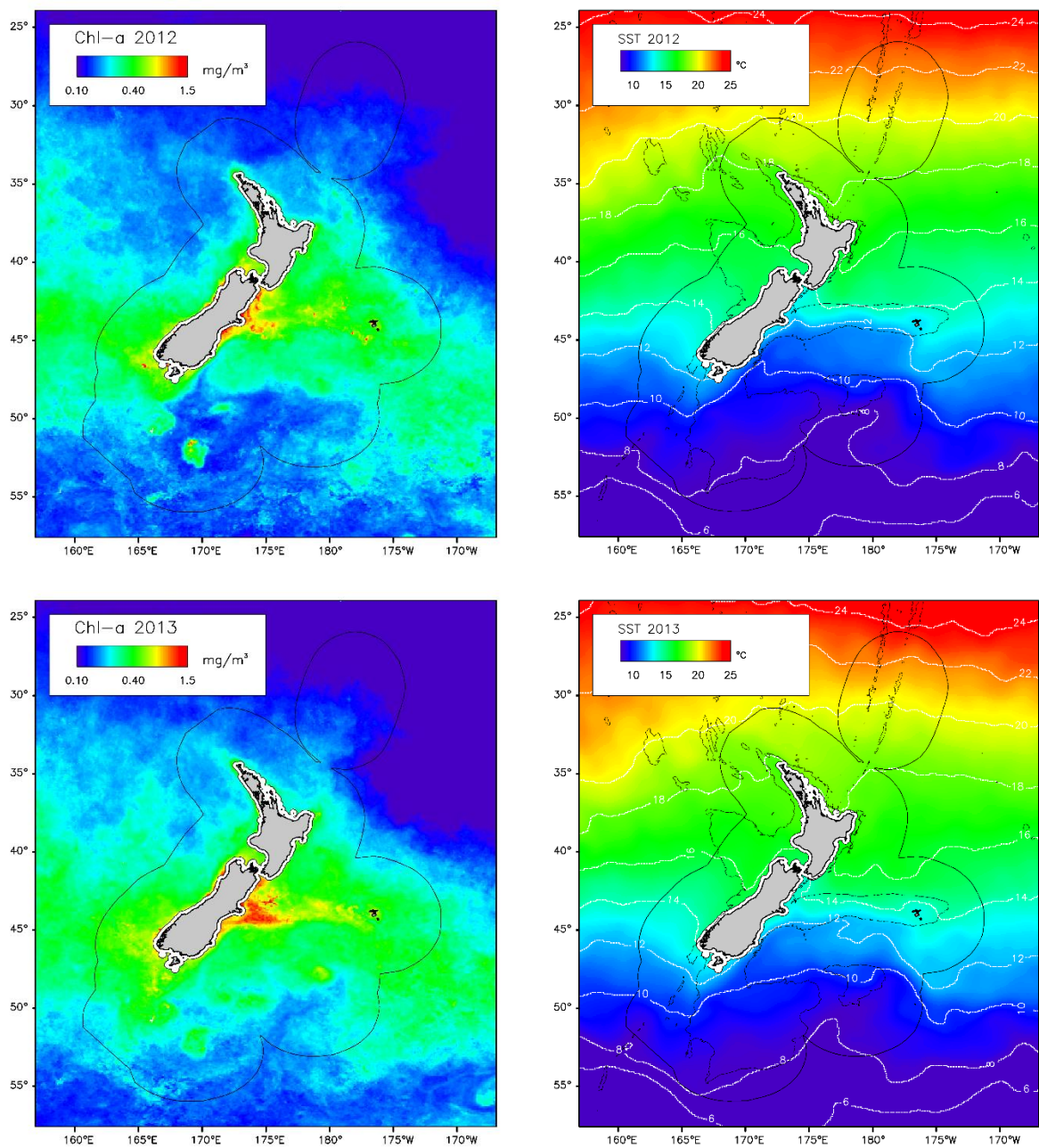


Figure B-1: Oceanic: Mean annual chl-a and SST. (Continued) Left: Mean annual chl-a by year from the merged dataset of SeaWiFS and MODIS-Aqua. Right: Mean annual SST from OISST v2.1 remapped to 9 km resolution with white contours showing 2° isotherms. The boundary of the New Zealand EEZ is also shown. Territorial seas (to 12 nautical miles offshore) are excluded from analysis (shown white).

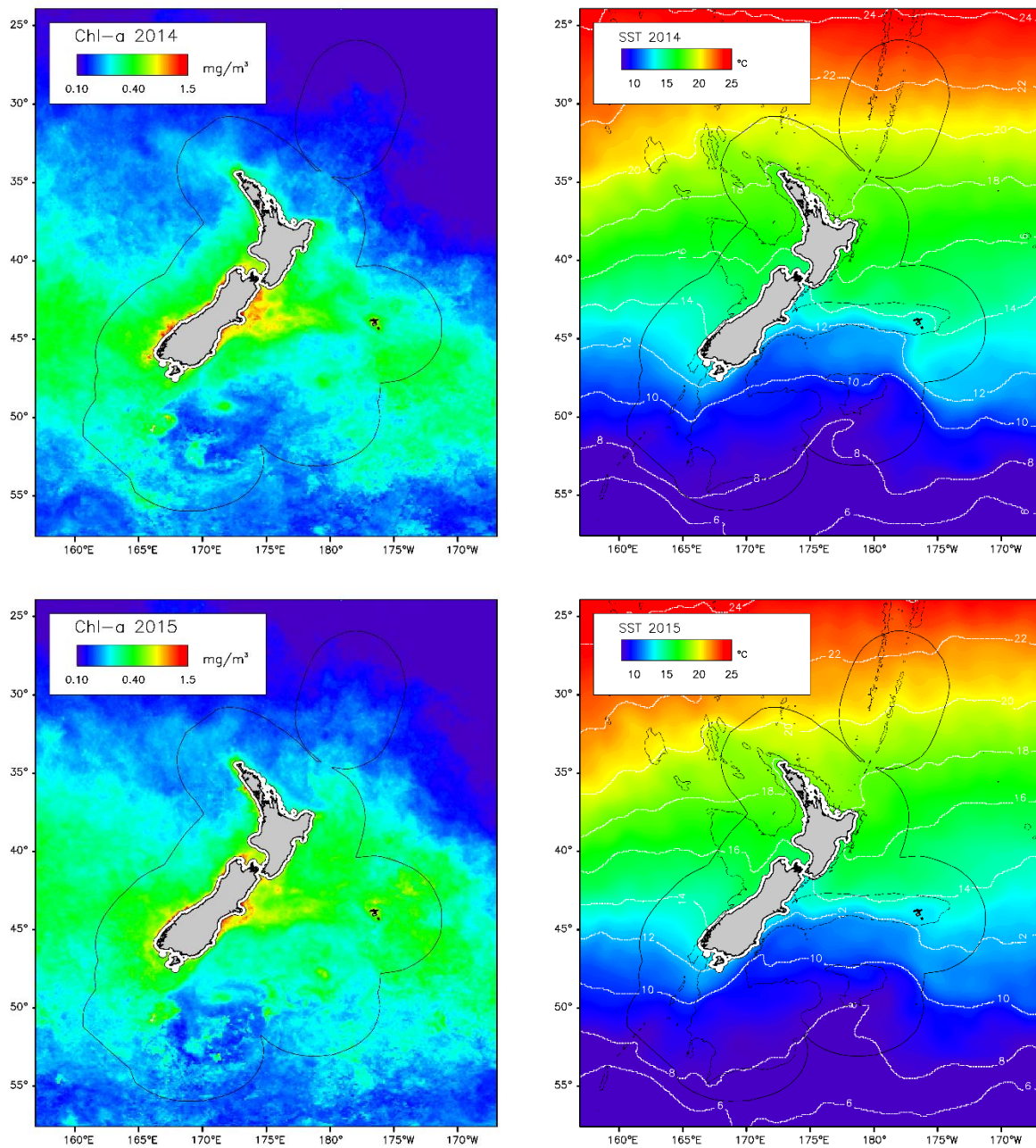


Figure B-1: Oceanic: Mean annual chl-a and SST. (Continued) Left: Mean annual chl-a by year from the merged dataset of SeaWiFS and MODIS-Aqua. Right: Mean annual SST from OISST v2.1 remapped to 9 km resolution with white contours showing 2° isotherms. The boundary of the New Zealand EEZ is also shown. Territorial seas (to 12 nautical miles offshore) are excluded from analysis (shown white).

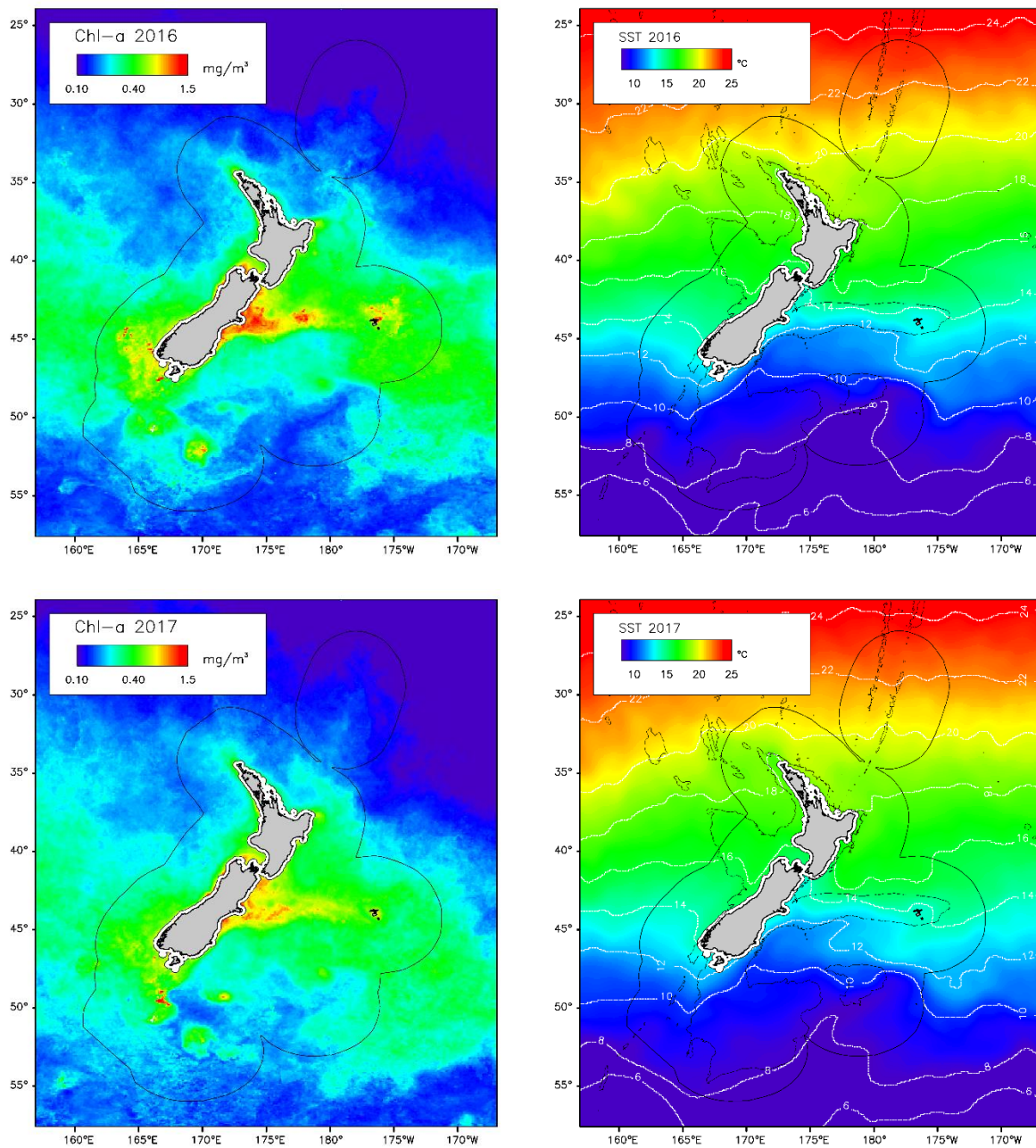


Figure B-1: Oceanic: Mean annual chl-a and SST. (Continued) Left: Mean annual chl-a by year from the merged dataset of SeaWiFS and MODIS-Aqua. Right: Mean annual SST from OISST v2.1 remapped to 9 km resolution with white contours showing 2° isotherms. The boundary of the New Zealand EEZ is also shown. Territorial seas (to 12 nautical miles offshore) are excluded from analysis (shown white).

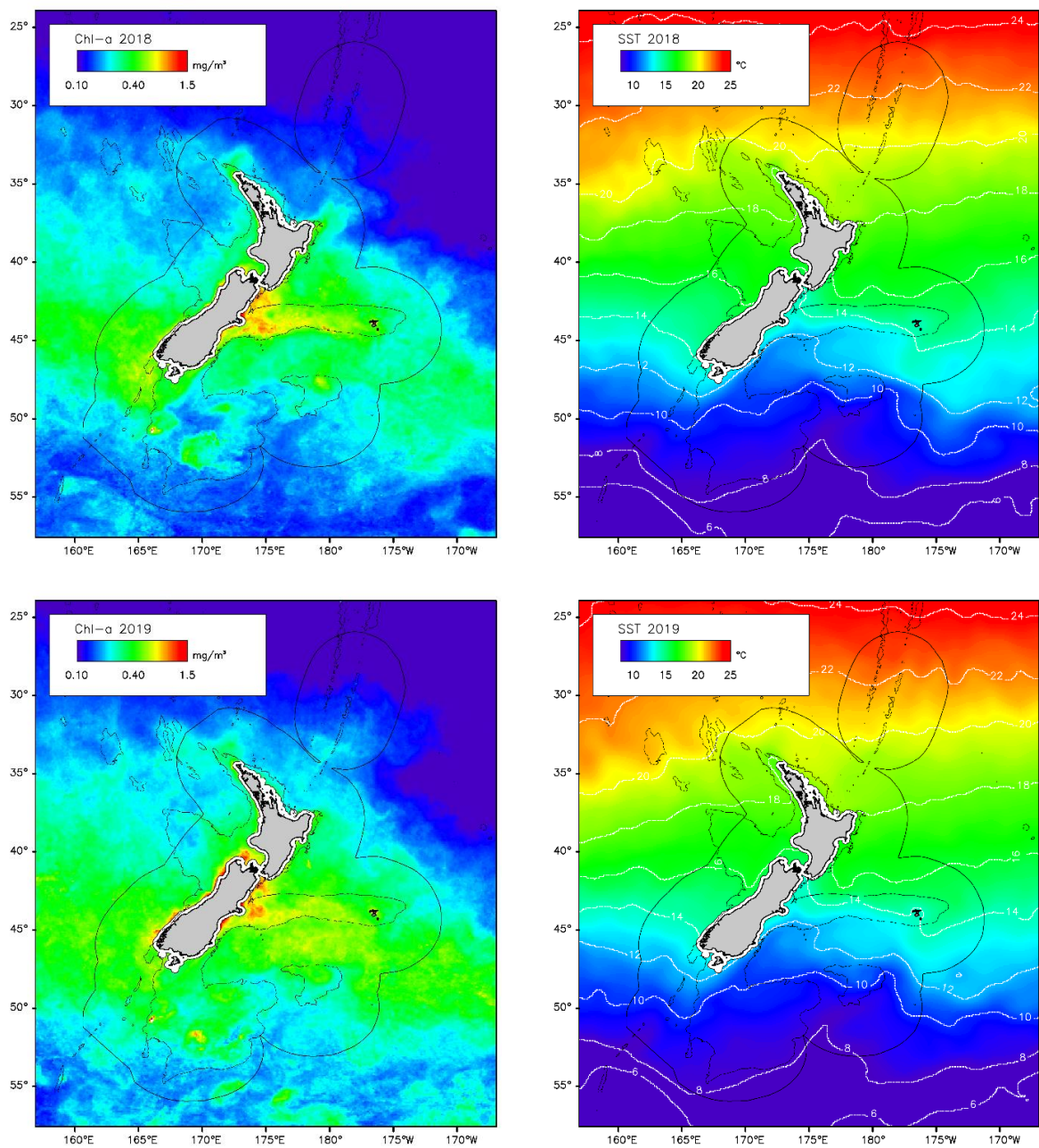


Figure B-1: Oceanic: Mean annual chl-a and SST. (Continued) Left: Mean annual chl-a by year from the merged dataset of SeaWiFS and MODIS-Aqua. Right: Mean annual SST from OISST v2.1 remapped to 9 km resolution with white contours showing 2° isotherms. The boundary of the New Zealand EEZ is also shown. Territorial seas (to 12 nautical miles offshore) are excluded from analysis (shown white).

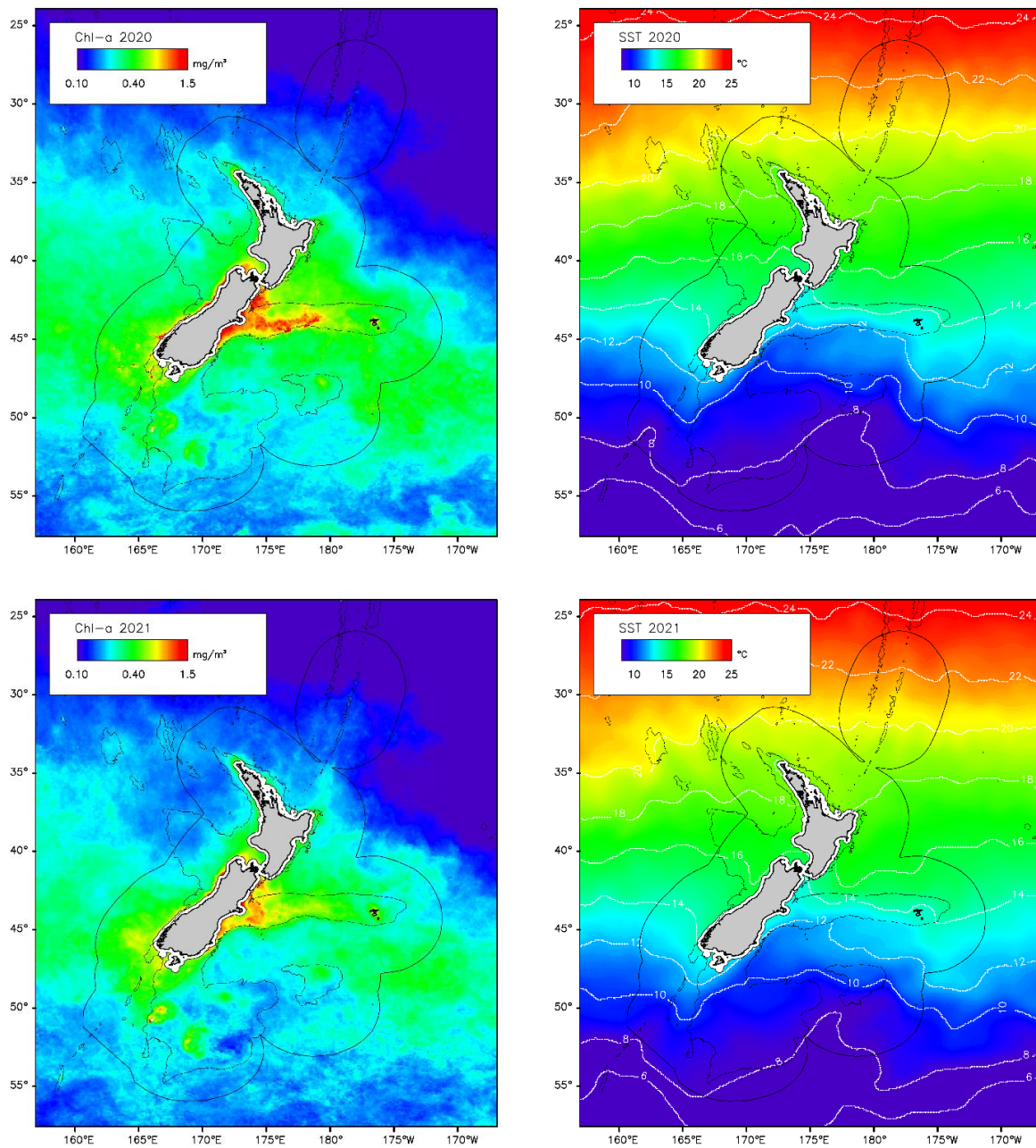


Figure B-1: Oceanic: Mean annual chl-a and SST. (Continued) Left: Mean annual chl-a by year from the merged dataset of SeaWiFS and MODIS-Aqua. Right: Mean annual SST from OISST v2.1 remapped to 9 km resolution with white contours showing 2° isotherms. The boundary of the New Zealand EEZ is also shown. Territorial seas (to 12 nautical miles offshore) are excluded from analysis (shown white).

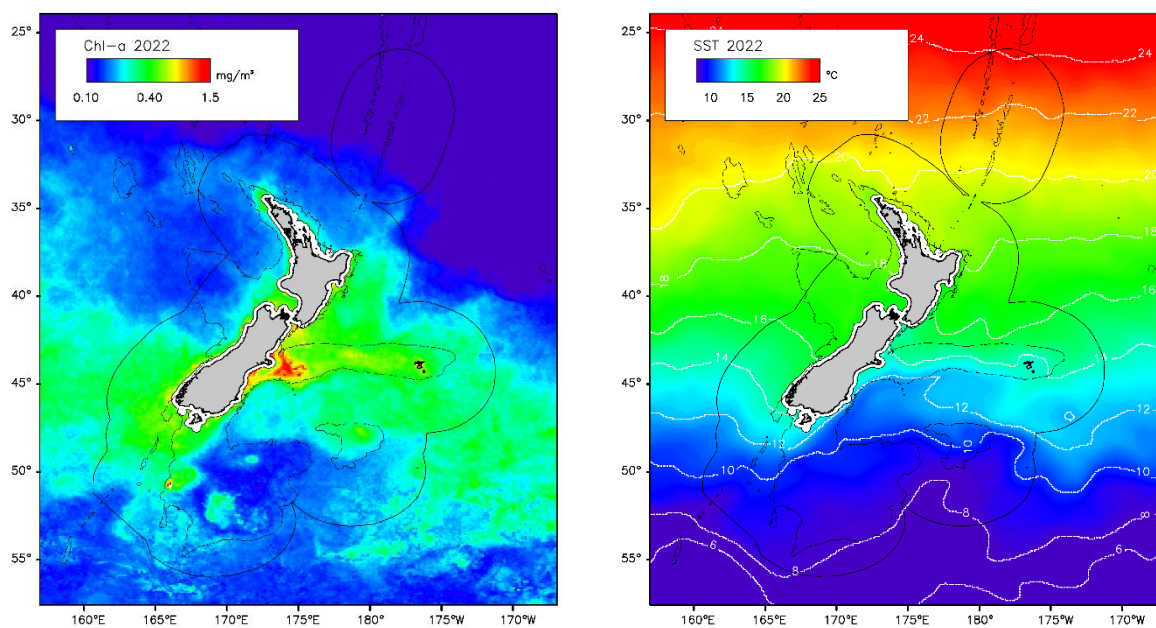


Figure B-1: Oceanic: Mean annual chl-a and SST. (Continued) Left: Mean annual chl-a by year from the merged dataset of SeaWiFS and MODIS-Aqua. Right: Mean annual SST from OISST v2.1 remapped to 9 km resolution with white contours showing 2° isotherms. The boundary of the New Zealand EEZ is also shown. Territorial seas (to 12 nautical miles offshore) are excluded from analysis (shown white).

Appendix C Ocean SST and chl-a annual anomalies

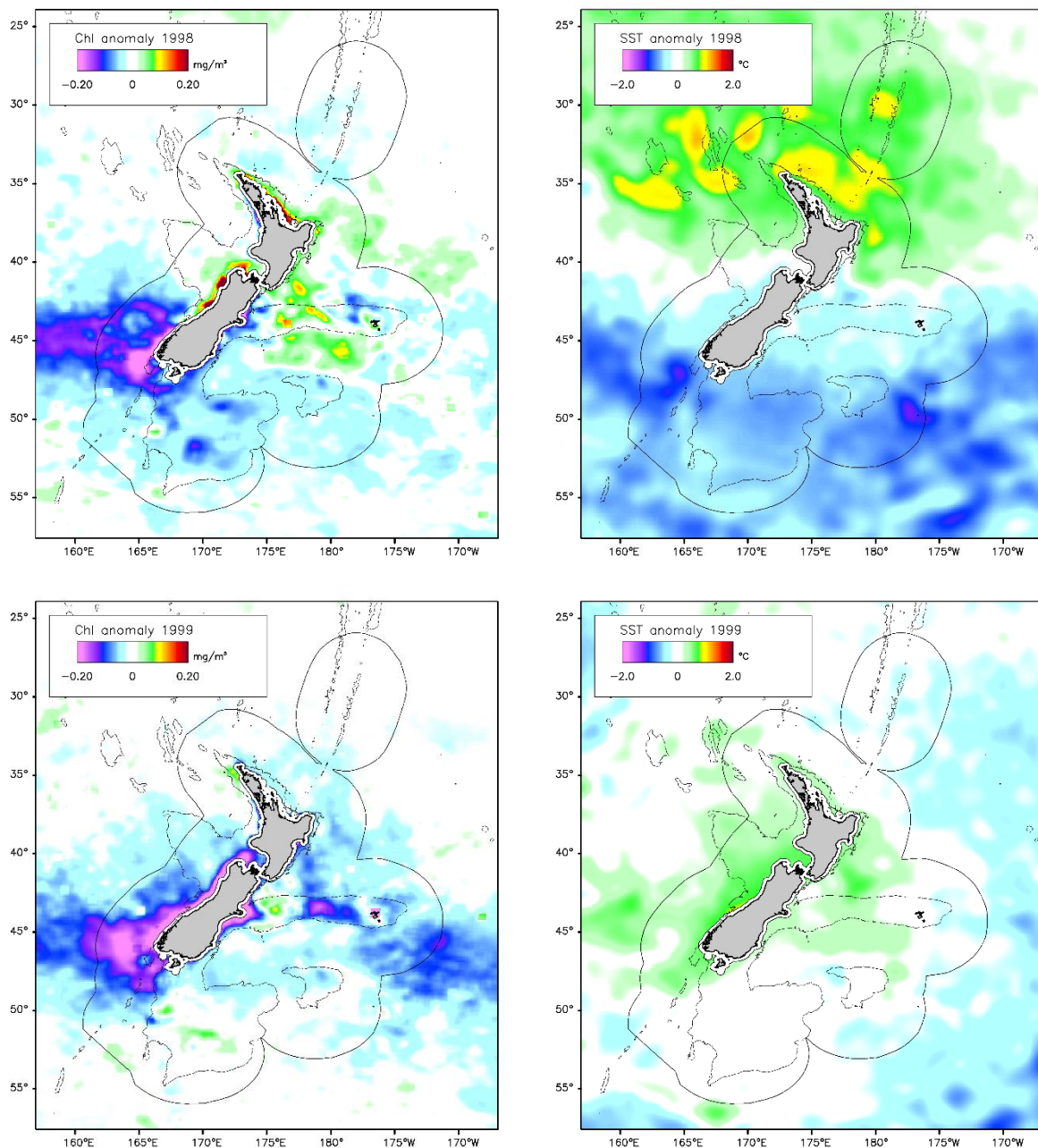


Figure C-1: Oceanic: Annual mean chl-a and sea-surface temperature (SST) annual anomalies by year. Left: chl-a annual anomalies from the merged dataset of SeaWiFS and MODIS-Aqua (1997–2018), spatially smoothed. Right: SST annual anomalies from AVHRR satellite data (1981–2018). “Annual anomalies” are the annual mean over each pixel minus the long-term mean. The boundary of the New Zealand EEZ is also shown.

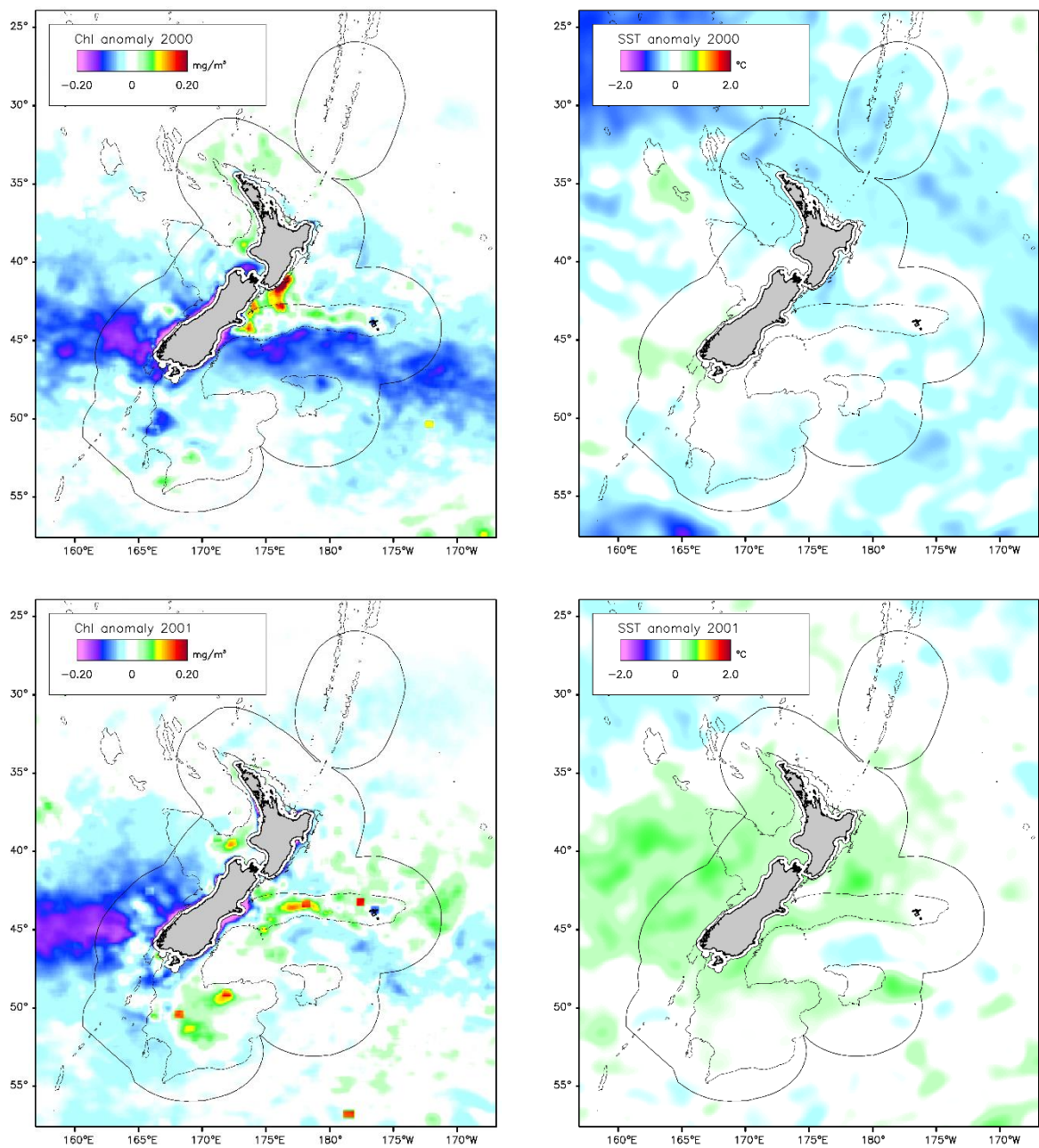


Figure C-1: Oceanic: Annual mean chl-a and sea-surface temperature (SST) annual anomalies by year. (Continued) Left: chl-a annual anomalies from the merged dataset of SeaWiFS and MODIS-Aqua (1997–2018), spatially smoothed. Right: SST annual anomalies from AVHRR satellite data (1981–2018). “Annual anomalies” are the annual mean over each pixel minus the long-term mean. The boundary of the New Zealand EEZ is also shown.

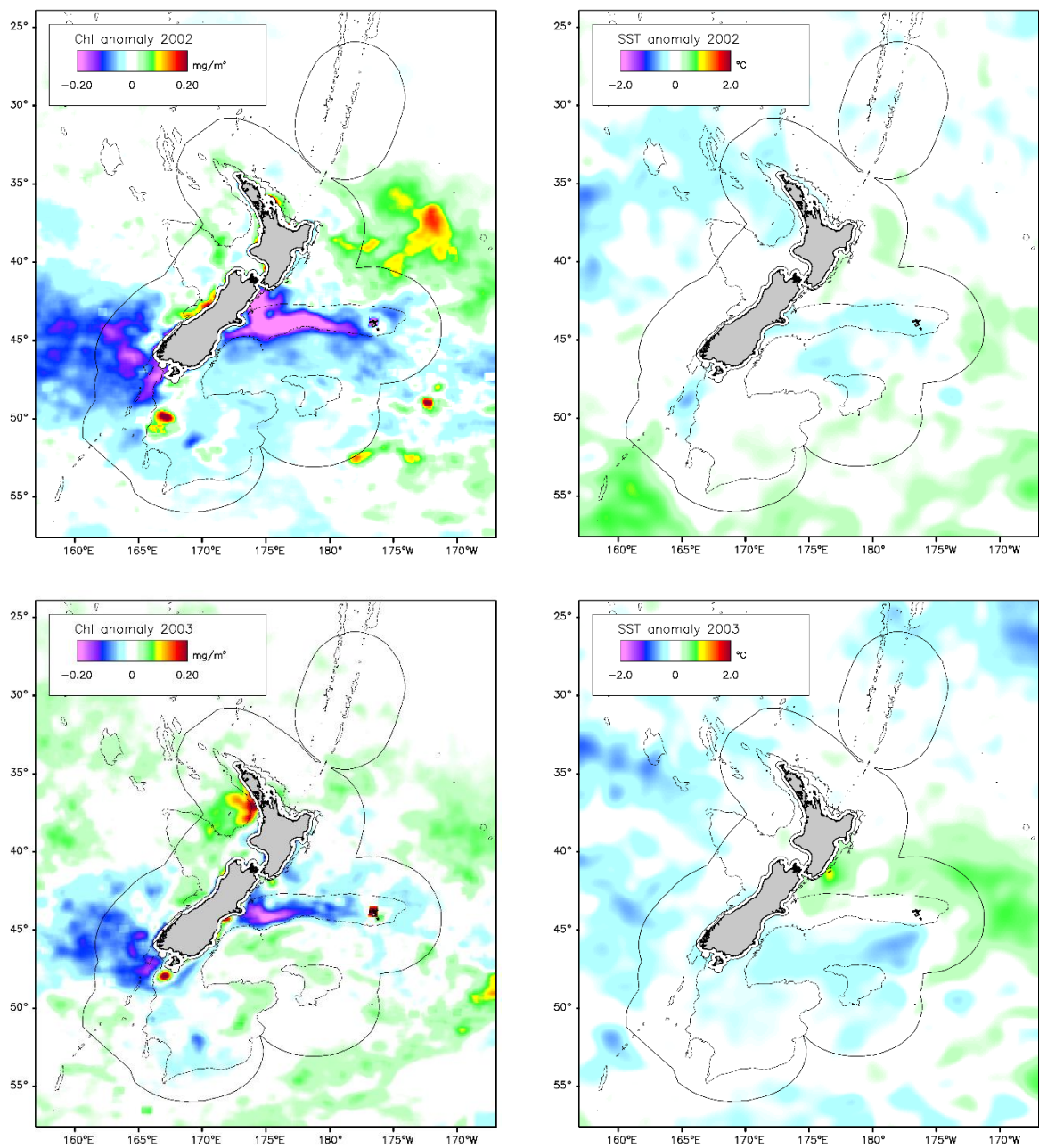


Figure C-1: Oceanic: Annual mean chl-a and sea-surface temperature (SST) annual anomalies by year. (Continued) Left: chl-a annual anomalies from the merged dataset of SeaWiFS and MODIS-Aqua (1997–2018), spatially smoothed. Right: SST annual anomalies from AVHRR satellite data (1981–2018). “Annual anomalies” are the annual mean over each pixel minus the long-term mean. The boundary of the New Zealand EEZ is also shown.

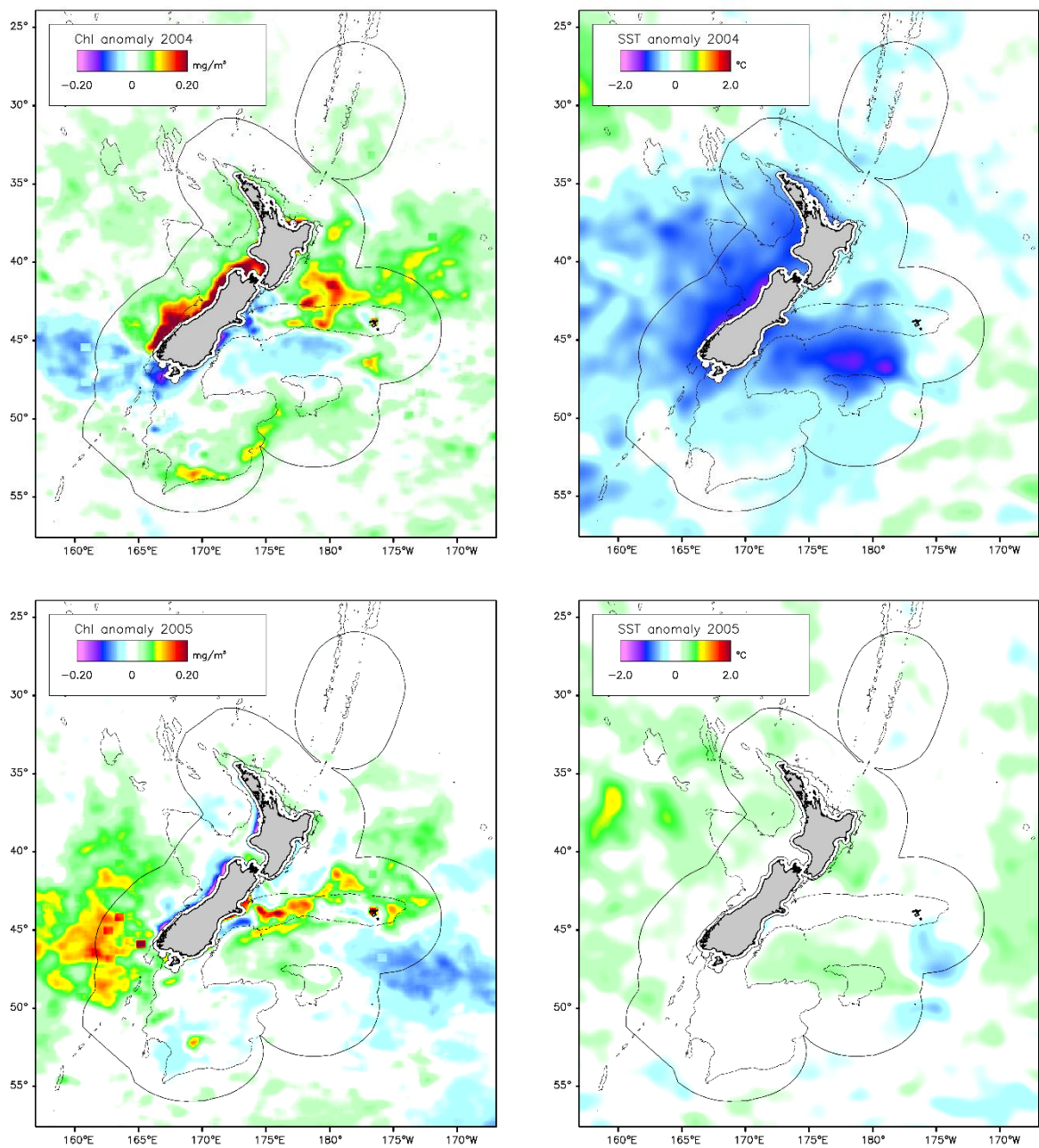


Figure C-1: Oceanic: Annual mean chl-a and sea-surface temperature (SST) annual anomalies by year. (Continued) Left: chl-a annual anomalies from the merged dataset of SeaWiFS and MODIS-Aqua (1997–2018), spatially smoothed. Right: SST annual anomalies from AVHRR satellite data (1981–2018). “Annual anomalies” are the annual mean over each pixel minus the long-term mean. The boundary of the New Zealand EEZ is also shown.

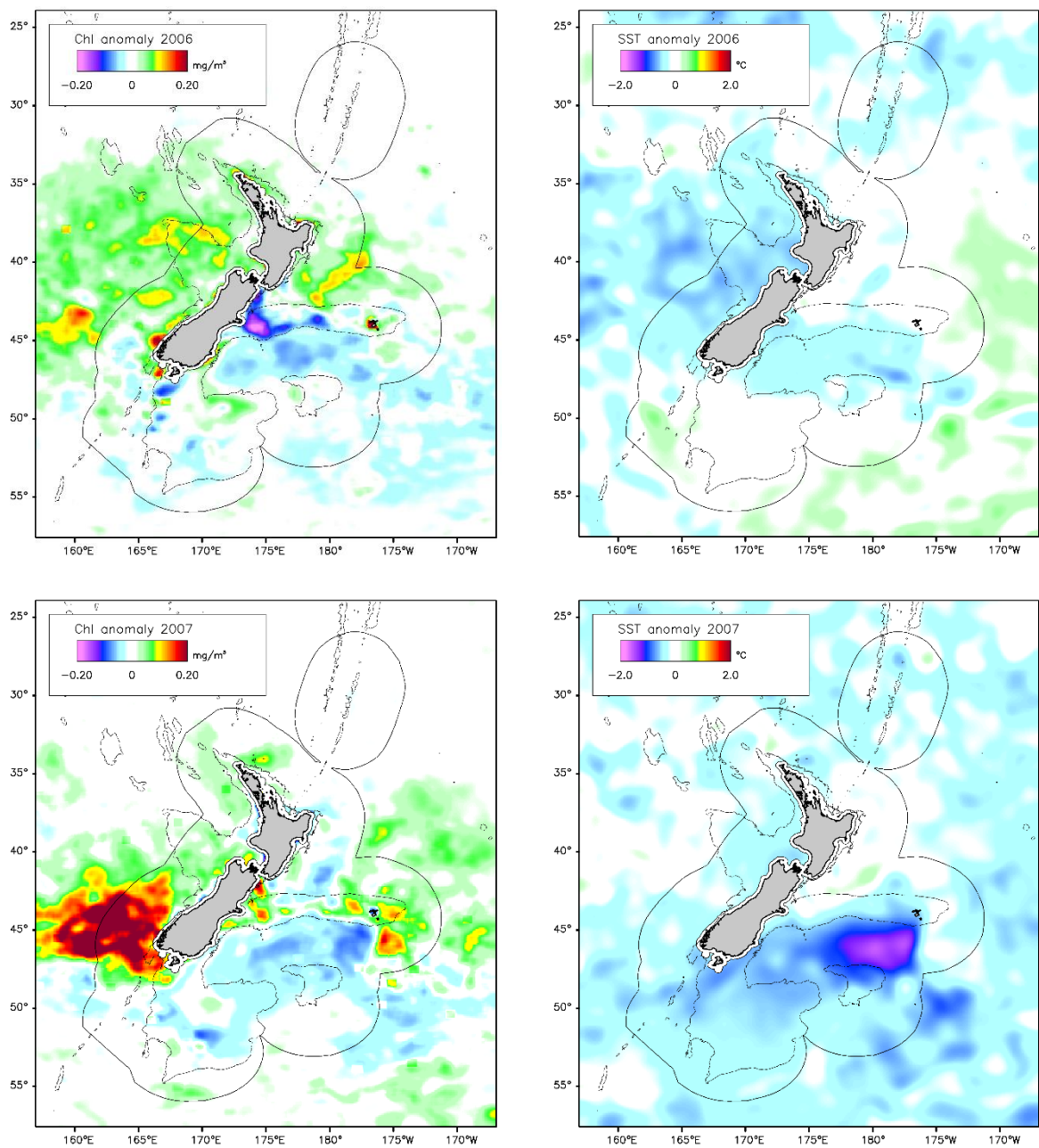


Figure C-1: Oceanic: Annual mean chl-a and sea-surface temperature (SST) annual anomalies by year. (Continued) Left: chl-a annual anomalies from the merged dataset of SeaWiFS and MODIS-Aqua (1997–2018), spatially smoothed. Right: SST annual anomalies from AVHRR satellite data (1981–2018). “Annual anomalies” are the annual mean over each pixel minus the long-term mean. The boundary of the New Zealand EEZ is also shown.

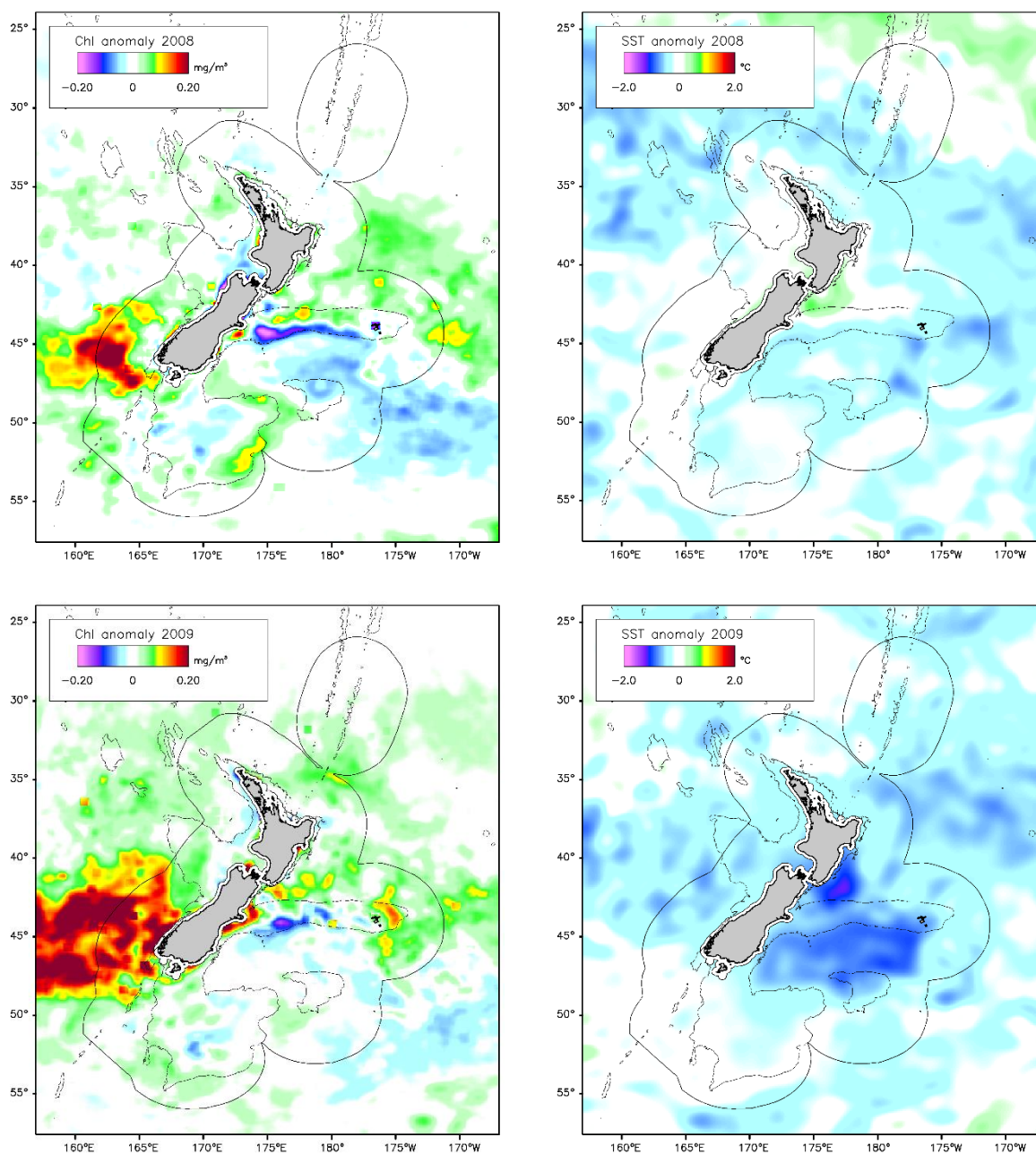


Figure C-1: Oceanic: Annual mean chl-a and sea-surface temperature (SST) annual anomalies by year. (Continued) Left: chl-a annual anomalies from the merged dataset of SeaWiFS and MODIS-Aqua (1997–2018), spatially smoothed. Right: SST annual anomalies from AVHRR satellite data (1981–2018). “Annual anomalies” are the annual mean over each pixel minus the long-term mean. The boundary of the New Zealand EEZ is also shown.

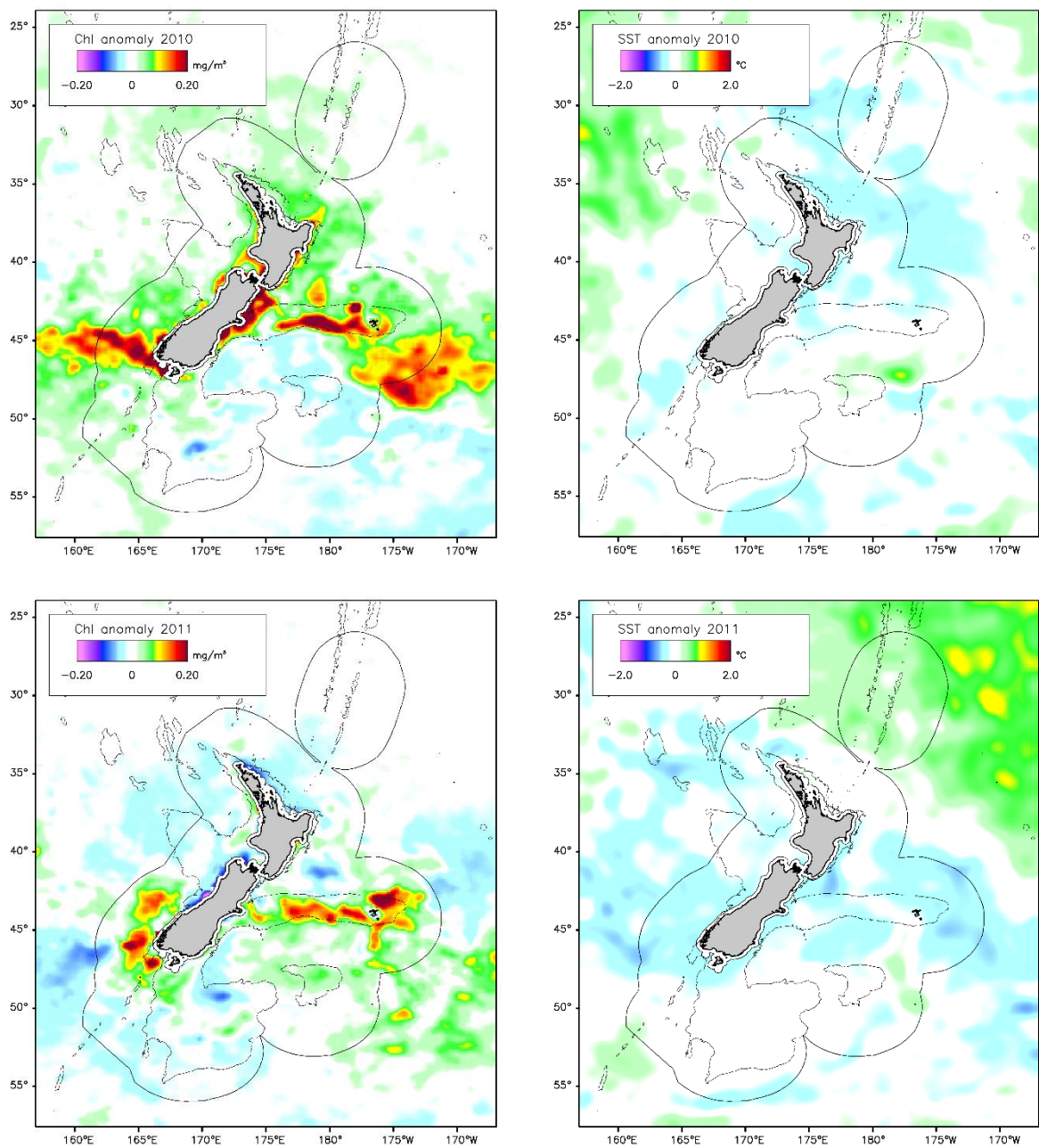


Figure C-1: Oceanic: Annual mean chl-a and sea-surface temperature (SST) annual anomalies by year. (Continued) Left: chl-a annual anomalies from the merged dataset of SeaWiFS and MODIS-Aqua (1997–2018), spatially smoothed. Right: SST annual anomalies from AVHRR satellite data (1981–2018). “Annual anomalies” are the annual mean over each pixel minus the long-term mean. The boundary of the New Zealand EEZ is also shown.

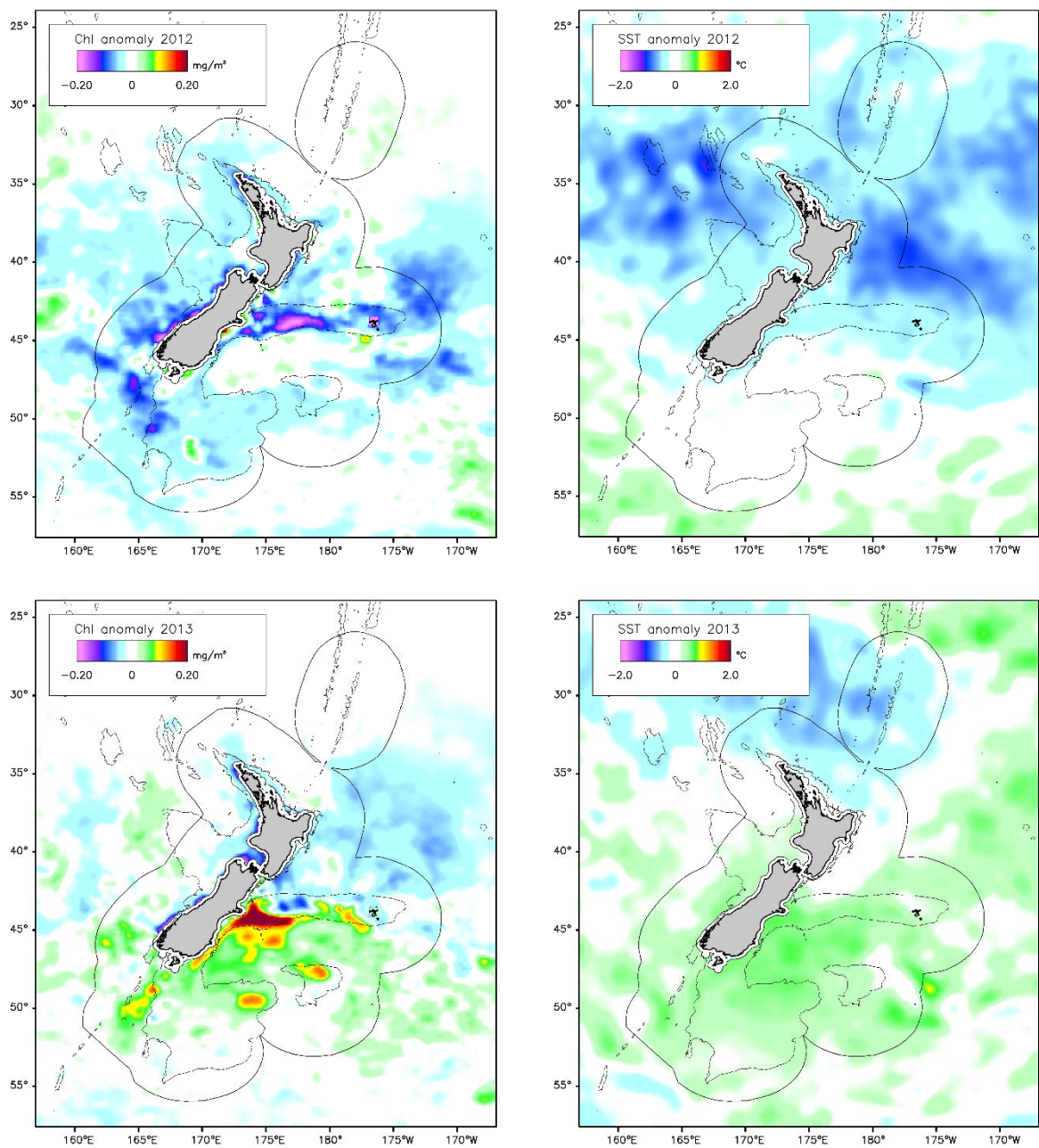


Figure C-1: Oceanic: Annual mean chl-a and sea-surface temperature (SST) annual anomalies by year. (Continued) Left: chl-a annual anomalies from the merged dataset of SeaWiFS and MODIS-Aqua (1997–2018), spatially smoothed. Right: SST annual anomalies from AVHRR satellite data (1981–2018). “Annual anomalies” are the annual mean over each pixel minus the long-term mean. The boundary of the New Zealand EEZ is also shown.

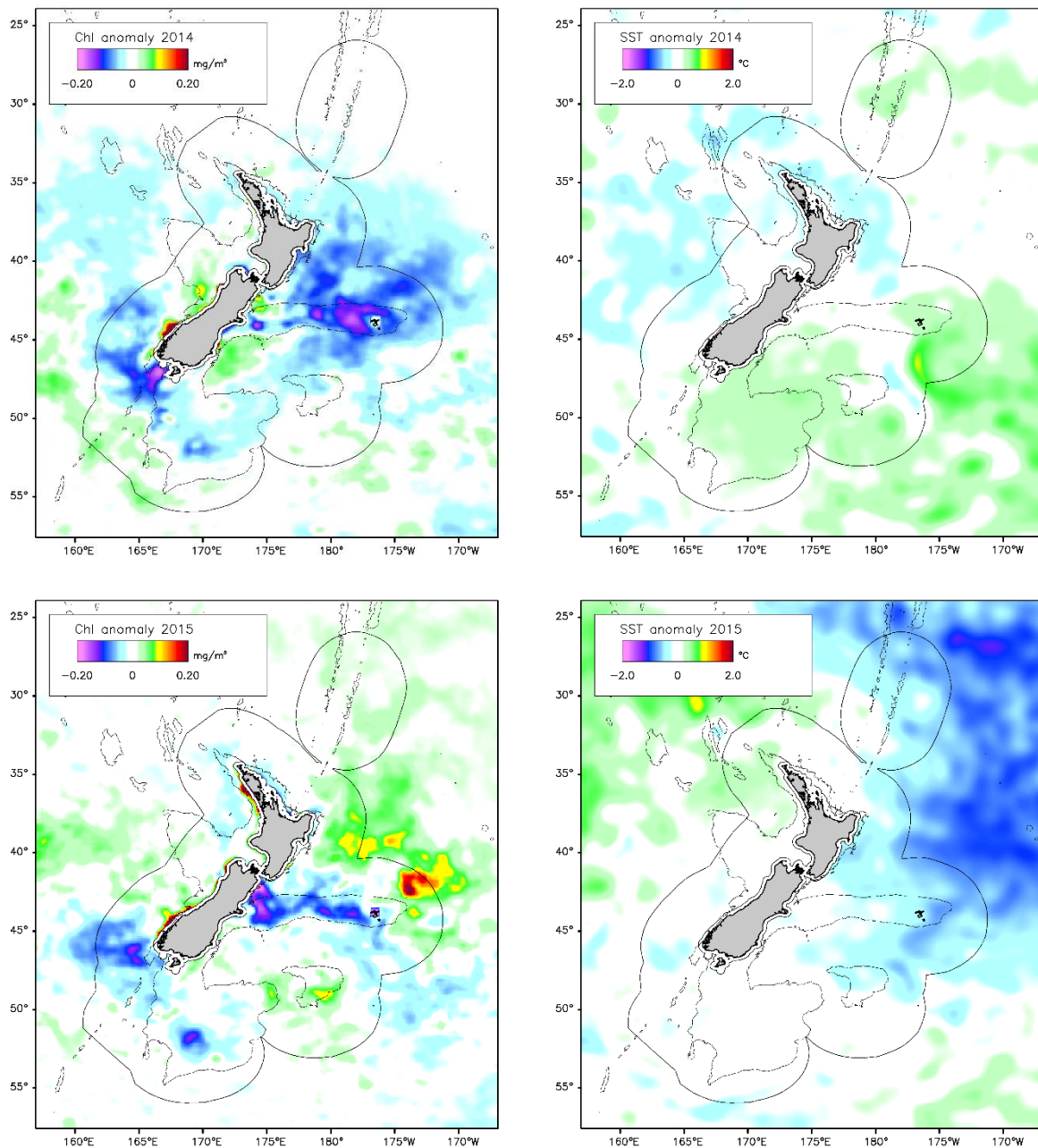


Figure C-1: Oceanic: Annual mean chl-a and sea-surface temperature (SST) annual anomalies by year. (Continued) Left: chl-a annual anomalies from the merged dataset of SeaWiFS and MODIS-Aqua (1997–2018), spatially smoothed. Right: SST annual anomalies from AVHRR satellite data (1981–2018). “Annual anomalies” are the annual mean over each pixel minus the long-term mean. The boundary of the New Zealand EEZ is also shown.

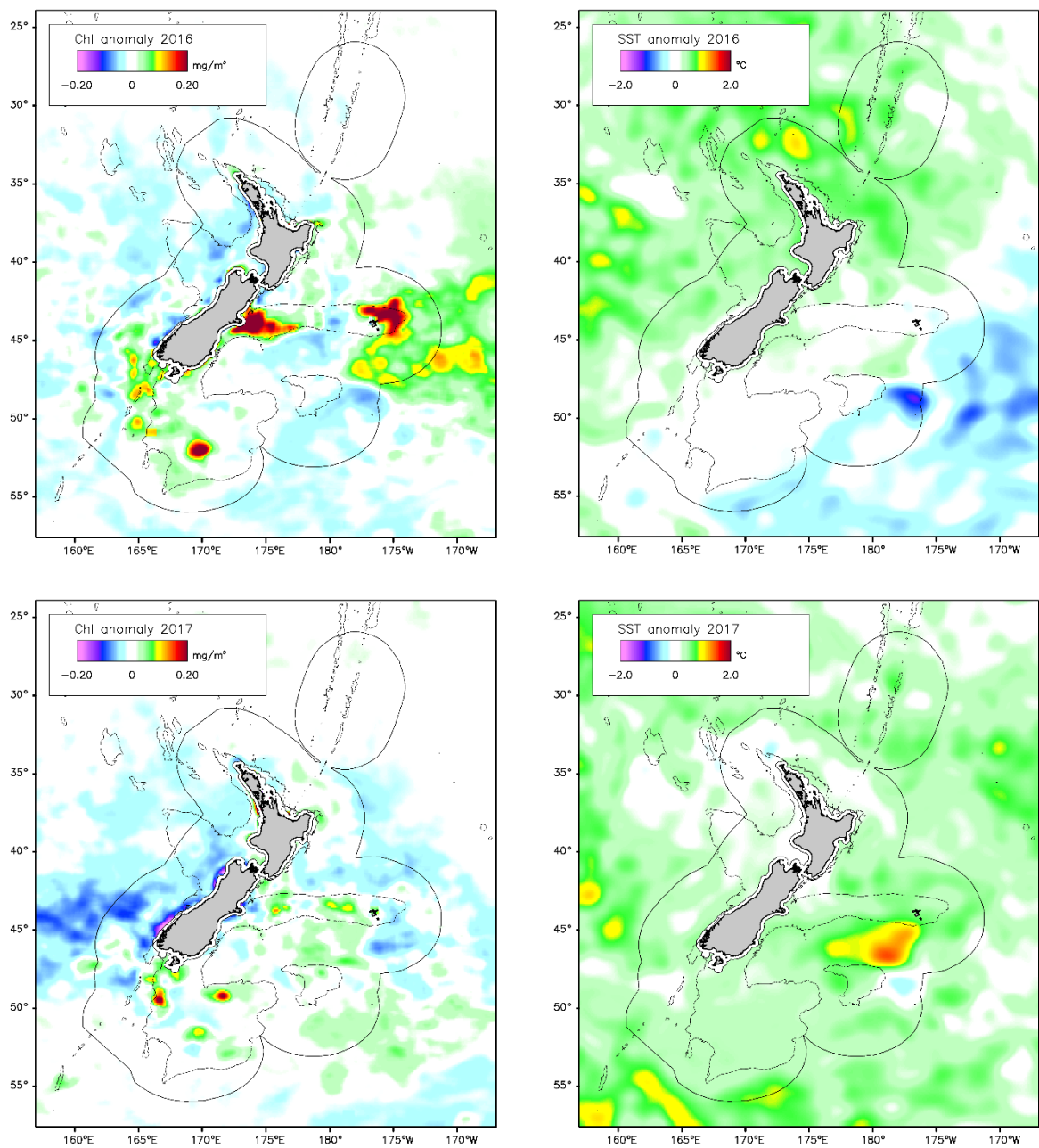


Figure C-1: Oceanic: Annual mean chl-a and sea-surface temperature (SST) annual anomalies by year. (Continued) Left: chl-a annual anomalies from the merged dataset of SeaWiFS and MODIS-Aqua (1997–2018), spatially smoothed. Right: SST annual anomalies from AVHRR satellite data (1981–2018). “Annual anomalies” are the annual mean over each pixel minus the long-term mean. The boundary of the New Zealand EEZ is also shown.

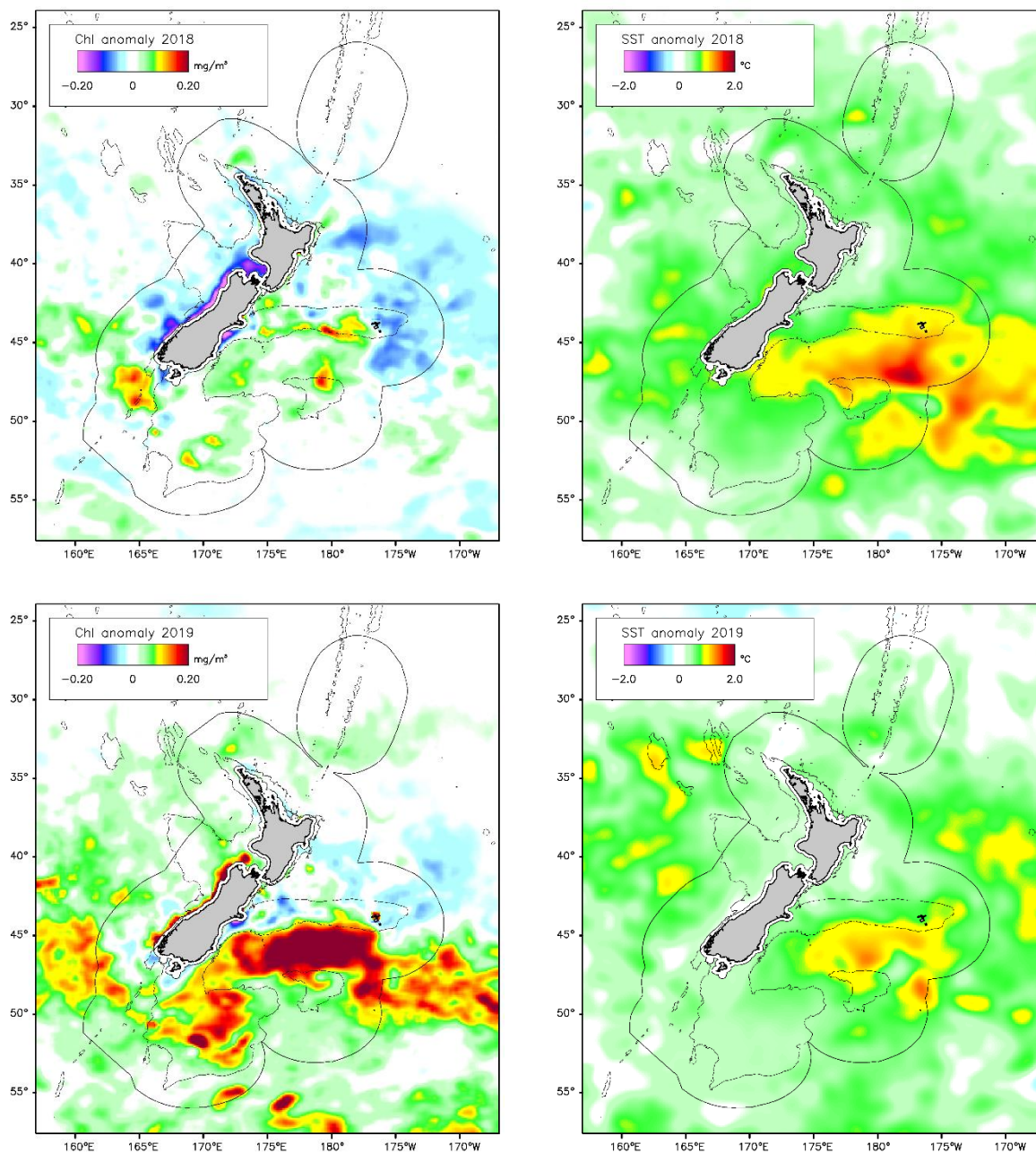


Figure C-1: Oceanic: Annual mean chl-a and sea-surface temperature (SST) annual anomalies by year. (Continued) Left: chl-a annual anomalies from the merged dataset of SeaWiFS and MODIS-Aqua (1997–2018), spatially smoothed. Right: SST annual anomalies from AVHRR satellite data (1981–2018). “Annual anomalies” are the annual mean over each pixel minus the long-term mean. The boundary of the New Zealand EEZ is also shown.

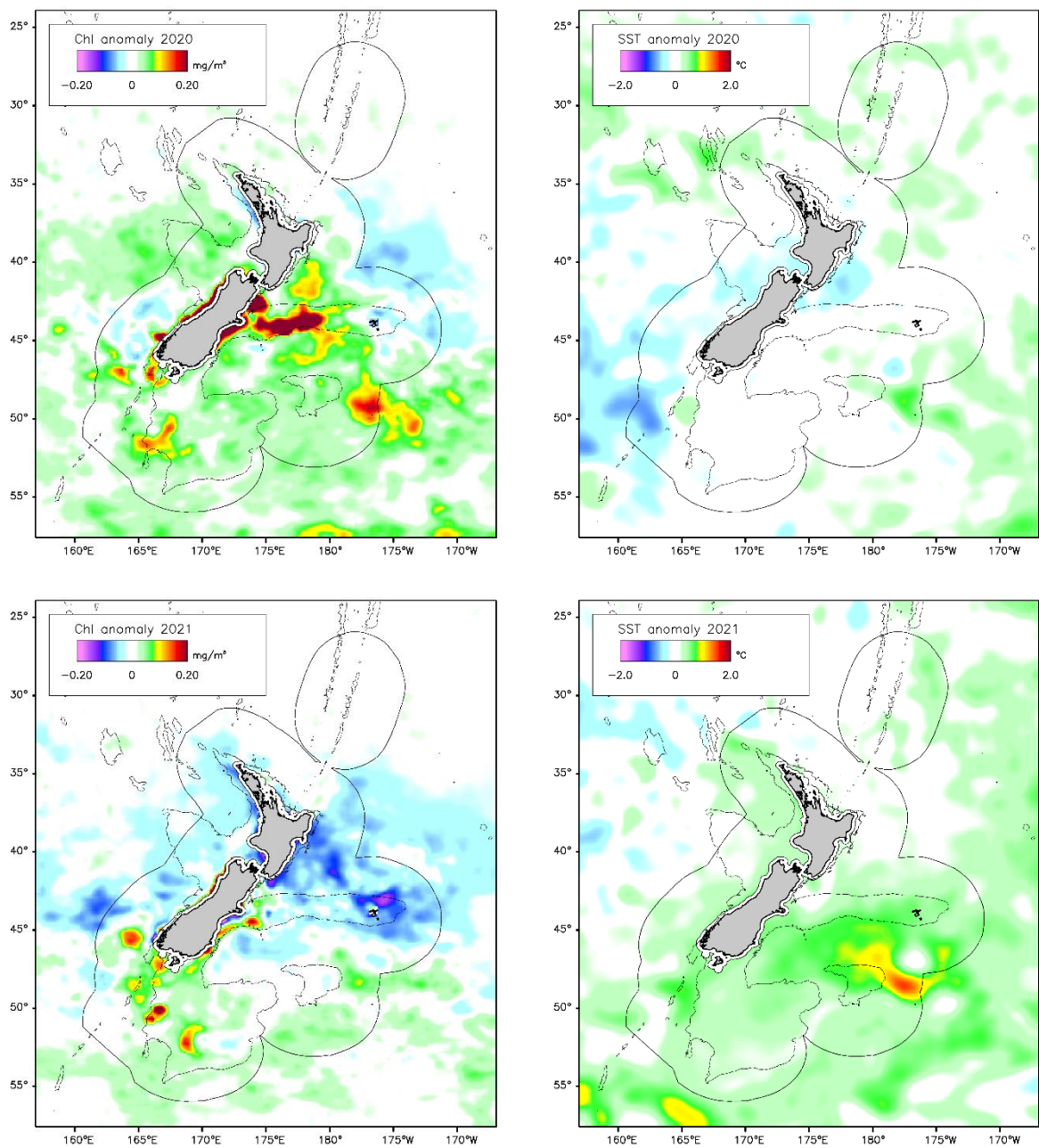


Figure C-1: Oceanic: Annual mean chl-a and sea-surface temperature (SST) annual anomalies by year. (Continued) Left: chl-a annual anomalies from the merged dataset of SeaWiFS and MODIS-Aqua (1997–2018), spatially smoothed. Right: SST annual anomalies from AVHRR satellite data (1981–2018). “Annual anomalies” are the annual mean over each pixel minus the long-term mean. The boundary of the New Zealand EEZ is also shown.

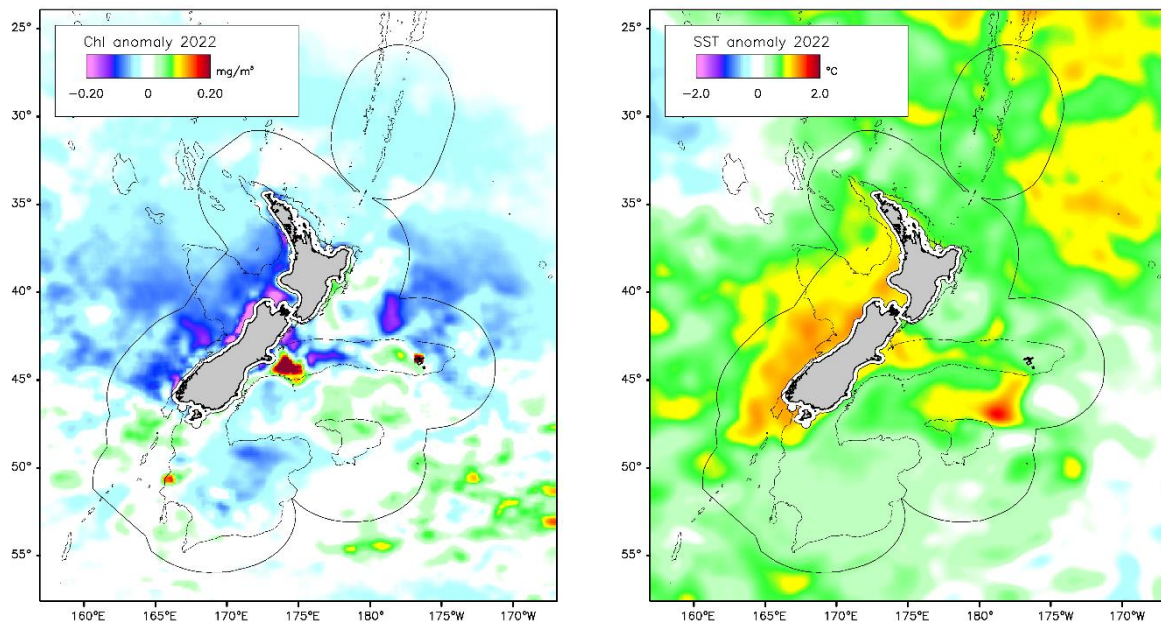


Figure C-1: Oceanic: Annual mean chl-a and sea-surface temperature (SST) annual anomalies by year. (Continued) Left: chl-a annual anomalies from the merged dataset of SeaWiFS and MODIS-Aqua (1997–2018), spatially smoothed. Right: SST annual anomalies from AVHRR satellite data (1981–2018). “Annual anomalies” are the annual mean over each pixel minus the long-term mean. The boundary of the New Zealand EEZ is also shown.

Appendix D Ocean SST and chl-a time-series

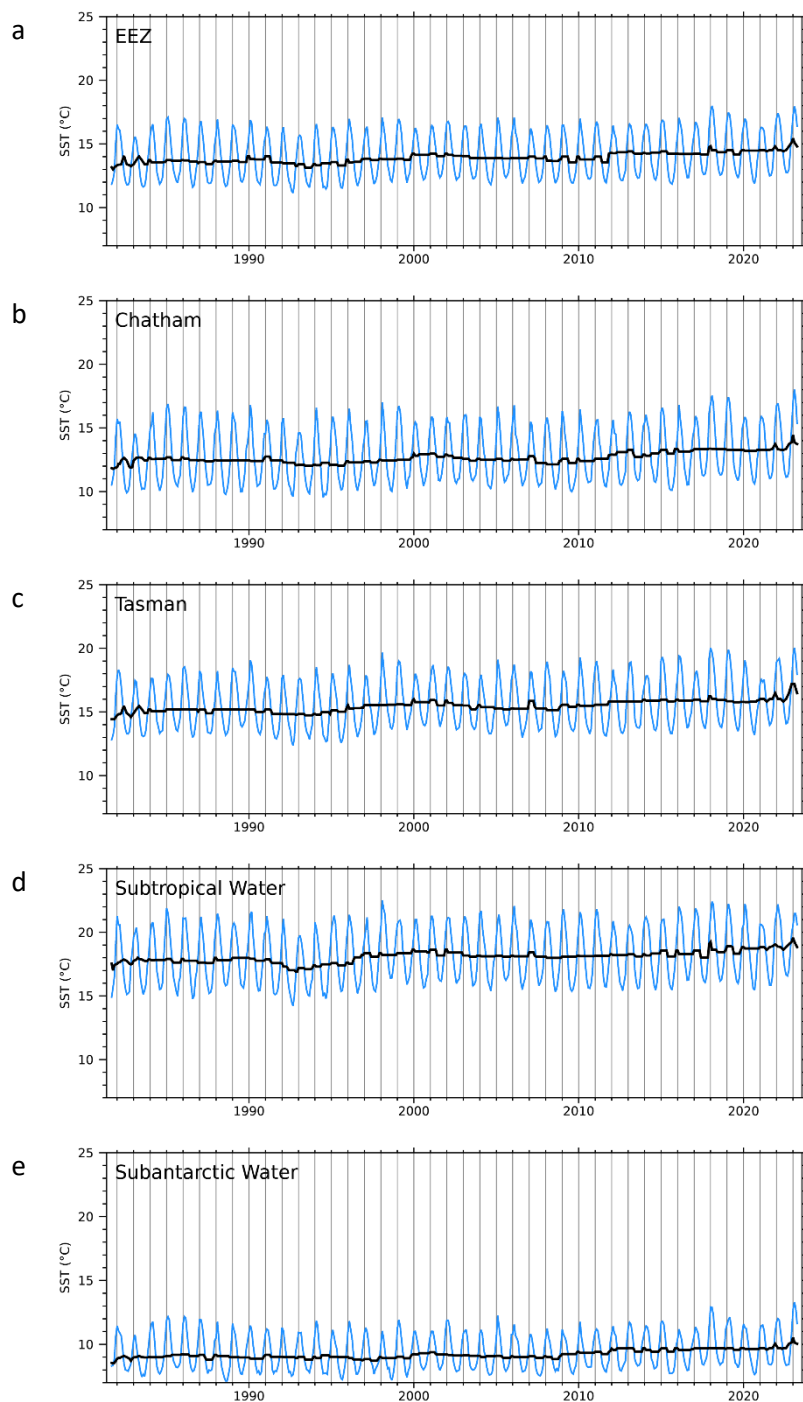


Figure D-1: Oceanic: Monthly mean SST for descriptive New Zealand regions. The regions (Figure 2-1) are: a: EEZ; b: Chatham Rise; c: Tasman Sea; d: Subtropical Water (STW); e: Subantarctic Water (SAW). These are OISST v2.1 (see Table 2 1). The 4-year running mean is shown black. The vertical grey lines divide different years.

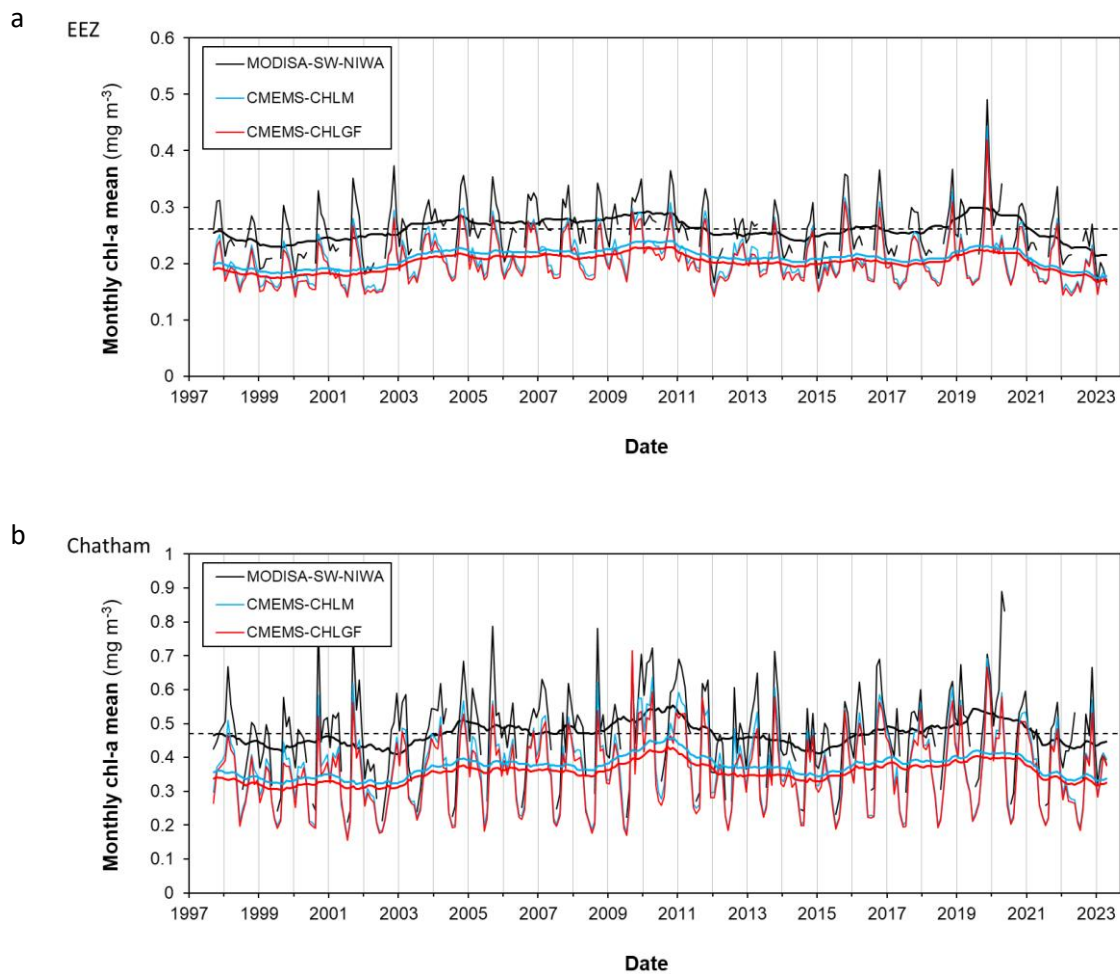


Figure D-2: Oceanic: Monthly mean chl-a for descriptive New Zealand regions. The regions (Figure 2-1) are: a: EEZ; b: Chatham Rise; c: Tasman Sea; d: Subtropical Water (STW); e: Subantarctic Water (SAW). The monthly data shown are the primary, secondary and tertiary datasets (Table 2 1). Monthly data are not shown where there was less than 80% data coverage for a given month in the region. Thick lines are smoothed with a 4-year running mean. The vertical grey lines divide different years. The dashed horizontal lines show the long-term mean of the primary data. Note that some panels have different scales. [continued below].

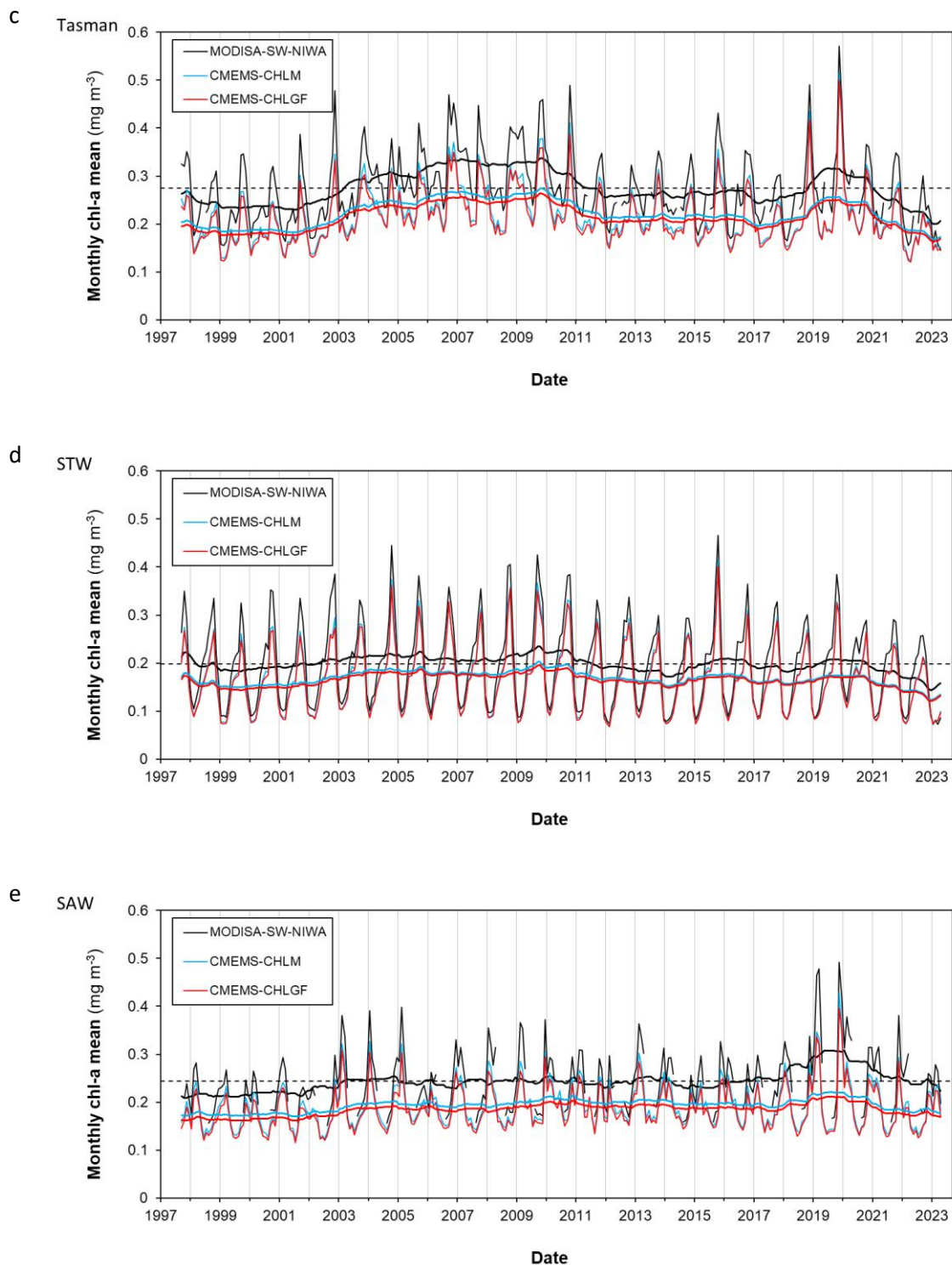


Figure D-2: Oceanic: Monthly mean chl-a for descriptive New Zealand regions. (Continued) The regions (Figure 2-1) are: a: EEZ; b: Chatham Rise; c: Tasman Sea; d: Subtropical Water (STW); e: Subantarctic Water (SAW). The monthly data shown are the primary, secondary and tertiary datasets (Table 2 1). Monthly data are not shown where there was less than 80% data coverage for a given month in the region. Thick lines are smoothed with a 4-year running mean. The vertical grey lines divide different years. The dashed horizontal lines show the long-term mean of the primary data. Note that some panels have different scales.

Appendix E Coastal SST, chl-a and TSS time-series

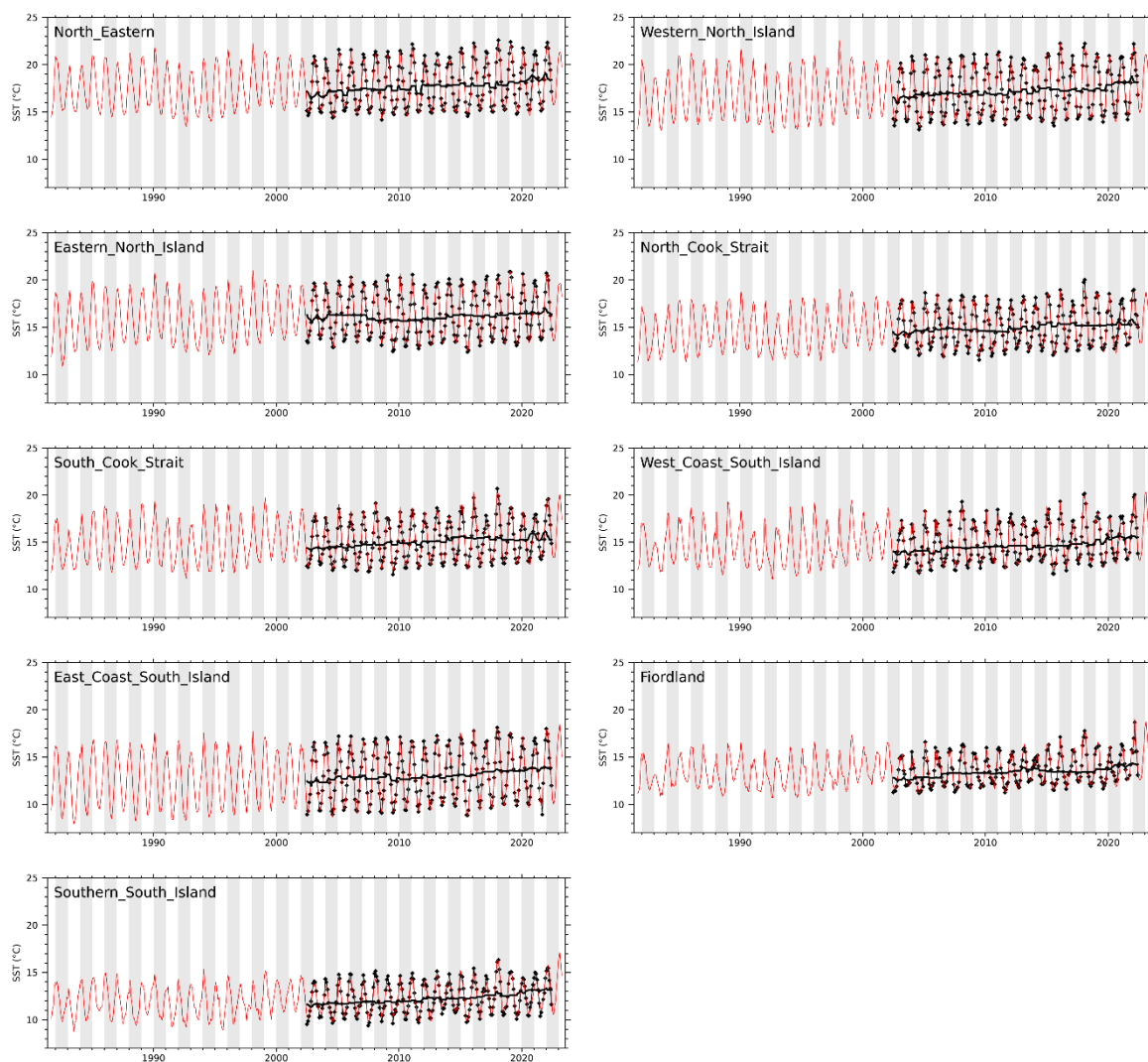


Figure E-1: Coastal sea-surface temperature (SST) means by month for coastal bio-regions. MODIS-Aqua (SCENZ SST v3.0) from 2002 (thin black and points) with a 4-year smoothed trend (thick black line). OISSTv2.1 data (red) are shown for comparison.

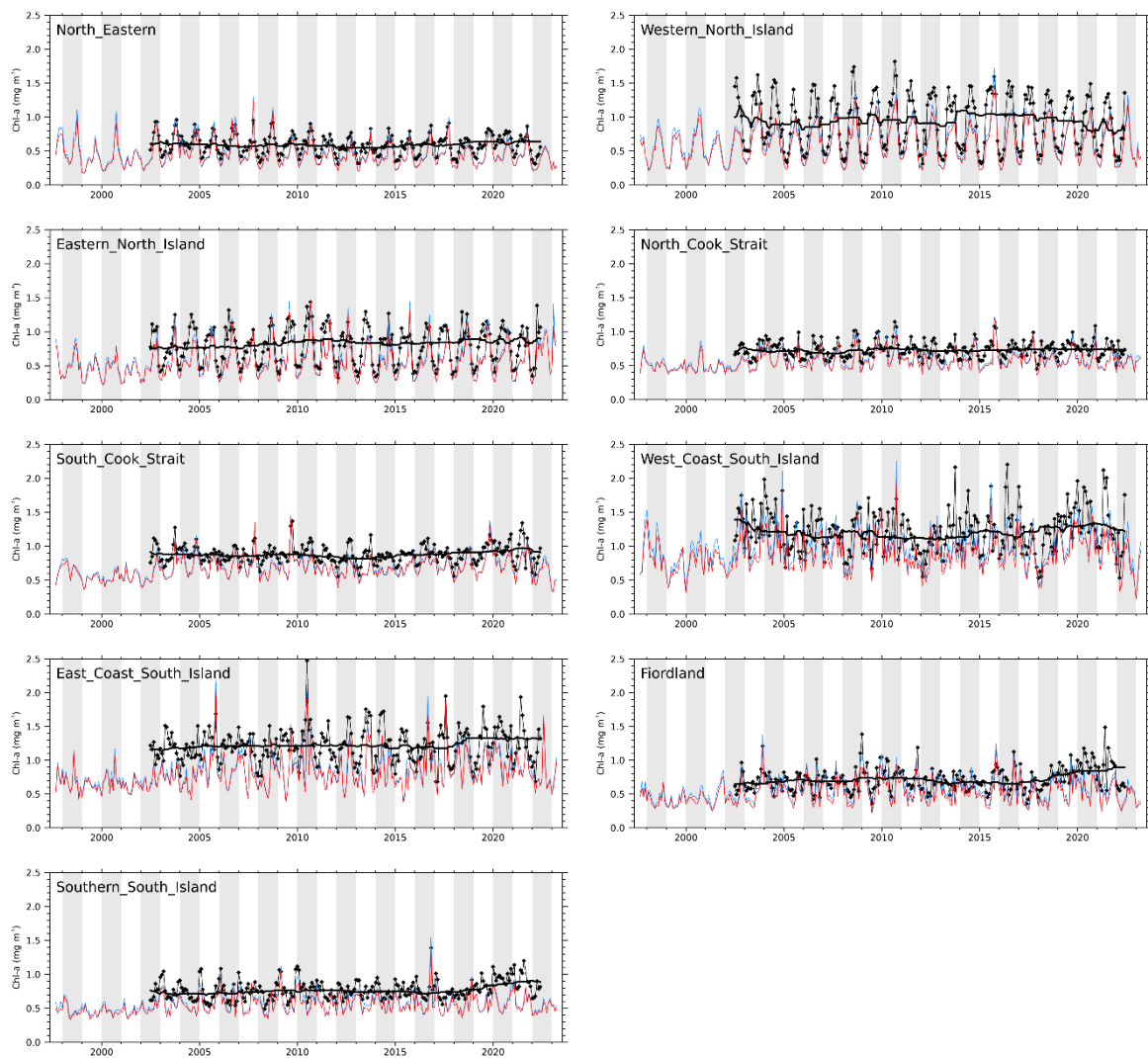


Figure E-2: Coastal chl-a anomalies by month for coastal bio-regions. [Continued below] MODIS-Aqua (SCENZ CHL v4.0) from 2002 are shown black with a 4-year smoothed trend (thick black line). CMEMS CHLM (blue) and CMEMS CHL-gap-free (red) are shown for comparison.

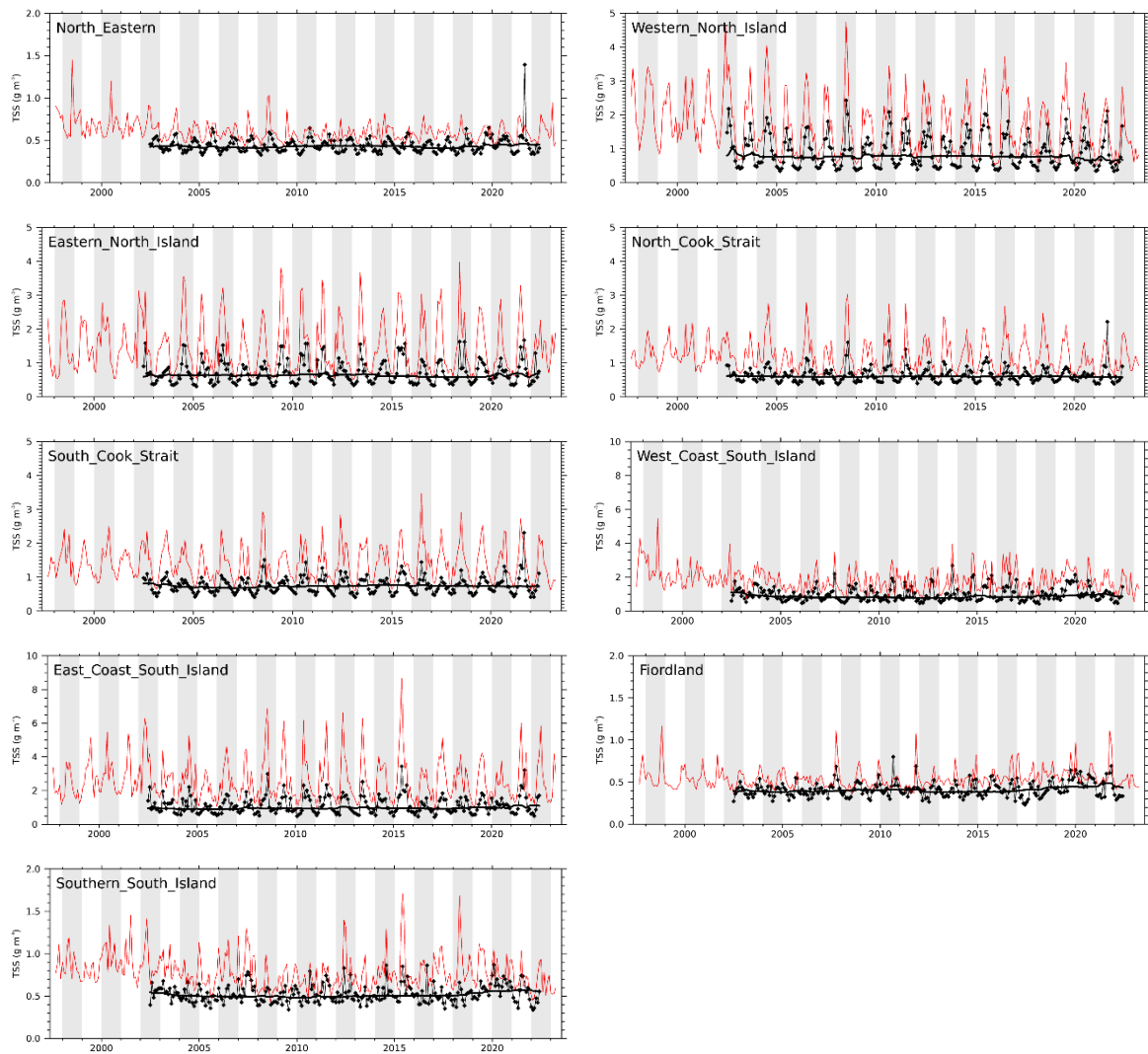


Figure E-3: Coastal TSS means by month for coastal bio-regions. [Continued below]. MODIS-Aqua (SCENZ TSS v3.0) from 2002 are shown black with a 4-year smoothed trend (thick black line). CMEMS SPM data are shown red for comparison.

Appendix F Oceanic MHW

Table F-1: Trend analysis for four marine heatwave (MHW) metrics for the NZ EEZ. The modified Mann Kendall test is applied to the yearly-averaged metrics in the EEZ. Corrected Zc: Z statistic after variance correction. Significance is shown: *** p<0.001; ** p<0.01; * p<0.05.

Region	MHW Metrics	Corrected Zc	p	Sen slope	Significance
EEZ	Number of MHW days	3.58	3E-04	16.83 days decade-1	***
	Number of events	4.77	2E-06	1.08 event decade-1	***
	Mean intensity	1.38	0.17	0.008 °C decade-1	
	Max intensity	2.06	0.04	0.04 °C decade-1	*
Chatham	Number of MHW days	5.23	2E-07	16.32 days decade-1	***
	Number of events	7.39	2E-13	1.06 event decade-1	***
	Mean intensity	0.44	0.66	0.007 °C decade-1	
	Max intensity	1.66	0.1	0.05 °C decade-1	
Tasman	Number of MHW days	5.35	9E-08	19.18 days decade-1	***
	Number of events	8.92	5E-19	1.15 event decade-1	***
	Mean intensity	1.05	0.29	0.01 °C decade-1	
	Max intensity	2.87	0.004	0.07 °C decade-1	**
STW	Number of MHW days	2.83	0.005	15.38 days decade-1	**
	Number of events	4.71	2E-06	1.16 event decade-1	***
	Mean intensity	-0.49	0.62	-0.007 °C decade-1	
	Max intensity	1.51	0.13	0.04 °C decade-1	
SAW	Number of MHW days	2.53	0.01	13.05 days decade-1	*
	Number of events	2.93	0.003	0.83 event decade-1	**
	Mean intensity	0.75	0.45	0.005 °C decade-1	
	Max intensity	1.09	0.28	0.02 °C decade-1	

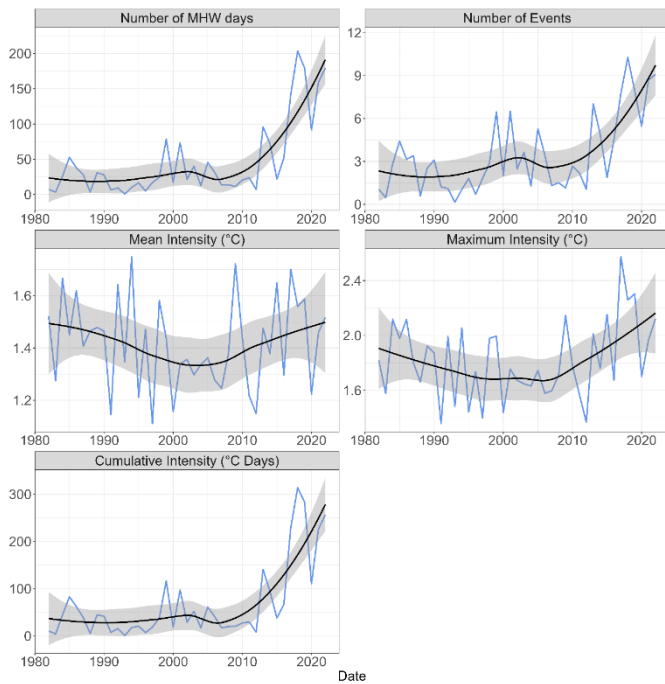


Figure F-1: Trends in MHW metrics for the NZ oceanic region “Chatham Rise” between January 1982 and December 2022 (blue line). The metrics are yearly, and grid-cell averaged.

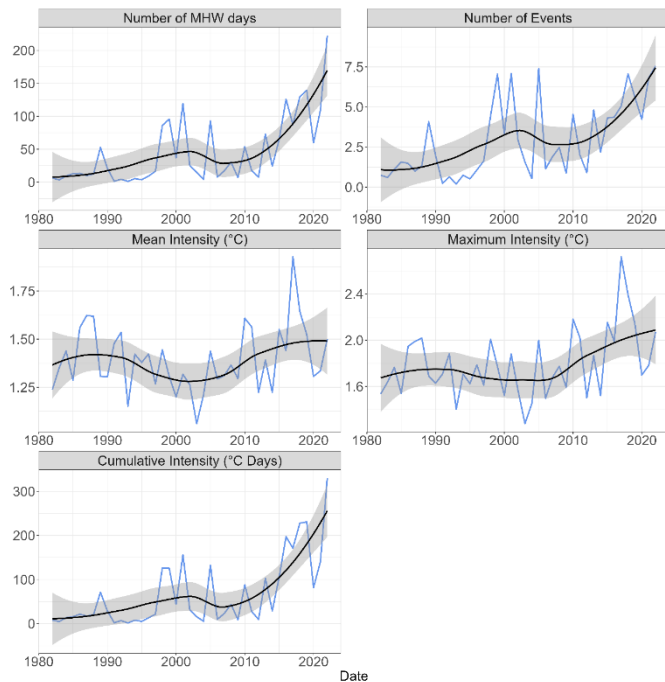


Figure F-2: Trends in MHW metrics for the NZ oceanic region “Tasman Sea” between January 1982 and December 2022 (blue line). The metrics are yearly, and grid-cell averaged.

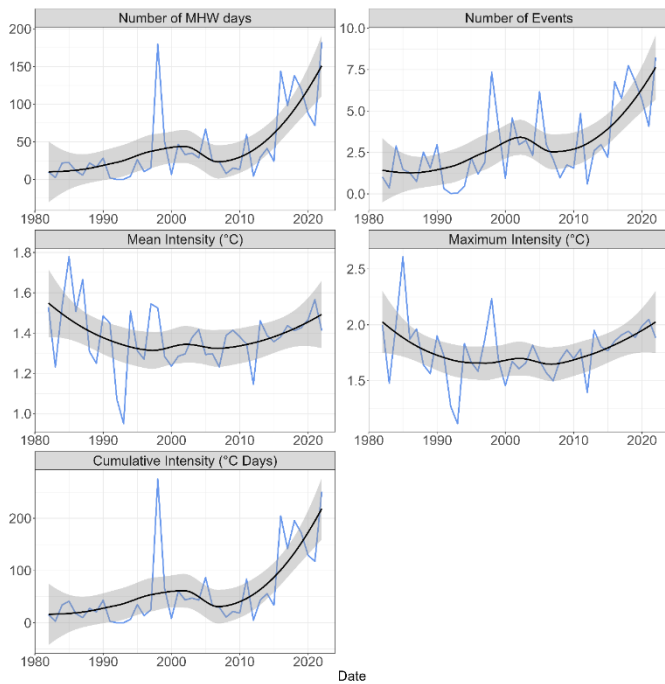


Figure F-3: Trends in MHW metrics for the NZ oceanic region “Subtropical Water” between January 1982 and December 2022 (blue line). The metrics are yearly, and grid-cell averaged.

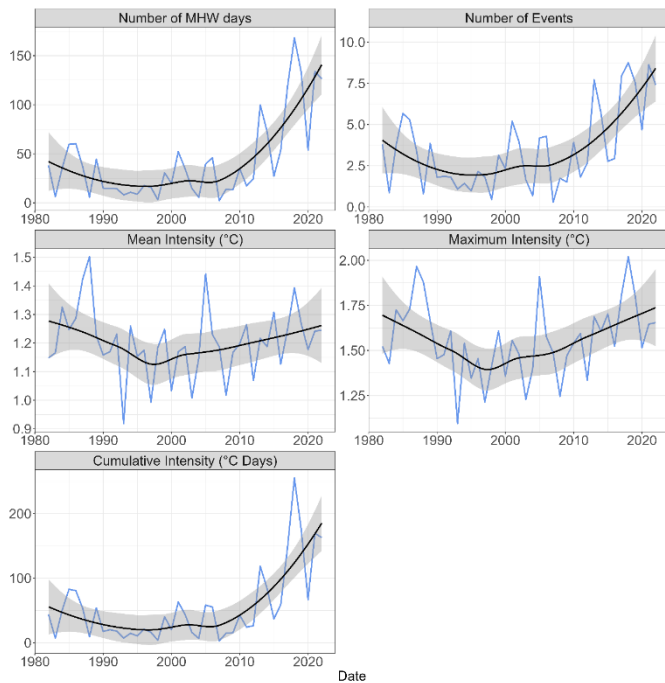


Figure F-4: Trends in MHW metrics for the NZ oceanic region “Subantarctic Water” between January 1982 and December 2022 (blue line). The metrics are yearly, and grid-cell averaged.

Appendix G Coastal MHW

Table G-1: Trend analysis for four marine heatwave (MHW) metrics for the NZ coastal regions. The modified Mann Kendall test is applied to the yearly-averaged metrics. Corrected Zc: Z statistic after variance correction. Significance is shown: *** p<0.001; ** p<0.01; * p<0.05.

Region	MHW Metrics	Corrected Zc	p	Sen slope	Sign'ce
North Eastern	Number of MHW days	3.72	2.00E-04	13.96 days decade-1	***
	Number of events	6.08	1.00E-09	0.97 event decade-1	***
	Mean intensity	1.88	0.06	0.03 °C decade-1	
	Max intensity	2.22	0.03	0.06 °C decade-1	*
Western North Island	Number of MHW days	3.73	2.00E-04	15.08 days decade-1	***
	Number of events	5.76	8.00E-09	0.96 event decade-1	***
	Mean intensity	0.51	0.61	0.01 °C decade-1	
	Max intensity	1.53	0.13	0.06 °C decade-1	
Eastern North Island	Number of MHW days	9.29	1.00E-20	12.53 days decade-1	***
	Number of events	8.35	7.00E-17	0.95 event decade-1	***
	Mean intensity	3.41	7.00E-04	0.06 °C decade-1	***
	Max intensity	4.31	2.00E-05	0.13 °C decade-1	***
North Cook Strait	Number of MHW days	5.51	4.00E-08	13.97 days decade-1	***
	Number of events	8.06	8.00E-16	10.12 event decade-1	***
	Mean intensity	-0.15	0.88	-0.002 °C decade-1	
	Max intensity	1.73	0.08	0.05 °C decade-1	
South Cook Strait	Number of MHW days	4.65	3.00E-06	16.07 days decade-1	***
	Number of events	7.31	3.00E-13	10.81 event decade-1	***
	Mean intensity	2.49	0.013	0.06 °C decade-1	*
	Max intensity	4.24	2.00E-05	0.16 °C decade-1	***
West Coast South Island	Number of MHW days	5.14	3.00E-07	17.46 days decade-1	***
	Number of events	6.59	4.00E-11	1.00 event decade-1	***
	Mean intensity	0.47	0.64	0.001 °C decade-1	
	Max intensity	3.08	0.002	0.12 °C decade-1	**
East Coast South Island	Number of MHW days	3.97	7.00E-05	17.70 days decade-1	***
	Number of events	5.95	3.00E-09	1.38 event decade-1	***
	Mean intensity	2.06	0.04	0.05 °C decade-1	*
	Max intensity	4.11	4.00E-05	0.15 °C decade-1	***
Southern South Island	Number of MHW days	3.09	0.002	14.00 days decade-1	**
	Number of events	6.27	4.00E-10	1.17 event decade-1	***
	Mean intensity	1.44	0.15	0.03 °C decade-1	
	Max intensity	3.25	0.001	0.12 °C decade-1	**
Fiordland	Number of MHW days	4.03	6.00E-05	13.28 days decade-1	***
	Number of events	5.78	8.00E-09	0.84 event decade-1	***
	Mean intensity	1.07	0.28	0.03 °C decade-1	
	Max intensity	2.68	0.007	0.14 °C decade-1	**

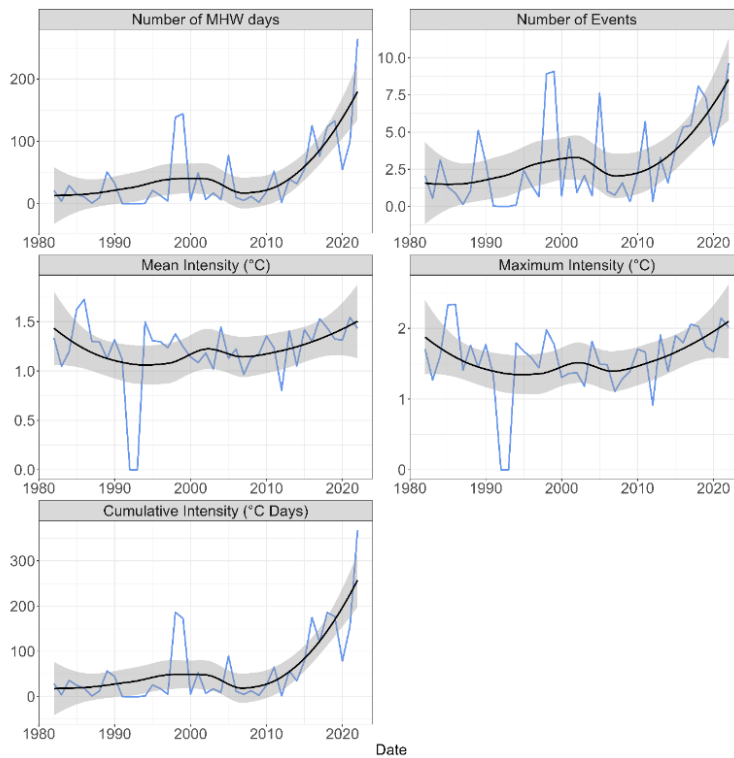


Figure G-1: Trends in MHW metrics for the NZ coastal region “North Eastern” between January 1982 and December 2022 (blue line). The metrics are yearly, and grid-cell averaged.

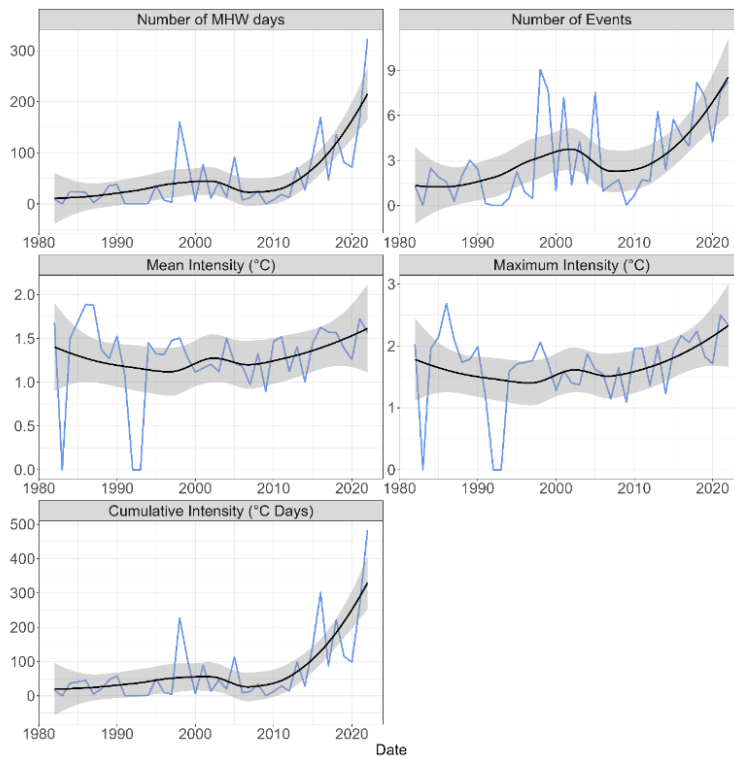


Figure G-2: Trends in MHW metrics for the NZ coastal region “Western North Island” between January 1982 and December 2022 (blue line). The metrics are yearly, and grid-cell averaged.

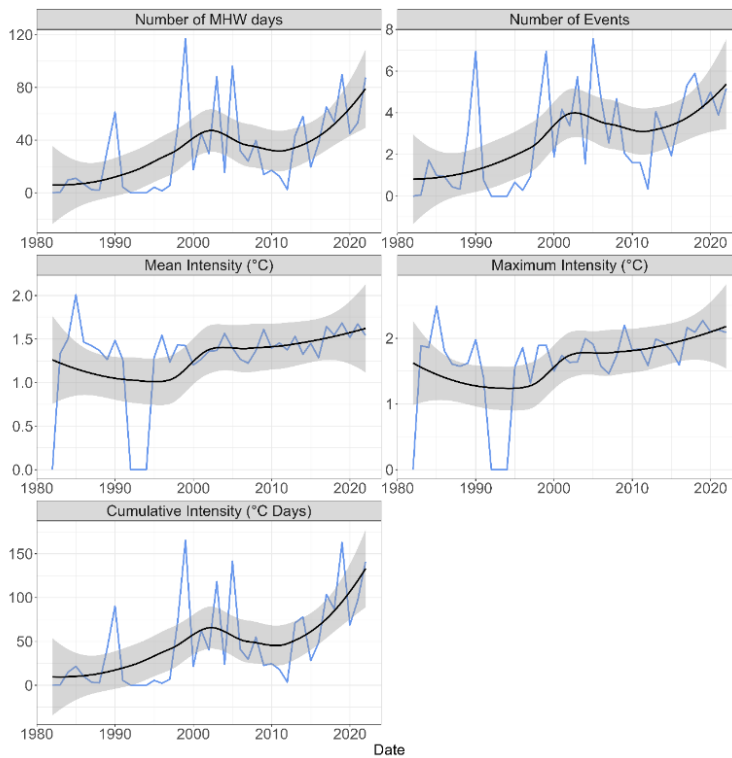


Figure G-3: Trends in MHW metrics for the NZ coastal region “Eastern North Island” between January 1982 and December 2022 (blue line). The metrics are yearly, and grid-cell averaged.

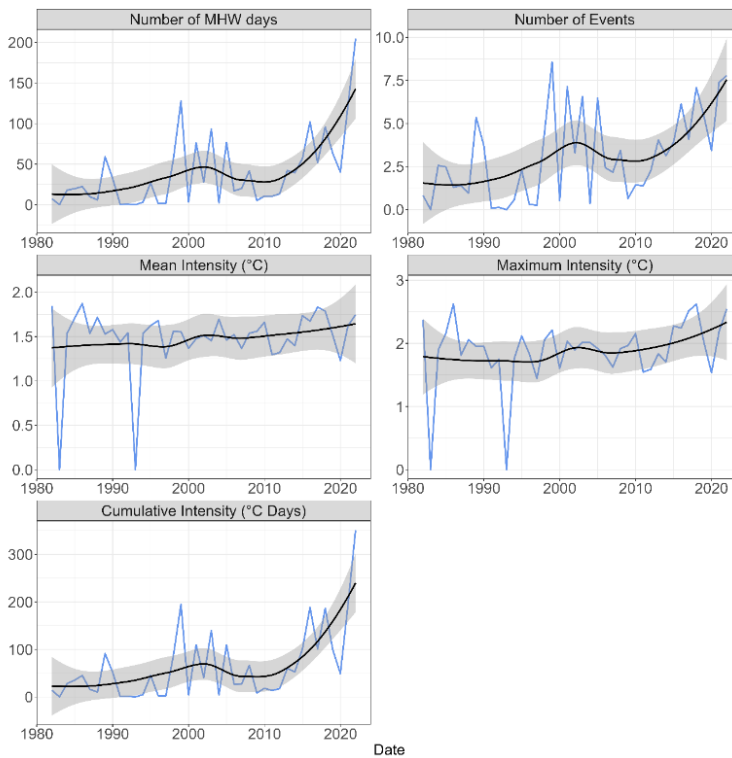


Figure G-4: Trends in MHW metrics for the NZ coastal region “North Cook Strait” between January 1982 and December 2022 (blue line). The metrics are yearly, and grid-cell averaged.

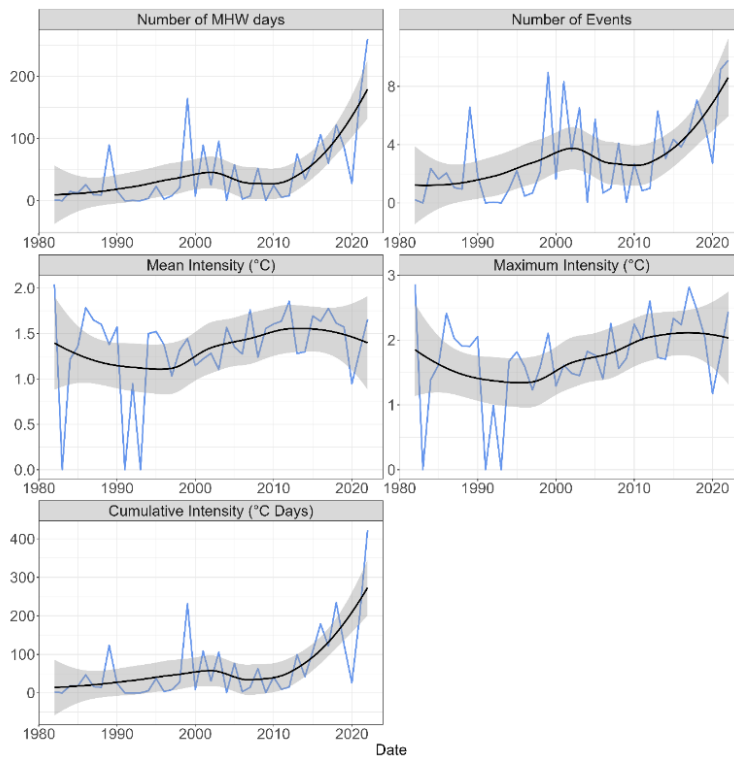


Figure G-5: Trends in MHW metrics for the NZ coastal region “South Cook Strait” between January 1982 and December 2022 (blue line). The metrics are yearly, and grid-cell averaged.

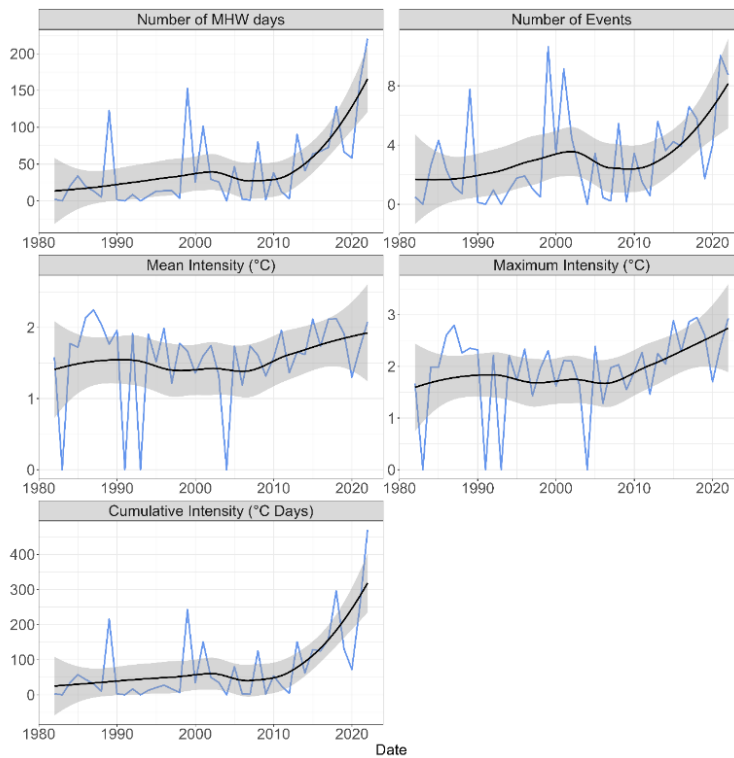


Figure G-6: Trends in MHW metrics for the NZ coastal region “West Coast South Island” between January 1982 and December 2022 (blue line). The metrics are yearly, and grid-cell averaged.

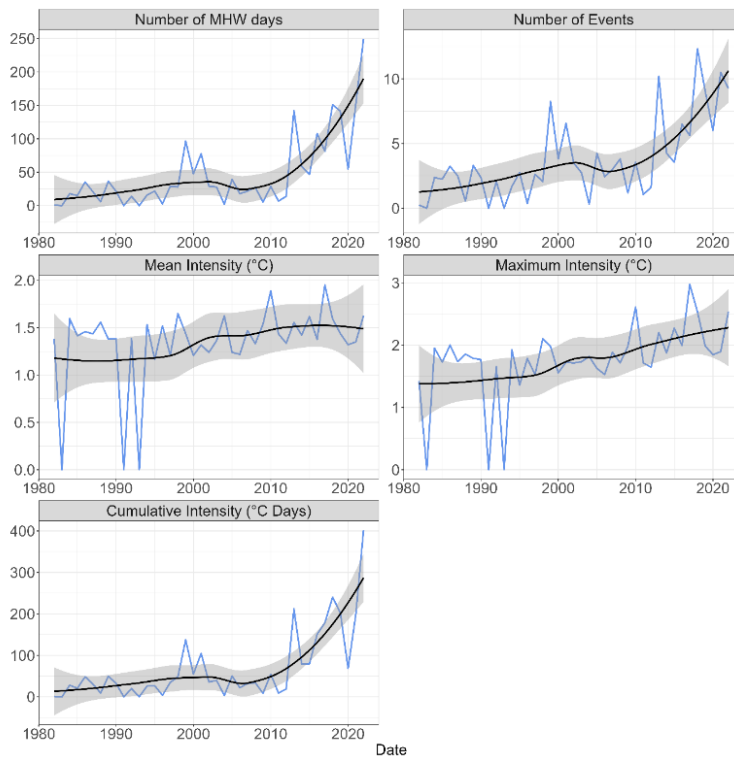


Figure G-7: Trends in MHW metrics for the NZ coastal region “East Coast South Island” between January 1982 and December 2022 (blue line). The metrics are yearly, and grid-cell averaged.

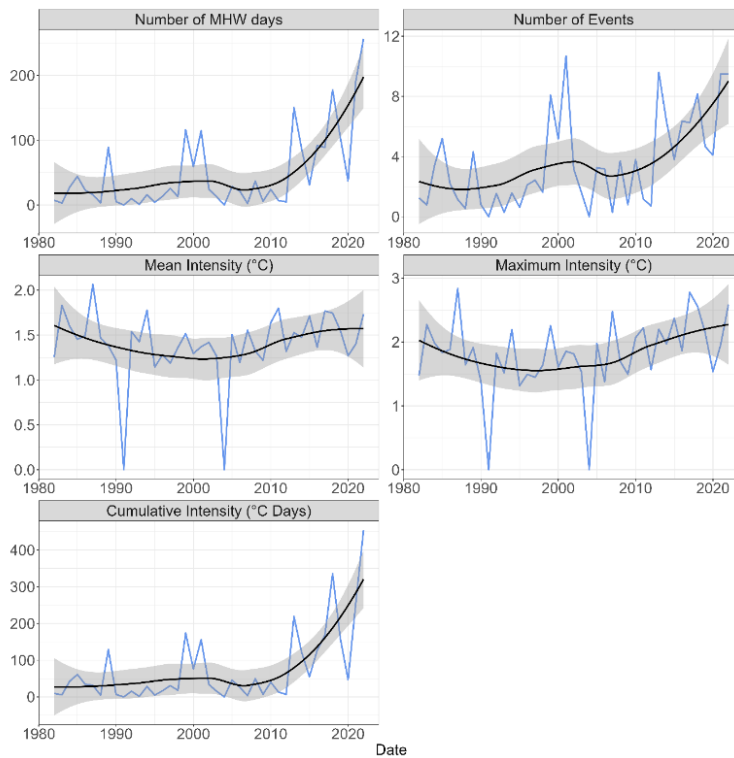


Figure G-8: Trends in MHW metrics for the NZ coastal region “Southern South Island” between January 1982 and December 2022 (blue line). The metrics are yearly, and grid-cell averaged.

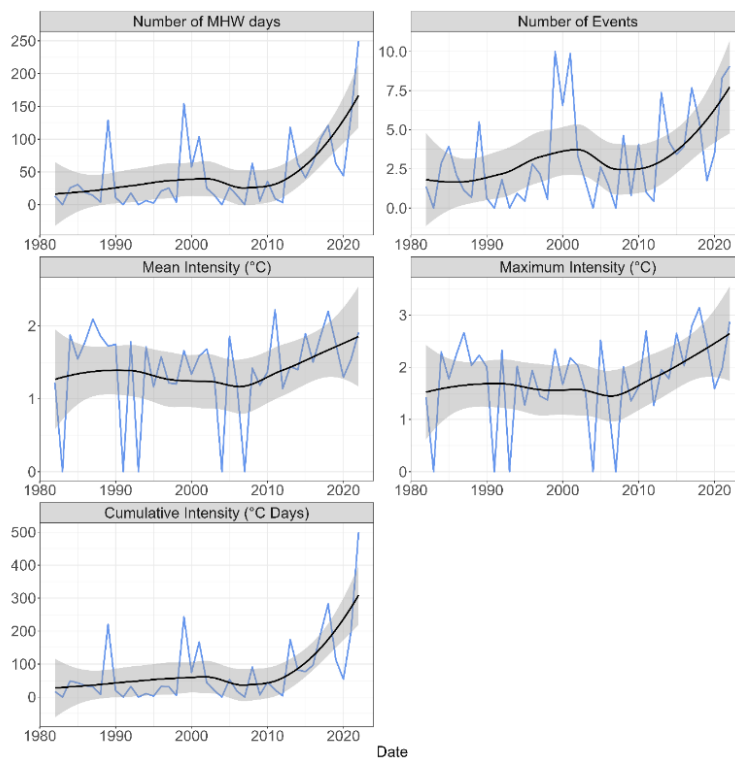


Figure G-9: Trends in MHW metrics for the NZ coastal region “Fiordland” between January 1982 and December 2022 (blue line). The metrics are yearly, and grid-cell averaged.